Universität Bremen

Groundwater pollution: Occurrence, Sources, Behavior, Transport and Fate of Mercury, Benzene and Nitrate in Soil–Groundwater systems in the Eastern Niger Delta, Nigeria

Dissertation

zur Erlangung des akademischen Grades
Doktor der Naturwissenschaften
(Dr. rer. nat.)
am Fachbereich Geowissenschaften
der Universität Bremen

vorgelegt von

Dogo Lawrence Aleku

Bremen, December 2024

Gutachter

Prof. Dr. Thomas Pichler
Fachgebeit Geochemie und Hydrogeologie
Fachbereich Geowissenschaften
Universität Bremen

Prof. Dr. Carl Renshaw
Fachbereich Geowissenschaften
Dartmouth College

Tag des Promotionskolloquiums: 13.12.2024

Versicherung an Eides Statt / *Affirmation in lieu of an oath*

gem. § 5 Abs. 5 der Promotionsordnung vom 28.04.2021 /

according to § 5 (5) of the Doctoral Degree Rules and Regulations of 28 April, 2021

Ich / I, _____
(Vorname / First *Name*, Name / *Name*, Anschrift / *Address*, ggf. Matr.-Nr. / *student ID no., if applicable)*

versichere an Eides Statt durch meine Unterschrift, dass ich die vorliegende Dissertation selbständig und ohne fremde Hilfe angefertigt und alle Stellen, die ich wörtlich dem Sinne nach aus Veröffentlichungen entnommen habe, als solche kenntlich gemacht habe, mich auch keiner anderen als der angegebenen Literatur oder sonstiger Hilfsmittel bedient habe und die zu Prüfungszwecken beigelegte elektronische Version (PDF) der Dissertation mit der abgegebenen gedruckten Version identisch ist. / *With my signature I affirm in lieu of an oath that I prepared the submitted dissertation independently and without illicit assistance from third parties, that I appropriately referenced any text or content from other sources, that I used only literature and resources listed in the dissertation, and that the electronic (PDF) and printed versions of the dissertation are identical.*

Ich versichere an Eides Statt, dass ich die vorgenannten Angaben nach bestem Wissen und Gewissen gemacht habe und dass die Angaben der Wahrheit entsprechen und ich nichts verschwiegen habe*. / I affirm in lieu of an oath that the information provided herein to the best of my knowledge is true and complete.*

Die Strafbarkeit einer falschen eidesstattlichen Versicherung ist mir bekannt, namentlich die Strafandrohung gemäß § 156 StGB bis zu drei Jahren Freiheitsstrafe oder Geldstrafe bei vorsätzlicher Begehung der Tat bzw. gemäß § 161 Abs. 1 StGB bis zu einem Jahr Freiheitsstrafe oder Geldstrafe bei fahrlässiger Begehung. / *I am aware that a false affidavit is a criminal offence which is punishable by law in accordance with § 156 of the German Criminal Code (StGB) with up to three years imprisonment or a fine in case of intention, or in accordance with § 161 (1) of the German Criminal Code with up to one year imprisonment or a fine in case of negligence.*

_____ _____

Ort / *Place*, Datum / *Date* Unterschrift / *Signature*

Abstract

The Benin Formation aquifer in the eastern Niger Delta of Nigeria faces many threats from anthropogenic activities. These activities include indiscriminate sewage disposal, the usage of pit latrines, and several impacts of oil and gas activities capable of releasing various pollutants into the environment. The Benin Formation aquifer is the primary source of drinking water for most of the region. Hence, the release of pollutants into the aquifer may cause adverse health effects on the population. Despite the area's high level of anthropogenic activities, the sources and processes affecting various groundwater pollutants remain understudied. This study investigated, for the first time, the occurrence, sources, transport and fate of mercury, benzene and nitrate in the groundwater of the eastern Niger Delta, Nigeria. The investigation was conducted across five communities (i.e., Alesa, Ogale, Ebubu, Alode and Okochiri). Results may be transferable to other locations with similar incidences.

At a site impacted by crude oil refining in Okochiri, hydrocarbon contamination in the ground and drinking water was already known. However, the concentration, source, speciation and mobility of mercury (Hg), an oil refining byproduct, was unknown. To address this, groundwater at the impacted site was investigated. Hg levels in groundwater along the wastewater discharge outlet (WDO) of the refinery ranged from 0.2 and 6 µg/L. 63 % of the Hg occurred as Hg bound to particles larger than 0.45 µm (Hg_{part}). Operationally-defined Hg speciation shows that 33 % occurred as inorganic, reactive Hg^{2+}, and 4 % as dissolved organic matter-bound Hg^{2+} despite the high DOC (up to 47 mg/L) and BTEX (up to 2,888 µg/L) levels, indicating that the DOC, which is mainly hydrocarbon, does not bind Hg. Overall, Hg levels in groundwater were elevated where oil and gas production wastewater was introduced into the aquifer.

The Hg concentration in sediments collected at the wastewater discharge point (WDP) was up to 529 µg/kg, and the carbon (C) content reached 40 %. The batch leaching experiments showed that up to 23.5 % of THg in the quartz-dominant sediment could be mobilized into groundwater under oxic conditions. In general, Hg retention in the sediment is controlled by the sediment's natural organic matter (NOM).

Abstract

The ground and drinking water in Alode, Ogale, and Okochiri, where several oil and gas production facilities are present, showed elevated BTEX levels, of up to 3,904 µg/L, 1,573 µg/L and 2,888 µg/L, respectively. Similarly, benzene levels were up to 3,500 µg/L, 1,300 µg/L and 2,700 µg/L in Alode, Ogale and Okochiri, respectively. Here, benzene was the dominant BTEX compound. DOC, which reflects the total hydrocarbon load in the groundwater, was up to 47 mg/L in Alode, 49 mg/L in Ogale and 33 mg/L in Okochiri. Benzene was detected in private supply wells (PSW) close to an underground petroleum pipeline passing through the three communities. Its concentration decreased with increasing distance from the pipeline, indicating probable leakage of petroleum from the pipeline into the aquifer.

The aquifer's dissolved oxygen level (up to 7.5 (95 %) mg/L) and BTEX biodegradation capacity (up to 2.11 mg/L for DO) appear sufficient to support the BTEX degradation. However, the degradation may be weakened by the high groundwater temperature (32.5 °C). As a result, based on the calculated benzene (0.128 to 0.693) and BTEX (0.086 to 0.556) daily attenuation rates for this study, up to 66.5 years and 85 years would be required to attenuate benzene and BTEX. Thus, active remedial measures are required to reduce the time required for complete benzene attenuation in the affected groundwater.

Given the extensive animal husbandry, pit latrine usage, and indiscriminate municipal and domestic waste disposal practices, the groundwater and municipal sewage were investigated for nitrate (NO_3^-) in Alesa, Ogale, Ebubu, Alode and Okochiri. NO_3^- levels in the groundwater were highly variable: up to 142 mg/L in Alesa, 211 mg/L in Ogale, 120 mg/L in Ebubu, 55 mg/L in Alode and 10 mg/L in Okochiri. The major ion comparison showed that 71 %, 90 %, 87 %, and 92 % of the groundwater samples exceeded the reference site concentrations for Ca^{2+}, Na^+, K^+, and Cl^-, respectively, suggesting anthropogenic (sewage) influence. Similarly, the NO_3^-/Cl^- ratio showed that 100 % (Alesa), 77 % (Ogale), and 84 % (Ebubu) of NO_3^- in the groundwater is derived from the ongoing anthropogenic activities (sewage). Furthermore, the isotopic evidence ($\delta^{15}N\text{-}NO_3^-$ and $\delta^{18}O\text{-}NO_3^-$) confirmed that the NO_3^- originates from sewage-derived NH_4^+ nitrification. Despite the high dissolved oxygen (DO) level, up to 8.9 mg/L, our results have shown evidence of denitrification in the area. This suggests that both biogeochemical processes occur simultaneously

in the groundwater. However, the high DO and NO_3^- levels do not support a complete NO_3^- attenuation in the affected communities, hence the need for safe domestic and municipal sewage management practices. Consequently, there is a risk of NO_3^- export from shallow aquifers into the nearby surface waters in Okochiri and into the coastal ocean.

It can be concluded that the ongoing anthropogenic activities in the eastern Niger Delta have contributed a substantial amount of pollutants (i.e., mercury, benzene and nitrate) to the ground and drinking water at levels above the WHO guideline values. The (1) high concentration of the pollutants, (2) their continuous release into the aquifer, and (3) the impact of the high groundwater temperature on the prevailing redox conditions in the aquifer appear to weaken the natural attenuation of these pollutants from the aquifer. To protect the health of the growing population in the affected areas, measures to encourage immediate discontinuous use of the contaminated wells and alternative safe water sources (e.g., bottled, sachet, or a centralized water supply system) should be explored. Also, the local authorities need to implement measures to ensure a decline in the concentration of the investigated pollutants, including the remediation of the contaminated sediments and groundwater.

Zusammenfassung

Der Grundwasserleiter der Benin-Formation im östlichen Niger-Delta von Nigeria ist auf vielfältige Weise durch anthropogene Aktivitäten bedroht. Dazu gehören die unstrukturierte Entsorgung von Abwässern, die Nutzung von Latrinen und verschiedene Auswirkungen der Öl- und Gasförderung, welche zu einer Freisetzung verschiedener Schadstoffe in die Umwelt führen können. Der Grundwasserleiter der Benin-Formation ist die Haupttrinkwasserquelle für den größten Teil der Region. Daher kann die Freisetzung von Schadstoffen in den Grundwasserleiter negative Auswirkungen auf die Gesundheit der Bevölkerung haben. Trotz des hohen Maßes an anthropogenen Aktivitäten in der Region sind die Quellen und Prozesse, die sich auf verschiedene Grundwasserschadstoffe auswirken, bisher nur unzureichend untersucht worden. In dieser Studie wurden zum ersten Mal das Vorkommen, die Quellen, der Transport und der Verbleib bzw. die mögliche Anreicherung von Quecksilber, Benzol und Nitrat im Grundwasser des östlichen Nigerdeltas in Nigeria untersucht. Die Untersuchung wurde in fünf Gemeinden durchgeführt (d.h. Alesa, Ogale, Ebubu, Alode und Okochiri). Diese Befunde lassen sich potentiell auf andere Orte mit vergleichbaren Kontexten übertragen.

An einem von der Erdölraffination betroffenen Standort in Okochiri war die Verunreinigung des Bodens und des Trinkwassers mit Kohlenwasserstoffen bereits bekannt. Die Konzentration, Quelle, Speziierung und Mobilität von Quecksilber (Hg), einem Nebenprodukt der Erdölraffination, war bisher jedoch unbekannt und aus diesem Grund wurde das Grundwasser an der betroffenen Stelle untersucht. Die Hg-Konzentrationen im Grundwasser entlang des Abwasserauslasses (WDO) der Raffinerie lagen zwischen 0,2 und 6 µg/L. Bis zu 63 % des Hg ist an Partikel größer als 0,45 µm gebunden(Hg_{part}). Die operational definierte Hg-Speziierung zeigt, dass 33 % als anorganisches, reaktives Hg^{2+} und 4 % als an gelöste organische Stoffe gebundenes Hg^{2+} vorliegt. Und das trotz der hohen DOC- (bis zu 47 mg/L) und BTEX-Werte (bis zu 2.888 µg/L), was darauf hindeutet, dass die DOC-Fraktion, welche hauptsächlich aus Kohlenwasserstoff besteht, Hg nicht effektivbindet. Insgesamt waren die Hg-Gehalte im Grundwasser dort erhöht, wo Abwässer aus der Öl- und Gasproduktion in den Grundwasserleiter gelangen konnten.

Die Hg-Konzentration in Sedimenten, die an der Abwasserausleitstelle der Raffinerie gesammelt wurden, betrug bis zu 529 µg/kg, und der Kohlenstoffgehalt (C) erreichte 40 %. Die Batch-Leachingversuche ergaben, dass bis zu 23,5 % des THg im quarzdominierten Sediment unter oxischen Bedingungen ins Grundwasser mobilisiert werden kann. Im Allgemeinen ist die Hg-Retention im Sediment wesentlich definiert durch die natürliche organische Substanz (NOM) des Sediments.

Das Grund- und Trinkwasser in Alode, Ogale und Okochiri, wo sich mehrere Öl- und Gasförderanlagen befinden, wies erhöhte BTEX-Werte von bis zu 3.904 µg/L, 1.573 µg/L bzw. 2.888 µg/L auf. In ähnlicher Weise lagen die Benzolwerte in Alode, Ogale und Okochiri bei bis zu 3.500 µg/L, 1.300 µg/L bzw. 2.700 µg/L. Hier war Benzol die häufigste BTEX-Verbindung. Der DOC-Wert, welcher die gesamte Kohlenwasserstoffbelastung des Grundwassers widerspiegelt, betrug bis zu 47 mg/L in Alode, 49 mg/L in Ogale und 33 mg/L in Okochiri. Benzol wurde ebenfalls in privaten Versorgungsbrunnen (PSW) in unmittelbarer Nähe zu einer unterirdischen Erdölpipeline nachgewiesen, welche durch die drei Gemeinden verläuft. Die Benzolkonzentration nahm mit zunehmender Entfernung von der Pipeline ab, was darauf hindeutet, dass aus dieser Pipeline möglicherweise Erdöl in den Grundwasserleiter austritt.

Der Gehalt an gelöstem Sauerstoff in dem Grundwasserleiter (bis zu 7,5 (95 %) mg/L) und die Kapazität für biologischen Abbau von BTEX (bis zu 2,11 mg/L für DO) erscheinen prinzipiell ausreichend für den natürlichen Abbau von BTEX. Allerdings könnte die Zersetzung durch die hohe Grundwassertemperatur (32,5 °C) verlangsamt werden. Ausgehend von den für diese Studie berechneten tagesbezogenen Abbaugeschwindigkeiten für Benzol (0,128 bis 0,693) und BTEX (0,086 bis 0,556) wären demzufolge bis zu 66,5 Jahre bzw. 85 Jahre erforderlich, um Benzol und BTEX-Kontamination natürlich abzubauen. Daher sind zusätzlich aktive Sanierungsmaßnahmen erforderlich, um die Zeit zu verkürzen, die für eine Verringerung der Benzolkontamination unter vernachlässigbare Grenzwerte im betroffenen Grundwasser benötigt wird.

Angesichts der umfangreichen Tierhaltung, sowie der Nutzung von Latrinen und der unstrukturierten Entsorgung von kommunalen und häuslichen Abfällen wurden das Grundwasser und die kommunalen Abwässer in Alesa, Ogale, Ebubu, Alode und Okochiri auf Nitrat (NO_3^-) untersucht. Die NO_3^--Gehalte im

Grundwasser deckten ein breites Spektrum ab: bis zu 142 mg/L in Alesa, 211 mg/L in Ogale, 120 mg/L in Ebubu, 55 mg/L in Alode und 10 mg/L in Okochiri. Der Vergleich der Hauptionenkonzentrationen zeigte, dass 71 %, 90 %, 87 % und 92 % der Grundwasserproben die Referenzkonzentrationen für Ca^{2+}, Na^{+}, K^{+}, bzw. Cl^{-} überschritten, was auf einen anthropogenen Einfluss (Abwasser) schließen lässt. Die NO_3^{-}/Cl^{-}-Verhältnisse weisen gleichermaßen darauf hin, dass 100 % (Alesa), 77 % (Ogale) und 84 % (Ebubu) des NO_3^{-} im Grundwasser aus den andauernden anthropogenen Aktivitäten (Abwässer) stammen. Darüber hinaus belegt auch die bestimmte Isotopie der Proben ($\delta^{15}N\text{-}NO_3^{-}$ and $\delta^{18}O\text{-}NO_3^{-}$), dass das NO_3^{-} aus der durch Abwasser verursachten NH_4^{+}-Nitrifikation stammen muss. Trotz des hohen Gehalts an gelöstem Sauerstoff (DO), bis zu 8,9 mg/L, ergeben sich aus unseren Ergebnissen auch Indizien für Denitrifikation in dem Gebiet. Dies deutet darauf hin, dass diese beiden biogeochemischen Prozesse simultan im Grundwasser ablaufen. Die Höhe der DO- und NO_3^{-}-Werte in den betroffenen Gemeinden, macht einen vollständigen bzw. hinreichenden natürlichen NO_3^{-} Abbau unwahrscheinlich, weshalb ein fundiertes sicheres Management für die Bewirtschaftung häuslicher und kommunaler Abwässer erforderlich ist. Folglich besteht aktuell die Gefahr, dass NO_3^{-} aus den flachen Grundwasserleitern in die nahe gelegenen Oberflächengewässer in Okochiri und in den Küstenozean gelangt.

In der Gesamtschau demonstrieren unsere Ergebnisse, dass durch die fortdauernden anthropogenen Aktivitäten im östlichen Nigerdelta eine beträchtliche Menge an Schadstoffen (d.h. Quecksilber, Benzol und Nitrat) in das Grund- und Trinkwasser gelangen, auf einem Niveau welches z.T. weit über den WHO-Richtwerten liegt. Die (1) hohe Konzentration der Schadstoffe, (2) ihre kontinuierliche Freisetzung in den Grundwasserleiter und (3) die Auswirkungen der hohen Grundwassertemperatur auf die vorherrschenden Redoxbedingungen im Grundwasserleiter scheinen den natürlichen Abbau bzw. die Ausleitung dieser Schadstoffe aus dem Grundwasserleiter zu beeinträchtigen. Um die Gesundheit der stetig wachsenden Bevölkerung in den betroffenen Gebieten zu schützen, sollten schnell Maßnahmen getroffen werden, die die sofortige Einstellung der Nutzung der kontaminierten Brunnen bewirken und ein Ausweichen auf alternative sicherere Wasserquellen (z. B. Flaschen- oder Beutelwasser oder ein zentrales Wasserversorgungssystem) sollte geprüft werden. Ferner müssen die lokalen

Behörden Maßnahmen ergreifen, um einen schnellen Rückgang der Kontaminationen der beschriebenen Schadstoffe zu gewährleisten, was auch eine umfassende Sanierung der kontaminierten Sedimente und des Grundwassers einschließt. (Übersetzt mit deepl.com).

Table of contents

1. Introduction

1.1 Ground and drinking water anthropogenic pollution

1.1.1 Overview

Groundwater, found in aquifers – rock fractures and sediments' pore spaces, constitutes about 98 % of the world's freshwater reserves (Velis et al., 2017). Globally, about 2.5 billion people rely on groundwater as their primary source of drinking water (Grönwall & Danert, 2020; UNESCO, 2012), especially in developing sub-Saharan countries like Nigeria, Chad, Niger, South Sudan, Angola, Central African Republic, Somalia, Djibouti, Eritrea, Cameroon, Uganda, Ethiopia, Burkina Faso and Chad, where 70 to 90 % of the domestic water users depend on it for their daily water needs (Danert & Theis, 2017; Grönwall et al., 2010; Kebede, 2012). Also, it is essential for industrial and irrigated agricultural purposes. It is, therefore, central to human development (Velis et al., 2017). However, due to the increased urbanization, industrialization and agricultural practices in recent years, groundwater quality worldwide has increasingly been threatened by both diffusive and point contributions from geogenic and anthropogenic pollutants (Margat & Van der Gun, 2013). Recently, several investigations reported groundwater pollution from anthropogenic sources, focusing on agricultural practices (e.g., Adjéï Kouacou et al., 2024; Alam et al., 2024), industrial spills (e.g., Adnan et al., 2024; Charlet et al., 2017; Lazareva et al., 2019) and landfill and municipal wastes (e.g., Dixit et al., 2022; Lalik & Dąbrowska, 2024). Such anthropogenic activities could lead to elevated levels of organic and inorganic pollutants in groundwater. The organic pollutants, which include pharmaceutical wastes, perfluorinated compounds, insecticides and herbicides, and hydrocarbon compounds (e.g., benzene), can deteriorate groundwater quality when released into the environment. Similarly, the inorganic pollutants, which include heavy metals (e.g., mercury, cadmium, copper, arsenic, lead, chromium, nickel, and zinc) and nitrogen species (i.e., nitrate, nitrite), can render groundwater unfit for consumption (Kurwadkar et al., 2020). Drinking polluted groundwater can cause several adverse health effects on humans.

In this study, we investigated three co-occurring anthropogenic pollutants (i.e., mercury, benzene and nitrate) in the groundwater resources of the eastern Niger Delta, Nigeria.

1.1.2 Ground and drinking water pollution by mercury

Mercury (Hg) is a transition metal with the atomic number 80, an atomic mass of 200.59, a density of 13.55 g/cm^3 and water solubility of 6 x 10^{-6} g^{-1} 100 mL at 25°C (e.g., De Laeter & Heumann, 1991; Kalisińska et al., 2019). It is the only known metal that exists in pure form as a liquid at ambient temperatures and has a high vapor pressure of 1.71 x 10^{-7} MPa at 20°C (Huber et al., 2006; Kalisińska et al., 2019; Levin, 2014). It has been used in the production of batteries, thermometers, barometers, blood pressure monitors, switches and relays, compact fluorescent lamps, high-pressure Hg vapor lamps, pesticides, biocides, topical antiseptics, cosmetics and dental amalgam restorations (WHO, 2017b). Also, Hg has been widely used for gold extraction in artisanal gold mining. However, due to its corresponding global pollution effects, the use of Hg has been strongly discouraged (Selin et al., 2018; UNEP, 2014). Furthermore, many countries, including the US, Sweden, Denmark, Norway and China placed a ban on the use of Hg-containing products (CIRS, 2017; Edlich et al., 2010; Ministry of the Environment, 2009).

Hg is regarded by WHO (2017b) as one of the “ten leading chemicals of concern” and can cause damage to the nervous system, gastrointestinal tract, lungs, kidneys, brain, immune system, and other essential organs of humans (Langford & Ferner, 1999; WHO, 2017a, 2017b). However, Hg toxicity depends on its species, which consist of inorganic (Hg^0 [metallic], Hg^+ [mercurous], and Hg^{2+} [mercuric]) and organic ($MeHg^+$ [methyl mercury], $EtHg^+$ [ethyl mercury], $PhHg^+$ [phenyl mercury], MMHg,$(CH_3Hg)^+$ [monomethyl mercury] and DMHg,$[(CH_3)_2Hg]$ [dimethyl mercury]) species. The organic species, for instance, MeHg, is the most toxic (Wang et al., 2020b), due to its ability to penetrate biological membranes, causing damage to the cerebellum and visual cortex (Gupta et al., 2018; Langford & Ferner, 1999; Lindberg et al., 2004). Nevertheless, the inorganic species, for instance, Hg^{2+}, is also toxic and capable of causing kidney disorders and damage to the human brain, which may result in death (Ha et al., 2017). Notably, all species of Hg are dangerous to the mammalian species (WHO, 2007), with each species having a unique toxicity profile, transport

mechanism and metabolic fate in the human body (Atsdr, 1999; Patrick, 2002). As a result, the World Health Organization (WHO) set various limits for Hg in the environment, including in drinking water. The WHO drinking water guideline value is 1 µg/L (WHO, 2011).

Naturally, Hg mostly occurs in cinnabar (HgS) and other minerals (e.g., timanite, tvalchrelidzeite, galkhaite, iorodaite, khakite) (Drott et al., 2013; Kozin & Hansen, 2013). Similarly, a substantial amount of Hg has been found in various geologic units, ore deposits, mine wastes, sediments and crude oil (Table 1.1). Over time, both geogenic and anthropogenic processes trigger the release of Hg into the environment (UNEP, 2018). However, anthropogenic processes remain the primary source of Hg to the environment, surpassing contribution from geogenic processes (i.e., ocean volatilization and emission from volcanoes and ore deposits) by a factor of 3 to 4 (UNEP, 2013). The major anthropogenic processes include artisanal and small-scale gold mining, coal combustion, non-ferrous metal production, cement production, disposal of Hg-added product wastes, ferrous-metal production, stationary combustion of other fuels, i.e., oil, gas and biomass and other sources, such as vinyl-chloride monomer (AMAP/UN, 2019). These processes are known to either (1) release Hg into the atmosphere and eventually deposit it on soils and surface water or (2) release Hg directly into soils and surface water (UNEP, 2002). Subsequently, the Hg may migrate into groundwater depending on the geological, hydrological and climatic conditions, land use, and soil characteristics (Barringer & Szabo, 2006; Leung & Jiao, 2006; Wang et al., 2004). Hg mobilization from geogenic or anthropogenic sources into an aquifer could lead to elevated concentrations in the groundwater. Important factors that could trigger the release and mobility of Hg into the corresponding groundwater were found to be changes in soil pH, soil organic matter (SOM), texture, slope, clay properties and redox conditions (Aleku et al., 2024; Barringer et al., 2013; Richard, 2016).

Table 1.1 Hg concentrations in various geologic units.

Geologic unit	Lithology	Hg (ug/kg)	References
Igneous	Granites	7.88 to 16.5	Tian et al. (2023)
	Granodiorites	6.24 to 9.52	Tian et al. (2023)
	Gabbros	8.65 to 19	Tian et al. (2023)
		26	Nekrasov and Timofeeva (1963)
	Tonalites	6.58 to 8.18	Tian et al. (2023)
	Basalts	70	Marowsky and Wedepohl (1971)
		20	Nekrasov and Timofeeva (1963)
		90	Turekian and Wedepohl (1961)
	Ultramafics	4	Marowsky and Wedepohl (1971)
Metamorphic	Gneiss, schist	0.21 to 7.8	Deng et al. (2022)
Sedimentary	Limestone	34.3	Grasby et al. (2019)
		18	Nekrasov and Timofeeva (1963)
	Clastic sedimentary rocks	62.4	Grasby et al. (2019)
	Sandstone	30	Turekian and Wedepohl (1961)
		12	Nekrasov and Timofeeva (1963)
	Shales	400	Marowsky and Wedepohl (1971)
		50	Nekrasov and Timofeeva (1963)
Sediments	Sea sediments	20 to 40	Leipe et al. (2013)
	River sediments	50	Craig (1986)
	Soils	20	Higueras et al. (2015)
Crustal averages	Upper crust	13.5 to 17.8	Tian et al. (2023)
	Middle crust	7.9	Gao et al. (1998)
	Lower crust	21	Wedepohl (1995)
Ores and sulfides	Limestone	1,198,000	Jonasson and Sangster (1975)
Mine wastes		1,500,000	Rytuba (2003)
Crude oil		600,000	Mashyanov (2021)
		33,000	COWI (2005)
		2,000	Shah et al. (1970)

Groundwater Hg pollution is a major concern, especially when the polluted groundwater serves as a drinking water source (Richard, 2016). Several investigations revealed varying Hg concentrations in groundwater. In pristine groundwater, for instance, Krabbenhoft et al. (1995) reported Hg concentrations between 0.0011 to 0.0033 µg/L in groundwater from Allequash Creek Watershed, Northern Wisconsin, USA. Also, 0.0008 to 0.0041 µg/L was reported for groundwater from Poznań, Poland (Kowalski et al., 2007) and 0.0002 to 0.005 µg/L was observed in the groundwater of

New Jersey, USA (Barringer & Szabo, 2006). Hg concentrations in groundwaters affected by geogenic processes ranged from 0.5 to 11.2 µg/L in coastal aquifers in Grosseto, Southern Tuscany, Italy (Grassi & Netti, 2000), 0.2 to 4.2 µg/L in alluvial and granitic matrix of the Ridaura Aquifer, Girona, Spain (Navarro et al., 2016), and up to 0.5 µg/L in volcanic aquifers of Italy and Guadeloupe (Bagnato et al., 2009). Higher Hg concentrations in groundwaters are attributed to anthropogenic activities, especially at legacy industrial sites and artisanal and small-scale gold mining sites (Kabir et al., 2002). Thus, Hg concentrations up to 230 µg/L were found in $HgCl_2$-contaminated groundwater at a site of a former wood impregnation facility in the Black Forest, South Germany (Bollen et al., 2008). Also, Omondi et al. (2023) reported Hg concentrations ranging from 80 to 760 µg/L in the groundwater of Migori County artisanal and small-scale gold mine sites in Kenya. An up-to-date overview of field studies on Hg groundwater pollution, sources and biogeochemistry for different locations worldwide can be found elsewhere (e.g., Aleku, Lazareva, et al., 2024).

Besides the pollution threat Hg poses to aquifers, Hg-contaminated groundwaters can be exported to nearby surface waters through exfiltration, thereby increasing the risk of Hg uptake by aquatic life and subsequent bioaccumulation in humans via fish consumption (Richard, 2016). Bradley et al. (2012) showed that groundwater discharge was the major source of Hg to the coastal plain stream of McTier Creek, South Carolina. Similarly, Ganguli et al. (2012) found indications that THg and MMHg fluxes to seawater, calculated at 0.41 and 0.15 nmol m^{-2} d^{-1}, respectively, were attributed to submarine groundwater discharge at the Southern California coastal lagoon system. An investigation carried out on the coastal plain stream in New Jersey, USA, showed the occurrence of Hg export from groundwater to surface water (Barringer et al., 2013).

1.1.3 Mercury in coastal sediments

Mercury is one of the least abundant elements in the upper Earth's continental crust, with an estimated concentration varying between 12.3 and 96 µg/kg (Gao et al., 1998; Rudnick, 2005; Shaw et al., 1976; Taylor, 1964; Tian et al., 2023; Wedepohl, 1995). In addition to the natural sources of Hg, anthropogenic activities have contributed to increased Hg levels in sediments (Aleku, Lazareva, et al., 2024). In coastal sediments, Hg enrichment is mostly a direct consequence of inputs from anthropogenic sources, as observed in Po River, Italy (Guerzoni et al., 1984; Pavoni

et al., 1987), Gulf of Trieste, Slovenia (Bussani & Princi, 1979), Marano and Grado lagoon, Italy (Bettoso et al., 2023), Wider Caribbean coastal region (Bolaños-Alvarez et al., 2024), Todos os Santos Ba, Brazil (Hatje et al., 2019), Hinda Bay, Philippines (Samaniego et al., 2024), Galveston Bay, USA (Dellapenna et al., 2020), Laizhou Bay, China (Wang et al., 2022), Qatari Coast, Qatar (Hassan et al., 2019), and Bandar Abbas (Persian Gulf), Iran (Elsagh et al., 2021). Notably, coastal sediments serve as a major sink for Hg, bridging terrestrial Hg export to the marine environment (Meng et al., 2019). Investigations have shown that Hg sediment contamination in coastal areas has become a major environmental concern due to the risks to the aquatic ecosystem and, indirectly, to human health (Ernst, 2012; Peña-Fernández et al., 2014).

Organic carbon (OC) can significantly control the distribution of Hg in sediments by providing sufficient strong binding sites in the sediment surface (Chakraborty et al., 2015b; Rutkowski et al., 2021; Wu et al., 2013). However, the ability of OC to bind trace metals depends on several factors, including the amount and type of OC present in the affected sediment, large surface area and sediment's cation-exchange capacity (Hirner et al., 1990; Horowitz, 1991; Saxby, 1969). A significant positive relationship between Hg and organic carbon (OC) has been observed in several investigations (e.g., Chakraborty et al., 2015b; Kainz & Lucotte, 2006; Kainz et al., 2003; Mirlean et al., 2003; Rutkowski et al., 2021; Wu et al., 2013). Nevertheless, there was no correlation between Hg and organic matter in polluted coastal sediments in other investigations (e.g., Kehrig et al., 2003; Wu et al., 2013), possibly due to sediments' heterogeneity (Vieira et al., 2021). Moreover, grain size distribution in sediments can also significantly influence the sediment's trace metal concentrations (Chakraborty et al., 2015a). Several investigations have shown that trace metals, such as Hg, favor binding to fine-grained sediment particles (Ligero et al., 2001; Scanu et al., 2016). For instance, a higher surface area increases the sediment's affinity to trace metals in clay-silt particles (Araújo et al., 1988; Cauwet, 1987; Thorne & Nickless, 1981). Nevertheless, other investigations have shown that sediment grain sizes do not exclusively control metal concentrations since high concentrations have been reported in coarser sediments (e.g., Krumgalz, 1989; Ramesh et al., 1990). These exceptions, however, indicate that several other factors, such as sediments' carbon content and metal loading, may also contribute significantly to controlling the accumulation and mobility of Hg in coastal sediments (Chakraborty et al., 2015a).

1.1.4 Ground and drinking water pollution by BTEX

Benzene, toluene, ethylbenzene and three forms of xylenes (o-, m-, p-) (BTEX, shown in Fig. 1.1) are a group of naturally occurring pollutants found in significant amounts in crude oil, various petroleum products, coal and gas deposits (Leusch & Bartkow, 2010). For instance, in gasoline, benzene, toluene, ethylbenzene and xylenes make up 11 %, 26 %, 11 %, and 52 % of its composition, respectively (Mitra & Roy, 2011). Similarly, gasoline contains up to 169,500 µg/kg BTEX concentrations (Pinedo et al., 2013). At room temperature, BTEX compounds are highly flammable. Although they co-occur, the physical and chemical properties of these volatile monoaromatic hydrocarbons vary, as shown in Table 1.2. According to Leusch and Bartkow (2010), BTEX compounds are among the most abundantly produced chemicals worldwide. Usually, during crude oil and natural gas extraction, BTEX and other aromatic compounds are captured at the wellhead as liquids. Subsequently, they are isolated and/or synthesized by catalytic reforming and cracking of naphtha and other chemical reactions (e.g., dealkylation, alkylation, and coal coking) (Bolden et al., 2015). These compounds are widely used in the manufacture of consumer products, such as rubber, leather, plastics, paints, polishes, ink, dyes, detergents, coatings, adhesives, degreasers, resins, cement and pesticides (Kwon et al., 2007; Sack et al., 1992). Similarly, they are also widely used in chemical and pharmaceutical industries as intermediates in synthesizing other organic compounds (Fishbein, 1985; Wiley, 2008).

Table 1.2 BTEX physical and chemical properties.

Pollutant	Benzene	Toluene	Ethylbenzene	o-Xylenes	m-Xylenes	p-Xylenes
Formula	C_6H_6	C_7H_8	C_6H_{10}	C_6H_{10}	C_6H_{10}	C_6H_{10}
Solubility (mg/L)[1,2]	1780	535	161	175	146	156
Molar weight[1]	78.11	92.13	106.16	106.16	106.16	106.16
Density (g/mL)[3,4]	0.8765	0.8669	0.867	0.88	0.87	0.86
VP (mm Hg)[2]	95.19	28.4	4.53	6.6	8.3	3.15
BP (°C)[3]	80.1	110.6	136.2	144.4	139.3	137
MP (°C)[3]	5.5	-95	-94.97	-25	-49.4	13
S-WPC[4]	97	242	622	570	570	570
Henry's law constant at 25°C (kPa*m^3/Mole)[5]	0.557	0.66	0.843	0.551	0.73	0.69
Overall reaction	$C_6H_6 + 7.5O_2 \rightarrow 6CO_2 + 3H_2O$	$C_7H_8 + 9O_2 \rightarrow 7CO_2 + 4H_2O$	$C_8H_{10} + 10.5O_2 \rightarrow 8CO_2 + 5H_2O$			

S-WPC: Soil-water partitioning coefficient, VP: Vapour pressure, BP: Boiling Point, MP: Melting Point. 1: Dean (1999), 2: Howard (2017), 3: Lide (2004), 4: Mitra and Roy (2011), 5: Farhadian et al. (2008).

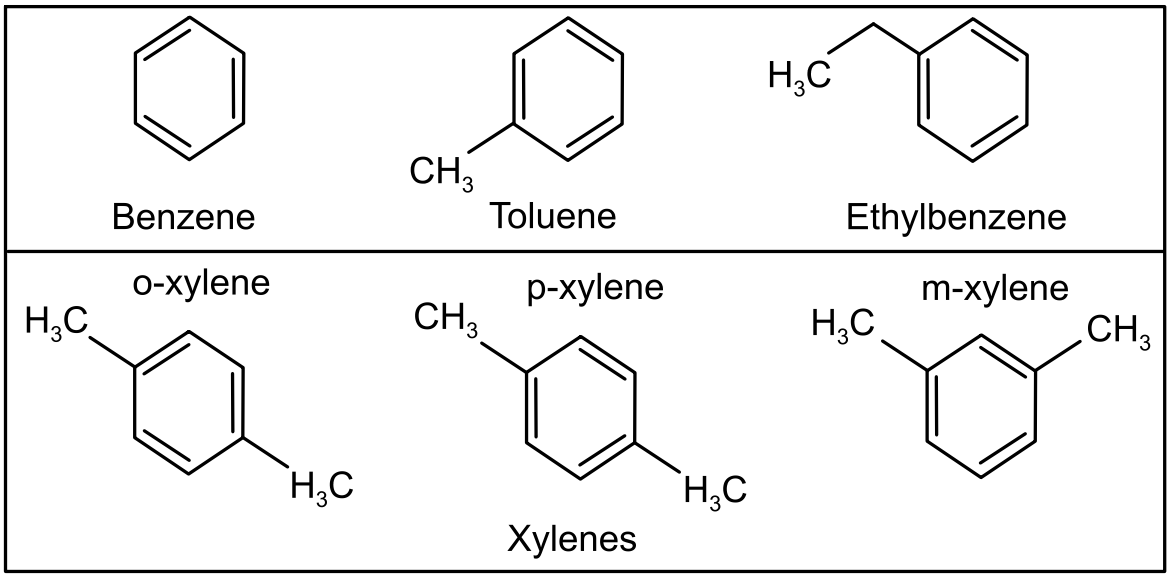

Fig. 1.1 BTEX skeletal chemical structure.

Generally, BTEX is released into the environment through various sources, including pyrogenic (i.e., coal combustion and the thermal cracking of petroleum), petrogenic and processed products (i.e., products from building and petrochemical industries) (Yu et al., 2022). The most prominent BTEX source of soil and groundwater pollution is the petrogenic source, which commonly occurs due to oil spills/leakages from exploration activities (e.g., > 4 million barrels of spilled oil in the Gulf of Mexico from deepwater drilling rig explosion in 2010) (Yu et al., 2022), underground storage tanks at gasoline stations (Rao et al., 2017), oil theft and artisanal refining of crude oil (Nwankwoala & Omofuophu, 2020), or petroleum transport (Lindén & Pålsson, 2013). BTEX sources and distribution in air, water and sediments are given in Table 1.3.

Table 1.3 BTEX in air, water and sediments

Location	BTEX	Unit	Source	Reference
Air (industrial/urban area with high traffic)				
Eleme, Nigeria	48.2	µg/m^3	Oil spill	(UNEP, 2011)
Limpopo, South Africa	4.45	µg/m^3	Traffic/industrial emissions	(Maswanganyi et al., 2024)
Orleans, France	3.6	µg/m^3	Urban emissions	(Jiang et al., 2017)
Kuwait, Saudi Arabia	2,351	µg/m^3	Gas station	(Al-Harbi et al., 2020)
Delhi, India	53.85	µg/m^3	Traffic emissions	(Kashyap et al., 2019)
Beijing, China	1,552.9	µg/m^3	Coal combustion	(Liu et al., 2015)
Tehran, Iran	2,055.75	µg/m^3	Bus terminal	(Golkhorshidi et al., 2019)
Tehran, Iran	2,742.84	µg/m^3	Gas station	(Baghani et al., 2019)
Tehran, Iran	137.31	µg/m^3	Urban emissions	(Dehghani et al., 2017)
Tehran, Iran	40.6	µg/m^3	Traffic emissions	(Miri et al., 2016)
Maragheh, Iran	74.07	µg/m^3	Traffic emissions	(Behnami et al., 2023)
Shiraz, Iran	91	µg/m^3	Bus terminal	(Dehghani et al., 2018)
Contaminated Surface water				
Ubeji, Nigeria	2,774	µg/L	Oil spill	(Asejeje et al., 2021)
Lagos, Nigeria	596.98	µg/L	Oil spill	(Doherty & Otitoloju, 2016)
Raša Bay, Croatia	0.81	µg/L	Coal-fired power plant	(Medunić et al., 2018)
Sabitri, India	1,500	µg/L	Industrial inputs	(Lokhande et al., 2009)
Contaminated Sediments				
Ubeji, Nigeria	11,700	µg/kg	Oil spills	(Asejeje et al., 2021)
Chanomi, Nigeria	97.075	µg/kg	Oil spills	(Onyena et al., 2023)
Lagos, Nigeria	450.53	µg/kg	Oil spills	(Doherty et al., 2016)
Lake İznik, NW Turkey	272.3	µg/kg	Agricultural/domestic/ industrial inputs	(Ünlü & Alpar, 2018)
Contaminated Ground and drinking water				
Rio de Janeiro, Brazil	3,600	µg/L	Gasoline station	(doRego & Pereira, 2007)
Shanxi, China	7.36	µg/L	Coking plant	(Wang eta al., 2024)
Northern Brazil	25.631	µg/L	Gas station	(Chira et al., 2024)
Yogyakarta, Indonesia	25,631	µg/L	Gas station	(Rahmawati et al., 2018)

Regarding pollution potential, BTEX is the most significant constituent of petroleum, considering that they are the most soluble and can readily migrate through soils and dissolve in groundwater when released into the environment (Johnson et al., 2003). However, where clay minerals are present, BTEX migration into the corresponding groundwater is usually restricted (Varona-Torres et al., 2017). Generally, the background levels of benzene, toluene, ethylbenzene and xylenes in groundwater are less than 1 µg/L, 3 µg/L, 0.1 µg/L and 0.1 µg/L, respectively (Yu et al., 2022). Nevertheless, in groundwater, up to 9,280 µg/L benzene was reported at the Ogoniland oil spill site (UNEP, 2011), 3,500 µg/L toluene was found in industrially contaminated sites, 28,000 µg/L ethylbenzene and 1,340 µg/L xylenes were reported at a solvent recovery facility (Leusch & Bartkow, 2010). Exposure to these compounds usually occurs either by ingestion (e.g., drinking contaminated water), inhalation (e.g., breathing contaminated air from spill sites or gas stations), or dermal contact (bathing or laundering with contaminated water) (Mitra & Roy, 2011; Tunsaringkarn et al., 2012). These toxic compounds can cause numerous adverse health effects, including damage to the central nervous and immune systems, liver and kidney (WHO, 2017a). Benzene, a known carcinogen, is considered the most dangerous and abundant compound of BTEX (IARC, 2010a; Loomis et al., 2017; WHO, 2017a). Due to the toxicity of BTEX compounds, the WHO (2017a) set 10 µg/L, 700 µg/L, 300 µg/L and 500 µg/L as drinking water guideline values for benzene, toluene, ethylbenzene and total xylenes, respectively. Similarly, the drinking water maximum allowable concentration set by the USEPA (2009) for benzene, toluene, ethylbenzene, and total xylenes are 5 µg/L, 1000 µg/L, 700 µg/L, and 10000 µg/L, respectively. Therefore, elevated levels of BTEX in drinking water may render it unfit for human consumption.

In groundwater, BTEX can be degraded either under aerobic or anaerobic conditions (Fig. 1.2). It, however, degrades most rapidly under aerobic conditions (An et al., 2001; Johnson et al., 2003). Under aerobic conditions, dissolved oxygen (DO) is required for (1) benzene ring activation and cleavage of the aromatic nucleus and (2) as the electron acceptor for the complete BTEX degradation by either bacteria, fungi or algae (Andreoni & Gianfreda, 2007; Kao & Prosser, 2001). Here, for a complete degradation to occur, the ring of the monoaromatic compound must undergo cleavage by oxygenases, as shown in Fig. 1.2 (Smith, 1990). In contrast, under anaerobic conditions, BTEX degradation can only occur when the DO level is less than

0.5 to 1 mg O_2/L (Christensen et al., 2000). However, to replace DO, terminal electron acceptors (TEAs) such as NO_3^-, Mn(IV), Fe(III), SO_4^{2-}, and CO_2 would be needed to serve as "sink" for the electrons transferred from the target BTEX compound by the mediating microorganisms (Johnson et al., 2003). The overall stoichiometry reactions for degradation of BTEX compounds are given in Table 1.2. Since our groundwater is oxic, only aerobic degradation of BTEX will be considered in this study.

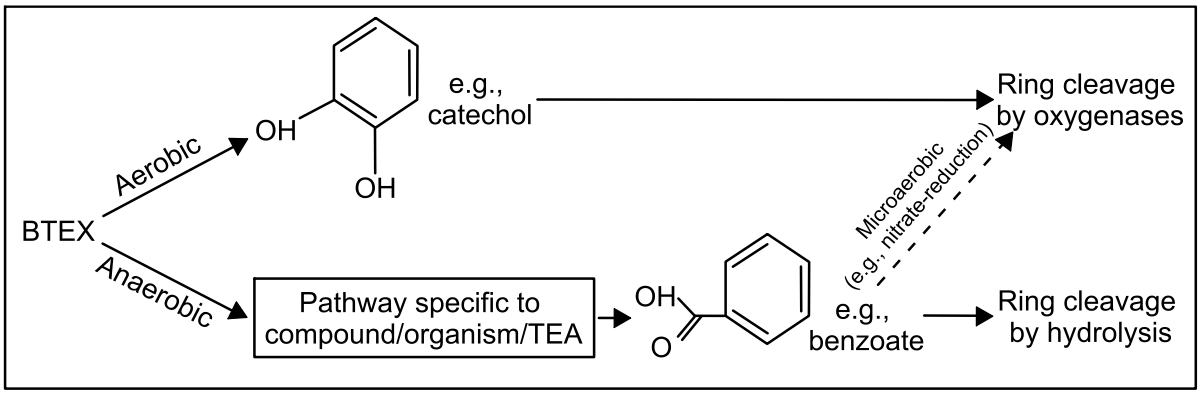

Fig. 1.2 Generalized pathway of BTEX degradation (after Johnson et al., 2003).

Under aerobic conditions, monooxygenase enzymes (e.g., toluene 4-monooxygenase, benzene and xylene monooxygenases) and dioxygenases enzymes (e.g., catechol 1–2 dioxygenase, ethylbenzene dioxygenase, and catechol 2,3-dioxygenase) are the two metabolic pathways for BTEX degradation (El-Naas et al., 2014; Olajire & Essien, 2014). In the monooxygenase (i.e., tol) pathway, methyl or ethyl substituents of the monoaromatic ring are attacked and eventually transformed into pyrocatechols or phenyl glyoxal, respectively (Khan et al., 2001; Tsao et al., 1998). In the dioxygenase (i.e., tod) pathway, however, the attacked monoaromatic ring forms 2-hydroxy-substituted compounds (Jindrova et al., 2002; Khan et al., 2001; Tsao et al., 1998). Both pathways eventually form (substituted) catechol intermediates (Andreoni & Gianfreda, 2007; Farhadian et al., 2008). While the main intermediate product for benzene degradation is catechol (Johnson et al., 2003; Tsao et al., 1998; Zhang et al., 2013), 3-methyl catechol and 3-ethyl catechol are the main intermediate products for the degradation of toluene and ethylbenzene, respectively (Jindrova et al., 2002; Zhang et al., 2013). For xylenes, according to Stephens (2011), the three isomers degrade to mono-methylated catechols (e.g., m-xylene transforms to 3-methyl catechol). In contrast, Oh et al. (1994) reported that p-xylene metabolizes to 3,6 dimethyl catechol. Eventually, these catechol intermediates are mineralized by either

enzyme catechol 1,2-dioxygenase or catechol 2,3-dioxygenase, which would subsequently open the monoaromatic ring and then degrade it (Al-Khalid & El-Naas, 2012; An et al., 2001; El-Naas et al., 2014). The rate and extent of aerobic degradation of BTEX can be affected by several physical, chemical and biological factors, including BTEX concentration, temperature, pH and microbial activity (Singh & Celin, 2010).

1.1.5 Ground and drinking water pollution by nitrate

Nitrate, an inorganic compound, is composed of 1 nitrogen (N) and 3 oxygen (O) atoms. In natural environments, N exists in several oxidation states (i.e., + 6 to – 3). In natural waters, for instance, N exists primarily as nitrate (NO_3^-), nitrite (NO_2^-), dissolved gas from the atmosphere (N_2), ammonia (NH_3) from rain and soil, and ammonium (NH_4^+) with + 5, + 3, 0, + 1 and – 3 oxidation states, respectively (Cantrell et al., 2023). Similarly, N also occurs as cyanide (CN^-) and other organic N compounds in aqueous systems (Stumm & Morgan, 2012). However, NO_3^-, which is highly mobile in groundwater, is the dominant N species over the entire pH range for oxic systems and consists of two stable isotopes of N ($\delta^{14}N$ and $\delta^{15}N$) and O ($\delta^{16}O$ and $\delta^{18}O$) that undergo significant transformation in the biogeochemical cycle (Cantrell et al., 2023). The behavior of NO_3^- and other N species in aqueous, sediment, and geochemical systems have been discussed elsewhere (e.g., Hem, 1986; Lindsay et al., 1981; Reddy et al., 1984; Small et al., 2014; Stumm et al., 1981).

In the environment, NO_3^- is either derived from geogenic or anthropogenic inputs (Huang et al., 2013; Kendall et al., 2007). The geogenic inputs include the (1) dissolution of nitrate-containing minerals (e.g., Chilean nitrate deposits in the Atacama Desert (Ericksen, 1983)) or soils containing soluble N compounds and (2) export of N-rich groundwater to surface waters. The anthropogenic N inputs are from agricultural sources (e.g., N fertilizers, organic fertilizers, sludge, animal wastes), industrial sources (e.g., fossil fuel combustion from vehicles and power plants emissions) and municipal inputs (e.g., sewage and landfill leachates) (Kendall et al., 2007). The major N sources, transport and transformations in the environment are shown in Fig. 1.3.

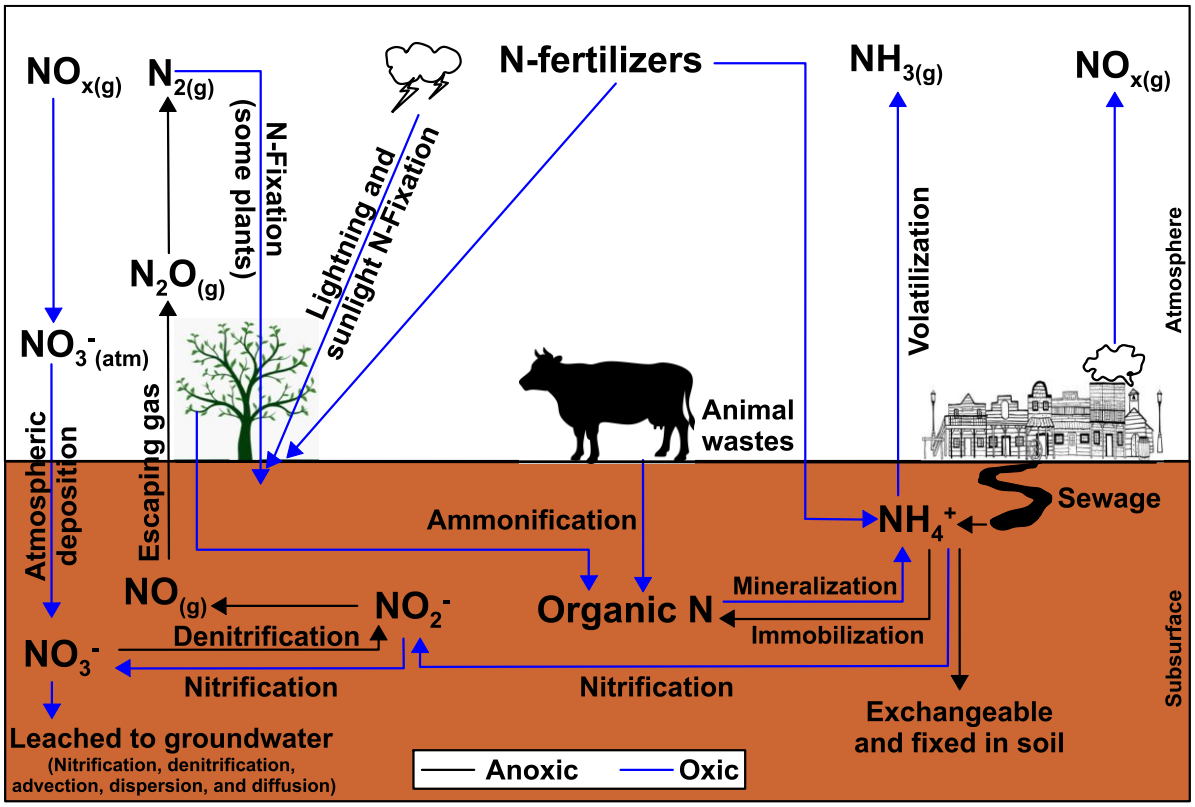

Fig. 1.3 N cycle showing pathways of N loading and the biogeochemical processes responsible for N transformation in the atmosphere, subsurface and groundwater (Modified after Gutiérrez et al., 2018).

Agricultural activities are likely the major source of various forms of N in the environment. Animal excreta, for instance, contributes N in the form of ammonia, urea and other organic N compounds, which, under oxygenated conditions, are either transformed to N gases, nitrite or nitrate. Similarly, chemical fertilizers contribute N as urea, ammonium salts and diammonium phosphate (Zaryab et al., 2023). Usually, they accumulate in the soils and vadose zone over a long period (Scanlon et al., 2008) before eventually leaching into the corresponding aquifer (Harris et al., 2022). The major biogeochemical processes of N inputs and transformations in the environment include N fixation, ammonification (also referred to as mineralization or re-mineralization), nitrification, denitrification, volatilization and atmospheric deposition. During the N fixation process, the N_2 molecules in the atmosphere are broken by bacteria (i.e., diazotrophs) and the resulting N reacts with available H^+ to form NH_3^+ (equation 1.1) that plants can absorb (Postgate, 1998). Subsequently, the plants'

organic matter is mineralized by bacteria or fungi to produce NH_4^+ under both oxic and anoxic conditions (Cameron et al., 2013).

$$N_2 + 3H_2 + 2NH_3 \quad - \quad - \quad - \quad - \quad (1.1)$$

Nitrification, which is an important process for NO_2^- and NO_3^- production, is a two-step process that is mediated by various autotrophic bacteria or archaea (Kendall et al., 2007). Firstly, NH_4^+ is oxidized into NO_2^- by ammonia-oxidizing bacteria e.g., *nitrosomonas spp.* as shown in equation 1.2 below (Zhou et al., 2015). In this process, N atoms originate from NH_4^+ and/or NO_2^- molecules, while O atoms originate from O_2 and/or H_2O (Kendall et al., 2007).

$$NH_4^+ + 1.5O_2 \rightarrow NO_2^- + 2H^+ + H_2O \quad - \quad (1.2)$$

Secondly, nitrification is completed as the available nitrite-oxidizing bacteria (e.g., *Nitrobacte*r *spp.*) convert NO_2^- to NO_3^- (equation 1.3).

$$NO_2^- + \frac{1}{2}O_2 \rightarrow NO_3^- \quad - \quad - \quad - \quad (1.3)$$

However, these processes are reversible through denitrification to remove NO_3^- from the environment. This process involves several steps with byproducts or intermediate N forms (i.e., NH_2OH, NO_2^- and NO and N_2O). Usually, denitrification only occurs under anoxic conditions when the DO level is < 0.5 mg/L (Hübner, 1986), mediated by certain strains of denitrifying bacteria that either use (1) organic C as electron donor and N oxides as electron acceptor or (2) inorganic compound (e.g., reduced Fe or S) as electron donor and N oxides as electron acceptor (Rivett et al., 2008; Tucker & Westerman, 1989). Similarly, to an extent, the effectiveness of denitrification to remove NO_3^- also depends on NO_3^- concentration, favorable temperature (i.e., 25 to 35°C), pH (5.5 to 8), electron donor and other trace nutrients in the affected environment (Rivett et al., 2008). Equation 1.4 below shows the generalized pathway for denitrification and simultaneous respiration of CO_2 from organic matter oxidation (Kendall et al., 2007).

$$4NO_3^- + 5CH_2O + 4H^+ \rightarrow 2N_2 + 5CO_2 + 7H_2O \quad - \quad (1.4)$$

Volatilization involves the loss of $NH_3(g)$ to the atmosphere, especially after applying fertilizer or manure in farmlands. The process, however, largely depends on the prevailing pH and temperature of the affected environment (Hübner, 1986; Tucker & Westerman, 1989).

Lastly, according to Kendall et al. (2007) dry or wet deposition of $NO_3^{-}{}_{(atm)}$ usually occurs when NO_x, which is released to the atmosphere through anthropogenic (e.g., fossil fuel combustion) or geogenic processes (biogenic soil emissions, lightning, biomass burning), is oxidized in the atmosphere. This reaction forms highly soluble HNO_3 which readily dissociates to NO_3^- which can be deposited as wet deposition. Similarly, other N species formed from this process can also be deposited as dry gas (e.g., NH_3, NO, peroxyacetyl NO_3^-, dry aerosols (particulate NO_3^-, particulate NH_4^+). Both dry and wet NO_3^- (atm) deposition contributes substantially to NO_3^- levels in the environment.

Notably, these N sources and transformations significantly influence the isotopic signatures of both N and O atoms, where the atoms are either enriched or depleted, causing $\delta^{15}N$ and $\delta^{18}O$ values to vary between the various N sources. For instance, $\delta^{15}N$ values of NO_3^- from atmospheric precipitation, chemical fertilizers or nitrification of organic manure vary between - 15 and + 15 ‰ whereas $\delta^{18}O$ values from these sources are > + 20 ‰, + 17 to + 25 ‰, and < + 15 ‰, respectively, (McMahon & Böhlke, 2006; Moore et al., 2006; Zhang et al., 2014). Typical isotopic signatures of major N sources in the environment are given in Table 1.4. However, the distinct isotope values generated from various N sources may overlap. Hence, distinguishing the various N sources would be a challenge. Several authors suggest various approaches to overcome this challenge, including (1) combining $\delta^{15}N$ and $\delta^{18}O$ values with contamination indicators (e.g., hydrochemical parameters such as Cl^-, Na^+, K^+, Ca^+, and total and fecal coliforms) (Cao et al., 2021; Minet et al., 2017) and (2) combining geochemical data and stable isotopes of hydrogen, oxygen, nitrogen, sulfur and boron (Biddau et al., 2023).

Table 1.4 Typical $\delta^{15}N$ and $\delta^{18}O$ values for major N sources in the environment (from Kendall et al., 2007).

N source	$\delta^{15}N$ ‰	$\delta^{18}O$ ‰
Atmospheric N_2 and O_2	0	Ca. + 23.5
Atmospheric NO_3^- and NH_4^+	- 15 to + 15	> 60
Bactria N fixation	- 3 to + 1	
Chemical fertilizers (e.g., urea, anhydrous ammonia, nitrate)	- 8 to + 7 (- 4 to + 4 in most cases)	+ 17 to + 25
Organic fertilizers (e.g., cover crops, plant composts and animal wastes	+ 2 to + 30	- 5 to + 15 (Chilean nitrate deposits: + 46 to + 58 ‰
Manure, septic wastes and biosolids	+ 8 to > + 25	< + 15
Soil NH_4	+3 to + 8	< + 15
Marine NO_3^-	+ 5 to + 15	+1 to + 20

Usually, natural background concentrations of NO_3^- in groundwater are usually < 5 to 10 mg/L (Panno et al., 2006). Groundwater with higher concentrations indicates contamination (Burkart & Kolpin, 1993), primarily due to anthropogenic influences, as observed in the White Volta River basin, Ghana where the NO_3^- levels were up to 431.17 mg/L (Anornu et al., 2017), Barrow Valley, Ireland, with 134.9 mg/L (Minet et al., 2017), Nile Delta, Egypt, with up to 652 mg/L (Kasem et al., 2024) and Alborz Province, Iran having 185 mg/L (Zaryab et al., 2024) (Table 1.5). However, intake of such high concentrations has been associated with several health implications, including the development of methaemoglobinaemia (i.e., cyanosis and "blue baby" syndrome) in infants (Majumdar, 2003), poor birth outcomes (e.g., preterm births (Sherris et al., 2021), low birth weights (Coffman et al., 2021) and congenital anomalies (Stayner et al., 2022). Also, other investigations suggest that a high NO_3^- intake in drinking water can cause colorectal cancer in humans (Schullehner et al., 2018). As a result, the International Agency for Research on Cancer (IARC) added that ingestion of high concentrations of NO_3^- or NO_2^-, which results in endogenous nitrosation formation in the gastrointestinal tract of humans, could be carcinogenic (IARC, 2010b). To protect humans against these adverse health implications, the World Health Organization has set a drinking water guideline value of 10 mg/L NO_3^- (as N) and 50 mg/L as NO_3^- (WHO, 2017a).

Besides the threat NO_3^- constitutes in groundwaters, discharge of NO_3^- contaminated groundwater to nearby surface waters can deteriorate the water quality, resulting in eutrophication of streams, reservoirs, estuaries, lakes, and blooms of toxic algae (Kaown et al., 2023; Qin et al., 2019; Zhu et al., 2019). Furthermore, according to Wang et al. (2023), elevated NO_3^- levels in surface waters are likely to increase anthropogenic biogenic N_2O emissions to the atmosphere. Thus, preventing or mitigating the NO_3^- levels in groundwater is important.

Table 1.5 NO_3^- occurrence and source identification using $\delta^{15}N$ and $\delta^{18}O$ in groundwater and surface water.

Location	NO_3^- (mg/L)	$\delta^{15}N$ ‰	$\delta^{18}O$ ‰	Source	Reference
Groundwater					
Barrow Valley, Ireland	2 to 134.9	+2.2 to +18	-2.4 to +10.9	N-fertilizers	Minet et al. (2017)
Southwest China	7.5 to 81.57	+6.5 to +24.4	-2 to +9.7	M & S	Cao et al. (2021)
South Korea	BDL to 93.1	+8.2 to +26	+2.9 to +17	M & S	Ju et al. (2023)
Chakari, Afghanistan	0.9 to 57.1	+4 to +10.2	+1.3 to +4	M & S	Zaryab et al. (2023)
Ghana	0.03 to 431.17	+6.75 to +22.1	+4 to +16	Manure	Anornu et al. (2017)
Southeast, Ghana	0.9 to 34	+5.4 to +38.9	−2.7 to +19.3	N-fertilizer, SON, and M & S	Saka et al. (2023)
Yangzhuang Basin, China	10.98 to 90.45	−2.27 to +11.75	−3.49 to +7.82	N-fertilizer, SON, and M & S	Wang et al. (2024)
Nile Delta, Egypt	0.42 to 652	-23.3 to +75	-13.6 to +39.62	SON and N-fertilizer	Kasem et al. (2024)
Ključ, Serbia	0.61 to 74.27	+6.7 to +12.9	+0.28 to +9.7	M & S	Perović et al. (2024)
Córdoba, Argentina	8.5 to 90	+4.7 to +12.6	−1.7 to +5.7	M & S	Becher Quinodoz et al. (2024)
China	0.44 to 70.9	−12 to +58.4	−8.7 to +38.1	M & S	Mao et al. (2024)
Alborz Province, Iran	4.6 to 185	+3 to +24.9	−0.3 to +18.9	Urban sewage	(Zaryab et al., 2024)
Surface water					
South Korea	0.32 to 52.6	−1.3 to +14.8	−4.4 to +10.5	SON and M & S	Shin et al. (2023)
Guizhou, China	BDL to 177	+1.3 to +9.8	+4.7 to +16.9	SON	Li et al. (2013)
Southeast, Ghana	0.45 to 10.63	+2.5 to +19.8	−3.8 to +11.5	N-fertilizer, SON, and M & S	Saka et al. (2023)

Note: S and P: Sewage and precipitation; SON: Soil Organic Nitrogen, M & S: Manure and sewage.

1.2 Study site overview

Most of the eastern Niger Delta population depend on groundwater as their primary source of drinking water. Also, groundwater serves industrial and other domestic uses in the region (Abam & Nwankwoala, 2020). Here, individuals are responsible for their water supply needs. Hence, most poorer households have shallow wells (i.e., hand-dug or motorized less than 30 m deep), and richer households and industries have deeper wells (up to 250 m deep) for their water supply. The ongoing anthropogenic activities in the region can release chemical pollutants into the soil and groundwater, as observed in parts of the region in Ogoniland (UNEP, 2011), to pose serious health risks to the growing population.

Geologically, the Niger Delta Basin is broadly subdivided into three lithostratigraphic units, representing prograde depositional facies (Obaje, 2009). The depositional sequences are distinguished based on the sand-shale ratio (Short & Stäuble, 1967). Depending on changes in the sea level, local subsidence and supply of sediments, the basin experienced various regressions and transgressions. The lithostratigraphic units are described in Table 1.6 below.

Table 1.6 Geological units of the Niger Delta region of Nigeria after Obaje (2009) and Adelana et al. (2008).

Age	Formation	Hydrostratigraphic unit	Lithology
Oligocene	Benin Formation (2.1 km thick)	Benin Aquifer	Continental sequence of massive and porous gravels, sands with clay lenses and lignites, silts, marine shales, and alluvial deposits. It has 70 to 100 % sand composition, deposited in the continental fluvial environment.
Eocene	Agbada Formation (3.7 km thick)	Agbada aquifer	A coastal sequence of alternating sandstones and shales of the transitional environment, with 30 to 70 % sand composition. It is considered as the hydrocarbon reservoir in the basin.
Paleocene	Akata Formation (7 km thick)	Akata shale aquitard	Thick basal marine shale and clay units with minor turbidite sand intercalations, turbidite sands, silts, and clays deposited in prodelta environment. The formation has < 30 % sand.

Due to the occurrence of clayey or silty strata at varying thicknesses, which act as confining layers and boundaries between distinct aquiferous zones, the basin developed a multilayered aquifer system in the upper 305 m (Nwankwoala et al., 2023). The aquifers vary from unconfined conditions at the surface to semi-confined and confined conditions at depths. According to Akpokodje et al. (1996), these aquifers are separated by highly discontinuous shale layers at various intervals that consist of a complex, non-uniform, discontinuous, and heterogeneous aquifer system. Additional details on hydrogeological and lithological details can be found elsewhere (e.g., Abam & Nwankwoala, 2020; Akpokodje, 1987; Akpokodje et al., 1996; Etu-Efeotor & Akpokodje, 1990; Etu-Efeotor & Odigi, 1983; Izeze, 1990; Lowden, 1972).

The Benin Formation aquifers serve as the region's groundwater reservoir (Eyankware et al., 2021). It is recharged mainly by infiltration from nearby surface waters, a more prolific aquifer, or precipitation (Ajaegwu et al., 2017; Nwankwoala et al., 2023). According to Ngah (1990), the recharge from surface waters increases the aquifer's vulnerability to pollution by dissolved toxic chemicals in the river. The groundwater is contained within the thick and extensive sand and gravel strata which are intercalated within the shale and clay layers of the formation. The sands are, however, poorly sorted, thus increasing the porosity and permeability of the aquifer (Nwankwoala et al., 2023). As a result, the Benin Formation aquifer has excellent water-yielding properties (Amajor, 1991b; Ngah & Eze, 2017), which makes it the target for both shallow and deeper wells in the Niger Delta. The average depth to the water table is 0.3 to 15 m (Offodile, 2002a). Based on the investigations carried out by Amajor (1989); Etu-Efeotor and Odigi (1983); and Etu-Efeotor and Akpokodje (1990), the freshwater aquifers of the Benin Formation are differentiated into three main zones: (1) a northern bordering zone that consists of shallow aquifers (< 100 m deep) of mainly continental deposits (coarse to very coarse sands), (2) a transitional zone, located towards the coast to the south, consists of intermixed marine and continental deposits (sand and gavels with clay intercalation), and (3) a coastal zone of marine deposits (coastal plain sands) that occurs at less than 200 m depth. At shallow depths, thicker lenses of marine clays and saline conditions capable of causing saltwater intrusion, especially when wells are over-abstracted, are prominent in the transitional and coastal zones. These conditions are absent in deep-seated aquifers.

1.3 Research motivation and objectives

1.3.1. Research needs

In the eastern Niger Delta, there are several ongoing anthropogenic activities capable of releasing pollutants into aquifers of the Benin Formation. These include:

1. Oil and gas industrial activities, including wastewater discharge from crude oil refining, leakage of petroleum pipelines and surface oil spillage.
2. Indiscriminate discharge of domestic and municipal sewage.
3. The presence of latrines.

Limited previous investigations have shown groundwater quality to be poor in the region. This is of particular concern for the residents, as many lack the means to afford safe drinking water (Aaron, 2005; Omofonmwan & Odia, 2009). The investigations, however, only focused on groundwater pollution by total petroleum hydrocarbons and polycyclic aromatic hydrocarbons (e.g., Anyakora & Coker, 2009; Edet et al., 2021; Odesa et al., 2024; Okechukwu et al., 2021; Ola et al., 2024), iron contamination in deep aquifers within the transition zones (e.g., Ngah, 2009), and saltwater intrusion (e.g., Atuchukwu et al., 2022; Mo et al., 2020). To date, Hg, C_6H_6, and NO_3^- groundwater pollution in the sandy aquifer of the Benin Formation has never been characterized in a single study, combining expertise in in-situ fieldwork and laboratory analyses. Since the residents' reliance on polluted ground and drinking water has resulted in an ongoing environmental and health catastrophe (Angaye et al., 2015; Ekhator, 2016; Obinna et al., 2017), a thorough investigation is necessary to identify the pollutants, their behavior, transport and fate in the soil-groundwater systems. Furthermore, many factors like redox conditions constitute a vital part of the chemical framework capable of influencing the behavior, fate and transport of pollutants in groundwater (Christensen et al., 2000). These factors are, therefore, important for groundwater assessment of pollutants' plume development downgradient, risk evaluation and evaluation of natural attenuation as a remediation option at polluted sites (Christensen et al., 2000). However, these factors that can influence the behavior, fate and transport of Hg, C_6H_6 and NO_3^- in sandy aquifers of the eastern Niger Delta have been so far not investigated. This study will provide an understanding of the groundwater pollution problems to raise awareness, thus preventing further consumption of polluted groundwater.

1.3.2. Thesis Objectives

This thesis investigated groundwater and sediment pollution in the eastern Niger Delta, focusing on the co-occurrence, source, transport, behavior and fate of Hg, benzene (C_6H_6) (and other TEX compounds) and nitrate (NO_3^-). The study was conducted on the sandy aquifer of Alesa, Ogale, Ebubu, Alode and Okochiri, which were influenced by (1) crude oil refining, (2) petroleum pipeline leakages, and (3) municipal and domestic sewage. Based on the groundwater pollution issues specified above, the three objectives of this thesis were to:

1) **Evaluate Hg concentration, source, speciation and retention in groundwater and sediments of the eastern Niger Delta.**

   To address this objective, groundwater samples were collected from the refinery-impacted site in Okochiri to estimate Hg concentrations and speciation for the first time. Also, the sediment samples were used for batch leaching experiments to determine the Hg retention capacity of the sediments. A redox diagram showing the stability of the various species of Hg in the groundwater was presented. A schematic representation of the Hg source, concentrations, speciation and mobility/retention in the groundwater and sediment of the eastern Niger Delta Region was also designed.

2) **Evaluate the current level and distribution of benzene and other TEX compounds, its source, and the potential for natural attenuation in the eastern Niger Delta region.**

   The objective was addressed by determining the hydrochemistry and benzene concentrations in the groundwater of Alode, Ogale and Okochiri. The samples were collected in wells next to the underground NNPCL and SPDC petroleum pipelines. Furthermore, the DO levels and groundwater temperatures were used to evaluate the aquifer's natural attenuation potential, limiting factors, and the time required to reach the benzene and BTEX remediation goal. Also, a site-specific recommendation was given to enhance the aquifer's biodegradation and natural attenuation capacities.

3) **Investigate NO_3^- source, transport, and fate across the eastern Niger Delta groundwater systems to improve management and remediation efforts.**

This objective was addressed by measuring the hydrochemistry and NO_3^- concentrations in the groundwater and municipal and domestic sewage in the Alesa, Ogale, Ebubu, Alode and Okochiri. $\delta^{15}N\text{-}NO_3^-$ and $\delta^{18}O\text{-}NO_3^-$ sewage and groundwater isotopic signatures were measured to establish the NO_3^- source and other ongoing geochemical processes influencing N transformation in the area. Furthermore, a schematic diagram of the source, transport, and fate of NO_3^- in the groundwater was designed. Site-specific recommendations were also made to improve management and remedial efforts.

1.4 Structure of the thesis

This thesis is a cumulative study that consists of five chapters. The introductory chapter (Chapter 1) presents reviews of the relevant literature on groundwater pollution, emphasizing pollution by mercury, benzene and nitrate in ground- and drinking water. It further provides the background for understanding the redox processes controlling the fate and transport of pollutants in groundwater. Furthermore, the study site overview and research needs are presented in this chapter. This chapter, therefore, provides the necessary background for the following sections, which form the main part of the thesis.

Chapter 2 addressed mercury pollution in the ground and drinking water in the coastal aquifer of the Okochiri, focusing on the estimate of Hg concentrations, source, speciation and retention in the groundwater and sediments of the Okochiri. This would be the first-time investigating mercury groundwater pollution in Nigeria and the first traced to influences of crude oil refining worldwide. Furthermore, a schematic representation was designed based on laboratory-scale experiments and the chemical data of the study. The paper was accepted for publication in the journal Applied Geochemistry.

Chapter 3 focused on the pipeline-related ground and drinking water pollution by benzene in the Alode, Ogale and Okochiri. Here, the current benzene (and the other TEX compounds) levels, source information and potential for natural attenuation are presented. The chapter was published in the Environments journal (Aleku et al., 2024).

Chapter 4 deals with nitrate pollution in the Alesa, Ogale and Ebubu, focusing on the source of nitrate in the shallow coastal aquifer to improve management and remediation efforts. Also, the role of parallel occurrence of nitrification and denitrification and other biogeochemical processes that could influence the transport and fate of nitrate in the aquifer were discussed. The paper was published in the journal Environmental Science and Pollution Research (Aleku, Dähnke, et al., 2024).

Chapter 5, the final chapter, provides the conclusion of the combined studies of this thesis with an outlook on further research.

Appendix A presents an up-to-date overview of Hg sources and concentrations in groundwater, emerging remedial technologies, complex biogeochemical processes, and a hydrogeochemical conceptual model for processes influencing Hg's mobility, fate and transport in groundwater. The paper was published in Applied Geochemistry (Aleku et al., 2024).

1.5 Declaration of co-author contributions

The thesis includes three research articles and one background chapter. The research articles were prepared according to the journal requirements to which they have been submitted. The style has been partially changed to the thesis. Figures, tables, and formulae/equations are numbered consecutively throughout the thesis. A list of complete references is given at the end. The supplementary data used for the manuscript is given in Appendix B. A detailed of the authors' contributions to each chapter is presented below.

Chapter 2: *Elevated mercury (Hg) in groundwater caused by oil and gas production*

Authors**:** Dogo Lawrence Aleku, Harald Biester and Thomas Pichler

Status: Submitted to *Applied Geochemistry* journal (in review)

DLA developed the research idea and conducted sample collection, preparation, and laboratory work. Furthermore, he interpreted the results and prepared the first version of the manuscript with all the figures and tables. HB provided the idea for the speciation analysis and contributed to the discussion. TP provided supervision, contributed to the

discussion, and edited the final draft of the manuscript. The three co-authors reviewed the manuscript before submission.

Chapter 3: Pipeline-related residential benzene exposure and groundwater natural attenuation capacity in the eastern Niger Delta, Nigeria

Authors**:** Dogo Lawrence Aleku, Harald Biester and Thomas Pichler

Status: Accepted for publication in *Environments* journal

DLA performed field sample collection, sample preparation, and laboratory work. Furthermore, he interpreted the results and prepared the first version of the manuscript. HB contributed content to the discussion. TP provided the idea for the study, provided supervision, contributed to the discussion, and edited the final draft of the manuscript. The three co-authors reviewed the manuscript before submission.

Chapter 4: *Source, transport and fate of nitrate in shallow groundwater in the eastern Niger Delta*

Authors**:** Dogo Lawrence Aleku, Kirstin Daehnke and Thomas Pichler

Status: Submitted to *Environmental Science and Pollution Research* journal (passed first round of revision)

DLA carried out the sample collection, sample preparation, and laboratory work. He also interpreted the results and prepared the first version of the manuscript. KD carried out the isotope analysis and contributed to the structure of the manuscript. She also contributed to the discussion and organization of the manuscript. TP conceptualized the study, supervised the study design, and edited the final draft of the manuscript.

Appendix A: *Mercury in Groundwater – Source, Transport and Remediation*

Authors**:** Dogo Lawrence Aleku, Olesya Lazareva and Thomas Pichler

Status: Published in Applied Geochemistry (2024)

Reference: Aleku, D. L., Lazareva, O., & Pichler, T. (2024). Mercury in Groundwater–Source, Transport and Remediation. Applied Geochemistry, 106060.

DLA developed the outline and prepared chapters 1, 2, 4, 6 and 7, the abstract, and summary and conclusion in the first version of the manuscript with all the figures (including the conceptual model in chapter 5) and tables. OL prepared chapters 3 and 5 in the first version of the manuscript and contributed content to other chapters. TP developed the idea for the manuscript and contributed content to the discussion of all chapters.

2. Elevated mercury (Hg) in groundwater caused by oil and gas production

Dogo Lawrence Aleku[a], Harald Biester[b] and Thomas Pichler[a,]

[a] *Institute of Geosciences, University of Bremen, 28359 Bremen, Germany*
[b] *Institute of Geoecology, Technical University Braunschweig, 38106 Braunschweig, Germany*

Abstract

From 1965 to 2017, the Port Harcourt Refining Company (PHRC) refined crude oil in the eastern Niger Delta and groundwater hydrocarbon contamination in the area is known. However, nothing is known about the concentration, source, speciation and mobility of mercury (Hg), a potential byproduct of oil refining. To address this, groundwater samples were collected along the wastewater discharge outlet (WDO) and around the PHRC. The Hg concentrations in groundwater near the WDO varied between 0.2 and 6 µg/L, compared to less than 0.01 µg/L at distances greater than 300 m from the WDO and reference sites away from the refinery. Up to 63 % of Hg were present as Hg bound to particles larger than 0.45 µm (Hg_{part}), suggesting the prevalence of Hg transport in the suspended colloidal phase in the aquifer. Operational-defined Hg speciation shows that 33 % of the total Hg (THg) occurred as inorganic, reactive Hg^{2+}. In comparison, only 4 % occurred as dissolved organic matter-bound Hg^{2+} despite high DOC and BTEX concentrations of up to 47 mg/L and 2,888 µg/L, respectively. Notably, the DOC is predominantly petroleum hydrocarbon, generated from the ongoing oil and gas activities at the site. This suggests that hydrocarbon-based-DOC does not bind Hg.

Sediment samples collected from the wastewater discharge point (WDP) contained Hg concentrations of up to 529 µg/kg, and the carbon (C) content reached 40 %. Sediment batch leaching experiments showed that up to 23.5 % of the Hg in the quartz-dominant sediment can be mobilized into groundwater under oxic conditions. Despite the presence of petroleum hydrocarbon, Hg retention was significantly controlled by the sediment's natural organic matter (NOM). Hence, the discharged oil

and gas production wastewater due to crude oil refining released Hg into the aquifer, where NOM ultimately controls fate and transport.

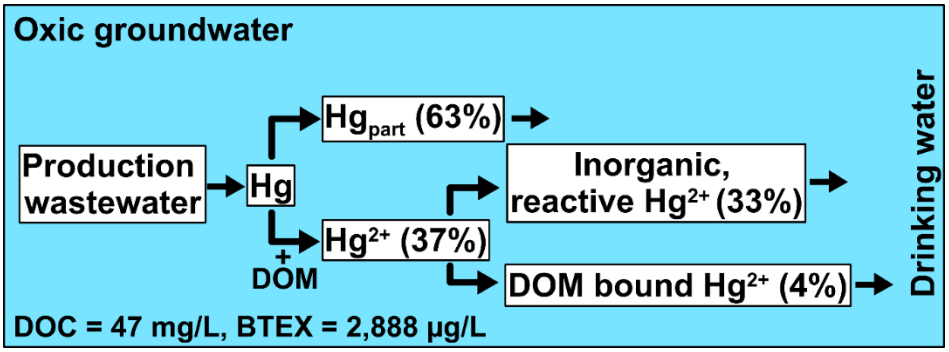

2.1 Introduction

Most oil and gas reservoirs naturally contain mercury (Hg) (Subirachs Sanchez, 2013). Hg appears to be mobilized into these reservoirs mostly from cinnabar (HgS) (Littlepage, 2013). It occurs in natural gas almost exclusively as elemental Hg (Hg^0), in gas condensate as Hg^0, Hg_2Cl_2, or $HgCl_2$ and crude oil mainly as Hg^0, inorganic compounds (e.g., HgS, HgSe and other salts) and organic compounds (Hg thiols) (UNEP, 2022). The dominant Hg species (> 50 %) in natural gas, gas condensate, and crude oil is Hg^0 (Wilhelm & Kirchgessner, 2001).

Although concentrations vary widely and published data are not always available, crude oils contain 1 to 33,000 µg/kg of Hg (COWI, 2005; Pacyna, 1987), depending on their origin and regional tectonism, seismicity and structural features (UNEP, 2022). According to the International Petroleum Industry Environmental Conservation Association (IPIECA) investigation of Hg in African crude oil, 1 % contained about 50 to 100 µg/kg, 27 % contained between 2 and 50 µg/kg, and 72 % contained ≤ 2 µg/kg (IPIECA, 2014). However, Shah et al. (1970) reported a higher Hg concentration for Libyan oil, up to 2,000 µg/kg. This suggests that crude oil can be an important sink for Hg if present in significant quantities (Krupp, 1988). In Nigeria, the Federal Ministry of Environment (2017) reported that the oil and gas industry accounts for 2 % of the total Hg released into the environment. Here, Hg concentrations in natural gas from the Niger Delta were reported at about 10 µg/Nm^3, and the Hg input of 777 kg Hg/yr was calculated for an average natural gas activity rate of 77,665,280,000 Nm^3/yr in 2015 and 2016. The estimated monthly Hg input from

crude oil was calculated at 369 kg Hg/yr for 108,575,075 t annual crude oil extraction, and an input of 10 kg Hg/yr was calculated for 3,053,689 t refined crude oil. The mass balance for Hg indicates that the majority is removed through refinery waste streams (Hoffman & Paulsen, 2009; Wilhelm, 2001), accounting for 0.1 % (0.56 t) of the total Hg released to aquatic systems (UNEP, 2018). The specific waste streams affected (i.e., wastewater, solids, and air emissions) were found to be highly dependent upon the sulfur levels in crude oil (IPIECA, 2014; Pacyna et al., 2006; Wilhelm, 2001). High sulfur-containing crude oils resulted in more significant accumulations of insoluble Hg-sulfide in crude oil and unprocessed gas condensates (IPIECA, 2014; Wilhelm & Bloom, 2000).

Due to the several issues that Hg poses to refineries (e.g., amalgamation with other metals, catalyst poisoning, and liquid metal embrittlement), Hg associated with crude oil is generally released during production and processing (Littlepage, 2013). Once released, Hg is captured in absorbent material-based Hg removal units (installed on production wellheads or at the refinery), removed, and disposed of in wastewater and solid waste streams (sludge) before oil and gas refining (UNEP, 2022). According to the IPIECA (2016) preliminary assessment, wastewater streams account for 13.5 t/y of Hg released to the environment during oil production globally. 90 % of those occur offshore (Munthe et al., 2019). In 2019, the Hg mass balance of two Korean refineries was calculated where Hg removal systems were not installed. The study showed that solid waste streams (sludge) accounted for 4.5 to 33.2 % of the Hg, and wastewater streams accounted for 3.1 to 5.6 % of the Hg released (UNEP, 2017). This process could release Hg into groundwater (Aleku, Lazareva, et al., 2024).

Between 1965 and 2017, the PHRC refined crude oil in the eastern Niger Delta. As a result, production wastewater was discharged to the nearby Okochiri Creek through a WDO. While Hg mass balance data for the PHRC is unavailable, unsafe discharge of wastewater streams from the refinery was observed. Hence, the production wastewater, which may contain Hg and several other toxic components, could have migrated into the Okochiri aquifer. Therefore, we hypothesize that the discharge of oil and gas production wastewater through the WDO to the aquifer could elevate Hg concentrations in the groundwater.

In this paper, we present the first estimate of (i) Hg concentrations, (ii) source information, (iii) speciation, and (iv) retention in groundwater and sediments in the Okochiri area of the eastern Niger Delta. A similar situation can be expected at other oil and gas locations, and hence, the results of this study may be transferable to different locations worldwide.

2.2 Materials and methods

2.2.1. Site description, geology, and hydrogeology

The PHRC, a subsidiary of the Nigerian National Petroleum Corporation Limited (NNPCL), is in Eleme, southeast of Port Harcourt in Rivers State, Nigeria. The company operates two oil refineries that specialize in refining crude oil. The first refinery commenced operation in 1965, processing 60,000 barrels (9,500 m^3) per stream day. The second refinery commenced operation in 1989 with 150,000 barrels (24,000 m^3) processing capacity per stream day. The PHRC stopped refining at both refineries in 2017. Before 2017, the wastewater from both refineries was discharged to the nearby Okochiri Creek through the WDO (Fig. 2.1). The creek is about 5 m away from the nearest residential house. The PHRC is approximately 12 m above sea level, and the Okochiri community, located on the edge of the refinery to the south, is approximately 4 m above sea level. The groundwater flow direction is to the SSW.

The geology of the Niger Delta region comprises three major lithostratigraphic units. The Paleocene to Recent 7 km thick Akata Formation consists of basal marine pro-delta thick shale units with less than 30 % sand intercalations and minor amounts of silt and clay (Adagunodo et al., 2017; Obaje, 2009). The Agbada Formation, Eocene to Recent, is 3.7 km thick. This formation is considered the primary source rock for petroleum hydrocarbons in the Niger Delta. It is characterized by a coastal sequence of alternating marine sands and shales, with sand percentages varying between 30 and 70 % (Ogbe et al., 2013; Tuttle et al., 1999). The Oligocene to Recent Benin Formation comprises mainly clay units, coarse-grained coastal plain sand and alluvial deposits of about 95 to 99 % quartz grains (Nwajide, 2013; Onyeagocha, 1980).

The Benin Formation has an excellent water-yielding capacity (Offodile, 2002a). Here, the aquifer predominantly comprises unconsolidated sand beds and

sandy gravels with minor intercalations of clays, lignite, and conglomerates at depths between 3 and 300 m (Adelana, 2008). The aquifer has 3.82 x 10^{-3} to 9 x 10^{-2} cm/sec hydraulic conductivity, 1.05 x 10^{-3} to 11.3 x 10^{-2} m^2/sec transmissivity, 1.07 x 10^{-4} and 3.53 x 10^{-4} storage coefficient, and 19.01 to 139.8 m^3/h/m (drawdown) specific capacity, indicating excellent water-yielding capacity (Offodile, 2002b). The regional groundwater flow is North-South and the aquifer's average hydraulic gradient is estimated at 3.8 x 10^{-4} (Abam & Nwankwoala, 2020). In Okochiri, private supply wells tap the aquifer of the Benin Formation. Several factors, such as the 2,800 to 4,000 mm/year precipitation rate, vast catchment area, geology, and presence of rivers and streams contribute to the Benin Formation's high perennial aquifer recharge (Abam & Nwankwoala, 2020; Ohwoghere-Asuma et al., 2023b). Consequently, the water infiltrates into the upper unit of the formation, leaving the aquifer vulnerable to potential pollution (Abam & Nwankwoala, 2020). Only deep-seated aquifers in the Benin Formation are considered safe and less susceptible to pollution threats (Abam & Nwankwoala, 2020). Groundwater from this formation mainly occurs as the $CaHCO_3$, $NaHCO_3$, NaCl, and $CaMgClSO_4$ water type (Eyankware et al., 2020; Owoyemi et al., 2019; Paschal et al., 2014). For this study, groundwater samples were collected from shallow wells (1 to 30 m) in the Benin Formation. For comparison, samples were collected from areas affected and unaffected by oil and gas production wastewater discharge.

2.2.2. Groundwater sampling

Fifty-three groundwater samples were collected along the WDO and next to the PHRC in 2021, 2022 and 2023 between 6:00 am and 2:00 pm. The samples were collected from public supply wells (PSW) and community supply wells (CSW) using a laboratory-constructed water bail made of polyvinyl chloride material or with an electric submersible pump. For sampling using bail, samples were collected during the early hours, between 6:00 and 8:00 am, when the wells were in use. The bail was rinsed three times with the groundwater to be sampled before collecting the samples. Those wells with installed electric submersible pumps were sampled by pumping. First, groundwater was pumped into an overhead storage tank to purge the wells for 30 minutes before sampling directly from the wellhead. However, measurements of the water table and well depth were impossible for most wells since the well heads

were sealed with concrete slabs to prevent surface contamination and theft of submersible pumps. In wells where measurement was possible, the water table and well depth ranged from 1.5 to 9 m and 9.8 to 30 m, respectively. The pH, conductivity (EC), total dissolved solids (TDS), temperature, dissolved oxygen (DO), salinity, redox potential (ORP) and resistivity were measured in the freshly pumped samples using a Hanna instrument HI98494 multiparameter. Also, the total alkalinity ($CaCO_3$) was determined in the field by colorimetric titration with 0.16 N H_2SO_4 in combination with a bromcresol green-methyl red indicator. The bromcresol green-methyl red indicator powder was added to 100 mL of the groundwater sample and titrated using a Hach digital titrator to a light pink color. The total alkalinity was reported as $CaCO_3$.

The samples were collected into MERX-T 60 mL certified autosampler vials for Hg (total (THg) and dissolved (Hg_{diss})) analysis. The Hg_{diss} samples were filtered through a 0.45 µm cellulose acetate (CA) membrane in the field and stabilized with 1 % HCl as described by Bloom (2000). During the 2023 sampling campaign, eight wells with the highest THg concentration were sampled for Hg speciation analysis. Samples were collected for DOC, cations, anions, and trace metal analysis. The BTEX samples were collected due to the strong petroleum odor in most wells next to the WDO. Samples were filtered through 0.45 µm cellulose acetate (CA) membrane filters and collected into 25 mL glass vials for DOC, 22 mL headspace vials for BTEX, 30 mL brown HDPE vials for major cations, and 20 mL Zinnser vials for anions and trace metals. The sub-samples for DOC and major cations were preserved with 2 % nitric acid (HNO_3). The sub-samples for BTEX were preserved with one spatula tip of $CuSO_4/Na_2SO_4$. The sampling for BTEX measurement was performed following the US EPA method 5021A (USEPA, 2003). The samples were stored at 4°C until transported to the laboratory for analysis. The groundwater well locations are shown in Fig. 2.1.

2.2.3. Sediment sampling

Since the PHRC stopped operations in 2017, sampling the wastewater for Hg analysis was impossible. Thus, sediment cores from the wastewater discharge point (WDP) were collected for Hg analysis. Eight 100 cm long sediment cores were collected at varying distances from the wastewater discharge point (WDP) in 2022 (Fig. 2.1). Five samples were collected at 20 cm depth intervals from each core. The

Eijkelkamp sand ruler with 10 fractions (art no. 080403) was used to determine and classify the grain size distribution of the core materials (Table 2.4S). Core S–1, nearest (4 m) to the WDO, was predominantly composed of quartz sands with little organic matter. In texture, the quartz sands were very fine to coarse at – 20 to – 40 cm, and a mixture of very fine to very coarse grains at – 60 to – 100 cm. S–2 was composed mainly of quartz sands; however, it had more organic matter than S–1. The texture of the quartz sands was generally very fine to highly coarse across all depths. S–3, highly rich in natural organic matter, was collected at the sediment deposition bank, where the wastewater flow velocity was strongest. Out of all the cores, S–3 had the strongest petroleum odor. As observed in S–3, S–4 also had a strong petroleum odor, and the grain sizes were very fine to highly coarse quartz sands across all depths. Similarly, the quartz-dominant S–5 sediments generally had a strong petroleum odor, with very fine to medium coarse quartz sands across all depths. In S–6, the organic matter and petroleum odor were comparatively less than in S–3, S–4 and S–5. Here, between – 20 to – 60 cm, the grain size distribution was generally very fine to medium coarse; however, at – 80 to – 100 cm, the grain sizes varied between medium fine and highly coarse. S–7, sampled towards the edge of another sediment deposition bank, had a strong petroleum odor. In texture, the cores at – 20 to – 60 cm were very fine to medium coarse and medium fine to highly coarse at – 80 to – 100 cm. S–8 was rich in natural organic matter and had a strong petroleum odor across all depths. The sediments were deposited as the wastewater flow was divided into two directions, SSE and SSW. The S–8 sediments were predominantly composed of quartz sands of highly fine to very coarse texture at – 20 to – 40 cm and medium fine to highly coarse texture at – 60 to – 100 cm. REF, collected at the reference site, was composed predominantly of quartz sands. The sands' texture was generally very fine to highly coarse across all depths. Little organic matter was observed in the core at – 20 cm; however, organic matter was not found at – 40 to – 100 cm. The core was collected in the Okochiri, within the same geologic settings as the study sediments. The sediments were collected into polypropylene bags and stored at 4°C until transported to the laboratory for analysis.

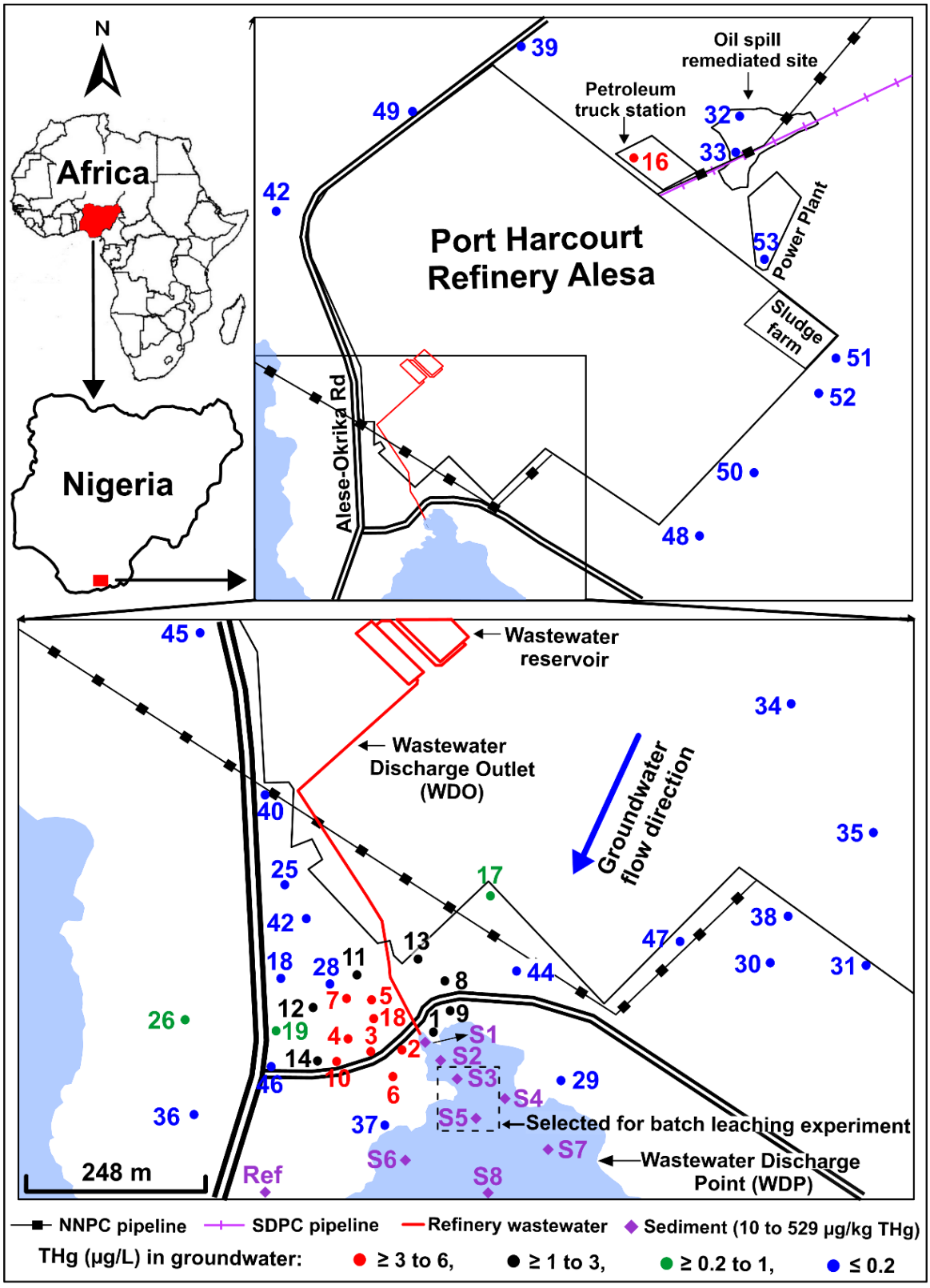

Fig. 2.1 Site map with well locations and spatial distribution of THg concentrations in the Okochiri groundwater (basemap: Google map). For color interpretation in this map, the reader is referred to the Web version of this article.

2.2.4. Analytical procedures

2.2.4.1. Total Hg (THg), dissolved Hg (Hg_{diss}) and speciation analyses (Hg^0, Hg^{2+}, and Hg_{part}) in groundwater

The THg and Hg_{diss} (filtered through a 0.45 µm CA membrane filter) analysis were conducted using a cold vapor atomic absorption spectroscopy (CV-AAS) (Hg-254 NE, Seefelder Messtechnik GmbH, Germany) for high-concentration samples, and a cold vapor absorption fluorescence spectrometry (CV-AFS) (Analytic Jena GmbH, Germany) for low concentration samples, following US EPA Method 1631 (2002). The groundwater samples were stabilized by adding 1 % by volume of 0.2 M bromine monochloride (BrCl) prepared according to Bloom et al. (2003). For complete oxidation of the organic Hg fractions, the samples (with the BrCl) were left for 24 hours as recommended by the US EPA Method 1631 (2002). Subsequently, hydroxylamine hydrochloride ($NH_2OH \cdot HCl$) was added to neutralize the BrCl, followed by the addition of tin(II) chloride ($SnCl_2$), which served as the Hg-reducing agent, before the samples were analyzed.

Operational-defined Hg speciation in the groundwater was determined following the method of Richard (2016), using CV-AAS. In addition to THg and Hg_{diss}, this method produces four distinct Hg fractions:

- Hg^0_{aq}: elemental Hg; purged from untreated groundwater samples,
- inorganic, reactive Hg^{2+}; purged after reduction with $SnCl_2$,
- Hg^{2+} bound to DOM; purged after BrCl and $SnCl_2$ treatment,
- Hg_{part}: Hg bound to particles; the difference between the Hg_{diss} and THg concentrations.

2.2.4.2. Total Hg (THg) and total carbon (% C) analyses in sediments

THg concentrations in the sediments were determined using a Milestone Direct Mercury Analyzer (DMA-80, Milestone Inc.) through thermal decomposition, amalgamation, and subsequent atomic absorption spectrometry. The samples were measured as dry mass. They were analyzed following EPA method 7473 (EPA, 2000). Approximately 50 mg of each milled sample aliquot was weighed into a nickel boat. After every 10 samples, two blanks, two Standard Reference Materials (SRMs) and two replicas were run to ensure the quality of the analysis. Certified soil reference

materials NCS DC 73019 (sediment) and NIST 1515 (apple leaves) were analyzed, and the results were within certified values.

The total carbon (% C) analysis was carried out using a DIMA 1000 C-N-S/VOC/IC. The quality of the analysis was ensured by certified reference material (CRM), i.e., B2178: Medium Organic Content Soil. One CRM, one blank, and two replicas were run after every 10 samples for quality control. The results were consistent with certified values.

2.2.4.3. Anion and cation measurements in groundwater

A Metrohm 883 Basic IC plus instrument with a 5 µL injection loop and a Metrosep A Supp5 (150 × 4.0 mm; 5 µm) column was used to determine the concentrations of anions in the groundwater samples. An internal standard was used to check the measurement's accuracy and precision. The errors recorded were < 10 %.

The cations and trace elements were determined by inductively coupled plasma-optical emission spectrometry (ICP-OES) using a Perkin Elmer Optima 7300 DV instrument. The measurement accuracy was checked using EnviroMAT Groundwater Low (ES-L-2) and High (ES-H-2) certified water from SCP Science, Canada. The errors recorded were < 3 % for all analytes. Also, the measurement's precision was checked using an internal standard, and errors < 4 % were recorded.

Furthermore, a Shimadzu TOC analyzer TOC-V CPN (Shimadzu Corporation) was used to determine dissolved organic carbon (DOC). The accuracy and precision of the method were checked using a certified Total Organic Carbon Standard of 50 mg/L (Aqua Solutions), showing errors of < 6 %. BTEX was measured following the "DIN 38407-F 43: 2014-10" method. Using the Shimadzu QP2020 with GC-2030 and HS-20 Trap. If necessary, the samples were diluted before measurement (Aleku, Biester, et al., 2024).

Statistical analyses were conducted using Microsoft Excel to test the correlations. Geochemist's Workbench (17.0.3 edition) was used to generate the Eh – pH diagram for Hg species in the groundwater and to evaluate the hydrochemistry

through the trilinear Piper diagram (Piper, 1944) based on the major ions. Surfer 12 was used to construct the Hg schematic diagram using data from this study.

2.3 Batch leaching experiment

The release of Hg under oxic conditions was investigated on sediment samples collected from the Okochiri WDP using a modified batch leaching procedure based on Koopmann et al. (2022), whose study examined the release of trace metal in sediments. Five sediment **c**ores (i.e., S3 B, S3 C, S3 D, S5 B, and S5 A) with the highest THg concentrations were selected for the experiment. The sediments were dried at room temperature for 14 days under a fume hood and powdered. Five batch vessels were filled with 0.5 g of the powdered sediment, and 10 mL of sodium acetate (NaOAc) solution (20.51 g in 250 ml of MQ water, pH = 8.2) was added as shown in Fig. 2.2. Notably, NaOAc solution has been used previously for THg (e.g., Ariza et al., 2000; Plouffe et al., 2001; Zhang et al., 2009) and $MeHg^{+}$ extraction (e.g., Tseng et al., 1999) in sediments. Furthermore, three vessels were filled with MQ water as blank samples for procedural control. Triplicates of each sample were also prepared for procedural control. The mixture was constantly shaken at 20 rpm for 2 h in an overhead shaker. Then, the samples were centrifuged at 4,000 rpm for 15 minutes, followed by a rinse with 5 mL MQ water and centrifuged at 4,000 rpm for 5 mins, decanted, and filtered through a 0.45 μm membrane. The aliquot was collected and analyzed for THg and TH_{diss} using CV-AFS.

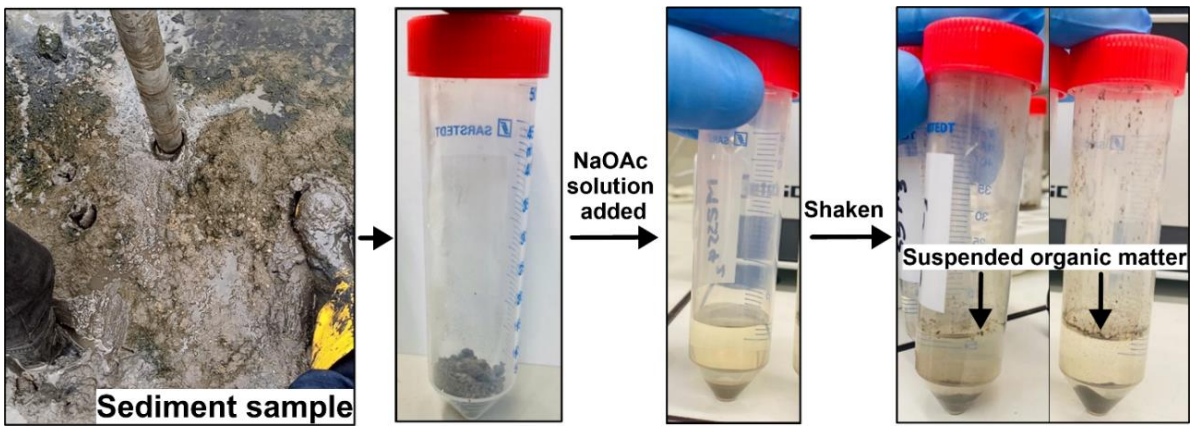

Fig. 2.2 Batch leaching experiment sample preparation.

2.4 Results and discussion

2.4.1 Results

2.4.1.1 Field measurements and chemical data

Minimum, maximum, median and mean are given in supplementary Tables 2.1S, 2.2S, 2.3S, 2.4S and 2.5S. The hydrogeochemical parameters of the groundwater collected in the reference and Hg-contaminated sites showed little variation (Table 2.1). The groundwater samples of the Hg-contaminated Okochiri site had concentrations of cations, anions, and trace metals similar to those of the reference site's groundwater. However, Hg was not detected (less than 0.01 µg/L) in the reference site samples.

Generally, the groundwater temperature varied between 25.3 and 32.5 °C. The pH was slightly acidic, ranging from 4 to 6.9. The low pH is attributed to microbial degradation of petroleum hydrocarbon, which forms organic acid (Lin et al., 2014). The DO and Eh ranged from 1.4 to 8.4 (median = 6.5 mg/L) (19 to 106 (median = 84) % saturation) and 117 to 801 (median = 506), respectively, indicating oxic groundwater conditions. None of the groundwater samples collected at the Hg-contaminated site were oxygen-saturated. Despite the coastal nature of the area, the groundwater was characterized by low EC (20 to 219, median = 56 mg/L), TDS (10 to 110, median = 28 mg/L) and salinity (0.01 to 0.1 PSU). This suggests that there is no occurrence of saltwater intrusion in the coastal Okochiri aquifer. The absence of correlation between the conservative elements (i.e., Cl, Na, Mg, Ca, and K) in the groundwater further supports this finding (Bagnato et al., 2009). The EC and TDS values were consistent with those reported by Eyankware et al. (2022), Nwankwoala and Walter (2012) and Abam and Nwankwoala (2020).

Ion concentrations ranged from 0.8 to 11 mg/L for Cl^-, less than 0.01 to 3.5 mg/L for NO_3^-, 1 to 12 mg/L for SO_4^{2-}, 0.3 to 2 mg/L for Ca, 1 to 15 mg/L for Na, 0.04 to 1 mg/L for K, 0.02 to 0.4 mg/L for Mg, and 0.5 to 2 mg/L for Si. The low concentrations of the ions are attributed to the dominance of quartz sands in the aquifer (up to 99 % quartz) (Onyeagocha, 1980). Under typical groundwater conditions, limited ion exchange and minimal dissolution are expected, given that

quartz is relatively inert. The groundwater belonged to the calcium–chloride (Ca–Cl) and sodium–chloride (Na–Cl) hydrochemical facies (Fig. 2.3).

The concentration of benzene, toluene, ethylbenzene, xylenes and trimethylbenzene varied between less than 0.1 and 2,700 µg/L, less than 0.1 to 20 µg/L, less than 0.1 to 3.8 µg/L, less than 0.1 to 24 µg/L and less than 0.1 to 140 µg/L. Overall, the total BTEX concentrations varied between less than 0.1 and 2888 µg/L (Aleku, Biester, et al., 2024).

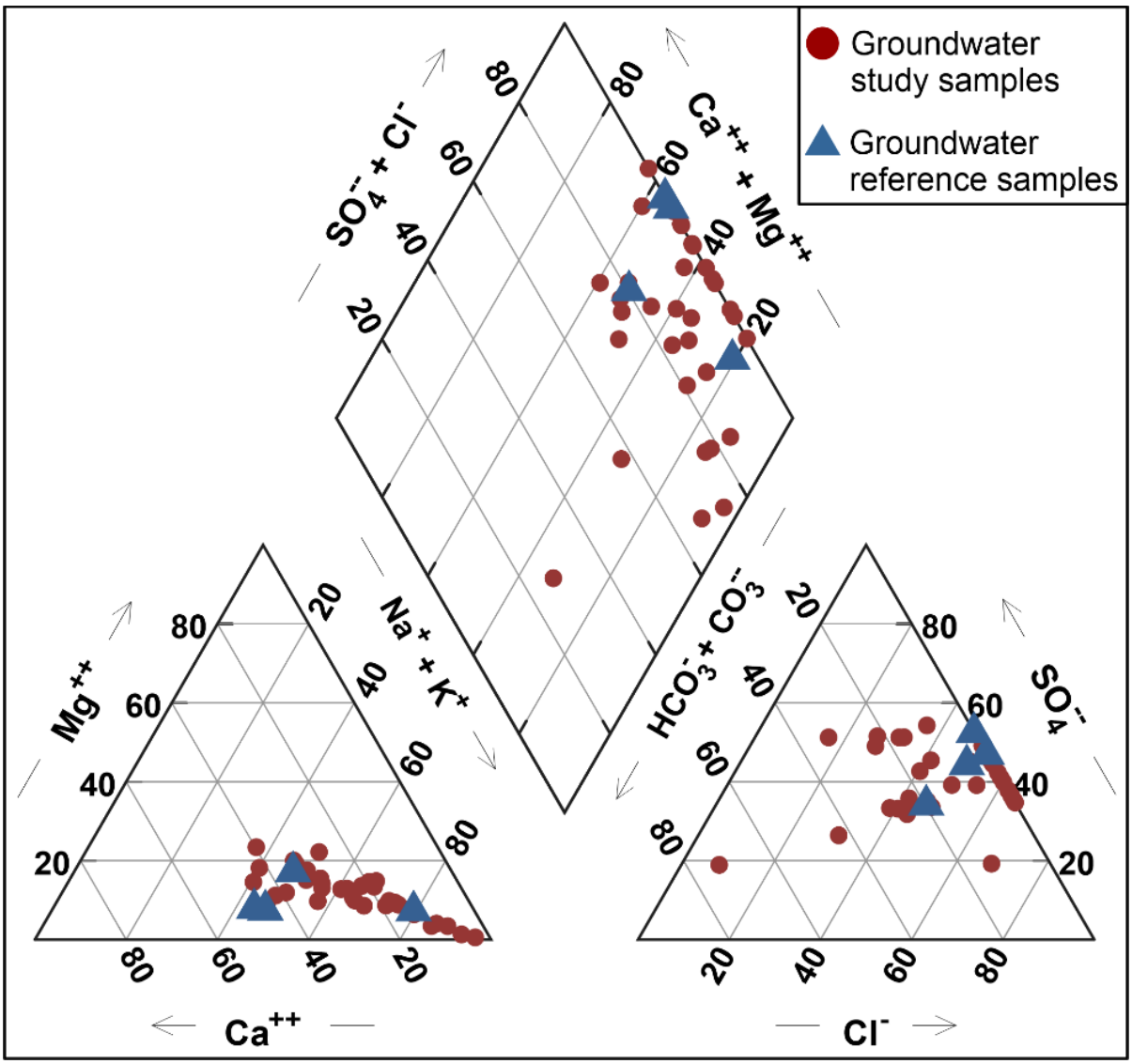

Fig. 2.3 Hydrochemical facies for groundwater in the Okochiri.

Table 2.1. pH, Eh, DO, TDS, temperature, anions, cations and Hg concentrations for contaminated and non-contaminated groundwater in the Okochiri.

Sample	pH	Eh	DO	DO	TDS	Temp.	Cl^-	NO_3^-	SO_4^{2-}	Ca^{2+}	Na^+	K^+	Mg^{2+}	DOC	BTEX	THg	Hg_{diss}
ID		mV	mg/L	%	mg/L	°C	mg/L	mg/L	mg/L	mg/L	mg/L	mg/L	mg/L	mg/L	µg/L	µg/L	µg/L
Hg-contaminated groundwater																	
PSW-1	5	341	5.1	64.2	21	27.2	11	3	6	1	5	0.1	0.1	18	623	2	0.1
PSW-2	5.5	450	4.3	55.4	60	28.4	2	1	12	0.2	11	0.1	0.0	18	62	3.8	0.04
PSW-3	5.5	742	7.3	97.2	13	29.5	5	2	8	1	4	0.3	0.2	26	4.4	6	3.8
CSW-4	4.7	542	3.3	41.5	18	28	2	2	2	0.3	2	0.3	0.2	23	0.3	3.7	3.2
PSW-5	4.5	797	6.6	83.7	18	27.6	2	2	7	0.3	2	0.3	0.2	21	1.3	4	1.9
PSW-6	4.6	716	4.8	61	20	28	2	2	4	1	4	0.2	0.3	22	186	4	0.3
PSW-7	4.8	734	5.7	78.8	10	32	1	3	1	1	1	0.1	0.1	26	0.1	3.2	0.7
PSW-8	4.5	450	5.2	67	16	28.5	1	<0.01	1	0.3	1	0.1	0.1	23	n.d.	1.7	<0.01
PSW-9	4.5	734	3.2	41.4	20	28	1	1	1	0.5	1	1	0.2	22	1305	1.5	0.7
PSW-10	6	576	7.2	96	15	29.7	5	3	6	0.5	3	0.4	0.2	2	0.2	3.3	1.6
PSW-11	5.8	80	7.1	95.6	9	29.7	5	2	7	0.4	2	0.2	0.2	14	0.8	2	0.7
PSW-12	5	728	6.5	84.3	16	28.3	5	2	7	0.5	2	0.2	0.2	23	0.3	1.9	1
PSW-13	5.6	336	7.4	96.7	40	28.8	4	2	11	1	10	0.3	0.2	22	86	1.7	0.1
PSW-14	5.6	737	7.3	92.8	12	27.2	1	4	5	0.4	3	0.2	0.2	29	n.d.	1.1	<0.01
PSW-15	5.2	769	4.7	63.9	12	30.6	4	2	6	0.3	1	0.4	0.1	26	n.d.	0.2	<0.01
PSW-16	4.9	561	7.5	95.2	10	27.1	1	<0.01	1	2	10	1	0.4	47	461	1.4	0.01
PSW-17	4.8	356	5.7	71.9	20	27.4	2	<0.01	5	1	2	0.1	0.2	33	1439	0.7	0.1
PSW-18	4.5	n.d.	4.8	62	16	28.4	5	3	7	1	3	0.3	0.2	22	n.d.	4.3	2.1
PSW-19	5.4	n.d.	7.3	95	8	28.5	4	2	6	0.4	1	0.3	0.1	n.d.	n.d.	0.8	<0.01
PSW-28	4.5	n.d.	7.2	94.1	9	28.3	4	1	6	1	1	0.2	0.1	n.d.	n.d.	0.01	<0.01
Non-contaminated (reference) groundwater																	
REF1	4	516	7.6	103	12	31	5	3	6	0.3	2	0.1	0.1	23	<0.01	<0.01	<0.01
REF2	4.3	497	7.5	101	9	31	5	3	6	1	1	0.1	0.1	35	<0.01	<0.01	<0.01
REF3	5.1	448	7.9	100.2	15	27.7	2	2	2	1	1	1	0.3	10	<0.01	<0.01	<0.01
REF4	4.6	418	6.6	83.5	9	27	4	<0.01	6	1	1	0.3	0.1	2	<0.01	<0.01	<0.01

Notes: PSW = Public Supply Well, n.d. = Not Determined, DOC = Dissolved Organic Carbon, DO = Dissolved Oxygen, TDS = Total Dissolved Solids, REF = Reference sample.

2.4.1.2. Hg distribution in groundwater

The THg and Hg_{diss} concentrations in the wastewater-influenced groundwater ranged from 0.2 to 6 µg/L and less than 0.01 to 3.8 µg/L, respectively (Table 2.1). Over the three sampling years (2021, 2022, and 2023), THg concentrations in wells near the WDO exceeded the WHO (2017a) drinking water guideline value of 1 µg/L. The highest concentrations were consistently observed in PSW–2, PSW–3, CSW–4, PSW–5, PSW–6, PSW–7, PSW–10, PSW–11 and PSW–18, collected along the groundwater flow direction. In contrast, all the wells on the opposite side of the WDO had consistently lower THg concentrations. Downgradient, along the groundwater flow direction, THg was 3.7 (Hg_{diss} = 3.2) µg/L at PSW–4, 3.8 (Hg_{diss} = 0.1) µg/L at PSW–2, 4 (Hg_{diss} = 1.9) µg/L at PSW–5, 4.3 (Hg_{diss} = 2.1) µg/L at

PSW–18, 4 (Hg_{diss} = 0.3) µg/L at PSW–6, and are highest (6 (Hg_{diss} = 3.8) µg/L) at PSW–3. At PSW–10, 131 m from the WDO, 3.3 (Hg_{diss} = 1.6) µg/L was found. At 210 m distance, only 0.8 (Hg_{diss} = 0.03) µg/L was detected (PSW–19). At 300 m distance, THg decreased to 0.2 (Hg_{diss} = less than 0.01) µg/L; at distances greater than 300 m and the reference sites, THg concentrations were less than 0.01 µg/L. Notably, the highest THg and Hg_{diss} concentrations were also rich in SO_4^{2-}.

2.4.1.3. Hg speciation in groundwater

The concentration of Hg_{part} (particulate Hg unable to pass through a 0.45 µm CA membrane filter) in the wastewater-influenced groundwater varied between 0.3 and 2.2 µg/L (median = 1.5 µg/L). Hg^{2+} (Hg^{IIa}) concentrations ranged from less than 0.01 to 3.5 µg/L (median = 0.8 µg/L). The concentration of Hg^{2+} (Hg^{IIb}) varied between 0.01 and 0.4 µg/L (median = 0.1 µg/L). Hg^0 was not detected in the groundwater. The percentage content for the species in the samples is given in Fig. 2.4.

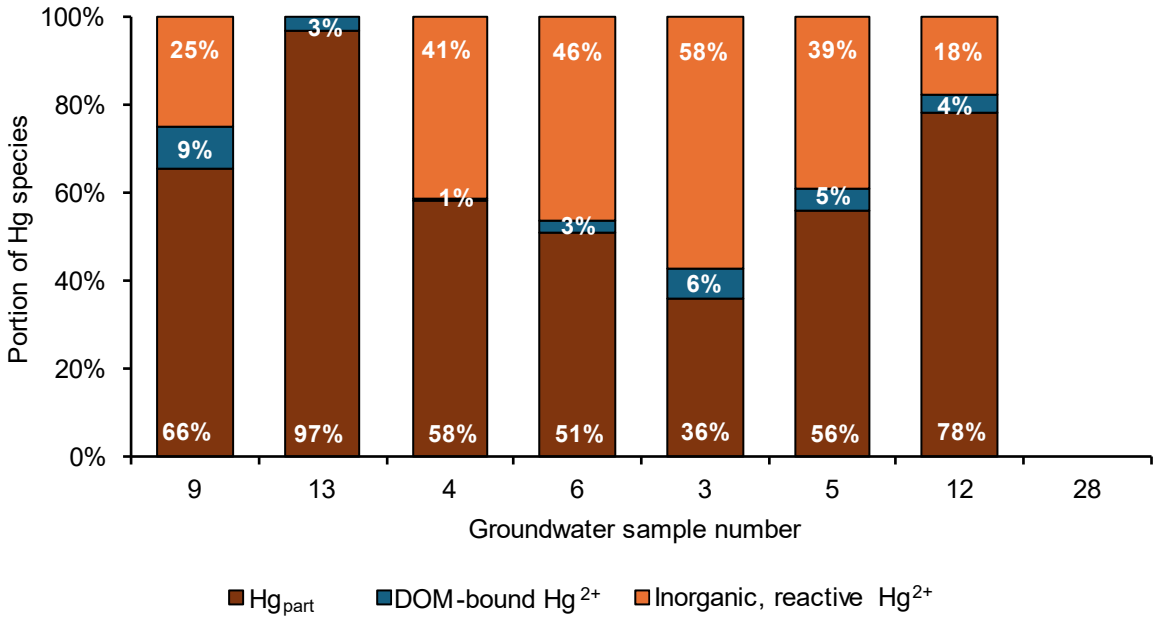

Fig. 2.4 Percentage content of Hg species in the Okochiri groundwater.

2.4.1.4. Hg distribution in sediments

Depth profiles for THg and total C concentrations in eight shallow sediment cores of the Okochiri WDP are shown in Fig. 2.5. The C is predominantly natural organic matter (NOM) generated from plant materials. The THg concentrations ranged from 10 to 529 µg/kg and C from 0.1 to 40 % across the eight shallow cores.

In core S–1, the THg concentration varied between 10 and 31 µg/kg. The concentration decreased with depth. Nevertheless, THg levels at all depths exceeded the average local reference value of 2 µg/kg. Despite the proximity of S–1 to the WDO, the THg concentration was low. This could be attributed to the low C content (0.3 to 0.8 %) and the absence of clay minerals that can retain the released Hg within the quartz-dominant sediment profile since organic matter is vital for Hg accumulation in sediments (Zhang et al., 2020). In S–2, the THg concentration ranged from 28 to 72 µg/kg, and the total C varied between 0.3 and 1.6 %. Unlike in S–1, the THg concentration in S–2 fluctuated with depth. The highest concentration occurred at a depth of 60 cm, and the lowest at 80 cm. The S–3 core had THg concentration that ranged from 258 to 529 µg/kg (median = 400 µg/kg), and the total C varied between 11 and 40 % (median = 20 %). Although S–3 was collected further from the WDO compared to S–1 and S–2, the core's high natural organic matter and low quartz content increased its Hg retention capacity (e.g., Zhang et al., 2020). Notably, the grain sizes were highly fine to medium fine across all depths. In S–4, the THg concentration ranged from 29 to 125 µg/kg (median = 42 µg/kg), and total C ranged from 0.2 to 19 % (median = 3 %). THg concentrations decreased consistently with depth. In cores S–5, S–6, and S–7, the THg concentration varied between 77 and 229 µg/kg, 38 to 87 µg/kg, and 65 to 142 µg/kg, respectively. The THg and C concentrations varied with depth. The THg concentration was relatively low in S–8, ranging from 34 to 54 µg/kg, and total C ranging from 0.1 to 4 %. Overall, the profile of THg and total C concentrations in the cores decreased with depth. While the THg concentrations were lowest at 100 cm depth in all eight cores, the concentrations were still above the local reference value. The lower C content at the 100 cm depths likely explains the lower THg concentrations at the bottom of the cores.

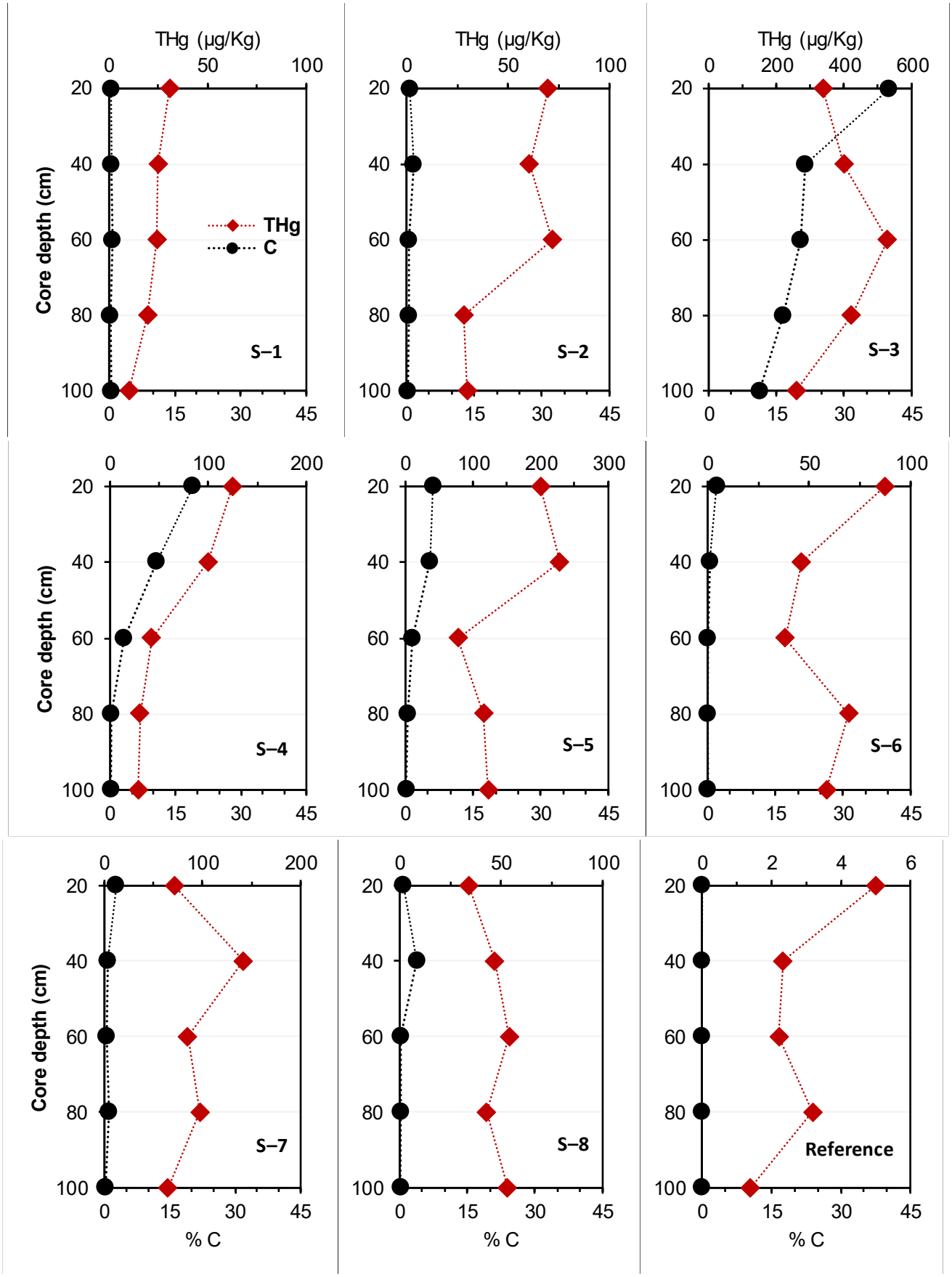

Fig. 2.5 Profiles of THg and % C in sediment cores collected from the WDP in Okochiri.

2.4.2. Discussion

2.4.2.1. Source, speciation and behavior of Hg in groundwater

THg concentrations in sediment samples have been used in several studies to trace Hg sources in groundwater (e.g., Bollen et al., 2008; González-Fernández et al., 2014; Kulikova et al., 2019; McLagan et al., 2022). This study compared the THg concentrations to those measured in the reference sediments collected within the same geological unit to identify Hg contamination.

As shown in Fig. 2.6, THg concentrations in sediments at the WDP were elevated compared to concentrations at the reference site. The sediments at the WDP had THg concentrations up to 230 times higher than the average value in the reference samples. Furthermore, during the operational period of the PHRC, the sediment accumulation rate was relatively constant in the area (i.e., 0.019 to 0.034 g cm^{-2} $year^{-1}$ over the last 80 years) (Omokheyeke et al., 2015). Hence, the fluxes of Hg in the accumulated sediments appeared to be influenced by the discharged production wastewater. Thus, an increase in the release of petroleum production wastewater could lead to increased Hg flux in the Okochiri.

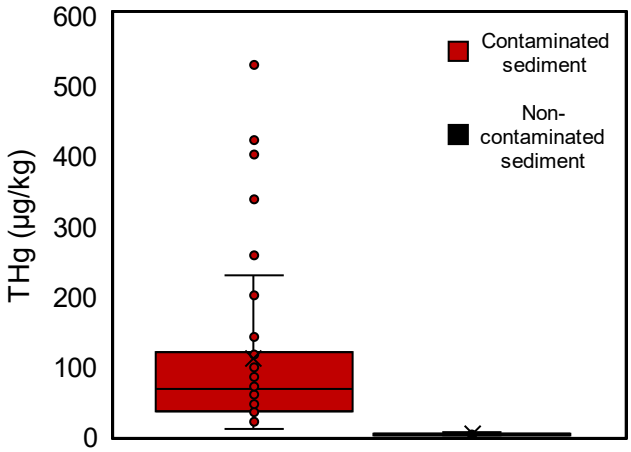

Fig. 2.6 Comparison between THg concentrations in the contaminated sediment and non-contaminated sediment (reference) collected within the same geological unit in Okochiri.

A general co-variation of THg and Hg_{diss} concentrations in the groundwater is given in Fig. 2.7a. It demonstrates a positive relationship between THg and Hg_{diss} concentrations in the groundwater, validating the reliability of our analytical

procedures. The elevated THg concentrations only occurred in wells next to the WDO. The WDO was constructed of concrete to prevent possible leakages into the underlying soil (see Fig. 2.1S). Nonetheless, cracks were evident within the WDO (see Fig. 2.2S); over time, Hg likely migrated in small amounts into the groundwater. Those cracks at different points within the WDO were most likely the only Hg entry point into the Okochiri groundwater. The wastewater in the WDO was the only possible source of Hg in the groundwater for the following reasons: (i) unlike in other coastal groundwater studies (e.g., Grassi & Netti, 2000; Spyropoulou et al., 2022), there was no positive correlation between THg and Cl or salinity in the Okochiri groundwater, suggesting that there was no Hg contribution from the nearby saltwater; (ii) all the PSWs and CSWs next to the WDO had THg concentrations varying between 0.2 and 6 µg/L, while concentrations consistently decreased with distance, and eventually to levels less than 0.01 µg/L in both PSWs and CSWs; (iii) the elevated THg concentrations in the sediments were only found in samples collected at the WDP. There, concentrations were up to 529 µg/kg, in contrast to the maximum of 5 µg/kg in sediments at the reference site. Hence, the WDO should be considered the only source of Hg for Okochiri groundwater. To identify Hg mobilization from the solid phase to the aqueous phase, a batch leaching experiment was conducted using sediments collected from the WDP. Results are discussed in Section 2.4.2.3.

SO_4^{2-} had a moderate positive correlation with THg ($r = 0.59$) and Hg_{diss} ($r = 0.58$) (Fig. 2.7b and c); the groundwater sample with the highest THg concentration (6 µg/L) was also among the richest in SO_4^{2-} (8.5 mg/L), suggesting that both Hg and SO_4^{2-} (e.g., Bagnato et al., 2009) in the Okochiri groundwaters were released simultaneously into the Okochiri aquifer as components of the petroleum production wastewater. The correlation supports the idea that petroleum production wastewater is the source of Hg in the groundwater.

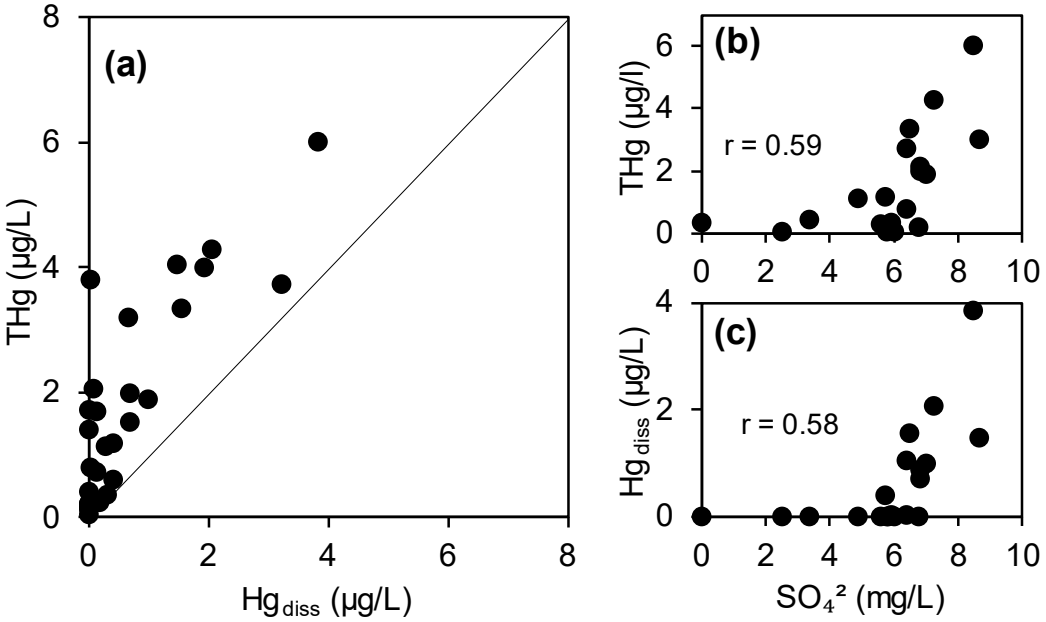

Fig. 2.7 (a) THg vs Hg_{diss} concentrations, **(b)** THg vs. SO_4^{2-}, and **(c)** Hg_{diss} vs. SO_4^{2-} for the wastewater-influenced groundwater in the Okochiri.

Although redox conditions in groundwater significantly influence the behavior and fate of Hg, Hg favors binding to DOM, where groundwater contains natural DOC (Wang et al., 2021). In this study, the DOC concentration ranged from 2 to 47 (median = 26) mg/L. However, this is not a naturally occurring DOC generated from plant materials at the land or subsurface, but petroleum hydrocarbon-based DOC generated from the ongoing oil and gas activities at the site. Notably, there was no correlation between the DOC and Hg in the groundwater, although they are both mobile, suggesting that petroleum hydrocarbon does not bind Hg. This further explains why there is a relatively low amount of Hg bound to DOM.

Nevertheless, due to the presence of a substantial amount of silica and organic carbon (OC) in the colloidal phase of the aquifer, it is more likely that the Hg here predominates as $Hg_{part,}$ as shown earlier. Furthermore, due to the presence of Cl^- and SO_4^{2-}, inorganic species of Hg (e.g., $HgCl_2$, HgClOH, $Hg(OH)_2$, $Hg(HS)_2$ or $HgHS_2$) can still occur in the groundwater. However, the occurrence and stability of these species would mainly depend on Eh and pH conditions in the groundwater (Bollen et al., 2008). The pH and Eh stability diagram based on groundwater data derived from this study is given in Fig. 2.8. In the groundwater, pH ranged from 4.4 to 6.1, and Eh varied between 238 and 801 mV (Table 2.1S). Thus, redox conditions favor the dominance of the inorganic species $HgCl_2(aq)$. However, the Hg also occurred

as $Hg(HS)_2$ and Hg(aq) (Fig. 2.8). Our laboratory data showed that Hg predominantly exists as Hg bound to particles (range: 36 to 97 %, mean: 63 %), suggesting the prevalence of Hg transport in the particulate phase in the Okochiri aquifer. However, the transport could be slightly lower than observed in the sample since groundwater pumping influences Hg mobilization in aquifers (Aleku, Lazareva, et al., 2024). Furthermore, 18 to 58 % (Mean: 33 %) exists as inorganic, reactive Hg (e.g., $HgCl_2$ and Hg_2Cl_2), while 1 to 9 % (mean: 4 %) exist as Hg bound to DOM. In contrast, Hg is unlikely to occur as $Hg(OH)_2$ due to the presence of Cl^- in the groundwater (up to 11 mg/L, Table 2.2S). Similarly, despite five samples plotting in the 'Hg^0(aq)' field and the possible dominance of Hg^0 in crude oil (UNEP, 2022; Wilhelm & Kirchgessner, 2001), Hg^0 was not found in the groundwater. This was possibly due to inaccuracies in the *in-situ* determination of Eh and pH or Hg^0 losses during sample collection.

The spatial distribution of Hg species in the groundwater shows that the proportion of reactive, inorganic Hg is highest in groundwater samples along the groundwater flow direction. This suggests that the soluble Hg species in the groundwater are highly mobile and can be transported over long distances.

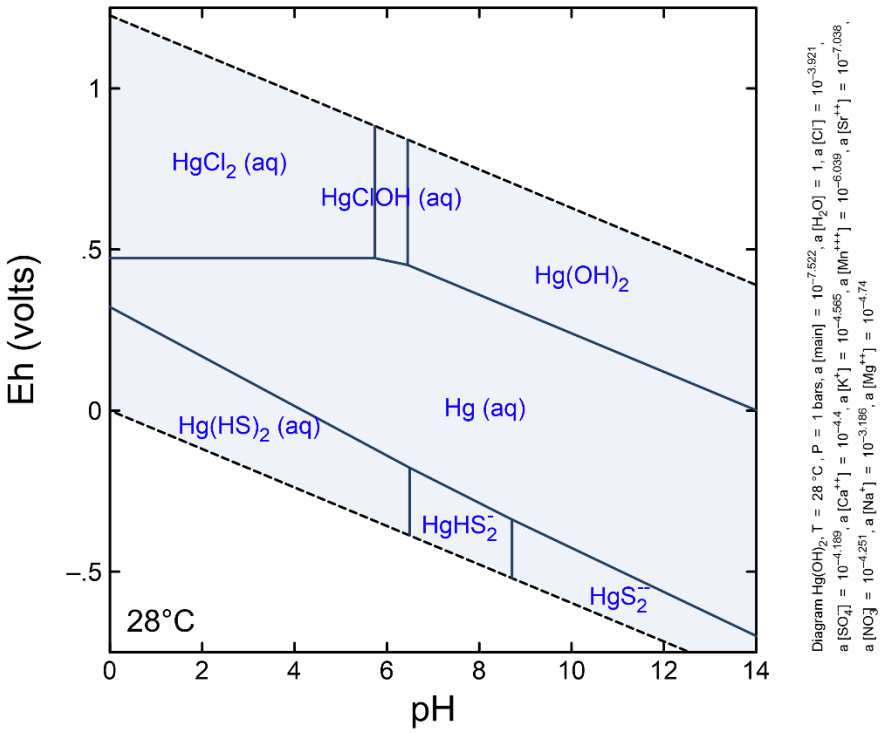

Fig. 2.8 Hg species as a function of pH and Eh, using calculated activities for the measured analytes and Miniteq thermodynamic data at 28°C. The diagram was generated using the Geochemist's Workbench (version 17.0.3). The stability diagram was constructed using chemical data from this study.

2.4.2.2. Role of organic matter on THg distribution in the sediments

In the combined data, a strong positive relationship between THg and % C was observed in the sediment cores (r = 0.79, *n* = 40, Fig. 2.9). Here, the % C in the sediments is predominantly naturally occurring organic matter generated from plant materials at the Creek. Nevertheless, due to several controlling factors (e.g., soil's C content, percentage of quartz grains, grain size distribution, and distance from the point source), the correlation between THg and % C was inconsistent across the eight sediment cores. THg had strong positive correlations with % C in S–4, S–5, and S–6 cores (r = 0.98, r = 0.86, and r = 0.75, respectively). This suggests homogeneously mixed surface materials associated with the point source of the contamination. The positive correlations in S–1 and S–2 cores were moderately positive (r = 0.34 and r = 0.42, respectively). In contrast, S7 and S8 had negative, weak correlations (r = – 0.23 and r = – 0.12, respectively), while there was no correlation in S1, suggesting heterogeneously mixed surface materials associated with the contamination. However, the significant correlation between THg and % C in the cores provides evidence that the transportation, distribution (lateral and depth) and binding of Hg in the wastewater-influenced sediments could be significantly influenced by the presence of NOM in the sediments (Chakraborty et al., 2015a; Outridge et al., 2007; Stern et al., 2009). In contrast, distance from the wastewater discharge point played a less significant role in Hg distribution in the sediments (Fig. 2.10a, b, c, d, and e).

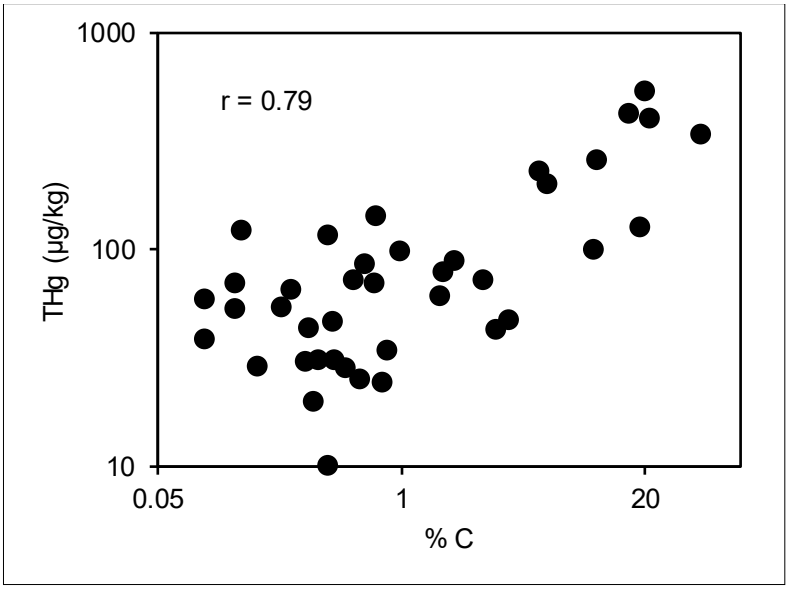

Fig. 2.9 Relationship between THg vs % C (all data plot) in the sediment cores.

Similarly, the sediment's grain size distribution had a relatively minor influence on the lateral distribution of Hg in the sediments. The sediments, mostly less than 1 mm in grain size, showed poor sorting and dominance of silty to sandy grain sizes across all depths (Table 2.4S). The highly permeable sediments (> 95 % quartz) and the NOM in the fine sediment fractions enhanced vertical Hg transport down the sediment core at our field site.

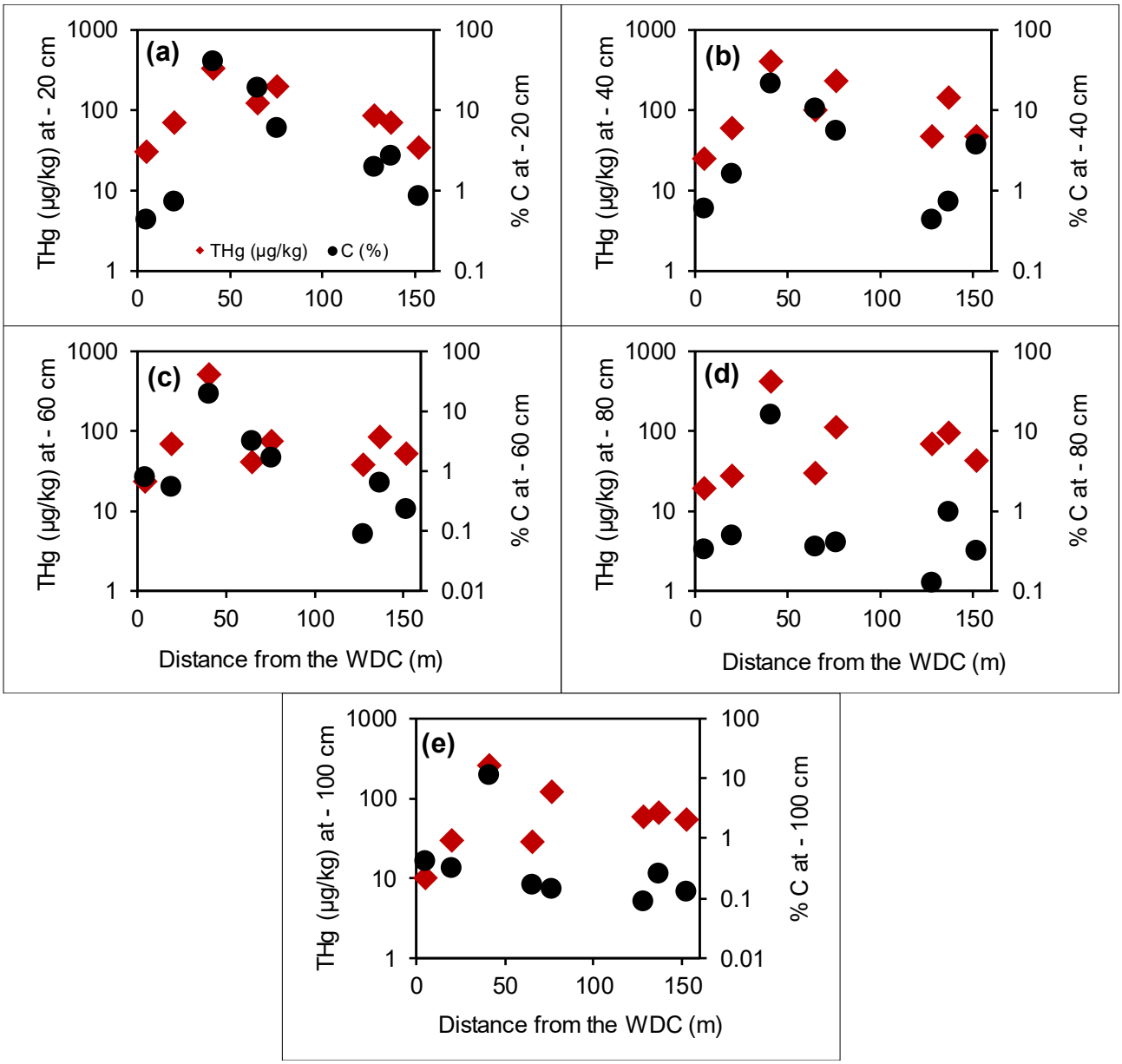

Fig. 2.10 Relationship between THg, % C and distance at **(a)** – 20 cm; **(b)** – 40 cm, **(c)** – 60 cm, **(d)** – 80 cm, and **(e)** – 100 cm core depths.

2.4.2.3 Hg retention in Okochiri aquifer

Our data suggests that elevated Hg concentrations in the groundwater were released from refinery production wastewater through the sediments in the Okochiri. Predicting the amount of Hg that can be released from the solid phase into the aqueous phase under oxic conditions is challenging; however, attempts have been made by carrying out batch-leaching experiments using the affected sediments (Bollen et al., 2008). Our results showed that the percentage of mobilized THg varied between less than 0.01 and 23.5 (median = 13.5) % as given in Fig. 2.11. Furthermore, the concentration of THg (extracted) and % C had a strong positive correlation (r = 0.78). In contrast, the concentration of Hg_{diss} was less than 0.01 µg/kg in all samples. The highest mobilization was found in S3-D. Before the experiment, the THg concentration found in sample S3-D (422 µg/kg) was the second highest in the sample set selected for the experiment. It was collected at a core depth of 80 cm with relatively little NOM present. Compared to the sample S3-C (collected at 60 cm depth from the same core) with an initial higher THg and % C concentration (529 µg/kg and 20 %, respectively), S3-D showed higher mobilization. This was due to the increased abundance of coarse grains and less organic matter in the S3-D sediment. As a result, the Hg retention capacity of the sediment was reduced, thereby increasing Hg mobility, unlike in S3-B and S3-C, which had a highly fine texture and higher C content (22 % C and 20 % C, respectively). Here, the retention is only controlled by NOM in the sediments. These conditions allowed Hg in S3-D to be easily mobilized, resulting in higher concentrations in the leachate. However, at lower concentrations (less than 199 µg/kg), Hg mobilization is unlikely to occur under oxygenated conditions. The result suggests that the mobilization of Hg in the Okochiri aquifer depends on the Hg concentration, amount of NOM and grain size distribution in the solid phase. This result supports the findings in Section 2.4.2.2.

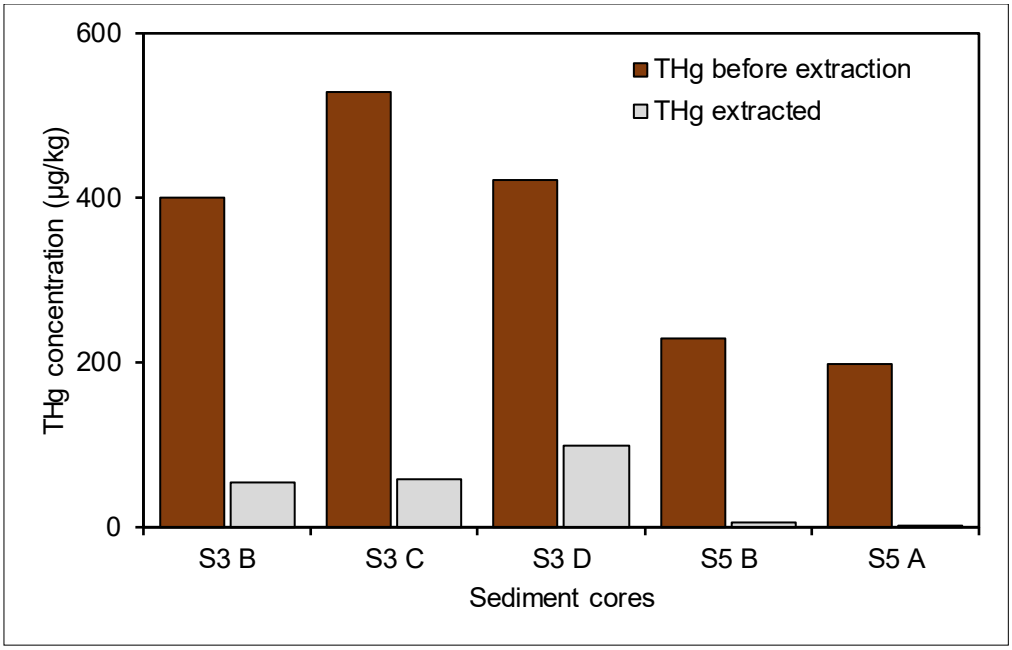

Fig. 2.11 Concentration of mobilized Hg in the study sediments. Sediment cores S3 B, S3 C, S3 D, S5 B, and S5 A were collected at – 40 cm, 60 cm, – 80 cm, – 40 cm, and – 20 cm depth, respectively.

Overall, the studies of the Hg-contaminated groundwater and sediment in Okochiri, eastern Niger Delta, have provided new information about the concentrations, source and speciation of Hg in a petroleum wastewater-affected area (Fig. 2.12).

The study showed that oil hydrocarbon is present in the groundwater and sediments. As a result, the concentrations of DOC and BTEX in groundwater at the Hg-contaminated site were elevated. Also, all sediment samples had a strong petroleum odor. Hence, the oil hydrocarbon contributed significantly to the OC load. Furthermore, Hg, along with SO_4^{2-}, was released from the wastewater reservoir and WDO into the Okochiri aquifer under oxic conditions (Fig. 2.12). Although Hg in the groundwater occurred as Hg_{part}, DOM-bound Hg^{2+} and inorganic, reactive Hg^{2+} species, DOM-bound Hg^{2+} was the least abundant despite the high concentration of BTEX and the hydrocarbon-based DOC. Moreover, in the sediments, Hg prefers binding to NOM rather than hydrocarbons. This shows that the OC generated from oil hydrocarbons has an insignificant influence on Hg retention or mobility in the groundwater and sediments in Okochiri. This, therefore, suggests that oil hydrocarbons do not bind to Hg. Here, NOM is the main component retaining Hg in the soil–groundwater system.

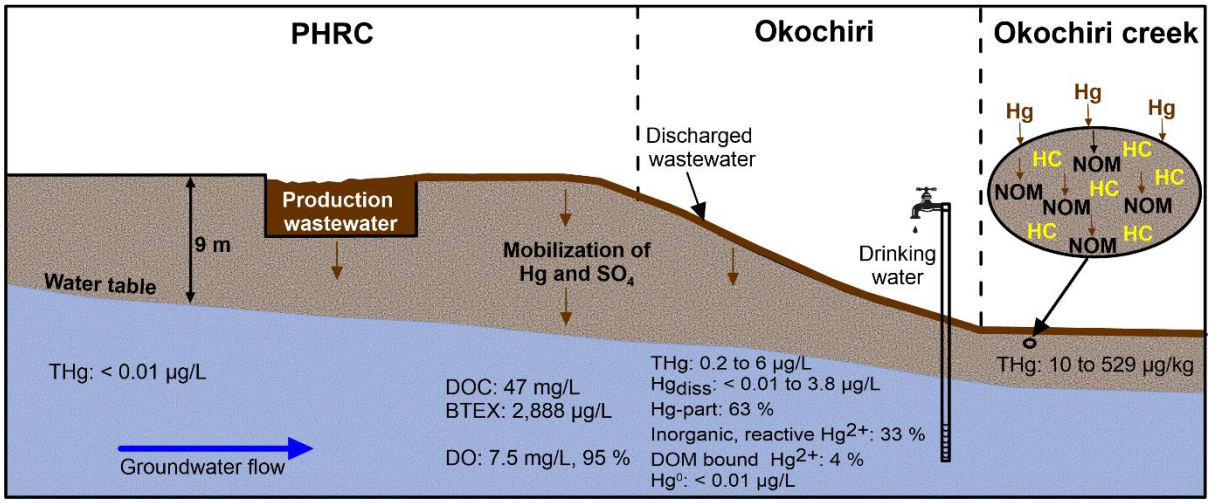

Fig. 2.12 Schematic representation (not to scale) of Hg source, concentrations, speciation and behavior in the groundwater and sediment of the eastern Niger Delta, Nigeria. *Notes: NOM: Natural organic matter, HC: Hydrocarbon.*

2.5 Conclusion

The groundwater and sediments of Okochiri contain elevated concentrations of Hg that were likely caused by the historical deposition of Hg due to petroleum production wastewater discharged into Okochiri Creek, which is also significantly influenced by NOM in the area. Hence, the binding of Hg to NOM is seemingly the most dominant process that controls the lateral and depth distribution of Hg in the Okochiri sediments.

In the groundwater, the elevated concentrations were found only in private supply wells and community supply wells next to the Okochiri wastewater discharge outlet (WDO). Through the WDO, the petroleum production wastewater was discharged into the Okochiri Creek. Our field observations suggest that cracks visible in the WDO allowed wastewater leakage into groundwater during the 52-year operational period of the Port Harcourt Refining Company. Assuming that the wastewater contained Hg, as demonstrated by our sediment data, cracks at different points within the WDO were most likely the Hg entry point into the Okochiri groundwater. The positive correlation between THg and Hg_{diss} vs SO_4^{2-} supported this result. The Hg occurred predominantly as Hg_{part}, accounting for 63 % of THg in the groundwater samples, indicating that most Hg in groundwater seems to be present and transported in the particulate phase. Despite the high DOC and BTEX levels,

inorganic, reactive Hg^{2+} and DOM-bound Hg^{2+} also occurred in the groundwater, accounting for the remaining 33 % and 4 % of the THg. This suggests that the groundwater Hg does not bind to petroleum hydrocarbon. Thus, the discharged oil and gas production wastewater from the refinery caused the increase in Hg concentrations in the aquifer.

3. Pipeline-related residential benzene exposure and groundwater natural attenuation capacity in the eastern Niger Delta, Nigeria

Dogo Lawrence Aleku[a], Harald Biester[b] and Thomas Pichler[a,*]

[a] *Institute of Geosciences, University of Bremen, 28359 Bremen, Germany*
[b] *Institute of Geoecology, Technical University Braunschweig, 38106 Braunschweig, Germany*

Abstract

Abstract This study was conducted to investigate the presence of benzene in the ground and drinking water in the eastern Niger Delta, where multiple oil and gas production facilities are present. Samples from drinking water wells were collected for measurements of benzene, toluene, ethylbenzene and xylenes (BTEX). Additionally, the dissolved organic carbon (DOC) concentration was determined for the first time to establish the groundwater's total hydrocarbon and non-hydrocarbon load. The groundwater BTEX and benzene levels were up to 3,904 µg/L and 3,500 µg/L, respectively. DOC concentrations were up to 49 mg/L. The highest benzene concentrations were detected in wells near an underground petroleum pipeline. However, the concentrations decreased with distance from the pipeline to levels less than 0.1 µg/L. Despite benzene contamination, the aquifer has shown promising aerobic attenuation potential, having up to 7.5 (95 %) mg/L DO level and 2.11 mg/L BTEX biodegradation capacity for DO. However, the high groundwater temperature of up to 32.5 °C may weaken attenuation. The benzene and BTEX point attenuation rates ranged from 0.128 to 0.693 day^{-1} and 0.086 to 0.556 day^{-1}, respectively. Hence, by natural attenuation alone, up to 66.5 and 85 years would be required to reach Nigeria's groundwater benzene and BTEX remediation goals, respectively.

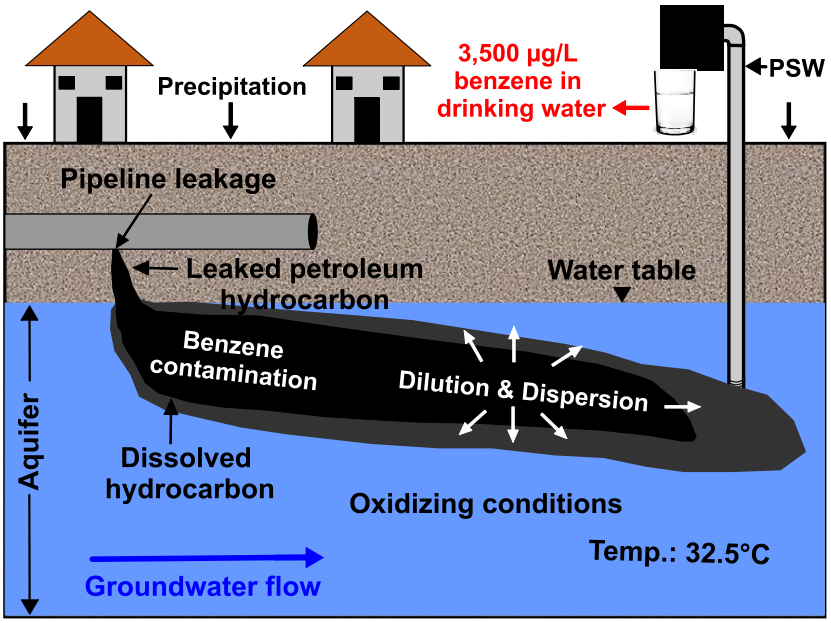

3.1 Introduction

Using pipelines to transfer oil and gas has become a widespread global practice because they are considered the safest and most economical, particularly when transporting over long distances (Ahmed et al., 2023; Feo et al., 2023). The Nigerian National Petroleum Corporation (NNPC) maintains a pipeline network of over 5000 km. Since the pipelines are constructed of carbon steel, leakage due to corrosion is a common problem (e.g., Unueroh et al., 2016). Additionally, problems of pipeline leakages resulting from oil theft/sabotage and vandalism (commonly called bunkering), aging infrastructure, corrosion, equipment failures, and operational failures have been frequently observed in oil and gas infrastructures worldwide (Ambituuni et al., 2015; Ekong et al., 2024; Feo et al., 2023; PHMSA, 2019; Umar et al., 2023). For instance, in Nigeria, Shell Nigeria reported 11,000 barrels per day of crude oil loss in their pipeline networks in 2018 due to leakages, an increment of about 550 % compared to the previous year's data (Ahmed et al., 2023). Such leaks are the main cause of oil losses and can lead to extreme environmental pollution, degradation and economic losses (Ambituuni et al., 2015; Ekong et al., 2024; Korlapati et al., 2022; Lu et al., 2020). Several studies have investigated the occurrence of pipeline leakages into groundwater (e.g., Baedecker et al., 1993; Baedecker et al., 1989; Bekins et al., 2020; Bennett et al., 1993; Cozzarelli et al., 2022; Cozzarelli et al., 1990; Essaid et al., 1995; McGuire et al., 2018), in the submarine environment (e.g., Lu et al., 2023;

Poursanidis et al., 2024; Zhao et al., 2024) and in soils (e.g., Ismailov & Nadjafova, 2022) for several locations worldwide. Also, investigations were reported for leakages in soils and groundwater near petroleum facilities and petroleum product spills (e.g., Adewuyi & Olowu, 2012; Gross et al., 2013; Nambi et al., 2017; Nwankwoala & Omofuophu, 2020; UNEP, 2011), petrol stations, and other gasoline-containing storage facilities (e.g., Chen et al., 2022; doRego & Pereira, 2007; Gomes et al., 2023; Joshua, 2020; Rao et al., 2017; Sivasankar & Gopalakrishna, 2017). As underground petroleum pipeline leaks, the frequently co-occurring monocyclic aromatic compounds, i.e., benzene, toluene, ethylbenzene, and the three forms of xylenes (o, m, p), commonly referred to as BTEX, might be released into groundwater along with other hydrocarbon constituents, including several polycyclic aromatic hydrocarbons and organochlorine compounds (An, 2004; Belpaire & Goemans, 2007; Gomes et al., 2023; Yang et al., 2023). These compounds, especially BTEX, can readily migrate through the soil (Kaur et al., 2023) and contaminate groundwater due to their highly soluble nature. The aqueous solubilities of benzene, toluene, ethylbenzene, and xylenes are 1780 mg/L, 515 mg/L, 161 mg/L, and 204 mg/L, respectively (Alexander, 1999; López et al., 2008; Mohammadi et al., 2020). To our knowledge, despite the substantial use of underground pipelines for crude oil transfer in the Niger Delta region (Umar et al., 2021), investigations on groundwater contamination from pipeline-related leakages are unavailable.

Of all the BTEX compounds, benzene is considered the most toxic (e.g., Behnami et al., 2023). Prolonged human exposure to benzene can lead to various health issues, including an attack on the central nervous system, the immune system, and the hematopoietic system and cause cancer (e.g., acute myeloid leukemia, myelodysplastic syndrome, aplastic anemia, pancytopenia), kidney conditions, liver damage, reduction in the size of women's ovaries, disruption of the menstrual cycle in women, and many other short-term health effects (IARC, 2018; WHO, 2017a, 2019). Exposure to the TEX compounds can also be detrimental to human health (e.g., Kuranchie et al., 2019; Zoleikha et al., 2017). As a result, the WHO (2017a) set a drinking water guideline value of 10 µg/L for benzene. Since groundwater is Nigeria's primary drinking water source, National Environmental Regulations (2011) set a remedial target value of 0.2 µg/L and an intervention value of 30 µg/L for benzene.

In groundwater, benzene undergoes several redox-controlled reactions. Under aerobic conditions, microbes can reduce benzene molecules into less toxic compounds, producing carbon dioxide and water: $C_6H_6 + 7.5O_2 \rightarrow 6CO_2 + 3H_2O$. Although benzene readily degrades under aerobic conditions (Bedics et al., 2022; Billersjö, 2013; Sohrabi et al., 2022), the extent of degradation depends on several factors, such as benzene concentration, the available population of microbes, availability of oxygen, available nutrients, prevailing pH conditions, and temperature (ATSDR, 2007; Bedics et al., 2022; Kaur et al., 2023). Degradation is slow if (1) the benzene concentration is very high and toxic to microbes (Vaishnav & Babeu, 1987), and (2) the conditions required to change the ring structure of the benzene to carbon dioxide gas molecules during benzene oxidation are not met (the process requires multiple electron transfer and substantial activation energies to remove electrons from the carbon atoms in the benzene ring) (Christensen et al., 2000). Nevertheless, the fate of benzene in contaminated groundwater systems seems to be primarily controlled by the availability of oxygen as a terminal electron acceptor (Vogt et al., 2011). Oxygen is rapidly depleted during benzene oxidation due to microbial respiration, creating anoxic conditions (Melkonian et al., 2021). Therefore, to further biodegrade the benzene, an alternative electron acceptor, such as NO_3^-, Mn^{4+}, Fe^{3+}, or SO_4^{2-}, and other benzene-degrading microbes capable of using the alternative electron acceptor must be available (Atashgahi et al., 2018; Toth et al., 2021; Wu et al., 2023). This process is, however, usually slow and is often associated with long lag times (Toth et al., 2021; Vogt et al., 2011), as benzene appears to be more persistent under anaerobic conditions than the TEX compounds (Vogt et al., 2011). Nevertheless, these natural processes, collectively referred to as natural attenuation (NA), can significantly reduce the concentration, mobility, bioavailability and toxicity of benzene in groundwater. As a well-known clean-up measure for petroleum-contaminated groundwater, assessing the NA potential at contaminated sites is important. Although NA has been widely applied (e.g., Choi & Lee, 2011; Cozzarelli et al., 2010; Kao & Prosser, 2001; Scow & Hicks, 2005; Wiedemeier et al., 1999), studies of its effectiveness in attenuating the petroleum-contaminated groundwater in the eastern Niger Delta have not been conducted.

The hydrocarbon-contaminated areas in the Niger Delta provide a unique opportunity to investigate benzene contamination and improve our understanding of

NA and the time required to reach Nigeria's groundwater clean-up goal by NA under aerobic conditions. To our knowledge, only a single study has been published on benzene occurrence in groundwater in the entire region (UNEP, 2011). That study reported concentrations that ranged from 0.155 to 48.2 µg/m^3 in indoor air and 161 to 9,280 µg/L in groundwater. Benzene data for Alode and Okochiri does not exist. Total petroleum hydrocarbon concentration in groundwater ranged from 649 to 86,100 µg/L in Nsisioken Agbi Ogale and 1,310 to 16,500 µg/L in Nkeleoken-Alode. Soil remediation was carried out in the affected community recently following UNEP recommendation, but published data on the current benzene level in the groundwater of Nsisioken Ogale and many other affected communities in the region are unavailable. Here, several investigations reported various disease symptoms associated with oil pollution, such as kidney diseases, respiratory problems, skin rashes, congenital disabilities, diabetes, headache, dizziness, throat irritation and chest pain (e.g., Nanadeinboemi et al., 2024; Nriagu et al., 2016; Ordinioha & Brisibe, 2013). Furthermore, Howard et al. (2021) and Enuneku et al. (2021) reported high cancer risk in the region due to oil pollution. Particularly detrimental is benzene since, through dermal absorption alone, the risk of contracting leukemia can increase by 70 % (e.g., Kalnas & Teitelbaum, 2000).

Since long-term exposure to benzene presents acute risks to human health (WHO, 2017a), assessing its concentration and fate remains essential to ensure the safe use of groundwater as a source of drinking water. This paper presents (i) the current level and distribution of benzene, (ii) source information and (iii) the potential and rates of NA and biodegradation capacity for benzene-contaminated groundwater in the eastern Niger Delta, Nigeria.

3.2 Materials and methods

3.2.1 Site description, geology, and hydrogeology

The study site is located in the eastern part of the petroleum-rich Niger Delta Region of Nigeria (Latitude 4°44′57′′N to 4°47′42′′N and Longitude 7°5′26′′E to 7°6′52′′E), where several oil spills were reported by UNEP (2011). Groundwater samples were collected from the Okochiri in the Okrika Local Government Area, Alode and Ogale in the Eleme Local Government Area of Rivers State. The sampling locations and the oil and gas production facilities are shown in Fig. 3.1. The Okochiri

is situated between the Port Harcourt Refinery (PHR) and the Okochiri Creek at approximately 4 m above sea level. Groundwater is flowing to the SSW. The community is characterized by (1) the Nigerian National Petroleum Corporation Limited (NNPCL) underground petroleum pipeline, which runs from the refinery to Umu Nwa (through Alode and Ogale), and Indorama Eleme Petrochemicals Plant (through Alode and Aleto), (2) Pipelines and Products Marketing Company (PPMC) 12-joint surface pipeline which runs from the refinery to the Nigerian Port Authority (Rivers Port Complex), and (3) wastewater discharge channel stretching for over 1 km from PHR (through the Okochiri) to Okochiri Creek. Alode is characterized by the presence of (1) the Shell Petroleum Development Corporation (SDPC) owned underground pipeline, (2) the NNPCL-owned refined petroleum product pipeline, and (3) two petroleum truck parking stations situated on the edge of the PHR to the north, and the north-west. Soil remediation for oil spill clean-up was completed at this location in April 2021. It was overseen by the Hydrocarbon Pollution Remediation Project (HYPREP) (an agency established in July 2012 under the Nigerian Ministry of Petroleum to manage the implementation of recommendations in the UNEP (2011) report).

Similarly, Ogale is characterized by (1) the presence of both SPDC and NNPCL-owned petroleum crude and product pipelines, (2) the intersection of several petroleum pipelines, including the SPDC-owned 28-inch trunk line which runs from Rumuekpe to Bomu, the 36-inch trunk line which runs from Nkpoku to New Ebubu and the abandoned 20-inch trunk line which runs from the Rumuekpe manifold to the Bomu manifold (UNEP, 2011), and (3) petroleum-contaminated drainage systems resulting from sales of petroleum products in plastic containers at roadside stalls. Although the pipelines run underground, visible signs indicate their routes and the width-extent in the three communities. Nevertheless, residential houses have been built next to the pipelines, the closest within 5 m from the pipelines.

Geologically, the region comprises three (3) major lithostratigraphic units: the (1) Benin Formation, (2) Agbada Formation, and (3) Akata Formation (Obaje, 2009). The Benin Formation is Oligocene to Recent in age. It mainly comprises coarse-grained, sub-angular to well-rounded, and poorly sorted coastal plain sand and alluvial deposits at shallow horizons (Avbovbo, 1978; Short & Stäuble, 1967). The formation, which extends to a depth of about 2 km (Tuttle et al., 1999), serves as a groundwater reservoir for the region (Ajaegwu et al., 2017). It also has excellent water-

yielding capacity, up to 6 to 9 L/s (Akujieze et al., 2003). The groundwater resources can be tapped within 3 to 300 m depth within the Formation (Adelana, 2008). Based on the hydrostratigraphic unit model developed by Akpokodje et al. (1996), the Benin Formation is considered homogeneous, and the groundwater flow direction is to the SSW. The Agbada Formation, Eocene to Recent, consists of a coastal sequence of alternating marine sands and shales (Ogbe et al., 2013; Short & Stäuble, 1967). It extends to a depth of up to 3.7 km (Tuttle et al., 1999). Obaje (2009) reported that sand percentage variation within the formation ranges between 30 to 70 %. The Paleocene – Recent Akata Formation consists of basal marine thick-shale units with < 30 % sand intercalations and little silt and clay (Obaje, 2009; Short & Stäuble, 1967). The formation extends up to 7 km depth (Adagunodo et al., 2017). The marine shales in the Agbada and the Upper Akata Formation are considered a source rock for the petroleum hydrocarbon in the region (Adiela & Odiri, 2018; Avbovbo, 1978; Diab et al., 2023; Ogbe, 2020).

Both shallow and deeper wells tap the aquifers of the Benin Formation. They comprise clay units, unconsolidated sand, and sandy gravels of about 95 to 99 % quartz grains (Onyeagocha, 1980). The 2,800 to 4,000 mm/year precipitation rate, vast catchment area, geology, North-Southwards groundwater flow, and rivers and streams contribute to the region's high perennial aquifer recharge (Abam & Nwankwoala, 2020; Ohwoghere-Asuma et al., 2023a). Consequently, the increased precipitation, sea level rise, flood and coastal erosion, poverty, coastal location, and intensive oil and gas industrial activities have left the shallow groundwater vulnerable to pollution (Adeniran et al., 2023; Ewim et al., 2023; Richard et al., 2023; Sam et al., 2023). However, deep-seated aquifers are considered safe and less vulnerable due to the intercalations of clay units (Abam & Nwankwoala, 2020). The protection of the Benin Formation's aquifers remains vital since the entire population in the region depends on them for their drinking water.

3.2.2 Groundwater sampling

Groundwater samples were collected in May 2021, April 2022 and April 2023 (50 samples in 2021 and 53 samples in 2022 and 2023) for DOC, cations, anions, and trace metal analysis. Samples were filtered through 0.45 µm cellulose acetate (CA) membrane filters and collected into 25 mL glass vials for DOC, 30 mL brown

HDPE vials for major cations, and 20 mL Zinnser vials for anions and trace metals. The sub-samples for DOC and major cations were preserved with 1 % concentrated hydrochloric acid (HCl) and stored at 4°C until transported to the laboratory for analysis. Samples were also collected for BTEX analysis during the 2022 and 2023 field campaigns.

The samples were collected from shallow wells (1 to 30 m) within the Benin Formation that serve as private supply wells (PSW) and community supply wells (CSW). Sampling locations were in three communities with suspected hydrocarbon contamination: Alode, Ogale, and Okochiri (Fig. 3.1). In Alode, 17 samples were collected from PSW within 350 m of the pipeline. In Ogale, 14 samples were collected from PSW within 640 m of the pipeline. Similarly, 22 samples collected in both PSW and CSW in Okochiri were within 285 m from the pipeline. In addition, 4 samples (REF 1 to REF 4) were collected in areas considered unaffected by oil and gas activities in Alode, Ogale and Okochiri (Fig. 3.1). The groundwater sampling for BTEX measurement followed the US EPA method 5021A (USEPA, 2003). Duplicate samples were collected unfiltered in 22 mL headspace vials, preserved with one spatula tip of $CuSO_4/Na_2SO_4$ and stored at 4°C until transported to the laboratory for analyses.

To ensure that “true or fresh” groundwater samples were collected, sampling was conducted during the early hours (between 6:00 and 8:00 a.m.) when residents were using the wells. Samples were collected by pumping where wells already had electric submersible pumps installed. First, groundwater was pumped into overhead storage tanks to purge the wells for 30 minutes before sampling directly from the wellhead. Manual sample collection was done with a water bail made of polyvinyl chloride. The bail was rinsed with water from the well three times before collecting a sample. All samples were collected fresh after pumping.

The pH, conductivity, total dissolved solids (TDS), temperature, dissolved oxygen (DO), salinity, redox potential (ORP), and resistivity were immediately determined *in situ* using a Hanna instrument HI98494 multiparameter. Total alkalinity ($CaCO_3$) was determined in the field by colorimetric titration with 0.16 N H_2SO_4 in combination with a bromcresol green-methyl red indicator. The bromcresol green-methyl red indicator powder was added to 100 mL of the groundwater sample and titrated using a Hach digital titrator to a light pink color. Total alkalinity was reported as $CaCO_3$.

During the sampling, a strong petroleum odor was observed in most wells, especially in Alode. Samples with strong petroleum odor also had free-phase petroleum hydrocarbon on the water surfaces, especially when left to sit for up to 10 minutes. Subsequently, a change in color, from colorless to reddish-brown, was observed in some samples collected within 5 m from the pipeline. Unfortunately, it was impossible to determine the water table and well depth for most wells because the well heads were sealed with concrete slabs (Fig. 3.1S) to prevent surface contamination and theft of submersible pumps installed in the wells. Most well owners rejected unsealing the wells for depth measurement during sampling. In those wells where measurement was possible, the water table and well depth ranged from 1 to 11 m and 9.8 to 30 m, respectively.

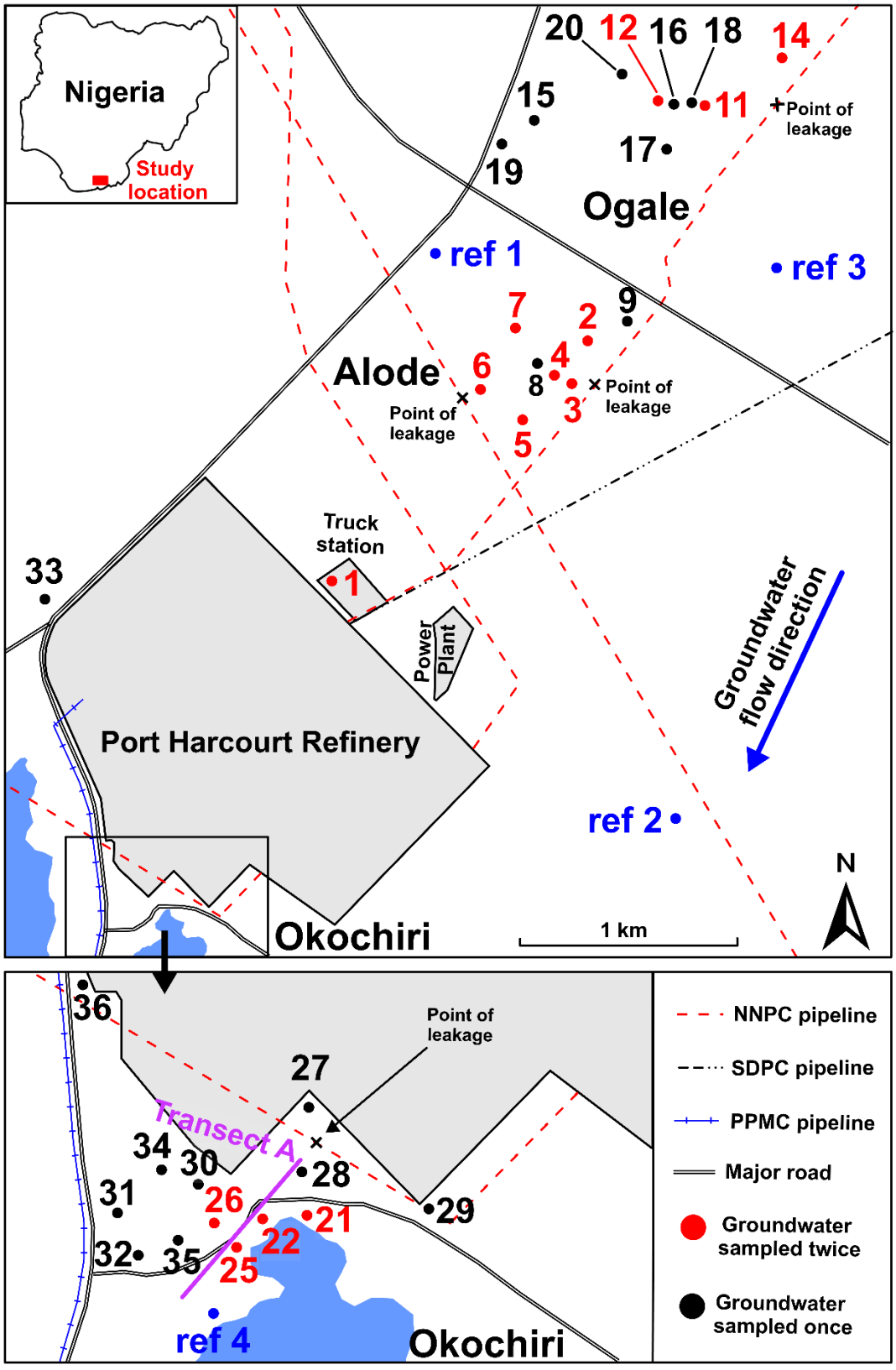

Fig. 3.1 Site map showing groundwater sample location and oil & gas production facilities. Transect A, indicated in purple, shows the groundwater flow path in the Okochiri.

3.2.3 Analytical procedures

3.2.3.1 Determination of BTEX and DOC

The BTEX measurements were performed using the "DIN 38407-F 43: 2014-10" method. The method combines gas chromatography and mass spectrometry using the static headspace technique (HS-GC/MS). The instrument used for the measurement was the Shimadzu QP2020 with GC-2030 and HS-20 Trap. If necessary, the samples were diluted before measurement. Five MilliQ water (Sartorius Inc., Göttingen, Germany) samples and five reference groundwater samples were measured, along with the study samples, for quality control.

Dissolved organic carbon (DOC), a fraction of organic carbon that can pass through 0.45 µm pore size, was determined using a Shimadzu TOC analyzer TOC-V CPN (Shimadzu Corporation, Kyoto, Japan). A certified Total Organic Carbon Standard of 50 mg/L (Aqua Solutions Inc., Texas, USA) was used to check the accuracy and precision of the method. The measurement error observed was < 6 %.

3.2.3.2 Anion and cation measurements

Major cations and trace metals were determined by inductively coupled plasma-optical emission spectrometry (ICP-OES) using a Perkin Elmer Optima 7300 DV instrument. Measurement precision was checked using EnviroMAT Groundwater Low (ES-L-2) and High (ES-H-2) certified water from SCP Science, Canada, showing errors of < 3 % for all analytes. Also, the accuracy of the measurement was checked using an internal standard, and errors < 4 % were observed. Anions were determined using a Metrohm 883 Basic IC plus instrument with a 5 µL injection loop and a Metrosep A Supp5 (150 × 4.0 mm; 5 µm) column. The accuracy and precision of the measurement were checked with an internal standard, and errors < 10 % were recorded.

3.2.3.3 Expressed biodegradation capacity and natural attenuation rate

Based on Wiedemeier et al. (1999), calculation of the expressed biodegradation capacity (EBC) was used to estimate the amount of BTEX degraded by a given terminal electron-accepting process (dissolved oxygen (DO) in this study):

$$\mathrm{EBC_{DO}} = \frac{[\mathrm{C_B} - \mathrm{C_P}]}{\mathrm{F}} \qquad (3.1)$$

where EBC_{DO} (mg/L) = expressed biodegradation capacity for dissolved oxygen, C_B (mg/L) = average background concentration of the DO, *C*P (mg/L) = the concentration of the DO within the plume, and *F* = the BTEX utilization factor using DO. Furthermore, point attenuation rates and half-lives were calculated for benzene and BTEX, following methods described by Newell (2002), McAllister and Chiang (1994) and Bockelmann et al. (2003) shown in equation (3.2), which is transformed into equation (3.3). The natural logarithm of benzene and BTEX concentrations were plotted against time to obtain the point attenuation.

$$C_t = C_0 e^{-kt} \quad (3.2)$$

$$\ln C_t = -kt \times \ln C_0 \quad (3.3)$$

where C_t = concentration of attenuated contaminant at time t (mg/L), C_0 = the initial concentration of contaminant (mg/L), t = time (days) after attenuation and k = the first-order attenuation (decay) rate constant (day^{-1}). The half-life, $t_{1/2}$ (days) (i.e., the time required to attenuate the initial concentration of the contaminant by 50 %) was computed using equation (3.4):

$$t_{1/2} = \ln(2)/k \quad (3.4)$$

Furthermore, using equation (3.5), the time required to reach the contaminant remediation goal can be estimated. Here, we used 1.3 mg/L, 0.620 mg/L, 1.0 mg/L and 0.460 mg/L as $C_{initial}$ for benzene and 1.305 mg/L, 0.6225 mg/L, 1.1194 mg/L, and 0.4609 mg/L as $C_{initial}$ for BTEX in samples W–21, W–22, W–12 and W–1, respectively, to calculate the time required to reach Nigeria's groundwater remediation goal for benzene (i.e., 0.2 µg/L) and BTEX (i.e., 0.8 µg/L) (National Environmental Regulations, 2011).

$$t_{goal} = [-\ln(C_{goal}/C_{initial})]/k \quad (3.5)$$

where t_{goal} = time (days) required to reach goal concentrations C_{goal} (mg/L), $C_{initial}$ = initial concentration of contaminant (mg/L).

3.3 Results and discussion

3.3.1 Results

3.3.1.1 Field measurements and chemical data

The groundwater's physicochemical and inorganic chemical composition showed slight variations in concentration between the three communities (Table 3.1). The pH was slightly acidic, in the range of 4.7 to 6.3, 4.1 to 6.6, and 4.5 to 6.1 in Alode, Ogale and Okochiri, respectively. Overall, the mean pH in the groundwater across the three communities showed only slight differences in the order of Ogale > Alode > Okochiri; however, the pH values were mainly below the WHO (2017a) drinking water guideline range of 6.5 to 8.5, a likely result of the breakdown of petroleum hydrocarbon into organic acid by microbes. Lin et al. (2014) observed a decrease in pH when microbes degraded hydrocarbons in aqueous systems.

The electrical conductivity (EC) values in the drinking water were relatively low across the three communities, ranging from 20 to 106 µS/cm, 20 to 364 µS/cm, and 21 to 207 µS/cm in Alode, Ogale and Okochiri, respectively. The EC values showed slight differences in the order of Alode > Okochiri > Ogale. Similarly, total dissolved solids (TDS) in the groundwater ranged from 10 to 53 mg/L, 10 to 183 mg/L, and 11 to 105 mg/L in Alode, Ogale and Okochiri, respectively. The wide range in EC and TDS values is controlled by salinity ($r = 0.99$) and Cl^- ($r = 0.53$) distribution in the study area. While the source of the salinity and Cl^- values has not been established yet, the concentrations might be heavily influenced by anthropogenic activities, e.g., indiscriminate disposal of household wastes into community drainages. Notably, the Cl^- concentrations were not influenced by the distance from the coast. The concentrations were lower in PSW near the coast and higher in PSW near the community drainages. Leachates from those drainages, which often contain contaminants, including Cl^-, infiltrate the groundwater and increase its Cl^- levels (Aweto et al., 2023). The EC, TDS, Cl^-, and salinity levels at the reference sites, which have comparatively less anthropogenic influence, had less variation, ranging from 19 to 24 µS/cm EC, 9 to 12 mg/L TDS, 4 to 6.6 mg/L Cl^- and 0.01 PSU salinity. The EC, TDS and Cl^- values were consistent with the findings by Eyankware et al. (2022), Nwankwoala and Walter (2012) and Abam and Nwankwoala (2020). Although the study area is in a coastal region, there was no indication of saltwater intrusion.

Groundwater salinity values ranged from 0.01 to 0.1 PSU (Alode), 0.01 to 0.17 PSU (Ogale), and 0.01 to 0.1 PSU (Okochiri).

The concentrations of the major ions and trace metals in the groundwater were generally within the acceptable drinking water guidelines set by the WHO (2017a). However, other trace metals (e.g., As, Cr, Ni, Co and Zn) were not detected in the groundwater. Since the aquifer comprises coastal plain sands of > 95 % quartz grains (Onyeagocha, 1980), limited ion exchange and minimal dissolution are expected, given that quartz is relatively inert under typical groundwater conditions. As such, the low TDS, EC and major ion values are attributed to the dominance of quartz grains in the aquifer.

Table 3.1. Groundwater chemical measurements in the study area

Parameter	Units	Okochiri (*n* = 15)	Ogale (*n* = 7)	Alode (*n* = 8)
pH		4.5 – 6.1 (5.4)	4.1 – 6.6 (5.2)	4.7 – 6.1 (5.1)
DO	mg/L	3.2 – 7.4 (6.3)	0.7 – 5.9 (4.2)	1.4 – 7.5 (5.5)
DO	%	41.4 – 97 (85)	9 – 74.5 (55.4)	19 – 95 (76)
Eh	mV	238 – 801 (652)	118 – 561 (427)	113 – 596 (401)
EC	µS/cm	21 – 207 (59)	20 – 364 (67)	20 – 106 (49)
TDS	mg/L	11 – 105 (30)	10 – 183 (33)	10 – 53 (25)
Temperature	°C	26.6 – 32.5 (29.3)	25.12 – 30.7 (29.4)	26.45 – 31 (30.8)
Salinity	PSU	0.01 – 0.1 (0.03)	0.01 – 0.17 (0.03)	0.01 – 0.1 (0.02)
Alkalinity	mg/L	0 – 25 (1)	0 – 100 (0)	0 – 30 (3)
DIC	mg/L	0 – 31 (1.3)	0 – 122 (0)	0 – 37 (4)
F^-	mg/L	< 0.01	< 0.01 – 0.2 (< 0.01)	< 0.01 – 3 (0.1)
Cl^-	mg/L	1 – 6 (5)	3 – 17 (8)	< 0.01 – 12 (4)
NO_2^-	mg/L	< 0.01	< 0.01 – 1 (< 0.01)	< 0.01 – 3 (< 0.01)
NO_3^-	mg/L	< 0.01 – 3 (2)	< 0.01 – 39 (2)	< 0.01 – 2 (< 0.01)
SO_4^{2-}	mg/L	1 – 14 (9)	1 – 23 (6)	1– 20 (6)
Ca	mg/L	0.5 – 1 (0.6)	0.2 – 13 (1)	0.5 – 12 (2)
Na	mg/L	0.6 – 15 (4)	1 – 14 (4)	0.6 – 10 (3)
K	mg/L	0.2 – 1 (0.4)	0.1 – 12 (1)	0.1 – 7 (1)
Mg	mg/L	0.04 – 0.4 (0.2)	0.02 – 4 (0.1)	0.1 – 1 (0.3)
Si	mg/L	0.5 – 5 (4)	0.3 – 4 (3)	1 – 4 (3.6)
Fe	mg/L	0.01 – 25 (0.2)	0.01 – 50 (2)	0.01 – 7 (1)
Mn	mg/L	0.01 – 0.3 (0.1)	0.01 – 0.2 (0.02)	0.01 – 0.2 (0.03)
Sr	mg/L	0.002 – 0.01	0.001 – 0.02 (0.003)	0.001 – 0.03 (0.01)
DOC	mg/L	3 – 33 (24)	9 – 49 (30)	16 – 47 (32)

Notes: DO: Dissolved Oxygen; DOC: Dissolved Organic Carbon; DIC: Dissolved Inorganic Carbon; EC: Electrical Conductivity; TDS: Total Dissolved Solids; NA: Not Analyzed; n: number of samples. The values in parentheses are the median.

Based on the major ions, the hydrochemical facies of the groundwater were evaluated through the trilinear Piper diagram (Piper, 1944). Two water types were identified: sodium–chloride (Na-Cl, 74 %) and calcium–chloride (Ca-Cl, 26 %) (Fig. 3.2). In Alode, the facies were 62 % Na-Cl and 38 % Ca-Cl type. In Ogale, the facies were 75 % Na-Cl and 25 % Ca-Cl type, whereas in Okochiri, closest to the coast, the facies were 83 % Na-Cl and 17 % Ca-Cl type. Despite the Na-Cl type dominance, there was no incidence of saltwater intrusion in the groundwater (salinity: 0.01 to 0.17 PSU). Anthropogenic influence, rather than mixing freshwater with saltwater, was likely responsible for the Na-Cl water type in this study.

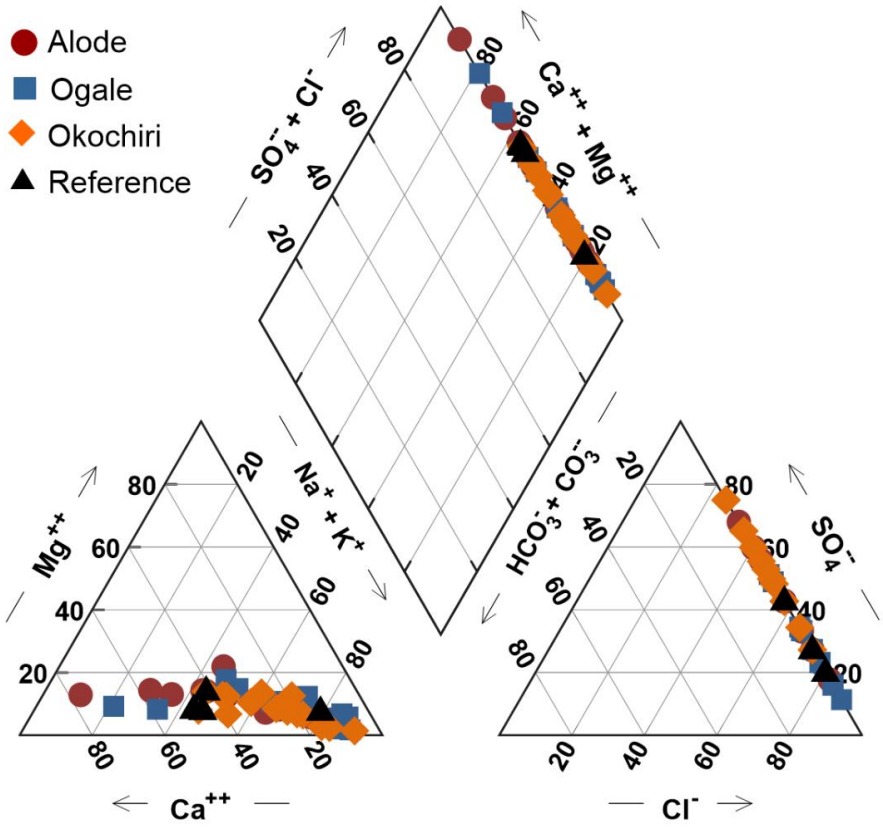

Fig. 3.2 Piper diagram for groundwater of the study area.

3.3.1.2 Benzene and TEX concentration

As shown in Fig. 3.3, the concentration of benzene, toluene, ethylbenzene, xylenes and trimethylbenzene varied between less than 0.1 and 3,500 µg/L, less than 0.1 to 210 µg/L, less than 0.1 to 370 µg/L, less than 0.1 to 360 µg/L and less than 0.1 to 220 µg/L. The total BTEX levels ranged from 0.1 to 3,904 µg/L.

Although benzene, toluene, ethylbenzene, trimethylbenzene and xylenes were released into the subsurface simultaneously, their concentrations vary significantly in the groundwater. The benzene concentration dominates in the wells, with a Pearson correlation coefficient of r = 0.97 in 2022 and 2023. Fig. 3.2S, 3.3S and 3.4S show the percentage comparison between concentrations of benzene, toluene, ethylbenzene, xylenes and trimethylbenzene in Alode, Ogale and Okochiri, demonstrating the dominance of benzene in the study groundwaters. Overall, the order of abundance was benzene > trimethylbenzene > ethylbenzene > xylenes > toluene. In 2022, benzene constituted 91 % in Alode, 72 % in Ogale and 97 % in Okochiri. In 2023, those values were 85 % in Alode, 66 % in Ogale, and 90 % in Okochiri.

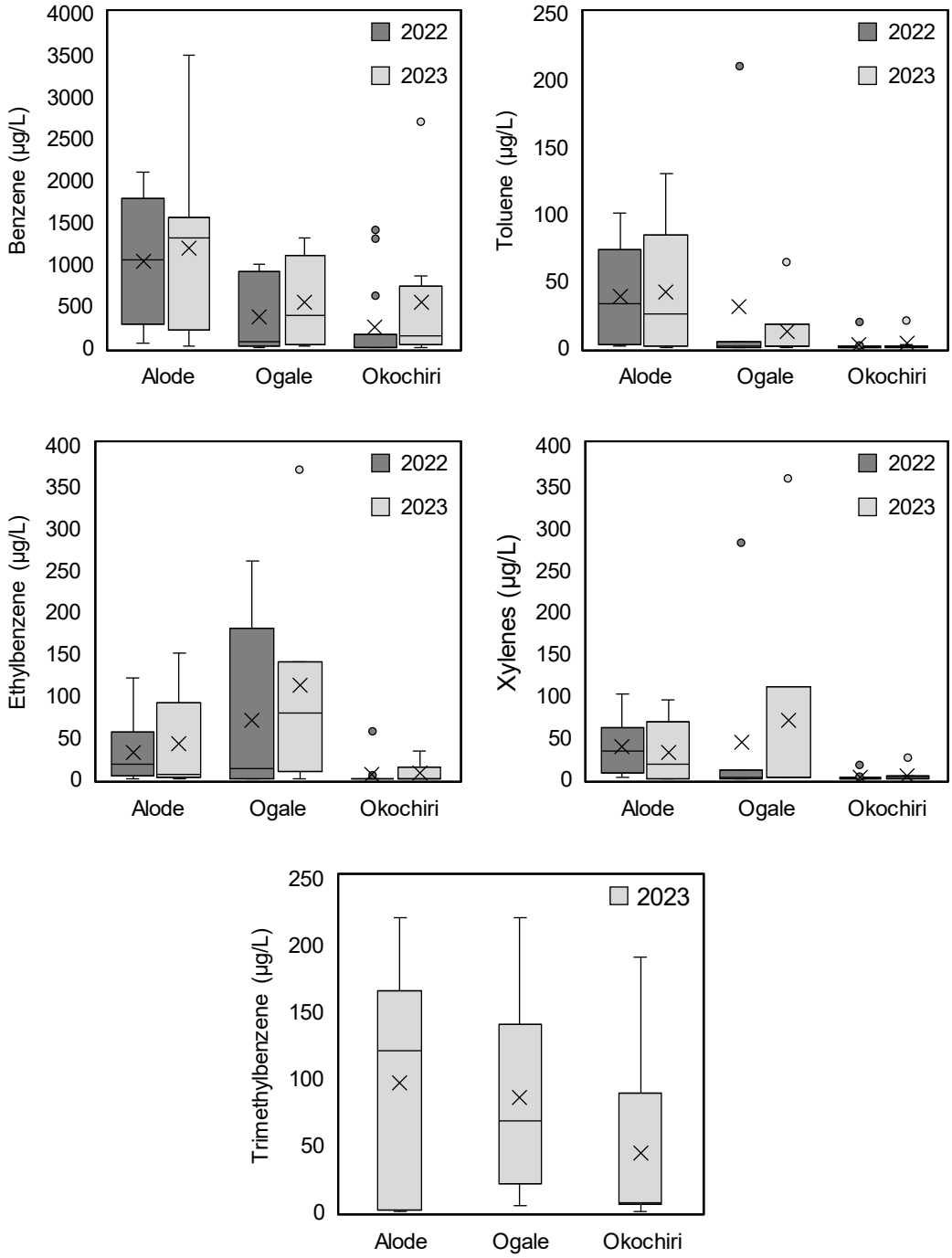

Fig. **3.3** Box plot of benzene, toluene, ethylbenzene, xylenes and trimethylbenzene concentrations in the study area. The edges of the box represent the 75th and 25th percentiles, respectively. The 'x' sign in the box represents the mean value. The solid line represents the median value. The branch gives the range of the data except for the outliers.

3.3.1.3 Dissolved organic carbon (DOC)

The DOC results are given in Fig. 3.4 and Table 3.1. The concentrations varied between 2.7 and 54 mg/L. Overall, high concentrations were observed in wells with strong hydrocarbon odor. Concentrations across the study sites were consistently within the same range throughout the sampling campaign, averaging 26 mg/L, 26 mg/L and 28 mg/L for Okochiri, Ogale and Alode, respectively.

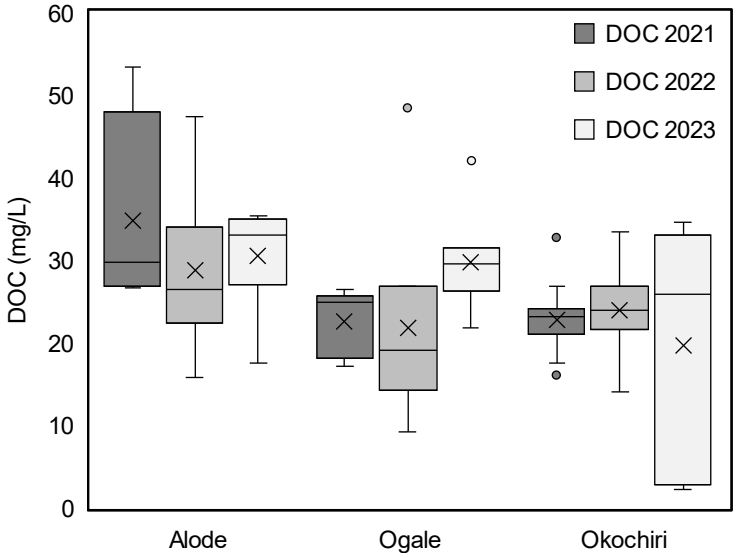

Fig. 3.4 DOC concentrations in the study area. The box's edges represent the 75th and 25th percentiles, respectively. In the box, the 'x' sign and the solid line represent the mean and median values, respectively. The branch gives the range of the data except for the outliers.

3.3.2 Discussion

3.3.2.1 Source, transport and fate of benzene

3.3.2.1.1 Source

At Alode, benzene concentration in the groundwater was up to 3,500 µg/L. The elevated benzene concentrations in the groundwater were found along the NNPCL petroleum pipeline, which runs from PHR to Umu Nwa, passing through Alode and Ogale. Samples from wells on the western side of the NNPCL pipeline had a strong hydrocarbon odor and free-phase hydrocarbon when left to sit for a few minutes. In contrast, the wells on the pipeline's eastern side do not show similar characteristics. As groundwater flows in the SSW direction, benzene is transported in

that direction, contaminating wells on the pipeline's eastern side. Concentrations ranging from 220 to 3,500 µg/L occur between 1 to 550 m distance, while lower concentrations occurred in PSW further away from the pipeline. Nevertheless, all the sampled wells in 2022 and 2023 had elevated benzene, up to 350 times higher than the WHO-recommended drinking water value of 10 µg/L.

In Ogale, the benzene level was up to 1,300 µg/L in the groundwater. Like the situation in Alode, wells on the western side of the NNPCL-owned petroleum pipeline had a strong hydrocarbon odor with free-phase hydrocarbon when left to sit for a few minutes. However, similar behavior was not observed in wells sited on the eastern side of the pipeline. Elevated benzene concentrations, up to 1,300 µg/L, were observed at a distance of up to 700 m from the pipeline, along the groundwater flow direction. UNEP (2011) observed high benzene concentration in PSW 11 (labeled 001-005-BH-102 in their study), but the concentration was approximately 8 times higher than our data in that well. This may be attributed to the NA effect due to DO availability and the soil remediation by HYPREP in Ogale in 2021.

In Okochiri (the host community to PHR), the benzene concentration was up to 2,700 µg/L in groundwater. The highest benzene concentrations were observed in PSW 21, 22, 27, and 28, close to the NNPCL underground petroleum pipeline, which runs from PHR to Umu Nwa through Alode and Ogale. Based on the groundwater samples taken along transect A in Okochiri (Fig. 3.1) along the groundwater flow direction, the benzene (and other TEX) concentration decreased significantly away from the pipeline leakage point (Fig. 3.5). Benzene and other TEX compounds were undetected in wells more than 250 m from the pipeline.

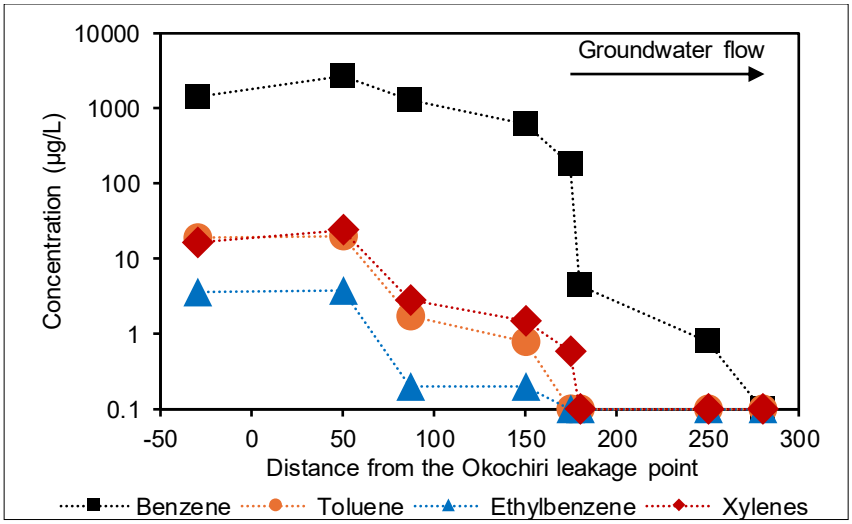

Fig. 3.5 Relationship between groundwater benzene and other TEX concentrations vs distance from the petroleum pipeline leakage point in Okochiri for groundwater samples taken along the flow direction (transect A). The wells plotted are, from left to right, PSW 27, 28, 21, 22, 25, 26, 35 and REF 4.

The presence, level and distribution of benzene in the groundwater of the three communities depend mainly on (1) the distance of PSWs and CSWs from the underground NNPCL petroleum pipeline, suggesting possible leakages of petroleum hydrocarbon into the corresponding groundwater, (2) the amount of hydrocarbon leakage from the NNPCL pipeline, and (3) the groundwater flow direction.

As the NNPCL petroleum pipeline leaks in the subsurface, benzene and other organic pollutants are released, contaminating groundwater. This occurs in three stages, as outlined by Zhang (2010) and Freeze and Cherry (1979): (1) the seepage stage, where gravitational and capillary forces influence the lateral migration of benzene from the oil-wetting zone in the soil into the corresponding groundwater, (2) seepage of the petroleum ceases when it reaches the water table and subsequently floats on the groundwater, and (3) the separate phase migration where vaporization and slight dissolution of some of the benzene into the groundwater occurs. The dissolution further leads to benzene lateral transport with the groundwater flow (Pantazidou & Sitar, 1993). However, concentrations usually decrease further away from the seepage source. Hence, in the study area, the high amount of precipitation facilitates benzene transport into the groundwater (Wadge & Salisbury, 1997), while the groundwater flow direction controls the extent and movement of the contamination plume.

Table 3.2 compares groundwater BTEX levels of the current study with previous results from the same locations and published results from other countries with similar underground petroleum leakage issues (e.g., Baedecker et al., 2011; Baedecker et al., 2018; Chen et al., 2022; Cozzarelli et al., 2022; Gomes et al., 2023; Joshua, 2020; UNEP, 2011). All other study locations, except Eleme (Ogale) in the Niger Delta of Nigeria (UNEP, 2011) and Utah, USA (Weidemeier et al., 1996), have lower groundwater benzene levels than the current study. The pipeline presence and the continuous transport of petroleum products from the PHR refinery to other parts of the country through the pipeline might be responsible for the high benzene levels observed in Ogale, Alode, and Okochiri groundwater compared to different locations. The groundwater benzene concentration was several orders higher than that of Brazil (Bragança), India (Bengaluru), China (Petrochemical Site near the Yangtze River), and Nigeria (Bonny) groundwater, as shown in Table 3.2. However, the current study's toluene, ethylbenzene, xylenes and trimethyl benzene concentrations are comparable to results published for other areas.

Table 3.2 Comparison of BTEX concentration (µg/L) in the eastern Niger Delta region groundwater with other groundwater studies.

Location	Benzene	Toluene	Ethyl-benzene	Xylenes	Trimethyl benzene	Source
Bragança, Brazil[1]	<0.1–0.6	<0.1–10.4	<0.1	<0.1–0.5	NA	UST at gas station
Bengaluru, India[2]	<0.1–485	<0.1–153	<0.1–80	<0.1–2,620	NA	UST at gas station
China	<0.1–644	<0.1–16.7	<0.1–209	<0.1–181	NA	Petrochemical site
Bonny, Nigeria[3]	<0.1–660	<0.1–800	<0.1–250	<0.1–4,200	NA	Petroleum spillage
Eleme, Nigeria[4]	161–9,280	NA	NA	NA	NA	Petroleum spillage
Minnesota, USA[5]	<0.1–2,550	<0.1–10.37	0.3–3.26	<0.1–1,230.7	<0.1–678.23	Pipeline rupture
Utah, USA[6]	<0.1–5600	<0.1–5870	2–950	36–9050	2–650	Hydrocarbon storage facility
Eleme/ Okrika, Nigeria[7]	<0.1–3,500	<0.1–210	<0.1–370	<0.1–360	<0.1–220	Pipeline leakage

ND: Not detected; NA: Not analyzed; Underground Storage Tank: UST; References 1: Gomes et al. (2023); 2: Joshua (2020); 3: Nwankwoala and Omofuophu (2020); 4: UNEP (2011), 5: Cozzarelli et al. (2022), 6: Weidemeier et al. (1996), 7:This study.

3.3.2.1.2 Benzene concentrations in relation to toluene, ethylbenzene, trimethylbenzene and xylenes

Being a soluble compound, and in the presence of the high BTEX concentration, aerobic removal of the more easily degraded TEX compounds may be

responsible for the abundance of benzene in the Ogale and Okochiri groundwater (Johnson et al., 2003). It has been shown that TEX compounds degrade at higher rates than benzene when specific benzene-degrading bacteria capable of oxidizing the aromatic ring are unavailable (El-Naas et al., 2014). Although oxygen appears to be available for degradation in the study area, the groundwater benzene levels remain high. In an experiment, Eziuzor et al. (2021) collected sediments from the study area, i.e., Eleme (Alode and Ogale), as well as other locations in the region (i.e., Tai, Gokana and Khana) to test the benzene degradation potential. The sediments were spiked with a mixture of benzene, ethylbenzene and naphthalene dissolved in acetone and left to sit for one year to monitor the potential for hydrocarbon degradation in the sediment. The result suggests that the benzene degradation is too slow to detect by analyzing benzene removal or that the benzene degraders were absent in the sediments. Relatively, sediments collected from Khana showed slightly higher degradation potential than sediments collected from Eleme (the study area), Gokana and Tai.

Few samples, however, have less dominance of benzene (e.g., PSW 11 had 55 % in 2022 and 54 % in 2023 and PSW 7 had 64 % in 2022 and 75 % in 2023). In contrast, sample PSW 17 had an ethylbenzene (11 µg/L) dominance, up to 91 %, with 1 % benzene, 1 % toluene, and 7 % total xylenes (Fig. 3.4S). The dominance of ethylbenzene in PSW 17, while benzene is dominant in all the other 52 samples, suggests the possible presence of distinct microbial communities that may preferentially degrade benzene, toluene, and xylenes over ethylbenzene. Since the groundwater is mainly oxygen-saturated, the aerobic microbial communities can break down the benzene, toluene and xylenes using the available oxygen as an electron acceptor. This process likely depleted the DO level in PSW 17 to 1.53 mg/L (19 %), making it the lowest in the 2022 data set. The role of DO in the natural degradation of benzene will be discussed in more detail in Section 3.3.2.2.

3.3.2.1.3 Dissolved organic carbon (DOC) in the eastern Niger Delta

The residents of Ogale and Alode suggested that oil spills resulting from pipeline failure first occurred in 2005 in Ogale. As a result, HYPREP carried out soil remediation to clean up the affected areas. Although the remediation activities ended in 2021 in Ogale and Alode, most wells in those communities still have a mild to

pungent hydrocarbon odor, and some well waters show free-phase hydrocarbon after sitting for about 10 minutes. Those wells, as well as a few other wells with little or no hydrocarbon odor, all have elevated DOC concentrations. The generally high DOC (> 4 mg/L), unusual for natural groundwater, indicates groundwater contamination derived from anthropogenically released organic pollutants (Regan et al., 2017). Most of the DOC is likely dominated by hydrocarbon degradation intermediates (Bekins et al., 2020; Bekins et al., 2016; Podgorski et al., 2018). The DOC levels, therefore, reflect the total hydrocarbon and non-hydrocarbon load in the groundwater. The shallow and sandy nature of the aquifer and the amount of precipitation in the area facilitate the infiltration of DOC from these sources into the aquifer (Chinago, 2020; McDonough et al., 2020).

In oxic groundwater where aerobic respiration is present, DOC typically shows an inverse relationship with DO (Rajendiran et al., 2023) that depends on the bioavailability of the DOC (Chapelle et al., 2012). In Alode and Ogale, DOC poorly correlates with DO, indicating either the absence of aerobic respiration or that DOC is not bioavailable for microbial respiration. In Okochiri, however, there seems to be a moderate negative trend (r = -0.43), suggesting possible microbial respiration ongoing in the aquifer. Generally, the microbes in the study area utilized the available oxygen to metabolize and break down the DOC into CO_2 and HCO_3^-, leading to its slight decrease in concentration (DOC vs HCO_3^- showed a moderate positive correlation, r = 0.5). In instances where a specific microbial population capable of degrading DOC is high in Alode, Ogale and Okochiri aquifers, DOC will be degraded, depleting DO in the process. When the DO is wholly consumed, electron acceptors such as NO_3^-, Mn^{4+}, Fe^{3+}, and SO_4^{2-}, if available, will further oxidize DOC (Christensen et al., 2000).

3.3.2.1.4 Fe contamination and influence on the fate of benzene

While the major ions and trace metal concentrations were relatively low or undetected in some wells, Fe^{2+} concentrations in some samples were elevated. Alode, Ogale and Okochiri concentrations varied between 0.01 to 7 mg/L, 0.01 to 50 mg/L, and 0.01 to 25 mg/L, respectively. The highest concentrations were observed in wells located near the NNPCL pipeline in Okochiri and Ogale. Wells situated further away have lower concentrations, usually between 0.01 to 0.3 mg/L of Fe, and in some cases, undetected. Along the NNPCL petroleum pipelines, accumulation of Fe precipitates as

stains (reddish-brown rust particles) were observed on surfaces of (1) polyvinyl chloride (PVC) overhead tanks used for storage of drinking water (Fig. 3.6) and (2) plumbing fixtures, as well as other domestic water containers (Fig. 3.5S). This phenomenon usually occurs under oxic conditions (Appelo & Postma, 2005; Ryan & Gschwend, 1992; White, 1990). The reddish-brown rust particles ($Fe(OH)_3$) resulted from the reaction between Fe and DO in the groundwater, as shown: $4Fe^{2+} + O_2 + 10H_2O \rightarrow 4Fe(OH)_3 + 8H^+$. The precipitation was also observed in samples left sitting for about 10 minutes after abstraction, suggesting the release of Fe from the nearby underground pipelines.

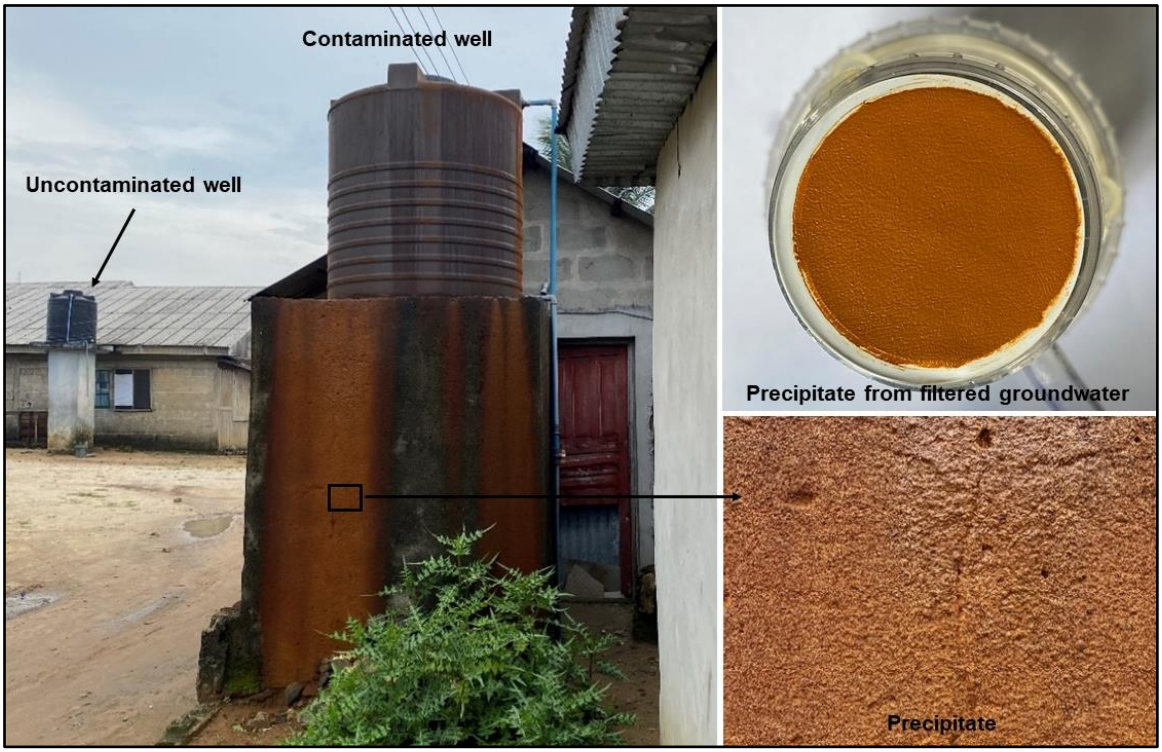

Fig. 3.6 Accumulated precipitates on PVC overhead drinking water storage tank situated directly above the NNPCL pipeline in Okochiri.

pH plays a significant role in the oxidation process, as the solubility and precipitation of Fe are pH-dependent. In the study wells, while > 95 % of Fe concentrations are < 4 mg/L, the elevated concentration shows a positive relationship with pH (r = 0.75 in 2022 and 0.54 in 2023, Fig. 3.7), demonstrating Fe precipitation under slightly alkaline conditions. As groundwater becomes more alkaline, Fe ions become less soluble and tend to come out of the solution, forming visible solid particles (i.e., the reddish-brown rust particles). Since rusts primarily contain Fe oxides, and the

groundwater samples were acidified to pH < 2 with 2 % HNO_3 after filtration, the low pH condition favored further dissolution of the rust, which was analyzed as Fe^{2+}.

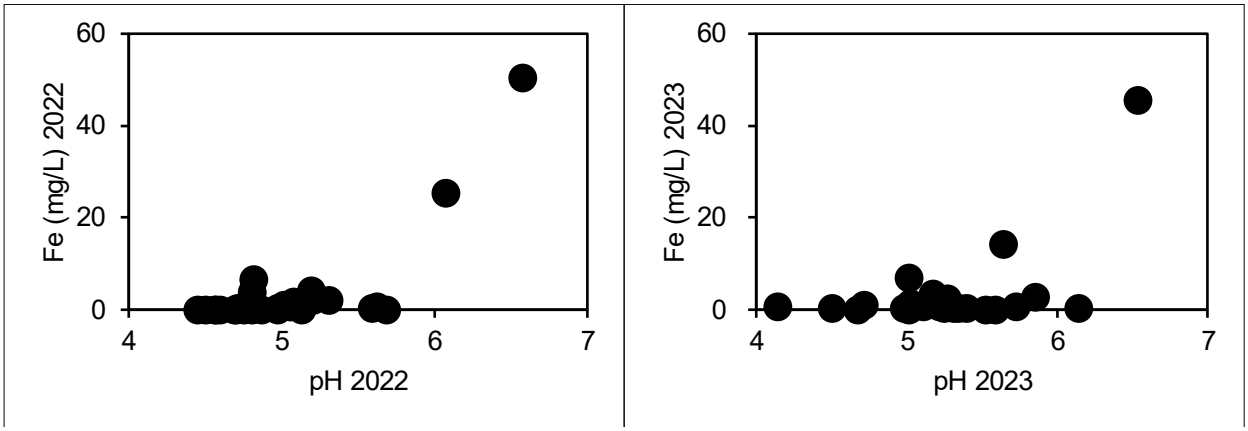

Fig. 3.7 Relationship of Fe vs pH in the groundwater in 2022 and 2023

Being an electron acceptor, iron is significant in anaerobic degradation of petroleum hydrocarbons (Castro et al., 2022). van Leeuwen et al. (2022) and Botton and Parsons (2006) showed that benzene was degraded under iron-reducing conditions in groundwater. From a thermodynamic perspective, such conditions occur when DO, NO_3^- and Mn^{4+} are consumed (Appelo & Postma, 2005). In Ogale, for instance, iron-reducing conditions occurred in PSW-11. Here, the DO, NO_3^-, Mn^{4+} and Fe^{3+} levels were 2.3 mg/L, 2 mg/L, 0.1 mg/L and 50 mg/L in 2022, and 0.7 mg/L, less than 0.01 mg/L, 0.1 mg/L and 46 mg/L in 2023, respectively. While the Fe^{3+} in the system decreased in 2023, the continuous release of benzene overwhelmed the iron-reducing capacity to attenuate benzene in the groundwater. Thus, the benzene level increased from 910 µg/L in 2022 to 1100 in 2023 µg/L. This suggests that benzene degradation by iron reduction may not have occurred. Furthermore, the SO_4^{2-} level was higher in 2023 (7 mg/L) than in 2022 (3 mg/L), indicating that SO_4^{2-} did not react with benzene.

3.3.2.2 Potential for natural attenuation of benzene

Since DO is considered the primary electron acceptor for hydrocarbon degradation (Marić et al., 2022), the available amount of DO in the studied groundwater shows considerable potential for the NA of benzene contamination. DO, however, poorly correlates with benzene in the groundwater (Fig. 3.8a). The lowest DO level (0.7 mg/L, 9 %) was observed in well PSW 11, which is located 111 m away from the NNPC underground petroleum pipeline in Ogale but is contaminated with

both benzene (1,100 µg/L) and Fe (45.6 mg/L). The high Fe content contributed to the depletion of oxygen levels in the groundwater. The Fe contamination was discussed in detail earlier in Fe contamination and influence on the fate of benzene section.

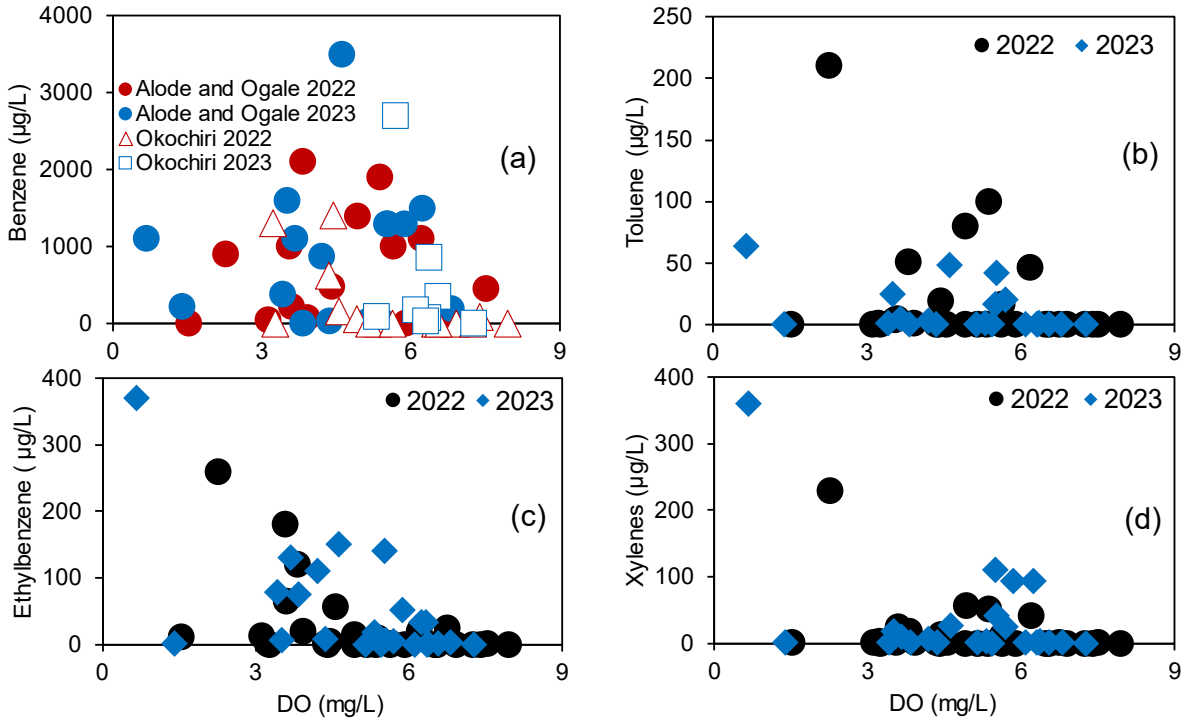

Fig. 3.8 Relationship between (a) benzene vs DO, (b) toluene vs DO, (c) ethylbenzene vs DO, and (d) total xylenes vs DO in Alode, Ogale and Okochiri groundwater.

Although DO and benzene have a weak negative correlation (r = -0.22 in 2022 and -0.11 in 2023, Fig. 3.8a), DO is consistently higher in wells with undetected benzene than in the contaminated wells. For instance, DO levels in the 5 reference wells with undetected benzene ranged from 6.4 (88 %) to 7.9 (102 %) mg/L. In contrast, the DO levels at the contaminated sites were lower in most wells, ranging from 0.7 (9 %) to 6.7 (86 %) mg/L. Data from Okochiri indicated that the considerable decrease in benzene must be related to the amount of DO available in the groundwater (Fig. 3.8a). For instance, the DO concentrations at PSW 21 were 3.2 (41.4 %) mg/L and 6.4 (85 %) mg/L, while the benzene concentrations were 1,300 µg/L and 850 µg/L in 2022 and 2023, respectively. Similarly, at well PSW 22, the DO concentrations were 4.4 (57%) mg/L (620 µg/L of benzene) and 6. 6 (88 %) mg/L (350 µg/L of benzene) in 2022 and 2023, respectively.

In 2022 and 2023, higher DO levels and corresponding lower benzene levels were consistently observed downgradient of the NNPCL product pipeline in Okochiri. Similarly, benzene levels in the groundwater samples taken along transect A in the Okochiri (shown earlier) showed an inverse relationship with DO along an established flow path (Fig. 3.9); DO levels increase as benzene concentration decreases. In Alode and Ogale, however, the relationship between DO and benzene was inconsistent. This may be affected by several factors, such as multidimensional groundwater flow directions and other contaminants.

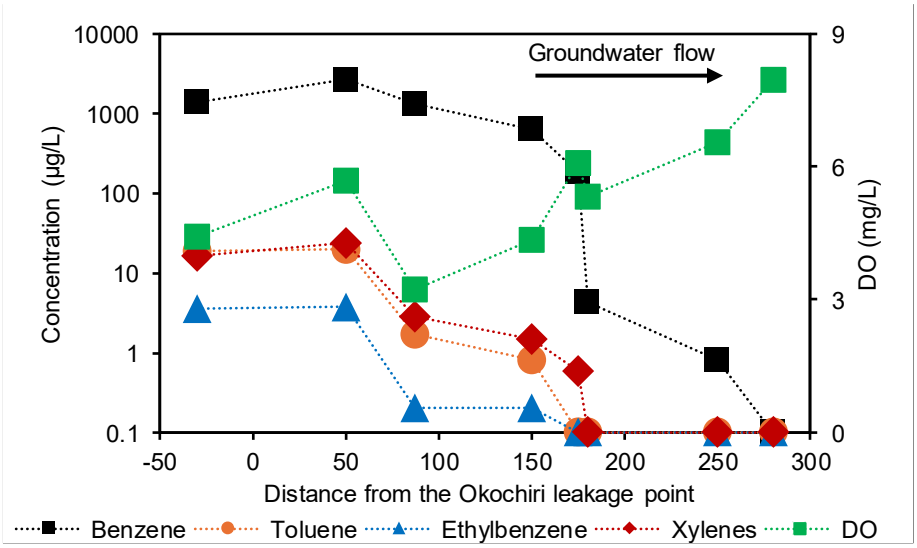

Fig. 3.9 Relationship between DO, benzene, toluene, ethylbenzene and xylenes concentrations along the groundwater flow direction (transect A) in Okochiri. From left to right, the wells plotted are PSW 27, 28, 21, 22, 25, 26, 35 and REF 4.

Despite the elevated benzene levels in the three communities, DO is still available due to constant recharge from precipitation. The precipitation, saturated with oxygen, continuously infiltrates the soils and the corresponding shallow and sandy aquifers in the study area. Since the area has permeable sandy soils, oxygen consumption in the soil zone is resupplied by gaseous oxygen transport through the soil, resulting in an insignificant oxygen consumption (e.g., Appelo & Postma, 2005) given that the depth to the aquifer is 11 m, 9 m and 1 m in Ogale, Alode and Okochiri, respectively. As a result, groundwater across the three communities remained saturated, up to 95 %, with an average of 66 %. Oxygen in the groundwater can initiate aerobic benzene degradation (Jindrová et al., 2002) under favorable conditions, such as appropriate pH levels (i.e., 6.5 to 8.5) (Finneran & Housewright, 2001; NRC, 2013)

and specific microbial populations capable of degrading benzene. In this process, aerobic bacteria, fungi, or algae utilize DO for both ring activation and cleavage of the aromatic nucleus and as an electron acceptor for the complete mineralization of the benzene, as presented in equation 1 (El-Naas et al., 2014).

$$C_6H_6 + 7.5O_2 \rightarrow 6CO_2 + 3H_2O \quad (1)$$

According to Jindrová et al. (2002), under ambient conditions, 8 to 12 mg/L of DO is sufficient to degrade 3,000 to 4,000 µg/L of benzene. However, such high DO levels were absent in the study area due to the high groundwater temperature, up to 32.5°C. Typically, 100 % DO saturation at 25°C is 8.45 mg/L and at 32.5°C, only 7.2 mg/L. The highest values for DO were 7.4 mg/L at Okochiri, 5.9 mg/L at Ogale and 7.5 mg/L at Alode. Similarly, the highest values for temperature were 32.5°C at Okochiri, 31°C at Ogale and 31°C at Alode. The groundwater temperature, therefore, appears to be a limiting factor to the aquifer's benzene NA potential. The rate and efficiency of benzene degradation, however, do not only depend on the oxygen availability but also the discontinuous release of BTEX from the pollutant source, temperature, nutrient availability, and the overall microbial activity in the groundwater environment (Ali et al., 2023; Eze, 2021; Seeger, 2013; Singh & Celin, 2010; Wu et al., 2023). In the case of Ogale, for instance, benzene concentration in well PSW 11 decreased from 9,280 µg/L (UNEP, 2011) to 910 µg/L (this study) in 11 years but increased from 910 µg/L to 1,100 µg/L in 1 year. Fig. 3.10 shows a general comparison between benzene levels in 2022 vs 2023. Besides two samples from Alode, which were significantly higher in 2023, benzene concentrations were similar for the two sampling campaigns. The lack of consistent decline between 2022 and 2023 concentrations suggests that there may be a continuous release of benzene from the pipeline into the groundwater. Also, benzene concentrations in the three communities appear to exceed the capacity of microbial degradation. Therefore, the high initial concentration or continuous benzene release overwhelmed the NA capacity, slowing the degradation.

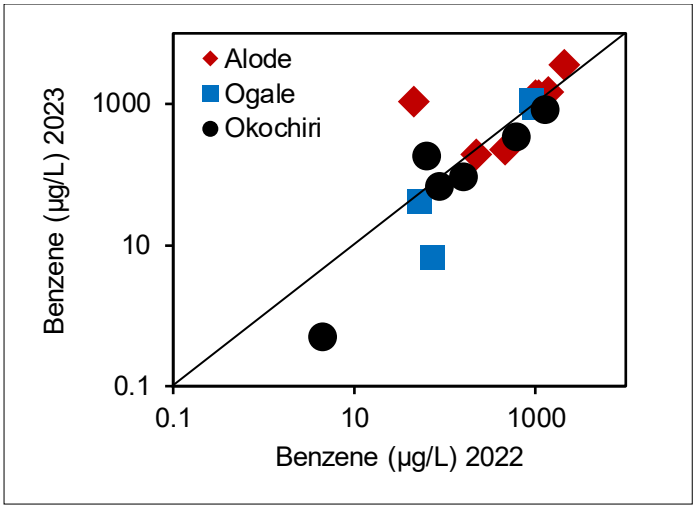

Fig. 3.10 Comparison between benzene concentrations in 2022 and 2023.

Nevertheless, the EBC calculations shown in Table 3.3 further suggest that the DO levels could be sufficient to support aerobic benzene-degrading bacteria to naturally attenuate the benzene-contaminated groundwater of Alode, Ogale and Okochiri. The EBC calculations were based on the lowest and the highest DO measured in the contaminated and reference groundwater in 2022 and 2023 samples. The calculated EBC_{DO} for BTEX levels ranged from 0.62 to 2.11 mg/L, which should be sufficient for BTEX removal (Choi & Lee, 2011).

Table 3.3 Results of EBC calculation

Year	Parameter	Alode	Ogale	Okochiri
2022	C_P (mg/L, DO)	3.6	1.53	3.23
	C_B (mg/L, DO)	8.89	8.17	8.44
	F	3.14	3.14	3.14
	EBC_{DO} (mg/L)	1.68	2.11	1.66
2023	C_P (mg/L, DO)	1.4	0.66	5.32
	C_B (mg/L, DO)	7.86	7.28	7.27
	F	3.14	3.14	3.14
	EBC_{DO} (mg/L)	2.06	2.11	0.62
Mean	EBC_{DO} (mg/L)	1.87	2.11	1.14

EBC: expressed biodegradation capacity; F: BTEX utilization factor using DO.

Furthermore, the point attenuation rate for benzene and BTEX were computed. Most wells, especially in Alode, showed fluctuated concentrations or insufficient data and were unsuitable for first-order decay calculation. Thus, only a few suitable samples were selected for the NA investigation. The computed point attenuation rates for benzene and BTEX are shown in Table 3.4. The BTEX point

attenuation rates varied between 0.086 and 0.556 day^{-1}, equivalent to half-lives of 51.7 years and 4.5 years, respectively. These attenuation rates were comparable to the 0.19 day^{-1} and 0.038 day^{-1} values reported for the sandy aquifer in Florida (Wilson et al., 1994) and Utah, USA (Weidemeier et al., 1996), respectively. The time required to reach the Nigerian remediation goal (0.8 µg/L total BTEX) was 9.2 to 85 years. Also, the point attenuation rates for benzene were smaller, varying between 0.128 and 0.693 day^{-1}, with half-lives of 4.6 to 32.8 years. To reach the Nigeria benzene remediation goal of 0.2 µg/L by NA alone, 11.2 to 66.5 years would be required. Notably, most of the NA at this site may be attributed to dilution due to the high precipitation rate, up to 4,000 mm/year, and dispersion enhanced by groundwater flow. Although the aquifer has a promising NA potential, active remediation measures would be required to reduce the time needed to reach the Nigerian benzene remediation goal. Due to the lack of sufficient data, it was impossible to estimate the study site's bulk attenuation rate.

Table 3.4 Estimated point attenuation rates for total BTEX and benzene

Sample	Site	Contaminant	Point attenuation (day^{-1})	Half-life (yr)	Remediation goal [a]	Remediation time (yr) [b]
W-21	Okochiri	Benzene	0.425	7.1	0.0002	20.7
		BTEX	0.383	7.7	0.0008	19.3
W-22	Okochiri	Benzene	0.572	4.6	0.0002	14.1
		BTEX	0.556	4.5	0.0008	12
W-12	Ogale	Benzene	0.128	32.8	0.0002	66.5
		BTEX	0.086	51.7	0.0008	85
W-1	Alode	Benzene	0.693	3.5	0.0002	11.2
		BTEX	0.4609	4.8	0.0008	9.2

[a] Groundwater remediation goal of Nigeria (National Environmental Regulations, 2011); [b] time required to reach the remediation goal.

3.4 Conclusion

The current study demonstrates that Alode, Ogale and Okochiri groundwater is heavily contaminated by benzene. Other drinking water quality parameters are within the WHO-recommended values. The maximum benzene concentration (3,500 µg/L) was recorded in Alode. Ogale and Okochiri had benzene concentrations up to 1,300 µg/L and 2,700 µg/L, respectively. Elevated values, however, were observed only in wells next to the NNPCL underground petroleum product pipeline, which runs from PHR to Umu Nwa through Alode and Ogale. The concentration decreased with distance from the pipeline. While the benzene

contamination is at a dangerous level, concentrations of the other co-occurring monocyclic aromatic compounds, i.e., toluene, ethylbenzene, trimethylbenzene, and the three forms of xylenes, are within the WHO-acceptable drinking water limits (i.e., 210 µg/L, 370 µg/L, 220 µg/L, and 360 µg/L, respectively). Additionally, DOC levels are elevated in most samples, up to 47 mg/L, 49 mg/L, and 33 mg/L in Alode, Ogale and Okochiri. The elevated DOC reflects the groundwater's total hydrocarbon and non-hydrocarbon load.

While both the benzene and DOC levels in the groundwater are high, the aquifer has shown promising potential for a possible aerobic degradation with its available level of DO (up to 7.5 (95 %) mg/L). The calculated BTEX biodegradation capacity for DO alone ranged from 0.62 to 2.11 mg/L. The point attenuation rates of benzene ranged from 0.128 to 0.693 day^{-1}. The time required to reach the groundwater benzene clean-up goal by NA alone was 11.2 to 66.5 years. Despite the promising potential for NA, the degradation rate appears to be too slow owing to (1) the elevated concentrations in the samples, (2) the continuous release of benzene into the groundwater, (3) the high groundwater temperature (up to 32.5°C), or (4) the possible absence of a specific benzene-degrading microbial population to utilize the available oxygen. Analysis and identification of the microbial population were not within this study's scope. Hence, considerable uncertainties and distinct unknowns on the nature and population of the appropriate microbial population needed for such attenuation remain.

Immediate measures are required to save the health of the growing population residing in the affected communities. These could include (1) using granular activated carbon or charcoal filters for benzene removal or (2) discontinuing the use of the contaminated groundwater. Water from safe sources (e.g., bottled or sachet) should be used instead. In the long term, the local authorities should (1) provide alternative drinking water sources in the form of a centralized water supply system where the quality of the drinking water can be controlled before being distributed to the affected communities, (2) implement measures to ensure a decline in benzene concentration and, (3) the NNPCL should carry out active remedial intervention on sediments and aquifers to facilitate the biodegradation and NA capacities in Alode, Ogale, and Okochiri. The benzene level in the affected communities already exceeded the National Environmental Regulations (2011)

drinking water target value at levels over 17,500 times and the intervention value at levels over 117 times.

4. Source, transport and fate of nitrate in shallow groundwater in the eastern Niger Delta

Dogo Lawrence Aleku[a], Kirstin Dähnke[b] and Thomas Pichler[a,*]

[a] *Institute of Geosciences, University of Bremen, 28359 Bremen, Germany*
[b] *Helmholtz-Zentrum Hereon, Institute for Carbon Cycles, 21502 Geesthacht, Germany*

Abstract

The eastern Niger Delta region in Nigeria is a hotspot for reactive nitrogen pollution due to extensive animal husbandry, pit latrine usage and agricultural practices. Despite the high level of human activity, the sources and processes affecting nitrogen in groundwater remain understudied. Groundwater nitrate (NO_3^-) concentrations are highly variable, with some areas recording values well above the safe drinking water threshold of 50 mg/L. This is particularly true near municipal sewage systems. Elevated nitrite (NO_2^-) and ammonium (NH_4^+) concentrations were also detected in the study area. Sewage analysis revealed NO_3^- concentrations ranging from 1 to 145 mg/L, NO_2^- from 0.2 to 2 mg/L, and notably high NH_4^+ concentrations. A comparison of major ions indicated that 71 %, 90 %, 87 %, and 92 % of groundwater samples surpassed reference site levels for calcium (Ca^{2+}), sodium (Na^+), potassium (K^+), and chloride (Cl^-), respectively, pointing to sewage as a likely source of contamination. The NO_3^-/Cl^- ratios at several sites suggested that most groundwater NO_3^- originates from human waste. Stable isotope analysis of NO_3^- showed a general enrichment in ^{15}N and, in some cases, a depletion in ^{18}O, indicating that the NO_3^- originates from sewage-derived NH_4^+ nitrification. Although nitrification is the primary biogeochemical process in the groundwater, there is evidence for simultaneous denitrification.

4.1 Introduction

Globally, excess nitrate (NO_3^-) in groundwater is an environmental problem threatening human health, either directly due to its adverse health effects or by inducing the release of toxic metals, such as cadmium (Cd) from the aquifer matrix (e.g., Kubier et al., 2020; Kubier et al., 2019; Ward et al., 2018). Migration of NO_3^- from groundwater to surface waters and subsequently into the coastal ocean has also become a cause of concern worldwide (e.g., Guo et al., 2021; Harris et al., 2022). As a result, various global organizations have implemented measures to reduce NO_3^- levels in groundwater. For instance, the European Union (EU) established a range of measures to reduce NO_3^- contributions from agricultural and non-agricultural sources in the EU (Stark & Richards, 2008). To this effect, the EU selected a concentration of 50 mg/L as the guideline value for NO_3^- in groundwater. Similarly, several countries, including Nigeria (NSDWQ, 2015), and organizations like the World Health Organization (WHO, 2017a) have set 50 mg/L as the guideline for NO_3^- in drinking water.

Various authors investigated the groundwater quality and geochemistry in Nigeria's urban and rural areas (Abanyie et al., 2023; Eludoyin & Fajiwe, 2023; Obrike et al., 2022; Raimi et al., 2023). Some studies included NO_3^- and concentrations reported were up to 2.1 mg/L in Nnewi, 4.2 mg/L in Awka (Ayejoto & Egbueri, 2023), 21.1 mg/L in Umunya (Egbueri et al., 2023), 36 mg/L in Ogbaru (Unigwe et al., 2022), 157 mg/L in Gboko (Omonona & Okogbue, 2021), and up to 770 mg/L in Maiduguri (Goni et al., 2019). NO_3^- sources were not identified in those studies, although agricultural activities, pit latrines and animal waste were hypothesized as possible sources. Similar investigations in other parts of the world suggested that, most commonly, anthropogenic sources such as nitrogen fertilizer, manure, municipal and domestic sewage discharge, pit latrines, soil organic nitrogen and atmospheric deposition contribute to NO_3^- loading of groundwaters (Biddau et al., 2023; Kendall et al., 2007).

To effectively reduce the excess levels of NO_3^- in groundwater, improved groundwater management practices that minimize the release of nitrogen compounds into the environment are required. Determining NO_3^- sources and variability is essential to improve nitrogen management practices. However, identifying a given source and its contribution can be complicated when multiple nitrogen sources exist.

Such uncertainty, for instance, is typical in urban areas where intensive agricultural activities involving nitrogen fertilizers are common (Minet et al., 2017). Hence, accurately identifying the NO_3^- source(s) in groundwater, evaluating the ongoing biogeochemical process in the aquifer and calculating NO_3^- contributions from different potential sources are necessary for effective management measures to reduce NO_3^- levels in groundwater.

Stable oxygen and nitrogen isotopic signatures of NO_3^- have been effectively applied to identify NO_3^- sources while also detecting nitrification, denitrification or dilution in groundwater (e.g., Anornu et al., 2017; Carrey et al., 2021; Guo et al., 2020; Harris et al., 2022). However, uncertainties remain during data interpretation, which include (1) significant overlaps resulting from multiple nitrogen sources during the early leaching process within unsaturated zones or as nitrification proceeds and (2) a mixing process between the multiple nitrogen sources, subsequent NO_3^- removal due to denitrification (Kendall et al., 2007), and the concurrent productions of NO_3^- during anaerobic ammonium oxidation under limited oxygen conditions (Granger & Wankel, 2016). This complicates nitrogen source identification in groundwaters (Kendall et al., 2007), hence the need for an approach that combines major ion and isotope data to reduce such uncertainties (Minet et al., 2017). This is possible because, for instance, municipal sewage and animal wastes are typically enriched with chloride (Cl^-), potassium (K^+), and sodium (Na^+), amongst many other contaminants, which are all released by decomposing organic matter (e.g., Ranjbar & Jalali, 2012).

With this in mind, we combined stable NO_3^- isotope data with hydrochemical markers (i.e., Ca^{2+}, Na^+, K^+, and Cl^-) for nitrogen source identification. It is important to note that there are no available studies on groundwater NO_3^- in the eastern Niger Delta, despite the widespread nitrogen-related anthropogenic activities. Hence, this study presents a unique opportunity to investigate NO_3^- and NO_2^- source, transport, and fate across the eastern Niger Delta groundwater systems to improve management and remediation efforts.

4.2 Materials and methods

4.2.1 Site description, geology, and hydrogeology

The study site is in the eastern Niger Delta Region of Nigeria (Latitude 4°44ˈ57ˈˈN to 4°47ˈ42ˈˈN and Longitude 7°05ˈ26ˈˈE to 7°09ˈ54ˈˈE) and comprises the following communities: Alesa, Ogale, Ebubu, Alode and Okochiri, with an uneven topography which varied between 0.1 m and 64.5 m above sea level. The area has two distinct seasons – the wet (March to October) and dry (November to February). The mean monthly temperature is high in March/April (up to 26.7°C) and low in July/August (24.4°C). Humidity ranges from 60 to 90 % and is associated with warm and dry northeastern winds (Hassan et al., 2020). Mean annual precipitation widely varies between 2,800 and 4,000 mm/year (Ohwoghere-Asuma et al., 2023a).

The sampling locations are shown in Fig. 4.1. Alesa, Ogale, and Ebubu are in the northern part of the study area, commonly characterized by the presence of (1) municipal and domestic sewage in the drainage systems and (2) unlined pit latrine toilets for human excrement. In these communities, the sewage flow was hindered by blockage resulting from indiscriminate solid waste disposal and the gentle nature of the topography (Fig. 4.1S). The municipal sewage was more commonly observed in Alesa than in Ogale and Ebubu. In contrast, sewage was not observed in the Alode and Okochiri drainage systems. The steep nature of the topography appears to play an essential role in aiding the free flow and eventual absence of municipal sewage (Fig. 4.2S).

Three major lithostratigraphic units have been identified within the Niger Delta Basin: the Benin Formation, Agbada Formation and Akata Formation (Obaje, 2009). The Oligocene to Recent Benin Formation is about 2 km thick and predominantly consists of clay units, coarse-grained, sub-angular to well-rounded, poorly sorted coastal plain sand and alluvial deposits of about 95 % to 99 % quartz grains at shallow depths (Nwajide, 2013). The Formation serves as a groundwater reservoir for the region (Adelana, 2008). The aquifer is recharged mainly by direct precipitation and exfiltration from major regional rivers (Abam & Nwankwoala, 2020). The sandy and permeable nature of the aquifer further facilitates rapid infiltration into the upper units of the formation (Abam & Nwankwoala, 2020). However, the anthropogenic activities in the region have left the shallow groundwater vulnerable to

pollution (Adeniran et al., 2023). The 3.7 km thick Agbada Formation, Eocene–Recent, is a transition zone considered the main source rock for the petroleum hydrocarbon in the region (Tuttle et al., 1999). The Formation consists of a coastal sequence of alternating marine sands and shales (Ogbe et al., 2013; Short & Stäuble, 1967; Tuttle et al., 1999). According to Obaje (2009), the sand percentage variation within the formation is between 30 to 70 %. The Paleocene – Recent Akata Formation, which extends up to 7 km depth, consists of mainly basal marine pro-delta thick-shale units with < 30 % sand intercalations and minor amounts of silt and clay (Adagunodo et al., 2017; Obaje, 2009; Sanuade et al., 2017; Short & Stäuble, 1967).

In the region, both shallow and deeper wells tap the aquifers of the Benin Formation at depths ranging between 3 to 300 m (Adelana, 2008). The aquifers mainly comprise sand beds with minor clays, lignite, and conglomerate intercalations (Amajor, 1991a). The aquifer's hydraulic conductivity (3.82 x 10^{-3} to 9 x 10^{-2} cm/sec), transmissivity (1.05 x 10^{-3} to 11.3 x 10^{-2} m^2/sec), storage coefficient (1.07 x 10^{-4} and 3.53 x 10^{-4}), and specific capacity (19.01 to 139.8 m^3/h/m of drawdown) shows that it has an excellent water-yielding capacity (Offodile, 2002a). According to Abam and Nwankwoala (2020), the aquifer is recharged mainly by direct precipitation at a 2,532 mm/year rate, and exfiltration from major regional rivers (Abam & Nwankwoala, 2020). Water quickly infiltrates deep into the upper unit of the formation, which is sandy and pervious (Abam & Nwankwoala, 2020; Amajor & Gbadebo, 1992; Dickey et al., 1987). However, the anthropogenic activities in the region have left the shallow groundwater vulnerable to pollution (Adeniran et al., 2023; Ewim et al., 2023; Richard et al., 2023; Sam et al., 2023). Nevertheless, deep-seated aquifers are considered safe and less vulnerable due to the intercalations of clay units (Abam & Nwankwoala, 2020).

4.2.2 Groundwater sampling

The groundwater samples for this study were collected from shallow wells (1 to 30 m) in the Benin Formation in April 2022 and April 2023. Groundwater and sewage samples were collected from communities with municipal and domestic sewage and areas considered relatively unaffected by municipal wastewater (i.e., reference sites 1 to 5). The reference samples were collected from Alode (Ref 1 and 2), Okochiri (Ref 3), Okrika Island (Ref 4) and Ogale (Ref 5) within the same geological unit in relatively new residential areas without municipal wastewater or other potential anthropogenic contamination sources.

The groundwater samples were collected either (1) manually, using a water bailer made of polyvinyl chloride, or (2) with an electric submersible pump in cases where those were installed in the wells. First, groundwater was pumped into the overhead storage tank to purge the wells for 30 minutes before sampling directly from the wellhead. The bailer was rinsed three times with the groundwater before sampling. Sampling was conducted during the early hours (between 6:00 and 8:00 a.m.) when the wells were actively used to ensure that fresh samples were collected. However, for most of the wells, water table and well depth measurements were not possible because well heads were sealed with concrete slabs (Fig. 2.3S) to protect wells from surface contamination and theft of submersible pumps. The well owners rejected unsealing the wells for depth measurement. Nevertheless, in those wells where measurement was possible, the water table varied between 1.5 and 9 m whereas well depths ranged from 9.8 to 30 m. In total, 180 samples (105 in 2022 and 75 in 2023) were collected from private supply wells (PSW) and community supply wells (CSW) next to municipal or domestic sewage drainages. In private residences, most wells were next to pit latrine toilets, usually between 2 and 9 m apart.

Immediately after collection, the samples were filtered through 0.45 µm cellulose acetate (CA) membranes and separated into aliquots for the different chemical analyses (isotopes, major ions, and dissolved organic carbon). The samples were stored in 25 mL glass vials for DOC, 30 mL brown HDPE vials for major cations and 20 mL clear HDPE vials for anions and isotopes. The sub-samples for DOC and major cations were preserved with 2 % concentrated nitric acid (HNO_3). All samples were stored at 4 °C until laboratory analyses.

The pH, conductivity (EC), total dissolved solids (TDS), temperature, dissolved oxygen (DO), salinity, redox potential (ORP), and resistivity were determined immediately *in situ* using a Hanna instrument HI98494 multiparameter. In the field, the total alkalinity ($CaCO_3$) was determined by colorimetric titration with 0.16 N H_2SO_4 in combination with a bromcresol green-methyl red indicator. The bromcresol green-methyl red indicator powder was added to 100 mL of the groundwater sample and titrated using a Hach digital titrator to a light pink color. The total alkalinity was reported as mg/L $CaCO_3$.

Additionally, 8 samples were collected from municipal and domestic sewage in Alesa, Ogale, and Ebubu. The samples were filtered through 0.45 µm cellulose acetate (CA) membrane filters and collected into 20 mL clear HDPE vials.

4.2.3 Analytical procedures

4.2.3.1 Cation, anion and DOC measurements

Major cations and trace elements were determined by inductively coupled plasma-optical emission spectrometry (ICP-OES) using a Perkin Elmer Optima 7300 DV instrument. The precision of the measurement was checked using EnviroMAT Groundwater Low (ES-L-2) and High (ES-H-2) certified water from SCP Science, Canada, showing errors of < 3 % for all analytes. Major anions (including NO_3^- and NO_2^-) were determined using a Metrohm 883 Basic IC plus instrument with a 5 µL injection loop and a Metrosep A Supp5 (150 × 4.0 mm; 5 µm) column. An internal standard was used to check the accuracy and precision of the measurement, and errors of less than 10 % were recorded.

Dissolved organic carbon (DOC), the fraction of organic carbon that can pass through a 0.45 µm pore size, was determined using a Shimadzu TOC analyzer TOC-V CPN (Shimadzu Corporation). A certified Total Organic Carbon Standard of 50 mg/L (Aqua Solutions) was used for quality control, and the measurement error was determined to be less than 6 %.

The ammonium (NH_4^+) was determined photometrically at 655 nm with salicylate following standard procedures (DIN 38406, 1983).

4.2.3.2 Determination of NO_3^- isotopes ($\delta^{15}N\text{-}NO_3^-$ and $\delta^{18}O\text{-}NO_3^-$)

A subset of 20 groundwater and 2 municipal wastewater samples were analyzed for stable isotopes, specifically from wells where their owners had granted permission to collect samples. The $^{15}N/^{14}N$ and $^{18}O/^{16}O$ ratios in dissolved NO_3^- were measured and expressed as $\delta^{15}N\text{-}NO_3^-$ and $\delta^{18}O\text{-}NO_3^-$. Isotope ratios were determined following the denitrifier method (Casciotti et al., 2002; Sigman et al., 2001). NO_3^- and NO_2^- are quantitatively converted to nitrous oxide (N_2O) by the denitrifying bacteria (*Pseudomonas aureofaciens*, ATCC#13985) that lack N_2O reductase. The sample volume for isotope determination was adjusted to achieve 10 nmol of N_2O. N_2O was extracted from the sample vials by purging with helium and measured with a

GasBench II (Thermo, Germany), coupled to an isotope ratio mass spectrometer (Delta Plus XP, Thermo, Germany). For quality assurance, two external standards (USGS34: δ ^{15}N: -1.8 ‰, δ ^{18}O: -27.9 ‰; IAEA-NO_3^-: δ^{15}N: +4.7 ‰, δ^{18}O: +25.6 ‰) and one internal standard were measured with each sample batch. The standard deviation of samples and standards was < 0.2 ‰ for δ ^{15}N-NO_3^- (n = 4) and < 0.5 ‰ for δ ^{18}O-NO_3^- (n = 4). Note that this method yields combined isotope values for NO_3^- + NO_2^-. In two samples, NO_2^- concentration exceeded 5 % of the nitrate concentration. These samples were excluded from the isotopic analysis.

4.3 Results

4.3.1 Groundwater hydrochemical characteristics

The supplemental information (SI) Tables 4.1S and 4.2S present data for all samples, including minimum, maximum, median and average. The pH ranged from 3.5 to 6.9, temperature from 25 to 34 °C, EC from 16 to 852 µS/cm, TDS from 8 to 427 mg/L, DO from 0.7 to 8.9 mg/L and salinity from 0.01 to 0.4 PSU. The EC ranged from 17 to 69 µS/cm at the reference site, and the TDS ranged from 9 to 32 mg/L.

Most groundwater quality parameters at the contaminated and reference sites were in accordance with WHO (2017) guidelines for drinking water. Nevertheless, the parameters associated with contamination from NO_3^- fertilizer and animal/human waste effluents (Cl^- and K^+) or animal/human wastes (Na^+) (Minet et al., 2017) showed higher concentrations at the contaminated sites than those at the reference sites. The concentrations of Na^+ in groundwater ranged from 1 to 56 mg/L, and 57 % of the samples exceeded the measured reference value range of 1 to 2 mg/L. The concentrations of K^+ ranged from 0.1 to 59 mg/L, and 33 % of the samples exceeded the 0.3 to 0.6 mg/L range at the reference sites. The concentrations of Cl^- ranged from 1 to 66 mg/L, with 25 % of the samples exceeding the 2 to 5 mg/L range at the reference site. Ca^{2+} ranged from 0.2 to 51 mg/L, and 71 % of the samples exceeded the 1 mg/L range at the reference sites. In the sewage, Na levels ranged from 5 to 363 mg/L, K^+ concentrations from 1 to 74 mg/L, Cl^- concentrations from 28 to 242 mg/L and Ca^{2+} concentrations from 22 to 65 mg/L. Generally, 90 %, 87 % and 92 % of the groundwater samples exceeded the Na^+, K^+ and Cl^- concentrations measured at the reference sites, respectively.

Similarly, although the Mg^{2+}, F^{-}, and SO_4^{2-} levels were relatively low in the groundwater and sewage, their concentrations exceeded the reference site values in several samples (Table 3.2S and 3.3S). Here, the Mg^{2+}, F^{-}, and SO_4^{2-} levels showed that 42 %, 34 %, and 18 % of the groundwater samples exceeded their respective reference site concentrations. NO_3^{-} vs Mg had a strong positive correlation (R = 0.9), likewise NO_3^{-} vs F^{-} (R = 0.53), and NO_3^{-} vs SO_4^{2-} (R = 0.64). Those elevated ion levels also indicated a possible anthropogenic influence, most likely sewage infiltration into the aquifer.

The concentration of dissolved NO_3^{-} in the water samples ranged from less than 0.01 up to 211 mg/L. Out of the 180 samples collected, 24 had concentrations that exceeded the maximum guideline value of 50 mg/L for NO_3^{-} in drinking water. Elevated concentrations were observed in 2022 and 2023 in Alesa, Ogale, and Ebubu. In general, the NO_3^{-} concentrations in groundwater were higher in the northern part of the study area (Alesa, Ogale, and Ebubu), where municipal sewage was frequently present. In contrast, in the southern part (Alode and Okochiri), where municipal sewage was absent, concentrations were comparably lower, not reaching the WHO guidelines (Fig. 4.2). In the sewage samples, NO_3^{-} concentrations, up to 145, 131 and 100 mg/L, were detected in Alesa, Ogale and Ebubu, respectively.

Eleven groundwater samples had nitrite (NO_2^{-}) concentrations that exceeded the NSDWQ (2015) drinking water guideline value of 0.2 mg/L. Concentrations up to 1 mg/L, 0.2 mg/L, 1 mg/L, 2 mg/L and 0.2 mg/L were detected in Alesa, Ogale, Ebubu, Alode and Okochiri groundwaters, respectively.

Ammonia (NH_4^{+}) was detected in five samples of the Alesa groundwater. The estimated concentration ranged from 0.02 to 1.6 mg/L. In Ogale, NH_4^{+} was detected in all the samples, with concentration estimates ranging from < 0.02 to 12.7 mg/L. In Ebubu, however, NH_4 was detected in only one sample (0.6 mg/L). Additionally, two sewage samples from Alesa were examined: EF 5 contained an estimated 4.8 mg/L, while NH_4^{+} in EF 2 exceeded the instrument's detection limit. These values might have been altered due to prolonged storage. Hence, those were considered only qualitatively.

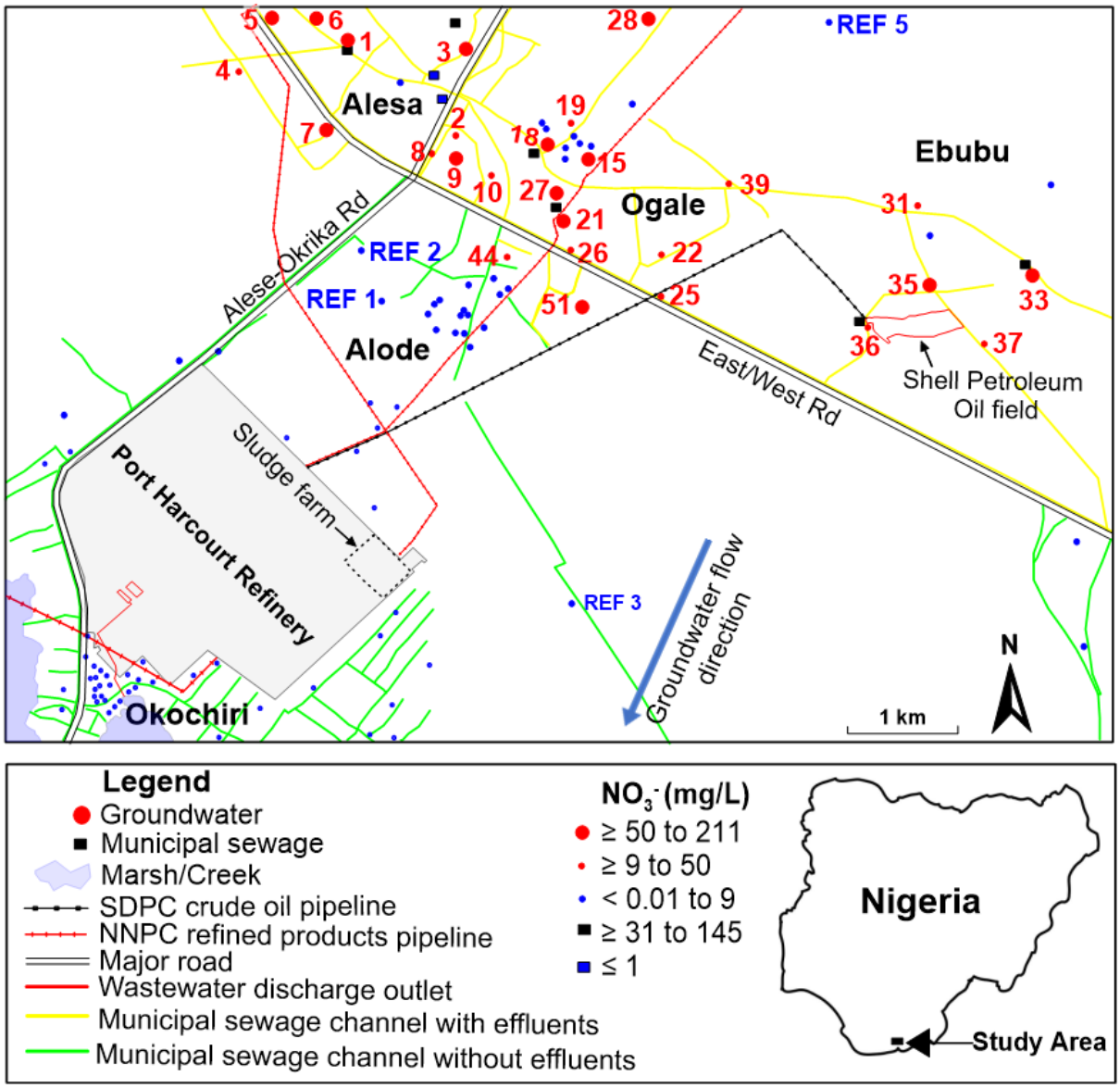

Fig. 4.1. The spatial distribution of NO_3^- concentrations in the groundwater and municipal sewage across the study area. Only samples with elevated NO_3^- concentrations were labeled on the map for clarity. For color interpretation in this map, the reader is referred to the Web version of this article.

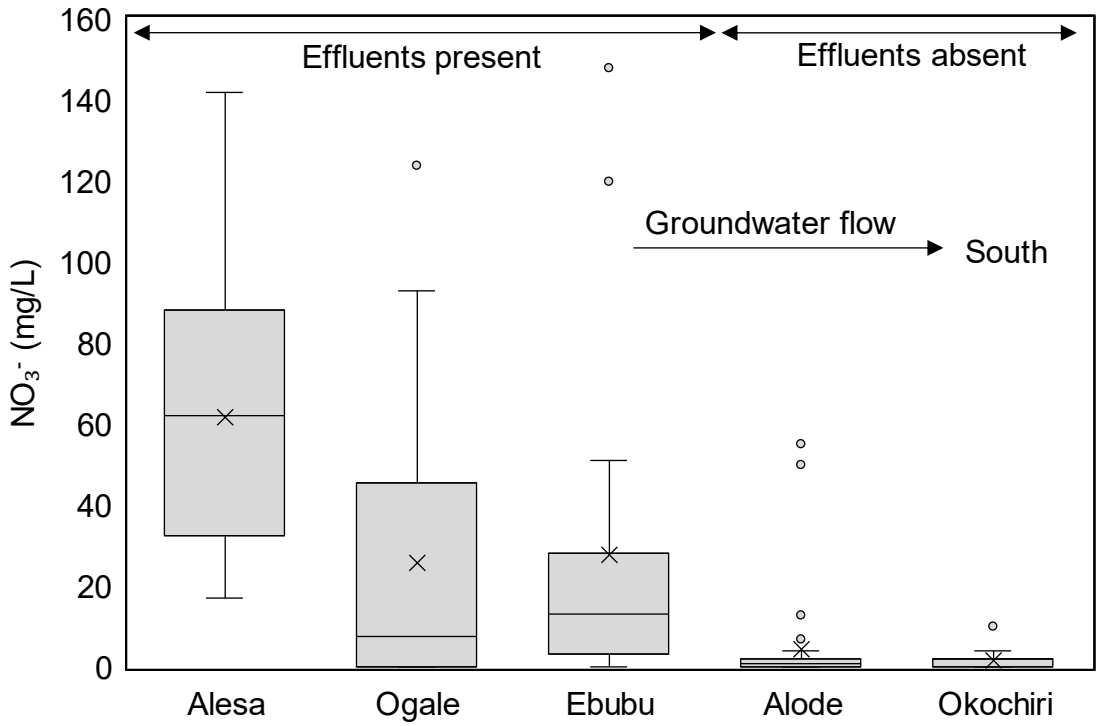

Fig. 4.2. Box plot of NO_3^- concentrations in the study area. Alesa, Ogale, and Ebubu are in the northern part of the study site, Alode is in the central part, whereas Okochiri is in the south. An outlier (211 mg/L) in Ogale was excluded from the plot. The edges of the box represent the 75th and 25th percentiles, respectively. The 'x' sign in the box represents the mean value. The solid line represents the median value. The branch gives the range of the data except for the outliers. Twenty samples were selected across Alesa, Ogale, and Ebubu for the δ^{15}N-NO_3^- and δ^{18}O-NO_3^- analyses.

4.3.2 Hydrochemical facies

Based on the major ions, the hydrochemistry of the groundwater was evaluated through the trilinear Piper (Piper, 1944), Druov (Durov, 1948) and Stiff diagrams using the Geochemist's Workbench 17.0.2. Based on the Piper diagram given in Fig. 4.3 a, two water types were identified from the groundwater samples: the Ca-Cl (23 %) and Na-Cl (77 %) water types. In the Alesa, the facies are 25 % Ca-Cl and 75 % Na-Cl type. In the Ogale, the facies are 10 % Ca-Cl and 90 % Na-Cl type whereas in the Ebubu, the facies are 50 % Ca-Cl and 50 % Na-Cl type. Similarly, in the trilinear Durov diagram shown in Fig. 4.3 b, all the groundwater samples have TDS less than 500 mg/L. Cl^- and SO_4^{2-} are the dominant anions and Na and Ca are the dominant cations. Furthermore, the Durov plot indicates the possible occurrence of

NO_3^-, Cl^- and SO_4^{2-} contamination in the investigated groundwater. As indicated by the Piper diagram, the Durov diagram also showed Na-Cl as the dominant water type in the study area. However, based on our salinity data, there was no incidence of saltwater intrusion in the groundwater despite the coastal nature of the area. The salinity values in the groundwater ranged from 0.04 to 0.2 (Alesa), 0.01 to 0.4 (Ogale), 0.01 to 0.2 (Ebubu and Alode) and 0.01 to 0.1 (Okochiri) PSU. Therefore, anthropogenic influence, rather than the mixing of freshwater with saltwater, was responsible for the Na-Cl water type in this study. All the groundwater samples in the study area showed freshwater facies. Notably, the elevated NO_3^- values were not specific to a particular water type, nevertheless, values of each major ion were higher in the NO_3^- contaminated sites (i.e., Alesa, Ogale and Ebubu) and lower in the uncontaminated sites (i.e., Alode and Okochiri) as shown in the Stiff diagram in Fig. 4.4S. Generally, the abundance of the anions and cations in the groundwater followed the order of $Cl^- > SO_4^{2-} > F^-$ and $Na^+ > K^+ > Ca^{2+} > Mg^{2+}$, respectively.

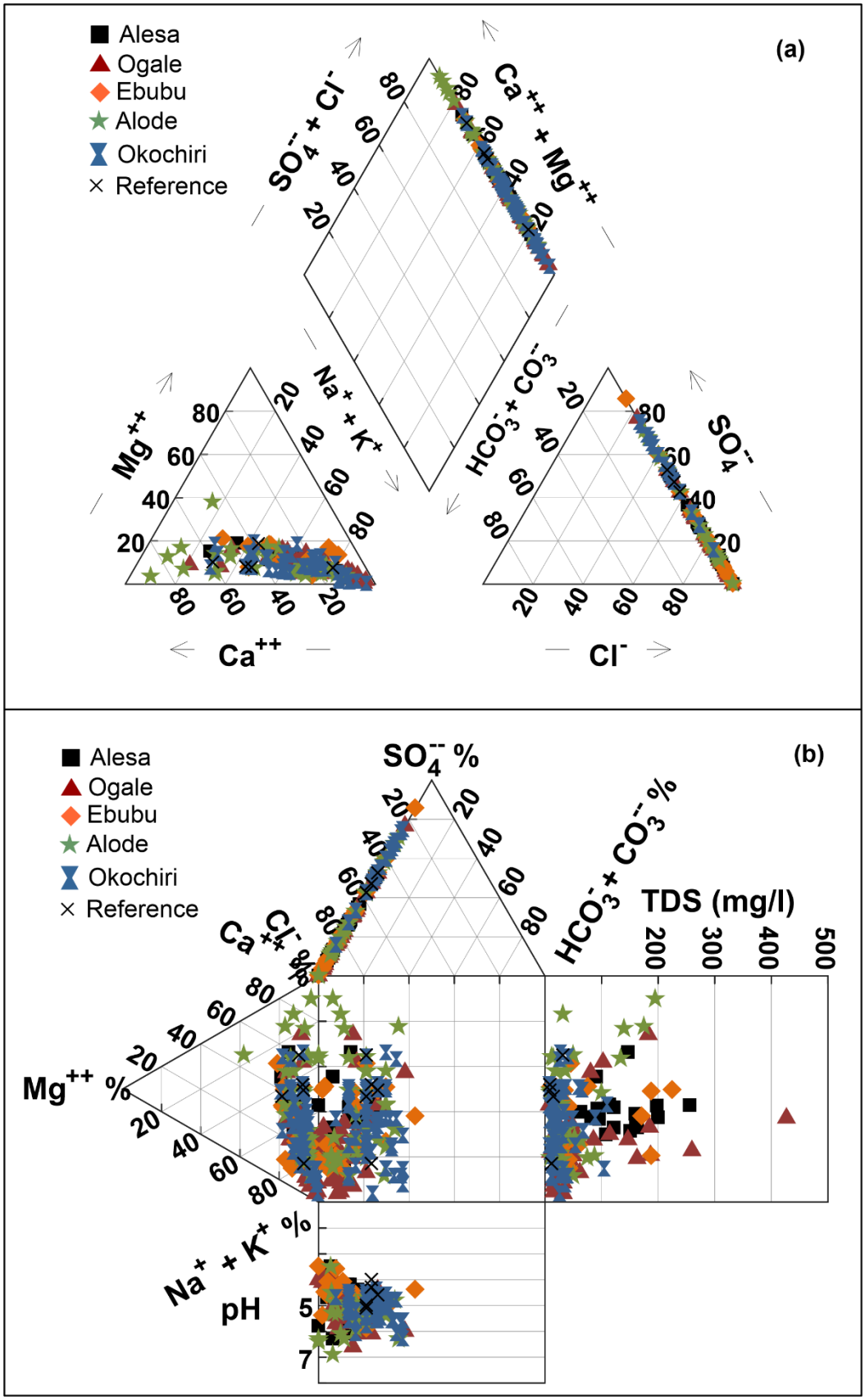

Fig. 4.3. (a) Piper and (b) Durov diagrams for groundwater of the study area.

4.3.3 $\delta^{15}N\text{-}NO_3^-$ and $\delta^{18}O\text{-}NO_3^-$

In the groundwater, the $\delta^{15}N\text{-}NO_3^-$ isotopic signatures varied between +8.9 to +25.6 ‰, and $\delta^{18}O\text{-}NO_3^-$ varied between +4.0 to +15.2 ‰ (Fig. 4.4 b, Table. 4.1). Overall, the variation in the $\delta^{15}N\text{-}NO_3^-$ and $\delta^{18}O\text{-}NO_3^-$ values across Alesa, Ogale, Ebubu, and Alode was small (Table 4.1). The $\delta^{18}O\text{-}NO_3^-$ values tended to increase with the $\delta^{15}N\text{-}NO_3^-$ values for the groundwater samples collected in Alesa and Ogale, while this trend was not observed in Ebubu. The $\delta^{15}N\text{-}NO_3^-$ and $\delta^{18}O\text{-}NO_3^-$ values in the shallow groundwater fitted the regression lines for Alesa and Ogale ($y = 0.58x + 0.21$, $r^2 = 0.71$).

In municipal sewage samples ($n = 2$), $\delta^{15}N$ and $\delta^{18}O$ values varied largely, ranging from -0.5 to +7.9 ‰ for $\delta^{15}N$, and +1.9 to +10.5 ‰ for $\delta^{18}O$.

Table 4.1: $\delta^{15}N$, $\delta^{18}O$ and NH_4 (estimates) values at each of the target communities

ID	Site	$\delta^{15}N$ (‰)	$\delta^{18}O$ (‰)	NH_4 (µmol/L) estimates	$\delta^{15}N$ /$\delta^{18}O$	NO_3^- (mg/L)	Cl^- (mg/L)	NO_3^-/Cl^-	Ln (NO_3^-)
1	Alesa	13.4	6.2	N.D.	2.17	106	41	2.6	4.66
2	Alesa	25.6	15.2	B.D.L	1.68	34	17	2	3.53
3	Alesa	13.9	8.8	N.D.	1.58	83	27	3.1	4.42
4	Alesa	13.6	9.4	0.03	1.45	17	9	1.9	2.83
5	Alesa	12.3	7.3	1.6	1.68	73	24	3	4.29
6	Alesa	13.7	7.8	B.D.L	1.76	53	18	2.9	3.97
7	Alesa	13.9	7.4	1.7	1.89	97	38	2.6	4.57
8	Alesa	15.1	9.9	0.4	1.52	32	11	2.9	3.47
9	Alesa	11.7	4	1.5	2.92	66	24	2.8	4.19
10	Alesa	10.2	4.1	N.D.	2.5	22	6	3.7	3.09
15	Ogale	18.8	11.5	13.5	1.64	64	49	1.3	4.16
21	Ogale	11.7	7.6	2.7	1.54	81	21	3.9	4.39
25	Ogale	9	8.2	N.D.	1.1	28	7	4	3.33
26	Ogale	11.5	8	0.6	1.45	22	6	3.7	3.09
27	Ogale	12.5	8.5	0.004	1.47	62	19	3.3	4.13
33	Ebubu	12.1	9	B.D.L	1.35	44	9	4.9	3.78
34	Ebubu	11.8	9	B.D.L	1.33	10	6	1.7	2.3
35	Ebubu	13.5	6.9	0.7	1.97	148	42	3.5	5
39	Ebubu	13.6	10.6	B.D.L	1.28	28	8.4	3.3	3.33
49	Alode	10.3	9.2	2.9	1.13	55	12	4.6	4.01
EF5	Alesa	7.9	10.5	5.1	0.75	145	123	1.1	4.98
EF2	Alesa	- 0.5	1.9	A.D.L.	-0.27	131	99	1.3	4.88

Notes: N.D. = Not Determined, B.L.D. = Below Detection Limit, A.D.L. = Above Detection Limit

4.4 Discussion

4.4.1 Source of NO_3^- in the groundwater

The groundwater samples with elevated ions were predominantly from Alesa, Ogale, and Ebubu. The elevated ion (i.e., Na^+, K^+, Cl^-, and Ca^{2+}) levels in the groundwater and sewage reflect the anthropogenic influence related to the discharge of animal/human waste effluents in the area (Minet et al., 2017). Furthermore, several strong positive correlations existed between the NO_3^- concentrations and the Na^+, K^+, Cl^-, Sr^{2+}, and Ca^{2+} concentrations. NO_3^- had a strong positive correlation with Na^+ (R = 0.9), indicating possible impacts from the municipal sewage on the NO_3^- loading (Liu et al., 2006). Furthermore, NO_3^- derived from septic effluents, human excreta, or animal wastes usually has a strong correlation with Cl^- (Liu et al., 2006). The groundwater NO_3^- in this study generally shows a strong positive correlation with Cl^- (R = 0.94) across the study area. The correlation appears to be stronger in Alesa (R = 0.98), Ogale (R = 0.9), and Ebubu (R = 0.99) compared to Alode (R = 0.59) and Okochiri (R = 0.09). The Cl^- and NO_3^- levels in the sewage were elevated, up to 242 mg/L and 58 mg/L, respectively. However, at the reference sites, Cl^- and NO_3^- levels in the sewage were relatively low, 14 and 2.4 mg/L, respectively, suggesting that municipal sewage is likely the major contributing source of the NO_3^- contamination in the groundwater. Meanwhile, the presence of pit latrine toilets containing leachates from human excreta may also contribute to the NO_3^- levels in the groundwater. Also, NO_3^- was positively correlated with K^+ (R = 0.83), Sr^{2+} (R = 0.88) and Ca^{2+} (R = 0.87) concentrations. These correlations, however, were mostly weak (R values ranged from 0.05 to 0.2) in all the groundwater quality parameters at the reference site. Notably, NO_3^- levels were consistently low (< 0.01 to 3 mg/L) at the reference sites. Therefore, the Na^+, K^+, Cl^- and Ca^{2+} concentrations suggest that the land use effect, i.e., leachate infiltration from domestic and municipal sewage and unlined pit latrine systems, is the point source of NO_3^- loading (e.g., Minet et al., 2017).

Similarly, although the Mg^{2+}, F^-, and SO_4^{2-} levels were relatively low in the groundwater and sewage, their concentrations exceeded the reference site values in several samples (Table 4.2S and 4.3S). NO_3^- vs Mg had a strong positive correlation (R = 0.9), likewise NO_3^- vs F^- (R = 0.53), and NO_3^- vs SO_4^{2-} (R = 0.64). Those elevated

ion levels also indicated a possible anthropogenic influence, most likely sewage infiltration into the aquifer.

In line with the elevated ion concentration, Alesa, Ogale, and Ebubu groundwater showed an influence from anthropogenic activities (e.g., indiscriminate waste disposal into the municipal drainages). Leachates from municipal sewages often contain various contaminants, including salts and chloride compounds, which may infiltrate the aquifer (e.g., Aweto et al., 2023). The EC and TDS values were consistent with the findings by Eyankware et al. (2022) and Abam and Nwankwoala (2020). EC and TDS, which principally comprises Ca^{2+}, Mg^{2+}, K^{+}, Na^{+}, Cl^{-}, SO_4^{2-}, HCO_3^{-} and small amounts of dissolved organic matter (WHO, 2017a), strongly correlated with NO_3^{-} (R = 0.93). Reference sites lacked such strong correlations, corroborating the influence of domestic and municipal sewage infiltration.

Furthermore, anthropogenic sources of NO_3^{-} can be identified using the NO_3^{-}/Cl^{-} molar ratio since Cl^{-} is widely distributed in natural waters (Torres-Martínez et al., 2021). According to Anornu et al. (2017) and Liu et al. (2006), this approach compares the molar ratios for NO_3^{-} and Cl^{-} with the assumption that halides, such as Cl^{-}, are chemically inert when introduced into the environment. This property makes Cl^{-}, which usually has minimal interaction with the subsoil (Guo et al., 2020), an ideal indicator of sewage, manure, and fertilizer when plotted against NO_3^{-} (Gibrilla et al., 2020). Generally, groundwater with high values of Cl^{-} against low NO_3^{-}/Cl^{-} ratios are associated with NO_3^{-} inputs from sewage and organic wastes, whereas high NO_3^{-}/Cl^{-} ratios with low Cl^{-} values suggest NO_3^{-} inputs from agrochemicals (Anornu et al., 2017). Moreover, the NO_3^{-}/Cl^{-} ratio is low in groundwater unaffected by anthropogenic activities (Jiang et al., 2016). In this study, the NO_3^{-}/Cl^{-} ratios in the groundwater across Alesa, Ogale, and Ebubu overall were elevated, suggesting an anthropogenic influence. The relationship of the NO_3^{-}/Cl^{-} vs Cl^{-} concentration appears to be constant, implying that the groundwater has a consistent, non-variable source of NO_3^{-} (Cao et al., 2021). All the samples showed significantly higher Cl^{-} levels with lower NO_3^{-}/Cl^{-} (Fig. 4.4 a), suggesting that the NO_3^{-} was derived from the ongoing anthropogenic activities in the area, which are likely leachates from the municipal sewage and the pit latrine systems. Interestingly, a subset of 4 samples deviated from the general trend, which we regard as an indication of nitrate removal in the study area, possibly due to denitrification (Fig. 4.4 a).

Also, several scientific research has shown that dual NO_3^- isotopes (i.e., $\delta^{15}N\text{-}NO_3^-$ and $\delta^{18}O\text{-}NO_3^-$) can assist in identifying NO_3^- sources, as well as revealing the ongoing biogeochemical processes (e.g., nitrification and denitrification) in the groundwater (Biddau et al., 2023; Boumaiza et al., 2023; Degnan et al., 2016; He et al., 2022; Ju et al., 2023; Kendall et al., 2007; Mao et al., 2023). The $\delta^{15}N\text{-}NO_3^-$ and $\delta^{18}O\text{-}NO_3^-$ values for this study (Fig. 4.4 b) are discussed in Section 4.2.1.

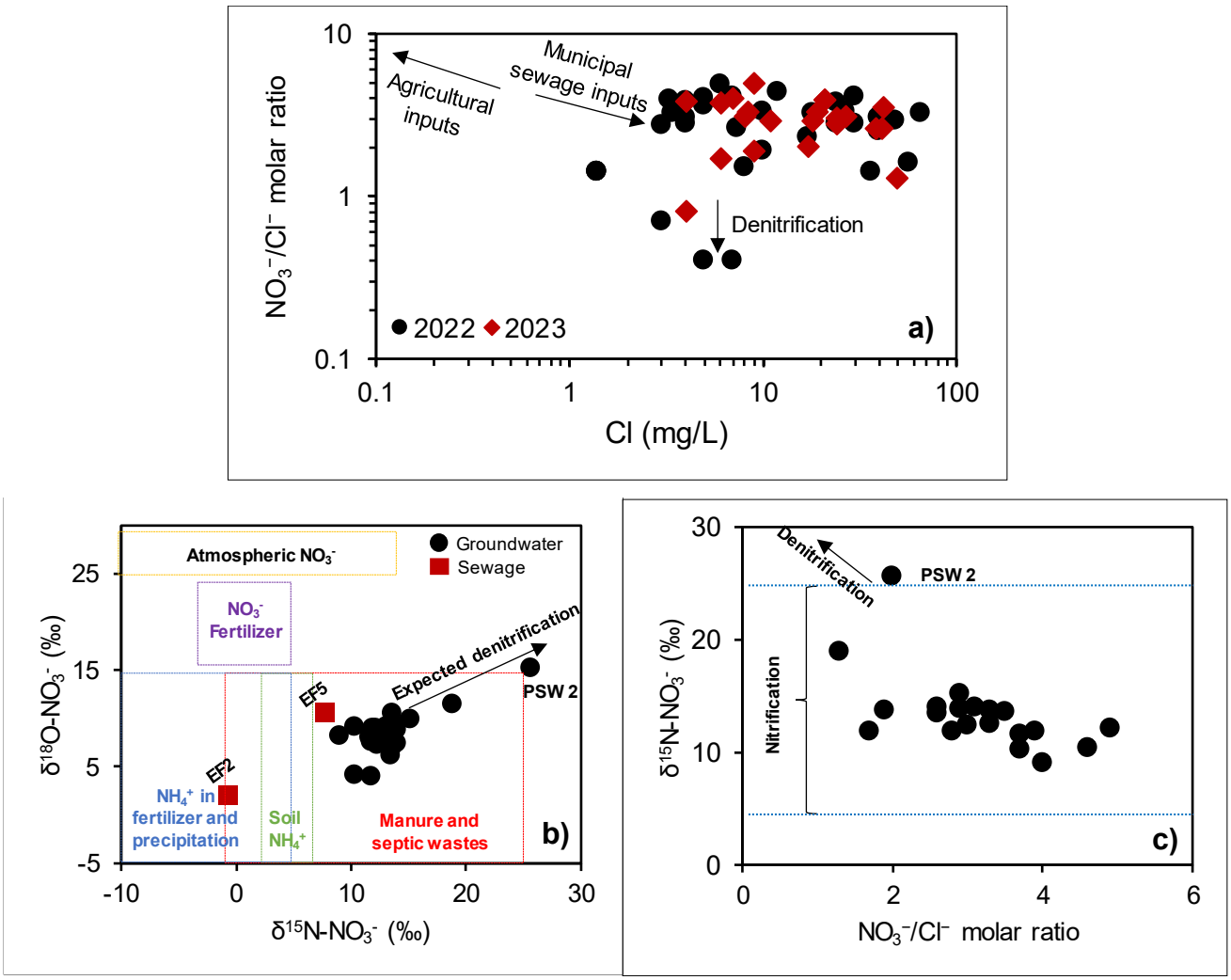

Fig. 4.4. (a) Relationship between Cl^- concentrations vs NO_3^-/Cl^- molar ratios, **(b)** A plot of $\delta^{15}N\text{-}NO_3^-$ vs $\delta^{18}O\text{-}NO_3^-$ isotopic values in Alesa, Ogale, and Ebubu groundwater and sewage. The diagram was modified from Kendall et al. (2007), showing typical values of $\delta^{15}N\text{-}NO_3^-$ and $\delta^{18}O\text{-}NO_3^-$ derived or nitrified from leachates originating from the municipal sewage and pit latrine systems. The arrow shows the expected denitrification of NO_3^- in the area. **(c)** A plot of $\delta^{15}N\text{-}NO_3^-$ vs. NO_3^-/Cl^- molar ratio variation in the Alesa, Ogale, and Ebubu groundwater.

4.4.2 Transport and fate of NO_3^- in the groundwater

4.4.2.1 Parallel occurrence of nitrification and denitrification?

While dual NO_3^- isotopes have been widely used for NO_3^- source assessment in various environments, a precise attribution is complicated by overlapping processes (e.g., nitrification and denitrification) (Granger & Wankel, 2016), fractionation effects (Yu et al., 2020), and mixing of different sources (Harris et al., 2022). For each NO_3^- source, there is a distinct dual isotope signature. For instance, $\delta^{18}O$ and $\delta^{15}N$ derived from nitrification of manure and sewage range from -10 to +15 ‰ and +8 to +25 ‰ for O and nitrogen isotopes, respectively (Kendall et al., 2007). In Alesa, Ogale, and Ebubu, groundwater DO content ranged from 1.5 to 8.9 mg/L, and such oxic conditions can favor nitrification as a nitrate source in the aquifer.

A first source attribution based on Kendall et al. (2007) shows that the data plotted in the “manure and sewage” zone (Fig. 4.4 b). As mentioned, the communities with elevated NO_3^- concentrations were characterized by drainage systems filled with domestic and municipal sewage (Fig. 4.7) and pit latrine toilets. Additional high NH_4^+ concentrations in the groundwater and sewage across the study communities can rapidly be converted to NO_3^- by nitrifiers in oxic groundwater. The high NO_3^-/Cl^- molar ratios (> 1), as well as the elevated $\delta^{15}N\text{-}NO_3^-$ values (> 5) in the groundwater (Fig. 4.4 c), further support that NH_4^+ from sewage or manure, is, upon nitrification, a significant source of NO_3^- in the groundwater.

Thus, while nitrification appears to be the primary biogeochemical process across the three sites, there is evidence for simultaneous denitrification. Denitrification, regarded as all nitrate respiration processes, is vital for NO_3^- removal in groundwater by transforming the dissolved NO_3^- to N_2O and N_2 (Cantrell et al., 2023), as expressed in Equation 4.1 below (Appelo & Postma, 2005). It is, however, more likely to occur under limited oxygen conditions and available organic carbon (Xue et al., 2009).

$$NO_3^-{}_{(aq)} \rightarrow NO_2^-{}_{(aq)} \rightarrow NO_{\ (enzyme\ complex)} \rightarrow N_2O_{(gas)} \rightarrow N_{2(gas)} \qquad (4.1)$$

In this process, as the NO_3^- decreases, both $\delta^{15}N\text{-}NO_3^-$ and $\delta^{18}O\text{-}NO_3^-$ of the NO_3^- residual increase simultaneously due to the fractionation and enrichment of the ^{18}O in the NO_3^- (Harris et al., 2022; Jiang et al., 2016; Kendall, 1998; Wassenaar, 1994). The relationship between $\delta^{15}N\text{-}NO_3^-$ vs $\delta^{18}O\text{-}NO_3^-$, and $\delta^{15}N\text{-}NO_3^-$ or $\delta^{18}O\text{-}NO_3^-$ vs

ln(NO_3^-) can provide information on the ongoing denitrification and mixing of NO_3^- from different sources in the aquifer (Harris et al., 2022; Zakaria et al., 2023; Zaryab et al., 2023). Usually, groundwaters undergoing denitrification will exhibit a linear correlation between $\delta^{15}N\text{-}NO_3^-$ and $\delta^{18}O\text{-}NO_3^-$ (Jiang et al., 2016; Wassenaar, 1994).

Despite the elevated groundwater DOC of up to 42 mg/L in Alesa, 49 mg/L in Ogale, 47 mg/L in Ebubu and 54 mg/L in Alode, our results (i.e., lack of distinct positive or negative correlation between $\delta^{15}N\text{-}NO_3^-$ or $\delta^{18}O\text{-}NO_3^-$ and NO_3^-) suggest that denitrification is not the primary process for nitrogen transformation in the area (Zaryab et al., 2023). Given oxic conditions in most samples, this is plausible. In most samples, DO was above the threshold oxygen level for denitrification of 2 mg/L (Xue et al., 2012). Nevertheless, the build-up of NO_2^- (0.2 to 2 mg/L, $n = 8$) and the observed slope of $\delta^{15}N\text{-}NO_3^-$ vs $\delta^{18}O\text{-}NO_3^-$ of 0.58 in the groundwater of Alesa and Ogale, are indicators of potential denitrification. In groundwater, denitrification theoretically follows a dual isotope slope of 0.5 (Mayer et al., 2002).

Furthermore, in Alsea and Ogale, a strong positive correlation between $\delta^{15}N\text{-}NO_3^-$ and $\delta^{18}O\text{-}NO_3^-$ indicated the occurrence of biological fractionation, likely due to denitrification (Anornu et al., 2017). The weak negative correlations between $\delta^{15}N\text{-}NO_3^-$ and $\delta^{18}O\text{-}NO_3^-$ vs. ln(NO_3^-) (Fig. 4.5 a) suggested that the isotopic enrichment of NO_3^- in the groundwater should have been caused by denitrification rather than dilution or mixing of NO_3^- from different sources (Xia et al., 2017). Also, the ratio of $\delta^{15}N\text{-}NO_3^-$ vs $\delta^{18}O\text{-}NO_3^-$ varied between 1.45 to 2.92. Those values are consistent with the reported ratios for groundwater denitrification, suggesting that simultaneous re-oxidation of NO_2^- occurred concurrently with NO_3^- reduction (Harris et al., 2022).

Also, DO appears to play a vital role in controlling denitrification in Alesa, Ogale, and Ebubu. Based on the thermodynamic principle, a complete depletion of oxygen is required for denitrification to proceed. Clearly, the NO_3^- decreased sharply when DO is ≤ 2 mg/L (Fig. 4.6 c). Also, $\delta^{15}N\text{-}NO_3^-$ composition in the groundwater increases with decreasing DO (Fig. 4.6 a, R = - 0.71), suggesting that DO is an overarching control on denitrification in the groundwater. A similar but weak negative

correlation (Fig. 4.6 b, R = - 0.38) is evident in the $\delta^{18}O\text{-}NO_3^-$ vs DO plot, across the three communities.

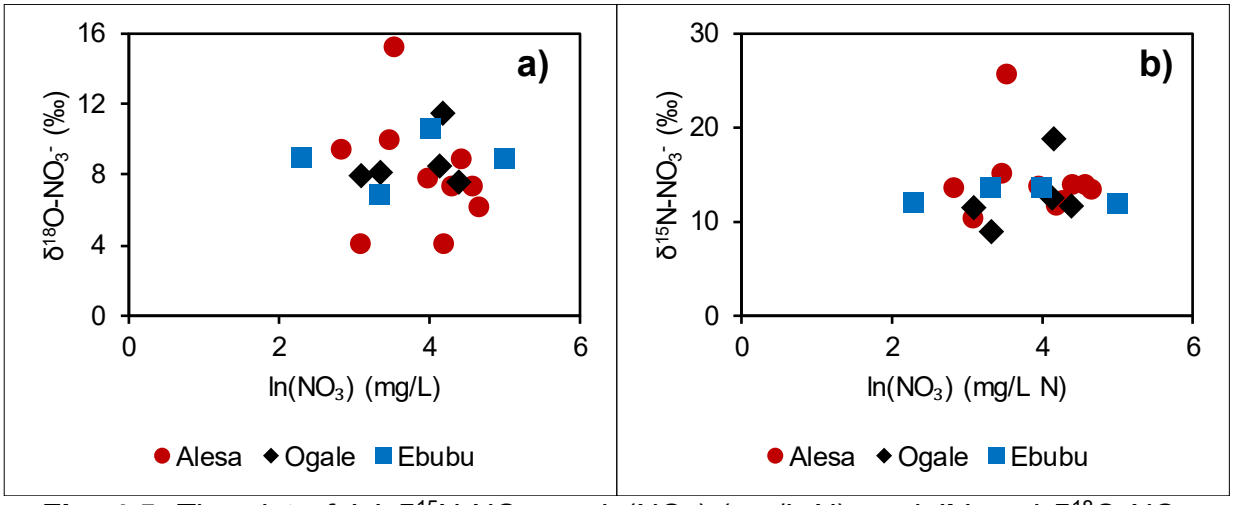

Fig. 4.5. The plot of **(a)** $\delta^{15}N\text{-}NO_3^-$ vs $\ln(NO_3)$ (mg/L N), and **(b)** and $\delta^{18}O\text{-}NO_3^-$ vs $\ln(NO_3)$ (mg/L N) for Ogale and Ebubu in the study areas.

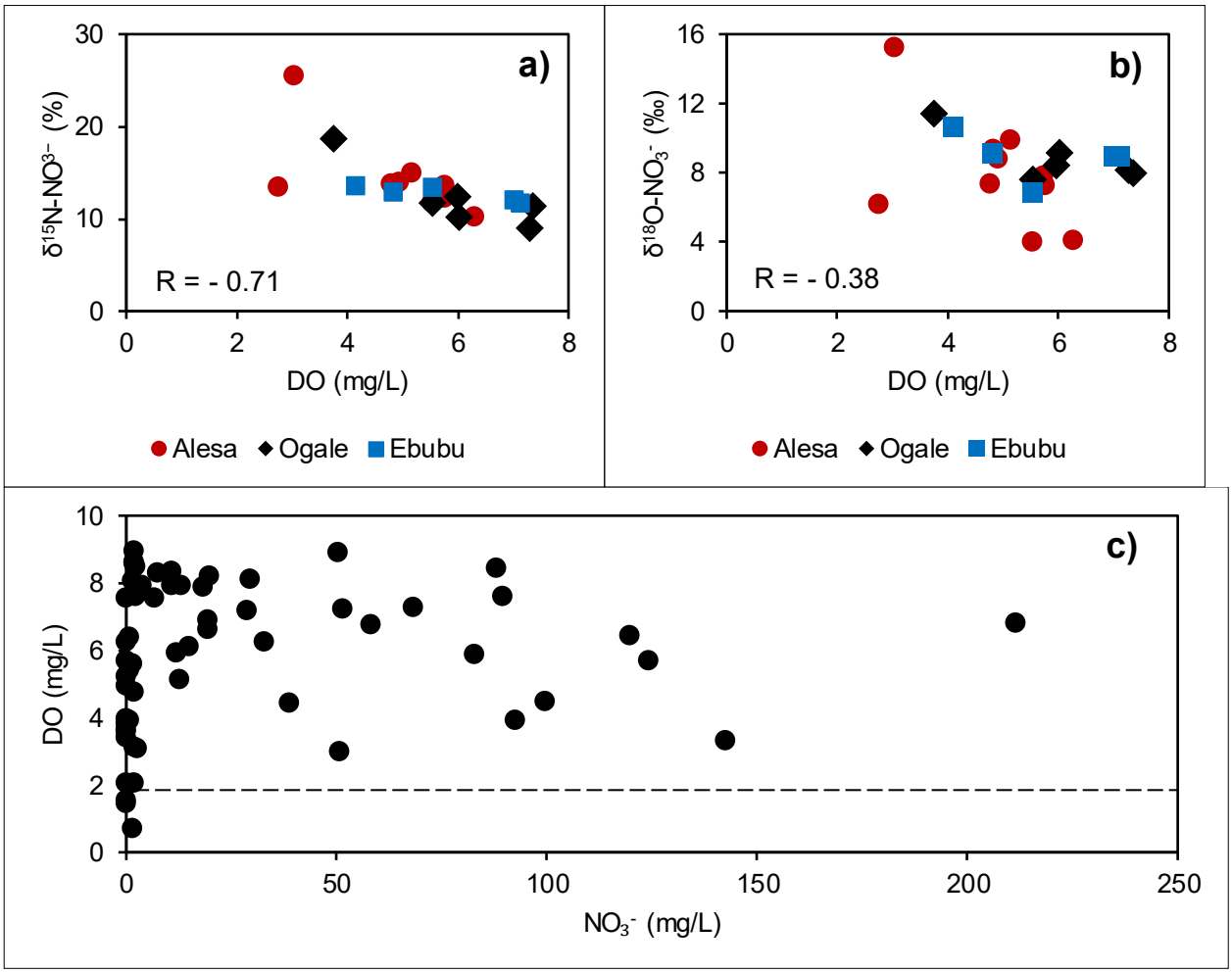

Fig. 4.6. The plot of **(a)** $\delta^{15}N\text{-}NO_3^-$ vs DO, **(b)** $\delta^{18}O\text{-}NO_3^-$ vs DO, and **(c)** DO vs NO_3^- in the study area.

In contrast, there was no relationship between DOC concentration and $\delta^{15}N\text{-}NO_3^-$ in the groundwater or between DOC concentration and NO_3^-. This suggests that the dissolved C fraction was not consumed during denitrification. The lack of a clear correlation between DOC and $\delta^{15}N\text{-}NO_3^-$ is consistent with the findings of Hinkle et al. (2007). They suggested that the dissolved carbon fraction is less relevant for denitrification than solid-phase organic carbon within the aquifer matrix. All the groundwater samples had elevated DOC levels of up to 54 mg/L, which we attribute to the ongoing oil and gas extraction activities in the Niger Delta. While such high DOC may not be consumed directly during denitrification, the labile organic carbon can act as a potential electron donor during groundwater denitrification by providing the necessary electrons needed for the reduction of NO_3^- or NO_2^- to N_2O or N_2 under depleted oxygen conditions. However, no conclusive evidence showed that DOC, as an electron donor, controlled the denitrification process in the study area.

Furthermore, despite the elevated DOC concentrations due to the heavy impacts of the oil and gas activities in the area, the DO level is still high. This is either due to (1) continuous recharge from precipitation or (2) the absence of aerobic respiration or that DOC is not bioavailable for microbial respiration. With a 2,800 to 4,000 mm/yr precipitation rate (Ohwoghere-Asuma et al., 2023a), DO, through the soil, is continuously introduced into the shallow and sandy aquifer of the investigated sites. Given the permeable and sandy nature of the soils and the low water table (1 to 11 m) in the areas, oxygen consumed in the soil zone is resupplied by gaseous oxygen transport through the soil, resulting in insignificant oxygen consumption (e.g., Appelo & Postma, 2005). Furthermore, according to (Rajendiran et al., 2023), in oxic groundwater where aerobic respiration is present, DO shows an inverse correlation with DOC. This relationship, however, depends on the bioavailability of the DOC (Chapelle et al., 2012). Nevertheless, in this study, DO poorly correlates with DOC, indicating either the absence of aerobic respiration or that DOC is not bioavailable for microbial respiration. Notably, the high groundwater temperature (up to 32.5°C), which affects the groundwater saturation level, appears to limit the DOC degradation potential in the investigated areas (Jindrová et al., 2002). Usually, DOC degradation depletes DO. When DO is completely used up, electron acceptors such as NO_3^-, Mn^{4+}, Fe^{3+}, and SO_4^{2-}, if available, will further oxidize DOC (Christensen et al., 2000). The low concentrations of Fe and Mn in this study are due to the dominance of quartz

grains (95 % to 99 %) in the aquifer (Nwajide, 2013) and less anthropogenic activities capable of releasing Fe and Mn into the aquifer. Nevertheless, the impact of the oil and gas industry released Fe in a portion of the Ogale, causing the occurrence of suboxic conditions (i.e., DO < 2 mg/L, NO_3^- < 0.5 mg/L and Fe ≥ 0.1 mg/L (Tesoriero et al., 2024)) in the affected portion. Here, the rusting of an underground NNPCL petroleum pipeline was observed as shown by the accumulation of Fe precipitates (reddish-brown rust particles) as stains on surfaces of (1) polyvinyl chloride overhead tanks used for storage of drinking water and (2) plumbing fixtures, as well as other domestic water containers in residential homes next to the underground pipeline (Fig. 4.5S). As a result, Fe concentrations were elevated, up to 50 mg/L in 2022 and 46 mg/L in 2023 while DO levels were low (Table 4.2S), prompting reducing conditions for NO_3^- and therefore denitrification observed in few samples in the Ogale, hence the low nitrate concentrations in those samples (Fig. 4.1).

Fig. 4.7. (a) and **(b)** municipal sewage in Alesa, **(c)** and **(d)** municipal sewage in Ogale with restricted flow, and **(e)** domestic sewage in Alesa with restricted flow. During rainfall, the sewage is transported to various parts of the community, infiltrating the aquifer. In flooding events, the sewage is transported to the nearby surface waters.

4.4.2.2 Biogeochemical processes of redox reaction on nitrogen (N) behavior in the groundwater

The oxidation/reduction (redox) reaction potential (Eh) is fundamental for most geochemical processes in aqueous environments. While nitrogen compounds actively undergo biogeochemical reactions in groundwater, changes in Eh and pH conditions control the occurrence and stability of the various nitrogen species (i.e., NO_3^-, NO_2^-, and NH_4^+) (Lidman et al., 2017; Reddy & D'angelo, 1997). In the Eh–pH diagram (Fig. 4.8), aqueous species of nitrogen in groundwater under standard conditions (25°C and 1 atm) are dominated by NO_3^- under highly oxidizing conditions, NH_4^+ under highly reducing conditions and NH_3^+ under highly basic and reducing conditions. At the same time, N_2 occupies a large area due to atmospheric influence (Fig. 4.8). In this study, changes in Eh and pH have been identified as an important controlling factor for the dominance of a particular aqueous species of nitrogen predicted to be present at 25°C with an activity value of 1×10^{-3} M dissolved nitrogen in the groundwater. The 1×10^{-3} M used is the NO_3^- activity value commonly found in NO_3^- polluted groundwaters (Appelo & Postma, 2005). It is, however, essential to note that changes in pressure do not necessarily introduce substantial errors in the Eh-pH boundaries calculated for 1 bar. Similarly, the influence of temperature on nitrogen transformation is usually in the same direction (e.g., the rate of chemical reaction speeds up with high temperature) (e.g., Thiagalingam & Kanehiro, 1973). This implies that slight fluctuations in temperature from 25 to 29°C may not significantly alter the stability fields in the Eh-pH diagram (Fig. 4.8).

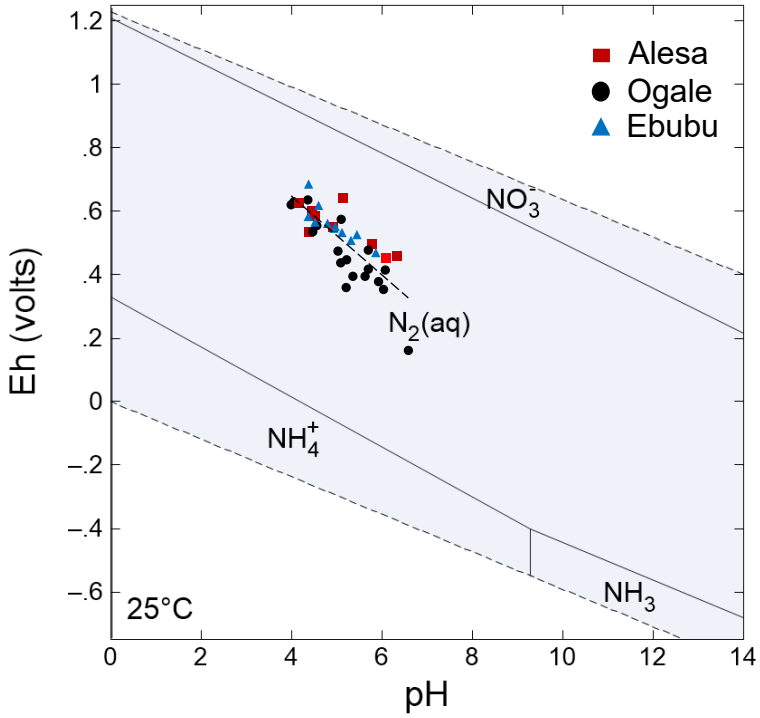

Fig. 4.8. Eh – pH for nitrogen species in Alesa, Ogale, and Ebubu groundwater. The diagram was generated using the Geochemist's Workbench software (17.0 edition).

The Eh values in the Alesa, Ogale, and Ebubu groundwater ranged from 113 to 641 mV (pH = 4 to 6.6), where the NO_3^- contamination was observed, and higher in Alode and Okochiri (Eh = 117 to 801 mV, pH = 4.4 to 6.9) where NO_3^- levels were relatively low. Both sites are characterized by highly oxidizing conditions favorable for nitrification. This explains the high NO_3^- concentrations in the groundwater (Takatert et al., 1999; Zhao et al., 2016). As shown in Fig. 4.8, the groundwater samples plotted in the field of $N_{2(aq)}$ stability between the boundary lines for NH_4^+ and NO_3^-. This supports the idea that nitrifying and denitrifying could be possible in groundwater at our study sites. This result is consistent with a similar investigation in the coastal aquifer of Lagos, Nigeria (Aladejana et al., 2020).

4.4.2.3 NO_3^- export potential and management implications

The schematic diagram of the NO_3^- source in the groundwater of the eastern Niger Delta is given in Fig. 4.9. The sewage availability, DO, and groundwater flow direction were the controlling factors influencing the distribution of NO_3^-. The nitrogen derived from the sewage likely migrated into the aquifer, where it was subsequently nitrified. The NO_3^- was transported along the groundwater flow direction within the groundwater system. The groundwater level in the oxic aquifers upgradient

(9 m) is relatively high compared to the oxic aquifers downgradient (1.5 m). Such differences have created pathways for NO_3^- to be transported, thereby presenting the potential for export to the nearby Okochiri River.

During the 2022 and 2023 sampling campaigns, some minor flooding occurred, due to the frequent heavy rainfall, improper design and maintenance of the drainage channels, and blockage of the municipal drainages. Consequently, sewage from the various drainages was transported to other areas within the community when the soil infiltration capacity was exceeded. This could cause a continuous rise in the groundwater levels facilitating the export of NO_3^- from shallow groundwater to the Okochiri River. Although the groundwater has shown evidence of denitrification, the prevailing redox conditions and the high groundwater NO_3^- load did not support a complete attenuation of NO_3^- in the affected communities. Denitrification, therefore, should not be relied upon for the effective NO_3^- reduction. Also, anthropogenic activities responsible for the elevated groundwater NO_3^- are still ongoing, posing the risk of further increases in the groundwater NO_3^- concentration. Hence, there is a need for urgent groundwater management measures to protect the groundwater.

The management measures should focus on the following:

1. Safe domestic and municipal sewage management practices should be introduced to reduce the amount of anthropogenic nitrogen reaching the aquifer via municipal and domestic sewage infiltration into the groundwater. Furthermore, responsible municipal and domestic sewage disposal will assist in freeing the clogged drainages, reducing the frequently occurring flooding and minimizing the potential spread of NO_3^- contamination.
2. Measures to encourage immediate discontinuous use of the contaminated PSW while alternative safe drinking water sources (e.g., sachet or bottled) are explored. The groundwater NO_3^- levels should, however, be monitored continuously to ensure that NO_3^- levels are within safe limits.

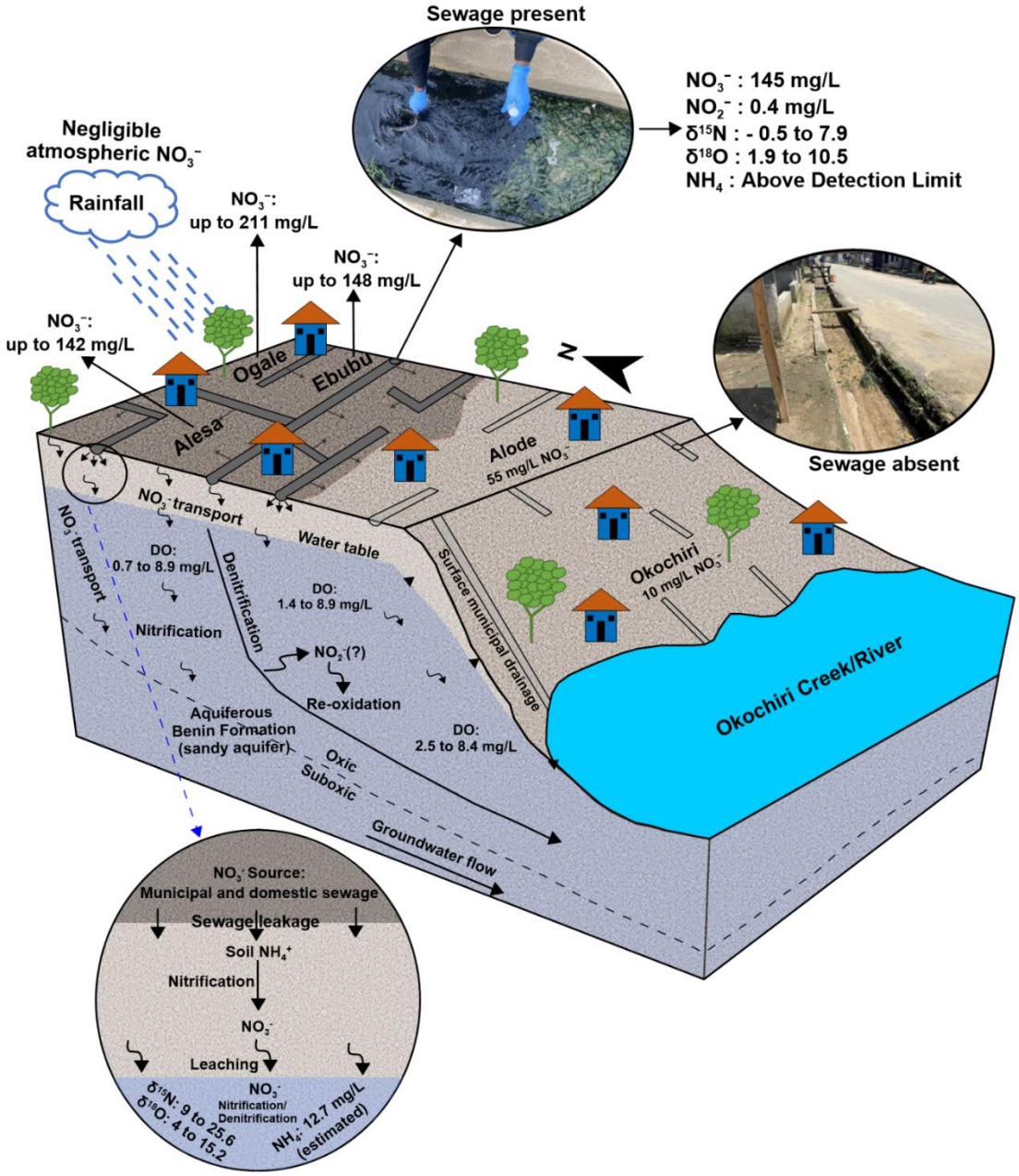

Fig. 4.9. Schematic diagram (not to scale) of the NO_3^- source, transport, and fate in the groundwater of the eastern Niger Delta Region of Nigeria.

4.5 Limitations and needs for further study

Since exposure to high levels of NO_3^- is dangerous to human health, the role of drinking water NO_3^- exposure in the Alesa, Ogale, Ebubu and Alode as a risk factor for specific cancers, adverse reproductive outcomes and other adverse health effects should be investigated. The findings from such investigations will provide public policymakers with a comprehensive understanding of the true health burden associated with NO_3^- contamination in the eastern Niger Delta region. Also, since the prevailing redox conditions do not support effective denitrification in the affected

communities, further studies on various NO_3^- removal techniques, including chemical and biological denitrification, ion exchange, reverse osmosis and adsorption, that use greener nanotechnologies (e.g., nanocomposites and nanorods) should be investigated and used for complete NO_3^- removal in the area.

4.6 Conclusion

The study revealed that the groundwater of Alesa, Ogale, and Ebubu in the eastern Niger Delta is contaminated with NO_3^-, at levels up to 142 mg/L, 211 mg/L, and 148 mg/L, respectively. The groundwater NO_3^- concentration decreased downgradient in Alode (55 mg/L) and Okochiri (10 mg/L). Similarly, NO_2^- groundwater contamination was observed in a few samples at up to 2 mg/L. To further assess the source of NO_3^-, we applied a dual isotope (δ^{15}N-NO_3^- and δ^{18}O-NO_3^-) and hydrochemical markers (major ions and NO_3^-/Cl^- ratio) approach. Our isotopic data were consistent with a sewage source of groundwater NO_3^-. It also showed that nitrification is the primary biogeochemical process controlling the groundwater NO_3^- levels. Our hydrochemical markers also revealed that the NO_3^- contamination is derived from sewage effluents, which likely released N-containing compounds before being nitrified. While nitrification is the primary ongoing biogeochemical process, the data also revealed that denitrification co-occurs in the groundwater, especially in Alesa and Ogale. Given the oxidizing condition of the groundwater, denitrification should not be relied upon for the complete attenuation of NO_3^- in the affected communities. Therefore, there is an urgent need to introduce safe domestic and municipal sewage management practices to protect groundwater. This will also prevent the potential NO_3^- movement into the surface and nearshore seawater.

5. Conclusions and outlook

5.1 Conclusions

This work aimed to investigate the groundwater pollution status of the eastern Niger Delta, focusing on the co-occurrence, source, transport, behavior and fate of Hg, C_6H_6 and NO_3^- in the sandy aquifer of the Benin Formation to improve management and remediation efforts. The primary objectives of the research were (i) the investigation of the occurrence and behavior of Hg, source information, speciation and mobility in the refinery-impacted sandy aquifer of the Benin Formation, (ii) the evaluation of benzene levels, source, and the natural attenuation potential in the oxic pipeline-impacted sandy aquifer**,** and (iii) the investigation of NO_3^- occurrence, source, transport and fate in the sewage-impact sandy aquifer**.** Aquifers of the Benin Formation serve as the major drinking water source for most of the eastern Niger Delta. Their water quality has been and still is being threatened by anthropogenic activities. The population's overreliance on heavily polluted groundwater as drinking water has resulted in environmental and health concerns (Angaye et al., 2015; Ekhator, 2016; Obinna et al., 2017). Meanwhile, the investigation of benzene in groundwater in the region has received little attention. Hg and NO_3^- investigations were unavailable. Thus, a thorough investigation of the occurrence of pollutants, their behavior, transport and fate is crucial in the soil-groundwater systems of the eastern Niger Delta. The findings may be transferable to other locations with similar incidences. The summary and key findings based on the research carried out in this thesis are presented below.

(1) Source of Hg in the sandy aquifer of the Benin Formation

Elevated Hg concentrations in Okochiri groundwater were found only in wells near the Okochiri wastewater discharge outlet (WDO) of the Port Harcourt refinery (Chapter 2). Naturally, most crude oils contain Hg (Subirachs Sanchez, 2013). Notably, crude oils with high sulfur contents are associated with high accumulations of insoluble Hg-sulfide (Wilhelm & Bloom, 2000). However, due to issues that Hg poses to refineries, Hg in crude oil is removed during refining (Littlepage, 2013), and the production waste streams, which may contain Hg, are discharged into the environment. This process could release Hg into the aquifer.

The positive correlation between THg and Hg_{diss} vs SO_4^{2-} in the Okochiri groundwaters indicated that both Hg and SO_4^{2-} were released into the groundwater simultaneously as components of the petroleum production wastewater. Thus, petroleum production wastewater is considered the only possible source of Hg in the Okochiri groundwater.

(2) Hg concentration and speciation in the sandy aquifer

Concentrations of THg and Hg_{diss} in the Okochiri groundwater varied between 0.2 and 6 µg/L. At distances greater than 300 m from the WDO, Hg concentration was less than 0.01 µg/L.

63 % of Hg was bound to particles (> 0.45 µm), 33 % occurred as inorganic, reactive Hg^{2+}, and 4 % as DOM-bound Hg^{2+} despite high DOC (up to 47 mg/L) and BTEX (up to 2,888 µg/L) levels. Notably, petroleum hydrocarbon-based DOC does not bind Hg.

The sediment contained Hg concentrations of up to 529 µg/kg. The carbon content reached 40 %. Here, the binding of Hg to the sediment's natural organic matter (NOM) controls the lateral and depth distribution of Hg in the Okochiri sediments. However, under oxic conditions, up to 23.5 % of the Hg in the quartz-dominant sediment can be mobilized into the Okochiri groundwater. Here, Hg mobilization was significantly controlled by the sediment's NOM despite the presence of petroleum hydrocarbon. Thus, NOM controls the fate and transport of Hg released in the aquifer.

(3) Source and concentration of benzene in the sandy aquifer of the Benin Formation

A vast network of underground oil pipelines characterizes the eastern Niger Delta, including the Nigerian National Petroleum Corporation Limited (NNPCL) underground petroleum pipeline, which runs from the refinery in Okochiri to Umu Nwa (through Alode and Ogale). Notably, drinking water wells next to the pipeline have shown elevated benzene concentrations, up to 3,500 µg/L, 1,300 µg/L and 2,700 µg/L in Alode, Ogale and Okochiri, respectively. In those wells, BTEX levels reached 3,904 µg/L, 1,573 µg/L and 2,888 µg/L in Alode, Ogale and Okochiri, respectively. However, the concentrations decreased with distance from the pipeline to levels less than 0.1 µg/L. DOC concentrations, which reflect the groundwater's total hydrocarbon and non-hydrocarbon load, were up to 47 mg/L, 49 mg/L, and 33 mg/L in Alode, Ogale, and Okochiri, respectively. Petroleum leakage from the NNPCL underground pipeline

could be responsible for the elevated benzene levels in the sandy aquifer of the eastern Niger Delta. However, well distance from the pipeline, the amount of leaked petroleum, and groundwater flow control the occurrence, concentration, and distribution of benzene in the impacted area.

(4) Groundwater potential to attenuate benzene

Despite benzene contamination, the sandy aquifer of the Benin Formation has shown promising aerobic attenuation potential, having up to 7.5 (95 %) mg/L DO level. The aquifer's BTEX biodegradation capacity for DO alone was up to 2.11 mg/L, and the point attenuation rates of BTEX and benzene varied between 0.086 and 0.556 day^{-1}, and 0.128 and 0.693 day^{-1}, respectively, consistent with the values reported for the sandy aquifer in Florida (Wilson et al., 1994) and Utah, USA (Weidemeier et al., 1996). Thus, by natural attenuation alone, 11.2 to 66.5 years would be required to reach Nigeria's groundwater benzene remediation goal. Similarly, 9.2 to 85 years would be required to reach the BTEX remediation goal. Notably, the (1) high groundwater temperature (up to 32.5°C), (2) continuous release of benzene into the groundwater, (3) high benzene levels, and (4) possible absence of a specific microbial population needed to utilize the available oxygen appears to slow down the attenuation rate. Thus, active remediation measures would be required to reduce the time required to reach the clean-up goal.

(5) Occurrence and source of nitrate in the sandy aquifer of the Benin Formation

Elevated NO_3^- concentrations in groundwater were found only in the northern part of the study area (i.e., Alesa, Ogale, and Ebubu), where nitrogen-related anthropogenic activities such as municipal and domestic sewage discharge are common. NO_3^- concentrations in the groundwater were at levels up to 142 mg/L, 211 mg/L and 148 mg/L in Alesa, Ogale and Ebubu, respectively. In the sewage, NO_3^- levels reached 145 mg/L, 131 mg/L and 100 mg/L in Alesa, Ogale and Ebubu, respectively.

The dual isotope ($\delta^{15}N\text{-}NO_3^-$ and $\delta^{18}O\text{-}NO_3^-$) and hydrochemical markers (major ions and NO_3^-/Cl^- ratio) data revealed that sewage is the source of excess nitrate (NO_3^-) in groundwater.

(6) Processes affecting nitrate transformation in the groundwater

Based on our $\delta^{15}N\text{-}NO_3^-$ and $\delta^{18}O\text{-}NO_3^-$ data, NH_4^+ nitrification is the primary biogeochemical process responsible for NO_3^- production in the groundwater. Furthermore, the data revealed that denitrification also occurs in the groundwater. While denitrification could reduce NO_3^- levels in groundwater, the high groundwater NO_3^- levels did not support an effective NO_3^- reduction. Also, nitrogen-related anthropogenic activities are ongoing; hence, NO_3^- levels in the groundwater could further increase. Thus, posing the risk of potential NO_3^- export to the Okochiri River.

5.2 Outlook

Overall, the findings of this study suggest several future research questions that need further investigation. For instance, a detailed investigation of the (1) Hg stable isotope signatures in the groundwater and (2) Hg speciation in the sediments is still required. A possible methodological approach is outlined elsewhere (e.g., McLagan et al., 2022). Furthermore, Hg and sulfur (S) in the sediments should be analyzed in different fractions of the organic matter. Results from such investigations will improve our understanding of the geochemical behavior and fate of Hg at sites impacted by crude oil refining. As such, *in situ* Hg transformation processes associated with changes in groundwater levels, redox conditions, and Hg binding to specific sizes of organic carbon can be demystified. Furthermore, the batch experiment could be repeated to allow for further conclusions on Hg binding to organic carbon in the Benin Formation aquifer. This time, the experiment should be conducted on different grain sizes of the sediments to understand further their role in the lateral and depth distribution of Hg released from crude oil refining.

Point attenuation rates and half-lives can be used to estimate the time required to reach the benzene remediation goal at a particular point within the plume. However, information on whether the benzene plume is expanding, showing slight change, shrinking, or if the plume has reached a dynamic steady state is still unclear. Hence, there is a need for further investigation of the bulk attenuation rate and biodegradation rate of the polluted site. This information can be used to design a site-specific benzene transport model for a long-term monitoring plan.

It is important to consider implementing immediate measures to prevent further release and eventual decline of mercury, benzene (and other TEX compounds)

and nitrate in the groundwater based on the source information provided in this study. For instance, the leaking pipeline could be fixed and active remedial intervention should be carried out on the sediments and aquifers to enhance the biodegradation and natural attenuation capacities of the impacted sites. Here, analysis and identification of the microbial population in the sediments should be conducted to understand the nature and population of the appropriate microbes needed for effective remedial intervention. Also, safe sewage management practices should be explored to prevent further release of nitrogen. Meanwhile, the residents should discontinue the use of the polluted groundwater. Alternatively, granular activated carbon or charcoal filters, for instance, should be used to remove benzene from the water before usage. In the long term, the local authorities should provide alternative drinking water sources (e.g., a centralized water supply system) to save the health of the growing population in the affected communities. Lastly, based on the locations and source information provided in this work, mercury, benzene (and other TEX compounds), and nitrate concentrations should be monitored continuously to ensure their levels are within safe limits.

Acknowledgments

I want to express my sincere gratitude to my advisor, Prof. Dr. Thomas Pichler, for the opportunity to complete my thesis in the Geochemistry and Hydrogeology working group at FB5, Universität Bremen. Your profound knowledge, patience, and rigorous approach to my research were crucial to my completion. A special thank you to Prof. Dr. Harald Biester for the opportunity to work in the Institute of Geoecology's laboratory at Technische Universität Braunschweig. Your knowledge and support were invaluable to the success of this work. I would also like to thank Prof. Stephen E. Obrike (Nasarawa State University, Keffi), who supervised and supported my sampling campaign in Nigeria in 2021 and 2022 despite security threats in the study location. Thank you to Prof. Dr. Carl Renshaw for reviewing this work.

I am grateful to the Petroleum Technology Development Fund (PTDF) Nigeria for providing me with a PhD scholarship opportunity to study in Germany. Thank you, everyone at the Geochemistry and Hydrogeology working group, for the invaluable support and assistance. Dr. Kay Hamer for contributing to this work. Dr. Hannah Roberts for teaching me how to conduct laboratory analysis for the first time. Dr. Henning Fröllje, Dr. Christian Hansen, Dr. Tobias Himmler, Laura Knigge-Stratmann, Janin Scheplitz, and Luis Fernandes-Nogueira for your essential laboratory support. Petra Schmidt and Adelina Calean for laboratory support during my time at the Technische Universität Braunschweig, Germany. Markus Ankele for laboratory support at Helmholtz-Zentrum Hereon, Institute for Carbon Cycles, Geesthacht, Germany. The Dr. Döring laboratory in Bremen for the excellent collaboration.

Special thanks to my committee members for their support, thought-provoking questions, invaluable guidance, and essential feedback. Your contributions have been integral to my completion.

A special thanks to my beloved wife, Faith Nyerma Aleku, for the care, support and love during my long distance. Also, thank you for your support during my sampling campaign in Nigeria. I am also deeply grateful to my amazing family in Nigeria and England for their invaluable support throughout my research. A special thank you to Dr. Holger Dierssen and Amelia for their invaluable support. I dedicate this work to you and the blessed memory of my mother, Mrs. Margaret Samaila Aleku. I hope I have made you all proud.

References

Aaron, K. K. (2005). Perspective: Big Oil, Rural Poverty, and Environmental Degradation in the Niger Delta Region of Nigeria. *Journal of Agricultural Safety and Health, 11*(2), 127-134. https://doi.org/https://doi.org/10.13031/2013.18178

Abam, T., & Nwankwoala, H. (2020). Hydrogeology of Eastern Niger Delta: A Review. *Journal of Water Resource and Protection, 12*(9), 741-777.

Abanyie, S. K., Apea, O. B., Abagale, S. A., Amuah, E. E. Y., & Sunkari, E. D. (2023). Sources and factors influencing groundwater quality and associated health implications: A review. *Emerging Contaminants*, 100207.

Adagunodo, T. A., Sunmonu, L. A., & Adabanija, M. A. (2017). Reservoir characterization and seal integrity of Jemir field in Niger Delta, Nigeria. *Journal of African Earth Sciences, 129*, 779-791. https://doi.org/10.1016/j.jafrearsci.2017.02.015

Adelana, SMA, Olasehinde, P., Bale, R., Vrbka, P., Edet, A., & Goni, I. (2008). An overview of the geology and hydrogeology of Nigeria. *Applied groundwater studies in Africa, 13*, 171-197.

Adelana, M. O., P. Bale, R. B. Vrbka, P. Edet, A. Goni, I. (2008). An overview of the geology and hydrogeology of Nigeria. In (pp. 171-197). https://doi.org/10.1201/9780203889497.ch11

Adeniran, M. A., Oladunjoye, M. A., & Doro, K. O. (2023, 2023-May-09). Soil and groundwater contamination by crude oil spillage: A review and implications for remediation projects in Nigeria [Review]. *Frontiers in Environmental Science, 11*. https://doi.org/10.3389/fenvs.2023.1137496

Adewuyi, G., & Olowu, R. (2012). Assessment of oil and grease, total petroleum hydrocarbons and some heavy metals in surface and groundwater NNPC oil depot, Apata, Ibadan, Nigeria. *International Journal of Aquatic Science, 13*, 45-76.

Adiela, U., & Odiri, N. (2018). Depositional Enviroment and Reservoir Characterization of the Z10 Reservoir sand, Niger Delta, Nigeria. *Int. J. Pure Appl. Sci. Technol, 38*(10), 008-012.

Adjéï Kouacou, B., Anornu, G., Adiaffi, B., & Gibrilla, A. (2024, 2024/08/01/). Hydrochemical characteristics and sources of groundwater pollution in Soubré and Gagnoa counties, Côte d'Ivoire. *Groundwater for Sustainable Development, 26*, 101199. https://doi.org/https://doi.org/10.1016/j.gsd.2024.101199

Adnan, M., Xiao, B., Ali, M. U., Xiao, P., Zhao, P., Wang, H., & Bibi, S. (2024). Heavy metals pollution from smelting activities: A threat to soil and groundwater. *Ecotoxicology and Environmental Safety, 274*, 116189.

Ahmed, S., Le Mouël, F., Stouls, N., & Lipeme Kouyi, G. (2023). Development and Analysis of a Distributed Leak Detection and Localisation System for Crude Oil Pipelines. *Sensors, 23*(9), 4298.

Ajaegwu, N., Ozumba, B., Anomneze, D., & Ugwueze, C. (2017). The impact of global drawdown of sea-level on the Messinian deposits of shallow offshore, Niger Delta, Nigeria. *Basic Phys. Res, 7*(1), 68-86.

Akpokodje, E. (1987). Engineering geology of the Niger Delta. Proc. 9th Reg. Conf. Soil Mech. and Foundation Engr. Lagos,

Akpokodje, E., Etu-Efeotor, J., & Mbeledogu, I. (1996). A study of environmental effects of deep subsurface injection of drilling waste on water resources of the Niger Delta. *CORDEC, University of Port Harcourt, Choba, Port Harcourt, Nigeria*.

Akujieze, C. N., Coker, S., & Oteze, G. (2003). Groundwater in Nigeria–a millennium experience–distribution, practice, problems and solutions. *Hydrogeology Journal, 11*, 259-274.

Al-Harbi, M., Alhajri, I., AlAwadhi, A., & Whalen, J. K. (2020). Health symptoms associated with occupational exposure of gasoline station workers to BTEX compounds. *Atmospheric Environment, 241*, 117847.

Al-Khalid, T., & El-Naas, M. H. (2012). Aerobic biodegradation of phenols: a comprehensive review. *Critical Reviews in Environmental Science and Technology, 42*(16), 1631-1690.

Aladejana, J. A., Kalin, R. M., Sentenac, P., & Hassan, I. (2020). Assessing the impact of climate change on groundwater quality of the shallow coastal aquifer of eastern Dahomey basin, southwestern Nigeria. *Water, 12*(1), 224.

Alam, S. K., Li, P., & Fida, M. (2024). Groundwater nitrate pollution due to excessive use of N-fertilizers in rural areas of Bangladesh: pollution status, health risk, source contribution, and future impacts. *Exposure and Health, 16*(1), 159-182.

Aleku, D. L., Biester, H., & Pichler, T. (2024). Pipeline-Related Residential Benzene Exposure. *Environments, 11*(10). https://doi.org/10.3390/environments11100221

Aleku, D. L., Dähnke, K., & Pichler, T. (2024). Source, transport and fate of nitrate in shallow groundwater in the eastern Niger Delta. *Environmental Science and Pollution Research*. https://doi.org/10.1007/s11356-024-35499-6

Aleku, D. L., Lazareva, O., & Pichler, T. (2024). Mercury in Groundwater–Source, Transport and Remediation. *Applied Geochemistry*, 106060.

Alexander, M. (1999). Biodegradation and Bioremediation. Academic Press San Diego CA. *Biodegradation and bioremediation. Academic Press, San Diego CA.*, -.

Ali, M., Song, X., Wang, Q., Zhang, Z., Zhang, M., Chen, X., Tang, Z., & Liu, X. (2023, 2023/08/05/). Thermally enhanced biodegradation of benzo[a]pyrene and benzene co-contaminated soil: Bioavailability and generation of ROS. *Journal of Hazardous Materials, 455*, 131494. https://doi.org/https://doi.org/10.1016/j.jhazmat.2023.131494

Amajor, L. (1989). Geological appraisal of groundwater exploitation in the Eastern Niger Delta. In *Groundwater and mineral resources of Nigeria* (pp. 85-100). Friedr vieweg and Sohn Braunschweig/Weisbaden.

Amajor, L. (1991a). Aquifers in the benin formation (miocene—recent), eastern Niger delta, Nigeria: Lithostratigraphy, hydraulics, and water quality. *Environmental Geology and Water Sciences, 17*, 85-101.

Amajor, L. (1991b). Aquifers in the benin formation (miocene—recent), eastern Niger delta, Nigeria: Lithostratigraphy, hydraulics, and water quality. *Environmental Geology and Water Sciences, 17*(2), 85-101.

Amajor, L., & Gbadebo, A. (1992). Oilfield brines of meteoric and connate origin in the Eastern Niger Delta. *Journal of Petroleum Geology, 15*(3), 481-488.

AMAP/UN, E. (2019). Technical Background Report for the Global Mercury Assessment 2018. Arctic Monitoring and Assessment Programme, Oslo, Norway/UN Environment Programme, Chemicals and Health Branch, Geneva, Switzerland. https://www.informea.org/sites/default/files/imported-documents/gma_tech.pdf

Ambituuni, A., Hopkins, P., Amezaga, J., Werner, D., & Wood, J. (2015). Risk assessment of a petroleum product pipeline in Nigeria: the realities of managing problems of theft/sabotage. *Safety and Security Engineering V*, 49-60.

An, H.-R., Park, H.-J., & Kim, E.-S. (2001). Cloning and expression of thermophilic catechol 1, 2-dioxygenase gene (catA) from Streptomyces setonii. *FEMS Microbiology Letters, 195*(1), 17-22.

An, Y.-J. (2004). Toxicity of benzene, toluene, ethylbenzene, and xylene (BTEX) mixtures to Sorghum bicolor and Cucumis sativus. *Bulletin of environmental contamination and toxicology, 72*, 1006-1011.

Andreoni, V., & Gianfreda, L. (2007). Bioremediation and monitoring of aromatic-polluted habitats. *Applied Microbiology and Biotechnology, 76*, 287-308.

Angaye, T. C. N., Ohimain, E. I., & Mieyepa, C. E. (2015). The Potability of Groundwater in Bayelsa State, Central Niger Delta Nigeria: A Review. *Journal of Environmental Treatment Techniques, 3*(2), 134-142. http://www.jett.dormaj.com

Anornu, G., Gibrilla, A., & Adomako, D. (2017). Tracking nitrate sources in groundwater and associated health risk for rural communities in the White Volta River basin of Ghana using isotopic approach (δ15N, δ18ONO3 and 3H). *Science of the total environment, 603*, 687-698.

Anyakora, C., & Coker, H. (2009). Assessment of the PAHs contamination threat on groundwater: a case study of the Niger Delta region of Nigeria. *International Journal of Risk Assessment and Management, 13*(2), 150-170.

Appelo, C. A. J., & Postma, D. (2005). *Geochemistry, groundwater and pollution*. CRC press.

Araújo, M. F. D., Bernard, P. C., & Van Grieken, R. (1988). Heavy metal contamination in sediments from the Belgian coast and Scheldt estuary. *Marine Pollution Bulletin, 19*(6), 269-273.

Ariza, J. G., Giráldez, I., Sánchez-Rodas, D., & Morales, E. (2000). Comparison of the feasibility of three extraction procedures for trace metal partitioning in sediments from south-west Spain. *Science of the total environment, 246*(2-3), 271-283.

Asejeje, G. I., Ipeaiyeda, A. R., & Onianwa, P. C. (2021). Occurrence of BTEX from petroleum hydrocarbons in surface water, sediment, and biota from Ubeji Creek of Delta State, Nigeria. *Environmental Science and Pollution Research, 28*, 15361-15379.

Atashgahi, S., Hornung, B., van der Waals, M. J., da Rocha, U. N., Hugenholtz, F., Nijsse, B., Molenaar, D., van Spanning, R., Stams, A. J. M., Gerritse, J., & Smidt, H. (2018, 2018/03/14). A benzene-degrading nitrate-reducing microbial

consortium displays aerobic and anaerobic benzene degradation pathways. *Scientific Reports, 8*(1), 4490. https://doi.org/10.1038/s41598-018-22617-x

ATSDR. (2007). Toxicological profile for benzene. Agency for Toxic Substances and Disease Registry. Atlanta, GA. http:// www.atsdr.cdc.gov/toxprofiles/tp3.html.

Atsdr, U. (1999). Toxicological profile for mercury. *Atlanta: Agency for Toxic Substances and Disease Registry, US Department of Health and Human Services*.

Atuchukwu, A. G., Amechi, B., Horsfall, O., & Udota, B. S. (2022). Investigation of Saline Water Intrusion In Selected Coastal Area Of Rivers State, South-South Nigeria. *Earth Science Malaysia (ESMY), doi. Org/10.26480/Esmy. 01.2022, 56*.

Avbovbo, A. A. (1978). Tertiary lithostratigraphy of Niger delta. *AAPG Bulletin, 62*(2), 295-300.

Aweto, K., Ohwohere-Asuma, O., Ovwamuedo, G., & Atiti, P. (2023). Hydro-geochemical characterization and Groundwater modelling of the subsurface around Ughelli West Engineered Dumpsite in the Western Niger Delta, Nigeria. *Nigerian Journal of Technological Development, 20*(2).

Ayejoto, D. A., & Egbueri, J. C. (2023, 2023/07/05/). Human health risk assessment of nitrate and heavy metals in urban groundwater in Southeast Nigeria. *Acta Ecologica Sinica*. https://doi.org/https://doi.org/10.1016/j.chnaes.2023.06.008

Baedecker, M. J., Cozzarelli, I., Siegel, D., Bennett, P., & Egan-house, R. (1993). Crude oil in a shallow sand and gravel aquifer. III. Biochemical reactions and mass balance modeling in anoxic groundwater. *Appl Geochem, 8*, 569586.

Baedecker, M. J., Eganhouse, R. P., Bekins, B. A., & Delin, G. N. (2011, 2011/11/01/). Loss of volatile hydrocarbons from an LNAPL oil source. *Journal of Contaminant Hydrology, 126*(3), 140-152. https://doi.org/https://doi.org/10.1016/j.jconhyd.2011.06.006

Baedecker, M. J., Eganhouse, R. P., Qi, H., Cozzarelli, I. M., Trost, J. J., & Bekins, B. A. (2018). Weathering of oil in a surficial aquifer. *Groundwater, 56*(5), 797-809.

Baedecker, M. J., Siegel, D. I., Bennett, P., & Cozzarelli, I. M. (1989). The fate and effects of crude oil in a shallow aquifer. US Geological Survey Toxic Substances Hydrology Program: Proceedings of the Technical Meeting, Phoenix, Arizona, September 26-30, 1988,

Baghani, A. N., Sorooshian, A., Heydari, M., Sheikhi, R., Golbaz, S., Ashournejad, Q., Kermani, M., Golkhorshidi, F., Barkhordari, A., & Jafari, A. J. (2019). A case study of BTEX characteristics and health effects by major point sources of pollution during winter in Iran. *Environmental pollution, 247*, 607-617.

Bagnato, Aiuppa, A., Parello, F., D'alessandro, W., Allard, P., & Calabrese, S. (2009). Mercury concentration, speciation and budget in volcanic aquifers: Italy and Guadeloupe (Lesser Antilles). *Journal of Volcanology and Geothermal Research, 179*(1-2), 96-106.

Barringer, L., J., Szabo, Z., Reilly, P. A., & Riskin, M. L. (2013). Variable contributions of mercury from groundwater to a first-order urban coastal plain stream in New Jersey, USA. *Water, Air, & Soil Pollution, 224*, 1-25.

Barringer, J. L., & Szabo, Z. (2006). Overview of investigations into mercury in ground water, soils, and septage, New Jersey coastal plain. *Water, Air, & Soil Pollution, 175*(1-4), 193-221. https://doi.org/10.1007/s11270-006-9130-1

Becher Quinodoz, F., Cabrera, A., Blarasin, M., Matteoda, E., Pascuini, M., Prámparo, S., Boumaiza, L., Matiatos, I., Schroeter, G., Lutri, V., & Giacobone, D. (2024, 2024/10/15/). Chemical and isotopic tracers combined with mixing models for tracking nitrate contamination in the Pampa de Pocho aquifer, Argentina. *Environmental Research, 259*, 119571. https://doi.org/https://doi.org/10.1016/j.envres.2024.119571

Bedics, A., Táncsics, A., Tóth, E., Banerjee, S., Harkai, P., Kovács, B., Bóka, K., & Kriszt, B. (2022). Microaerobic enrichment of benzene-degrading bacteria and description of Ideonella benzenivorans sp. nov., capable of degrading benzene, toluene and ethylbenzene under microaerobic conditions. *Antonie van Leeuwenhoek, 115*(9), 1113-1128.

Behnami, A., Jafari, N., Benis, K. Z., Fanaei, F., & Abdolahnejad, A. (2023). Spatio-temporal variations, ozone and secondary organic aerosol formation potential, and health risk assessment of BTEX compounds in east of Azerbaijan Province, Iran. *Urban Climate, 47*, 101360.

Bekins, B. A., Brennan, J. C., Tillitt, D. E., Cozzarelli, I. M., Illig, J. M., & Martinović-Weigelt, D. (2020). Biological effects of hydrocarbon degradation intermediates: is the total petroleum hydrocarbon analytical method adequate for risk assessment? *Environmental science & technology, 54*(18), 11396-11404.

Bekins, B. A., Cozzarelli, I. M., Erickson, M. L., Steenson, R. A., & Thorn, K. A. (2016). Crude oil metabolites in groundwater at two spill sites. *Groundwater, 54*(5), 681-691.

Belpaire, C., & Goemans, G. (2007). Eels: contaminant cocktails pinpointing environmental contamination. *ICES Journal of Marine Science, 64*(7), 1423-1436.

Bennett, P., Siegel, D., Baedecker, M. J., & Hult, M. (1993). Crude oil in a shallow sand and gravel aquifer—I. Hydrogeology and inorganic geochemistry. *Applied Geochemistry, 8*(6), 529-549.

Bettoso, N., Pittaluga, F., Predonzani, S., Zanello, A., & Acquavita, A. (2023). Mercury levels in sediment, water and selected organisms collected in a coastal contaminated environment: the Marano and Grado lagoon (northern Adriatic Sea, Italy). *Applied Sciences, 13*(5), 3064.

Biddau, R., Dore, E., Da Pelo, S., Lorrai, M., Botti, P., Testa, M., & Cidu, R. (2023, 2023/04/01/). Geochemistry, stable isotopes and statistic tools to estimate threshold and source of nitrate in groundwater (Sardinia, Italy). *Water Research, 232*, 119663. https://doi.org/https://doi.org/10.1016/j.watres.2023.119663

Bloom, N. S. (2000). Analysis and stability of mercury speciation in petroleum hydrocarbons [Article; Proceedings Paper]. *Fresenius Journal of Analytical Chemistry, 366*(5), 438-443. https://doi.org/10.1007/s002160050089

Bloom, N. S., Preus, E., Katon, J., & Hiltner, M. (2003). Selective extractions to assess the biogeochemically relevant fractionation of inorganic mercury in sediments and soils. *Analytica Chimica Acta, 479*(2), 233-248.

Bockelmann, A., Zamfirescu, D., Ptak, T., Grathwohl, P., & Teutsch, G. (2003). Quantification of mass fluxes and natural attenuation rates at an industrial site with a limited monitoring network: a case study. *Journal of Contaminant Hydrology, 60*(1-2), 97-121.

Bolaños-Alvarez, Y., Ruiz-Fernández, A. C., Sanchez-Cabeza, J.-A., Asencio, M. D., Espinosa, L. F., Parra, J. P., Garay, J., Delanoy, R., Solares, N., & Montenegro, K. (2024). Regional assessment of the historical trends of mercury in sediment cores from Wider Caribbean coastal environments. *Science of the Total Environment, 920*, 170609.

Bolden, A. L., Kwiatkowski, C. F., & Colborn, T. (2015). New look at BTEX: are ambient levels a problem? *Environmental science & technology, 49*(9), 5261-5276.

Bollen, A., Wenke, A., & Biester, H. (2008). Mercury speciation analyses in HgCl2-contaminated soils and groundwater - Implications for risk assessment and remediation strategies [Article]. *Water Research, 42*(1-2), 91-100. https://doi.org/10.1016/j.watres.2007.07.011

Botton, S., & Parsons, J. (2006, 11/01). Degradation of BTEX compounds under iron-reducing conditions in contaminated aquifer microcosms. *Environmental toxicology and chemistry / SETAC, 25*, 2630-2638. https://doi.org/10.1897/06-004R.1

Boumaiza, L., Ben Ammar, S., Chesnaux, R., Stotler, R. L., Mayer, B., Huneau, F., Johannesson, K. H., Levison, J., Knöller, K., & Stumpp, C. (2023, 2023/11/01/). Nitrate sources and transformation processes in groundwater of a coastal area experiencing various environmental stressors. *Journal of Environmental Management, 345*, 118803. https://doi.org/https://doi.org/10.1016/j.jenvman.2023.118803

Bradley, P. M., Journey, C. A., Lowery, M. A., Brigham, M. E., Burns, D. A., Button, D. T., Chapelle, F. H., Lutz, M. A., Marvin-DiPasquale, M. C., & Riva-Murray, K. (2012). Shallow groundwater mercury supply in a Coastal Plain stream. *Environmental science & technology, 46*(14), 7503-7511.

Burkart, M. R., & Kolpin, D. W. (1993). *Hydrologic and land-use factors associated with herbicides and nitrate in near-surface aquifers* (0047-2425).

Bussani, M., & Princi, M. (1979). Mercurio nel golfo di Trieste.

Cameron, K. C., Di, H. J., & Moir, J. L. (2013). Nitrogen losses from the soil/plant system: a review. *Annals of applied biology, 162*(2), 145-173.

Cantrell, K., Zachara, J., Dresel, P., Krupka, K., & Serne, R. (2023, 11/03). Geochemical Processes Data Package for the Vadose Zone in the Single-Shell Tank Waste Management Areas at the Hanford Site.

Cao, X., Yang, S., Wu, P., Liu, S., & Liao, J. (2021). Coupling stable isotopes to evaluate sources and transformations of nitrate in groundwater and inflowing rivers around the Caohai karst wetland, Southwest China. *Environmental Science and Pollution Research, 28*, 45826-45839.

Carrey, R., Ballesté, E., Blanch, A. R., Lucena, F., Pons, P., López, J. M., Rull, M., Solà, J., Micola, N., & Fraile, J. (2021). Combining multi-isotopic and molecular

source tracking methods to identify nitrate pollution sources in surface and groundwater. *Water Research, 188*, 116537.

Castro, A. R., Martins, G., Salvador, A. F., & Cavaleiro, A. J. (2022). Iron Compounds in anaerobic degradation of petroleum hydrocarbons: A review. *Microorganisms, 10*(11), 2142.

Cauwet, G. (1987). Influence of sedimentological features on the distribution of trace metals in marine sediments. *Marine chemistry, 22*(2-4), 221-234.

Chakraborty, P., Sarkar, A., Vudamala, K., Naik, R., & Nath, B. N. (2015a). Organic matter—a key factor in controlling mercury distribution in estuarine sediment. *Marine Chemistry, 173*, 302-309.

Chakraborty, P., Sarkar, A., Vudamala, K., Naik, R., & Nath, B. N. (2015b, 2015/07/20/). Organic matter — A key factor in controlling mercury distribution in estuarine sediment. *Marine Chemistry, 173*, 302-309. https://doi.org/https://doi.org/10.1016/j.marchem.2014.10.005

Chapelle, F. H., Bradley, P. M., McMahon, P. B., Kaiser, K., & Benner, R. (2012). Dissolved oxygen as an indicator of bioavailable dissolved organic carbon in groundwater. *Groundwater, 50*(2), 230-241.

Charlet, L., Blancho, F., Bonnet, T., Garambois, S., Boivin, P., Ferber, T., Tisserand, D., & Guedron, S. (2017). Industrial Mercury Pollution in a Mountain Valley: A Combined Geophysical and Geochemical Study. *Procedia Earth and Planetary Science, 17*, 77-80. https://doi.org/https://doi.org/10.1016/j.proeps.2016.12.040

Chen, X., Zhang, S., Yi, L., Liu, Z., Ye, X., Yu, B., Shi, S., & Lu, X. (2022). Evaluation of Biodegradation of BTEX in the Subsurface of a Petrochemical Site near the Yangtze River, China. *International journal of environmental research and public health, 19*(24), 16449.

Chinago, A. (2020). Analysis of rainfall trend, fluctuation and pattern over Port Harcourt, Niger Delta coastal environment of Nigeria. *Biodiversity International Journal, 4*(1), 1-8.

Chira, P., Mendes, R., Ferrari, S., Rocha, C., da Silva, E., Farias, J., & do Carmo, R. (2024). Groundwater Contamination by Gas Stations in Two Eastern Amazonian Towns (Northern Brazil). *Applied Sciences, 14*(13), 5529.

Choi, H.-M., & Lee, J.-Y. (2011). Groundwater contamination and natural attenuation capacity at a petroleum spilled facility in Korea. *Journal of Environmental Sciences, 23*(10), 1650-1659.

Christensen, T. H., Bjerg, P. L., Banwart, S. A., Jakobsen, R., Heron, G., & Albrechtsen, H.-J. (2000). Characterization of redox conditions in groundwater contaminant plumes. *Journal of Contaminant hydrology, 45*(3-4), 165-241.

CIRS. (2017). *China Enforcing Mercury Convention* http://www.cirs-reach.com/news-and-articles/China-Enforcing-Mercury-Convention.html#:~:text=From%201%20January%202021%2C%20the,with%20mercury%20less%20than%202%25

Coffman, V. R., Jensen, A. S., Trabjerg, B. B., Pedersen, C. B., Hansen, B., Sigsgaard, T., Olsen, J., Schaumburg, I., Schullehner, J., & Pedersen, M. (2021). Prenatal exposure to nitrate from drinking water and markers of fetal growth restriction:

a population-based study of nearly one million Danish-born children. *Environmental Health Perspectives, 129*(2), 027002.

COWI, A. (2005). *Assessment of Mercury Releases from the Russian Federation. Reduction of Atmospheric Mercury Releases from Arctic States*. http://hdl.handle.net/11374/14

Cozzarelli, I. M., Baedecker, M. J., Mumford, A. C., Jaeschke, J. B., & Spencer, T. A. (2022). Understanding the Evolution of Groundwater-Contaminant Plume Chemistry Emanating from Legacy Contaminant Sources: An Example from a Long-Term Crude Oil Spill. *Groundwater Monitoring & Remediation, 42*(4), 30-42.

Cozzarelli, I. M., Bekins, B. A., Eganhouse, R. P., Warren, E., & Essaid, H. I. (2010). In situ measurements of volatile aromatic hydrocarbon biodegradation rates in groundwater. *Journal of contaminant hydrology, 111*(1-4), 48-64.

Cozzarelli, I. M., Eganhouse, R. P., & Baedecker, M. J. (1990). Transformation of monoaromatic hydrocarbons to organic acids in anoxic groundwater environment. *Environmental Geology and Water Sciences, 16*, 135-141.

Craig, P. (1986). Organomercury compounds in the environment. In *Organometallic compounds in the environment* (pp. 65-110). Longman Harlow.

Danert, K., & Theis, S. (2017). Professional Management of Water Well Drilling Projects and Programmes Online Course 2018; Report for Course Participants. *UNICEF-Skat Foundation Collaboration, 2019*.

De Laeter, J., & Heumann, K. (1991). Atomic weights of the elements 1989. *Journal of physical and chemical reference data, 20*(6), 1313-1325.

Dean, J. A. (1999). *Lange's handbook of chemistry*.

Degnan, J. R., Bohlke, J., Pelham, K., Langlais, D. M., & Walsh, G. J. (2016). Identification of groundwater nitrate contamination from explosives used in road construction: isotopic, chemical, and hydrologic evidence. *Environmental science & technology, 50*(2), 593-603.

Dehghani, M., Fazlzadeh, M., Sorooshian, A., Tabatabaee, H. R., Miri, M., Baghani, A. N., Delikhoon, M., Mahvi, A. H., & Rashidi, M. (2018). Characteristics and health effects of BTEX in a hot spot for urban pollution. *Ecotoxicology and environmental safety, 155*, 133-143.

Dehghani, M. H., Sanaei, D., Nabizadeh, R., Nazmara, S., & Kumar, P. (2017, 2017/03/01). Source apportionment of BTEX compounds in Tehran, Iran using UNMIX receptor model. *Air Quality, Atmosphere & Health, 10*(2), 225-234. https://doi.org/10.1007/s11869-016-0425-0

Dellapenna, T. M., Hoelscher, C., Hill, L., Al Mukaimi, M. E., & Knap, A. (2020). How tropical cyclone flooding caused erosion and dispersal of mercury-contaminated sediment in an urban estuary: The impact of Hurricane Harvey on Buffalo Bayou and the San Jacinto Estuary, Galveston Bay, USA. *Science of the Total Environment, 748*, 141226.

Deng, C., Geng, H., Xiao, T., Chen, D., Sun, G., & Yin, R. (2022, 2022/06/01/). Mercury isotopic compositions of the Precambrian rocks and implications for tracing mercury cycling in Earth's interior. *Precambrian Research, 373*, 106646. https://doi.org/https://doi.org/10.1016/j.precamres.2022.106646

Diab, A. I., Sanuade, O., & Radwan, A. E. (2023, 2023/01/01). An integrated source rock potential, sequence stratigraphy, and petroleum geology of (Agbada-Akata) sediment succession, Niger delta: application of well logs aided by 3D seismic and basin modeling. *Journal of Petroleum Exploration and Production Technology, 13*(1), 237-257. https://doi.org/10.1007/s13202-022-01548-4

Dickey, P. A., George, G., & Barker, C. (1987). Relationships among oils and water compositions in Niger Delta. *AAPG Bulletin, 71*(10), 1319-1328.

DIN 38406. (1983). German standard procedures for water, wastewater and sludge testing; cations (group E); Determination of ammonium nitrogen (E 5), DIN Deutsches Institut für Normung e.V., Berlin. https://dx.doi.org/10.31030/1209472

Dixit, A., Singh, D., & Shukla, S. K. (2022). Assessment of Human Health Risk Due to Contaminated Groundwater Nearby Municipal Solid Waste Disposal Site: A Case Study in Kanpur City. International Conference on Trends and Recent Advances in Civil Engineering,

Doherty, V.F., & Otitoloju, A. A. (2016). Occurrence and distribution of monocyclic aromatic hydrocarbons (BTEX) and the impact on macrobenthic community structure in Lagos lagoon, Nigeria. *Environmental monitoring and assessment, 188*, 1-17.

Doherty, V. F., & Otitoloju, A. A. (2016, 2016/09/17). Occurrence and distribution of monocyclic aromatic hydrocarbons (BTEX) and the impact on macrobenthic community structure in Lagos lagoon, Nigeria. *Environmental Monitoring and Assessment, 188*(10), 571. https://doi.org/10.1007/s10661-016-5576-9

doRego, E. C. P., & Pereira, N. A. D. (2007). PAHs and BTEX in groundwater of gasoline stations from Rio de Janeiro City, Brazil. *Bulletin of environmental contamination and toxicology, 79*, 660-664.

Drott, A., Björn, E., Bouchet, S., & Skyllberg, U. (2013, 2013/05/07). Refining Thermodynamic Constants for Mercury(II)-Sulfides in Equilibrium with Metacinnabar at Sub-Micromolar Aqueous Sulfide Concentrations. *Environmental Science & Technology, 47*(9), 4197-4203. https://doi.org/10.1021/es304824n

Durov, S. (1948). Natural waters and graphic representation of their composition. Dokl Akad Nauk SSSR,

Edet, A., Nyong, E., Ukpong, A., & Edet, C. (2021). Evaluation and risk assessment of polycyclic aromatic hydrocarbons in groundwater and soil near a petroleum distribution pipeline spill site, Eleme, Nigeria. *Sustainable Water Resources Management, 7*(4), 50.

Edlich, R. F., Rhoads, S. K., Cantrell, H. S., Azavedo, S. M., & Newkirk, A. T. (2010). Banning mercury amalgam. Meeting Materials of the Dental Products Panel. Washington DC: Food and Drug Administration,

Egbueri, J., Agbasi, J., Ikwuka, C., Chiaghanam, O., Khan, M., Khan, M., Khan, N., & Uwajingba, H. (2023). Nitrate health risk and geochemical characteristics of water in a semi-urban: implications from graphical plots and statistical computing. *International Journal of Environmental Analytical Chemistry*, 1-21.

Ekhator, E. O. (2016). Public Regulation of the Oil and Gas Industry in Nigeria: An Evaluation. *Annual Survey of International & Comparative Law, 21*(1). https://digitalcommons.law.ggu.edu/annlsurvey/vol21/iss1/6

Ekong, A. P., James, G. G., & Ohaeri, I. (2024). Oil and Gas Pipeline Leakage Detection using IoT and Deep Learning Algorithm. *Journal of Information Systems and Informatics, 6*(1), 421-434.

El-Naas, M. H., Acio, J. A., & El Telib, A. E. (2014). Aerobic biodegradation of BTEX: progresses and prospects. *Journal of Environmental Chemical Engineering, 2*(2), 1104-1122.

Elsagh, A., Jalilian, H., & Aslshabestari, M. G. (2021). Evaluation of heavy metal pollution in coastal sediments of Bandar Abbas, the Persian Gulf, Iran: Mercury pollution and environmental geochemical indices. *Marine Pollution Bulletin, 167*, 112314.

Eludoyin, A. O., & Fajiwe, A. A. (2023). Groundwater resources in Nigeria: Case study of distribution and quality at a medium-size urban settlement-scale. In *Case Studies in Geospatial Applications to Groundwater Resources* (pp. 183-206). Elsevier.

Enuneku, A., Ogbeide, O., Okpara, B., Kubeyinje, B. F., Job, O., Asemota, C. O., Imoobe, T., & Ezemonye, L. I. (2021). Ingestion and dermal cancer risk via exposure to polycyclic aromatic hydrocarbon–contaminated soils in an oil-producing community, niger delta, Nigeria. *Environmental Toxicology and Chemistry, 40*(1), 261-271.

EPA. (2000). Method 7473, Mercury in solids and solutions by thermal decomposition, amalgamation, and atomic absorption spectrophotometry. https://www.epa.gov/esam/epa-method-7473-sw-846-mercurysolids-and-solutions-thermal-decomposition-amalgamation

Ericksen, G. E. (1983). The Chilean Nitrate Deposits: The origin of the Chilean nitrate deposits, which contain a unique group of saline minerals, has provoked lively discussion for more than 100 years. *American Scientist, 71*(4), 366-374.

Ernst, W. (2012). Overview of naturally occurring Earth materials and human health concerns. *Journal of Asian Earth Sciences, 59*, 108-126.

Essaid, H. I., Bekins, B. A., Godsy, E. M., Warren, E., Baedecker, M. J., & Cozzarelli, I. M. (1995). Simulation of aerobic and anaerobic biodegradation processes at a crude oil spill site. *Water Resources Research, 31*(12), 3309-3327.

Etu-Efeotor, J., & Akpokodje, E. (1990). Aquifer systems of the Niger Delta. *Journal of Mining and Geology, 26*(2), 279-284.

Etu-Efeotor, J., & Odigi, M. (1983). Water supply problems in the eastern Niger Delta. *Journal of Mining and Geology, 20*(1-2), 183-193.

Ewim, D. R. E., Orikpete, O. F., Scott, T. O., Onyebuchi, C. N., Onukogu, A. O., Uzougbo, C. G., & Onunka, C. (2023). Survey of wastewater issues due to oil spills and pollution in the Niger Delta area of Nigeria: a secondary data analysis. *Bulletin of the National Research Centre, 47*(1), 1-20.

Eyankware, M., Akakuru, O., Ulakpa, R., & Eyankware, E. (2022). Hydrogeochemical approach in the assessment of coastal aquifer for domestic, industrial, and agricultural utilities in Port Harcourt urban, southern Nigeria. *International Journal of Energy and Water Resources*, 1-19.

Eyankware, M. O., Akakuru, O. C., Ulakpa, R. O. E., & Eyankware, O. E. (2021). Sustainable management and characterization of groundwater resource in coastal aquifer of Niger delta basin Nigeria. *Sustainable Water Resources Management, 7*, 1-17.

Eyankware, M. O., Aleke, C. G., Selemo, A. O. I., & Nnabo, P. N. (2020, 2020/04/01/). Hydrogeochemical studies and suitability assessment of groundwater quality for irrigation at Warri and environs., Niger delta basin, Nigeria. *Groundwater for Sustainable Development, 10*, 100293. https://doi.org/https://doi.org/10.1016/j.gsd.2019.100293

Eze, M. O. (2021). Metagenome analysis of a hydrocarbon-degrading bacterial consortium reveals the specific roles of BTEX biodegraders. *Genes, 12*(1), 98.

Eziuzor, S., Schmidt, M., & Vogt, C. (2021, 02/01). Anaerobic benzene mineralization by natural microbial communities from Niger Delta. *Biodegradation, 32*, 1-16. https://doi.org/10.1007/s10532-020-09922-x

Farhadian, M., Vachelard, C., Duchez, D., & Larroche, C. (2008). In situ bioremediation of monoaromatic pollutants in groundwater: a review. *Bioresource Technology, 99*(13), 5296-5308.

Federal Ministry of Environment, N. (2017). *Minamata Convention on Mercury Initial Assessment Report for Nigeria*. https://www.mercuryconvention.org/sites/default/files/documents/minamata_initial_assessment/Nigeria_MIA_2017.pdf

Feo, A., Pinardi, R., Scanferla, E., & Celico, F. (2023). How to Minimize the Environmental Contamination Caused by Hydrocarbon Releases by Onshore Pipelines: The Key Role of a Three-Dimensional Three-Phase Fluid Flow Numerical Model. *Water, 15*(10), 1900. https://www.mdpi.com/2073-4441/15/10/1900

Finneran, K. T., & Housewright, M. E. (2001). Enhanced anaerobic bioremediation of BTEX and TCE in groundwater. *In Situ and On-Site Bioremediation, Volume 7. Battelle Press.*

Fishbein, L. (1985). An overview of environmental and toxicological aspects of aromatic hydrocarbons III. Xylene. *Science of the total environment, 43*(1-2), 165-183.

Freeze, R., & Cherry, J. (1979). Groundwater. Englewood Cliffs, N. J.: Prentice-Hall, Inc.

Ganguli, P. M., Conaway, C. H., Swarzenski, P. W., Izbicki, J. A., & Flegal, A. R. (2012, 2012/02/07). Mercury Speciation and Transport via Submarine Groundwater Discharge at a Southern California Coastal Lagoon System. *Environmental Science & Technology, 46*(3), 1480-1488. https://doi.org/10.1021/es202783u

Gao, S., Luo, T.-C., Zhang, B.-R., Zhang, H.-F., Han, Y.-w., Zhao, Z.-D., & Hu, Y.-K. (1998). Chemical composition of the continental crust as revealed by studies in East China. *Geochimica et cosmochimica acta, 62*(11), 1959-1975.

Gibrilla, A., Fianko, J. R., Ganyaglo, S., Adomako, D., Anornu, G., & Zakaria, N. (2020). Nitrate contamination and source apportionment in surface and groundwater in Ghana using dual isotopes (15N and 18O-NO3) and a Bayesian isotope mixing model. *Journal of Contaminant Hydrology, 233*, 103658.

Golkhorshidi, F., Sorooshian, A., Jafari, A. J., Baghani, A. N., Kermani, M., Kalantary, R. R., Ashournejad, Q., & Delikhoon, M. (2019). On the nature and health impacts of BTEX in a populated middle eastern city: Tehran, Iran. *Atmospheric pollution research, 10*(3), 921-930.

Gomes, K. J. M., Oliva, P. A. C., da Rocha, H. O., de Alcantara Mendes, R., da Costa, A. C. G., dos Santos Miranda, C., & de Oliveira Almeida, N. (2023). Evaluation of the contamination of the subsurface and groundwater by monoaromatic hydrocarbons in an eastern Amazonian town in northern Brazil. *Environmental Earth Sciences, 82*(1), 23.

Goni, I. B., Sheriff, B. M., Kolo, A. M., & Ibrahim, M. B. (2019). Assessment of nitrate concentrations in the shallow groundwater aquifer of Maiduguri and environs, Northeastern Nigeria. *Scientific African, 4*, e00089.

González-Fernández, B., Menéndez-Casares, E., Asensio, M., Fernández, S., Ramos-Muñiz, F., Cruz-Hernández, P., & González Quirós, A. (2014). Sources of mercury in groundwater and soils of west Gijón (Asturias, NW Spain). *Science of The Total Environment, 481*, 217–231. https://doi.org/10.1016/j.scitotenv.2014.02.034

Granger, J., & Wankel, S. D. (2016). Isotopic overprinting of nitrification on denitrification as a ubiquitous and unifying feature of environmental nitrogen cycling. *Proceedings of the National Academy of Sciences, 113*(42), E6391-E6400.

Grasby, S. E., Them II, T. R., Chen, Z., Yin, R., & Ardakani, O. H. (2019). Mercury as a proxy for volcanic emissions in the geologic record. *Earth-Science Reviews, 196*, 102880.

Grassi, S., & Netti, R. (2000). Sea water intrusion and mercury pollution of some coastal aquifers in the province of Grosseto (Southern Tuscany — Italy). *Journal of Hydrology, 237*(3), 198-211. https://doi.org/https://doi.org/10.1016/S0022-1694(00)00307-3

Grönwall, J., & Danert, K. (2020). Regarding groundwater and drinking water access through a human rights lens: Self-supply as a norm. *Water, 12*(2), 419.

Grönwall, J. T., Mulenga, M., & McGranahan, G. (2010). *Groundwater, self-supply and poor urban dwellers: A review with case studies of Bangalore and Lusaka*. IIED.

Gross, S. A., Avens, H. J., Banducci, A. M., Sahmel, J., Panko, J. M., & Tvermoes, B. E. (2013). Analysis of BTEX groundwater concentrations from surface spills associated with hydraulic fracturing operations. *Journal of the Air & Waste Management Association, 63*(4), 424-432.

Guerzoni, S., Frignani, M., Giordani, P., & Frascari, F. (1984). Heavy metals in sediments from different environments of a Northern Adriatic Sea area, Italy. *Environmental Geology and Water Sciences, 6*, 111-119.

Guo, X., Zhu, A., & Chen, R. (2021). China's algal bloom suffocates marine life. *Science, 373*(6556), 751-751.

Guo, Z., Yan, C., Wang, Z., Xu, F., & Yang, F. (2020). Quantitative identification of nitrate sources in a coastal peri-urban watershed using hydrogeochemical indicators and dual isotopes together with the statistical approaches. *Chemosphere, 243*, 125364.

Gupta, R. C., Milatovic, D., Lall, R., & Srivastava, A. (2018). Chapter 31 - Mercury. In R. C. Gupta (Ed.), *Veterinary Toxicology (Third Edition)* (pp. 455-462). Academic Press. https://doi.org/https://doi.org/10.1016/B978-0-12-811410-0.00031-3

Gutiérrez, M., Biagioni, R. N., Alarcón-Herrera, M. T., & Rivas-Lucero, B. A. (2018). An overview of nitrate sources and operating processes in arid and semiarid aquifer systems. *Science of the total environment, 624*, 1513-1522.

Ha, E., Basu, N., Bose-O'Reilly, S., Dórea, J. G., McSorley, E., Sakamoto, M., & Chan, H. M. (2017). Current progress on understanding the impact of mercury on human health. *Environmental research, 152*, 419-433.

Harris, S. J., Cendón, D. I., Hankin, S. I., Peterson, M. A., Xiao, S., & Kelly, B. F. (2022). Isotopic evidence for nitrate sources and controls on denitrification in groundwater beneath an irrigated agricultural district. *Science of The Total Environment, 817*, 152606.

Hassan, H., Abou Elezz, A., Abuasali, M., & AlSaadi, H. (2019). Baseline concentrations of mercury species within sediments from Qatar's coastal marine zone. *Marine pollution bulletin, 142*, 595-602.

Hassan, I., Kalin, R. M., Aladejana, J. A., & White, C. J. (2020). Potential impacts of climate change on extreme weather events in the Niger delta part of Nigeria. *Hydrology, 7*(1), 19.

Hatje, V., Andrade, R., Jesus, R., Masqué, P., Albergaria-Barbosa, A., de Andrade, J., & Santos, A. (2019). Historical records of mercury deposition in dated sediment cores reveal the impacts of the legacy and present-day human activities in Todos os Santos Bay, Northeast Brazil. *Marine pollution bulletin, 145*, 396-406.

He, S., Li, P., Su, F., Wang, D., & Ren, X. (2022, 2022/04/01/). Identification and apportionment of shallow groundwater nitrate pollution in Weining Plain, northwest China, using hydrochemical indices, nitrate stable isotopes, and the new Bayesian stable isotope mixing model (MixSIAR). *Environmental Pollution, 298*, 118852. https://doi.org/https://doi.org/10.1016/j.envpol.2022.118852

Hem, J. (1986). Study and Interpretation of Chemical Characterizations of Natural Water. *Water-Supply Paper, 2254*.

Higueras, P., Fernández-Martínez, R., Esbrí, J. M., Rucandio, I., Loredo, J., Ordónez, A., & Alvarez, R. (2015). Mercury soil pollution in Spain: a review. *Environment, energy and climate change I: environmental chemistry of pollutants and wastes*, 135-158.

Hinkle, S. R., Böhlke, J. K., Duff, J. H., Morgan, D. S., & Weick, R. J. (2007). Aquifer-scale controls on the distribution of nitrate and ammonium in ground water near La Pine, Oregon, USA. *Journal of Hydrology, 333*(2-4), 486-503.

Hirner, A. V., Kritsotakis, K., & Tobschall, H. J. (1990, 1990/07/01/). Metal-organic associations in sediments—I. Comparison of unpolluted recent and ancient sediments and sediments affected by anthropogenic pollution. *Applied Geochemistry, 5*(4), 491-505. https://doi.org/https://doi.org/10.1016/0883-2927(90)90023-X

Hoffman, V. J., & Paulsen, S. (2009). Bay Area Petroleum Refinery Mercury Air Emissions, Deposition, and Fate.

Horowitz, A. (1991). A Primer on sediment-trace element chemistry. *Lewis publish, 136*.

Howard, I. C., Okpara, K. E., & Techato, K. (2021). Toxicity and risks assessment of polycyclic aromatic hydrocarbons in river bed sediments of an artisanal crude oil refining area in the Niger Delta, Nigeria. *Water, 13*(22), 3295.

Howard, P. (2017). *Handbook of environmental fate and exposure data: for organic chemicals, volume III pesticides*. Routledge.

Huang, T., Pang, Z., & Yuan, L. (2013). Nitrate in groundwater and the unsaturated zone in (semi) arid northern China: baseline and factors controlling its transport and fate. *Environmental earth sciences, 70*, 145-156.

Huber, M. L., Laesecke, A., & Friend, D. G. (2006). The vapor pressure of mercury. *National Institute of Standards and Technology, NISTIR, 6643*.

Hübner, H. (1986). Chapter 9 – ISOTOPE EFFECTS OF NITROGEN IN THE SOIL AND BIOSPHERE.

IARC. (2010b). International Agency for Research on Cancer: Ingested nitrate and nitrite and cyanobacterial peptide toxins. In *Ingested nitrate and nitrite and cyanobacterial peptide toxins* (pp. 450-450).

IARC. (2018). Benzene. Volume 120. Lyon, International Agency for Research on Cancer (IARC Monographs on the Evaluation of Carcinogenic Risks to Humans, Volume 120; . http://publications.iarc.fr/Book-And-Report-Series/Iarc-Monographs-On-The-Identification-Of-Carcinogenic-Risks-To-Humans/Benzene-2018

IPIECA. (2014). *Mercury management in petroleum refining: An IPIECA Good Practice Guide*. https://www.ipieca.org

IPIECA. (2016). International Petroleum Industry Environmental Conservation Association, Mercury Emissions in the Oil & Gas industry, November 2016. UNEP Discussions.

Ismailov, N., & Nadjafova, S. (2022, 10/06). Experience in Assessing Environmental Risks of Main Oil Pipelines in Azerbaijan through the Prism of Soil Biogeoresistance to Crude Oil Pollution. *Moscow University Soil Science Bulletin, 77*, 196-202. https://doi.org/10.3103/S014768742203005X

Izeze, I. (1990). Aquifer characteristics of the coastal plain sands of the southern Nigeria. *Unpublished M. Sc. thesis, University of Port Harcourt, Port Harcourt, Nigeria*.

Jiang, W., Wang, G., Sheng, Y., Zhao, D., Liu, C., & Guo, Y. (2016). Enrichment and sources of nitrogen in groundwater in the Turpan-Hami area, northwestern China. *Exposure and Health, 8*, 389-400.

Jiang, Z., Grosselin, B., Daële, V., Mellouki, A., & Mu, Y. (2017, 2017/01/01/). Seasonal and diurnal variations of BTEX compounds in the semi-urban environment of Orleans, France. *Science of The Total Environment, 574*, 1659-1664. https://doi.org/https://doi.org/10.1016/j.scitotenv.2016.08.214

Jindrova, E., Chocova, M., Demnerova, K., & Brenner, V. (2002). Bacterial aerobic degradation of benzene, toluene, ethylbenzene and xylene. *Folia microbiologica, 47*, 83-93.

Jindrová, E., Chocová, M., Demnerová, K., & Brenner, V. (2002, 2002/04/01). Bacterial aerobic degradation of benzene, toluene, ethylbenzene and xylene. *Folia Microbiologica, 47*(2), 83-93. https://doi.org/10.1007/BF02817664

Johnson, S. J., Woolhouse, K. J., Prommer, H., Barry, D. A., & Christofi, N. (2003, 2003/11/01/). Contribution of anaerobic microbial activity to natural attenuation of benzene in groundwater. *Engineering Geology, 70*(3), 343-349. https://doi.org/https://doi.org/10.1016/S0013-7952(03)00102-9

Jonasson, I., & Sangster, D. (1975). Variations in the mercury content of sphalerite from some Canadian sulphide deposits. *Assoc. Expl. Geochem*, 313-332.

Joshua, R. E. (2020). *Evaluation of Btex Contamination in Bengaluru Groundwater and Remediation of Contaminated Water Samples*

Ju, Y., Koh, D.-C., Kim, D.-H., Mayer, B., & Kwon, H.-i. (2023). Evaluating the sources and fate of nitrate in riparian aquifers under agricultural land using in situ-measured noble gases, stable isotopes, and metabolic genes. *Water Research, 231*, 119601.

Kabir, Y., Sengupta, R., Agrawal, G. D., & Chopra, R. (2002). Mercury Contamination Of The Groundwater In Bhopal. 1 - 8. https://peoplesscienceinstitute.org/PDF%27s/EQMG/mercury%20in%20bhopal.pdf

Kainz, M., & Lucotte, M. (2006). Mercury concentrations in lake sediments–revisiting the predictive power of catchment morphometry and organic matter composition. *Water, air, and soil pollution, 170*, 173-189.

Kainz, M., Lucotte, M., & Parrish, C. C. (2003). Relationships between organic matter composition and methyl mercury content of offshore and carbon-rich littoral sediments in an oligotrophic lake. *Canadian Journal of Fisheries and Aquatic Sciences, 60*(7), 888-896.

Kalisińska, E., Łanocha-Arendarczyk, N., & Kosik-Bogacka, D. I. (2019). Mercury, Hg. *Mammals and Birds as Bioindicators of Trace Element Contaminations in Terrestrial Environments: An Ecotoxicological Assessment of the Northern Hemisphere*, 593-653.

Kalnas, J., & Teitelbaum, D. T. (2000, 2000/04/01). Dermal Absorption of Benzene: Implications for Work Practices and Regulations. *International Journal of Occupational and Environmental Health, 6*(2), 114-121. https://doi.org/10.1179/oeh.2000.6.2.114

Kao, C., & Prosser, J. (2001). Evaluation of natural attenuation rate at a gasoline spill site. *Journal of hazardous materials, 82*(3), 275-289.

Kaown, D., Koh, D.-C., Mayer, B., Mahlknecht, J., Ju, Y., Rhee, S.-K., Kim, J.-H., Park, D. K., Park, I., & Lee, H.-L. (2023). Estimation of nutrient sources and fate in groundwater near a large weir-regulated river using multiple isotopes and microbial signatures. *Journal of Hazardous Materials, 446*, 130703.

Kasem, A. M., Xu, Z., Jiang, H., Liu, W., Zhang, J., & Nosair, A. M. (2024). Nitrate source and transformation in groundwater under urban and agricultural arid environment in the southeastern Nile Delta, Egypt. *Water, 16*(1), 22.

Kashyap, P., Kumar, A., & Kumar, K. (2019). Btex concentrations and associated health risks at urban vegetative sites in Delhi, India. *Environmental Claims Journal, 31*(4), 349-365.

Kaur, G., Lecka, J., Krol, M., & Brar, S. K. (2023, 2023/10/15/). Novel BTEX-degrading strains from subsurface soil: Isolation, identification and growth evaluation. *Environmental Pollution, 335*, 122303. https://doi.org/https://doi.org/10.1016/j.envpol.2023.122303

Kebede, S. (2012). *Groundwater in Ethiopia: features, numbers and opportunities*. Springer Science & Business Media.

Kehrig, H., Pinto, F., Moreira, I., & Malm, O. (2003). Heavy metals and methylmercury in a tropical coastal estuary and a mangrove in Brazil. *Organic Geochemistry, 34*(5), 661-669.

Kendall, C. (1998). *Isotope Tracers in Catchment Hydrology. Elsevier, pp. 519–576*.

Kendall, C., Elliott, E. M., & Wankel, S. D. (2007). Tracing anthropogenic inputs of nitrogen to ecosystems. *Stable isotopes in ecology and environmental science*, 375-449.

Khan, A. A., Wang, R.-F., Cao, W.-W., Doerge, D. R., Wennerstrom, D., & Cerniglia, C. E. (2001). Molecular cloning, nucleotide sequence, and expression of genes encoding a polycyclic aromatic ring dioxygenase from Mycobacterium sp. strain PYR-1. *Applied and Environmental Microbiology, 67*(8), 3577-3585.

Koopmann, S., Prommer, H., & Pichler, T. (2022). Molybdenum Release Triggered by Dolomite Dissolution: Experimental Evidence and Conceptual Model. *Environmental Science & Technology, 56*(17), 12325-12335.

Korlapati, N. V. S., Khan, F., Noor, Q., Mirza, S., & Vaddiraju, S. (2022). Review and analysis of pipeline leak detection methods. *Journal of pipeline science and engineering, 2*(4), 100074.

Kowalski, A., Siepak, M., & Boszke, L. (2007). Mercury Contamination of Surface and Ground Waters of Poznań, Poland. *Polish Journal of Environmental Studies, 16*(1).

Kozin, L. F., & Hansen, S. C. (2013). *Mercury handbook: chemistry, applications and environmental impact*. Royal society of chemistry.

Krabbenhoft, D. P., Benoit, J. M., Babiarz, C. L., Hurley, J. P., & Andren, A. W. (1995). Mercury cycling in the Allequash Creek watershed, northern Wisconsin. *Water, Air, and Soil Pollution, 80*, 425-433.

Krumgalz, B. S. (1989, 1989/12/01/). Unusual grain size effect on trace metals and organic matter in contaminated sediments. *Marine Pollution Bulletin, 20*(12), 608-611. https://doi.org/https://doi.org/10.1016/0025-326X(89)90397-4

Krupp, R. (1988). Physicochemical aspects of mercury metallogenesis. *Chemical Geology, 69*(3-4), 345-356. https://doi.org/10.1016/0009-2541(88)90045-9

Kubier, A., Hamer, K., & Pichler, T. (2020, Jan). Cadmium Background Levels in Groundwater in an Area Dominated by Agriculture. *Integr Environ Assess Manag, 16*(1), 103-113. https://doi.org/10.1002/ieam.4198

Kubier, A., Wilkin, R. T., & Pichler, T. (2019). Cadmium in soils and groundwater: A review. *Applied Geochemistry, 108*, 104388. https://doi.org/10.1016/j.apgeochem.2019.104388

Kulikova, T., Hiller, E., Jurkovič, Ľ., Filová, L., Šottník, P., & Lacina, P. (2019). Total mercury, chromium, nickel and other trace chemical element contents in soils at an old cinnabar mine site (Merník, Slovakia): anthropogenic versus natural

sources of soil contamination. *Environmental Monitoring and Assessment, 191*(5), 263. https://doi.org/10.1007/s10661-019-7391-6

Kuranchie, F. A., Angnunavuri, P. N., Attiogbe, F., & Nerquaye-Tetteh, E. N. (2019). Occupational exposure of benzene, toluene, ethylbenzene and xylene (BTEX) to pump attendants in Ghana: Implications for policy guidance. *Cogent Environmental Science, 5*(1), 1603418.

Kurwadkar, S., Kanel, S. R., & Nakarmi, A. (2020). Groundwater pollution: Occurrence, detection, and remediation of organic and inorganic pollutants. *Water Environment Research, 92*(10), 1659-1668.

Kwon, K.-D., Jo, W.-K., Lim, H.-J., & Jeong, W.-S. (2007). Characterization of emissions composition for selected household products available in Korea. *Journal of hazardous materials, 148*(1-2), 192-198.

Lalik, M., & Dąbrowska, D. (2024). Groundwater Chemical Status Assessment in the Area of the Waste Landfill in Chorzów—Southern Poland. *Sustainability, 16*(2), 763.

Langford, N. J., & Ferner, R. E. (1999). Toxicity of mercury. *Journal of Human Hypertension, 13*(10), 651-656. https://doi.org/10.1038/sj.jhh.1000896

Lazareva, O., Sparks, D., Landis, R., Ptacek, C., & Ma, J. (2019). Investigation of legacy industrial mercury in floodplain soils: South River, Virginia, USA. *Environmental Earth Sciences, 78*. https://doi.org/10.1007/s12665-019-8253-9

Leipe, T., Moros, M., Kotilainen, A., Vallius, H., Kabel, K., Endler, M., & Kowalski, N. (2013, 2013/10/01/). Mercury in Baltic Sea sediments—Natural background and anthropogenic impact. *Geochemistry, 73*(3), 249-259. https://doi.org/https://doi.org/10.1016/j.chemer.2013.06.005

Leung, C.-M., & Jiao, J. J. (2006). Heavy metal and trace element distributions in groundwater in natural slopes and highly urbanized spaces in Mid-Levels area, Hong Kong. *Water Research, 40*(4), 753-767. https://doi.org/https://doi.org/10.1016/j.watres.2005.12.016

Leusch, F., & Bartkow, M. (2010). *A short primer on Benzene, Toluene, Ethylbenzene and Zylenes (BTEX) in the Environment and in Hydraulic Fracturing Fluids*. Griffith University.

Levin, L. (2014). Mercury in the Environment. *Mercury Control: for Coal-Derived Gas Streams*, 1-12.

Li, S.-L., Liu, C.-Q., Li, J., Xue, Z., Guan, J., Lang, Y., Ding, H., & Li, L. (2013, 2013/01/01). Evaluation of nitrate source in surface water of southwestern China based on stable isotopes. *Environmental Earth Sciences, 68*(1), 219-228. https://doi.org/10.1007/s12665-012-1733-9

Lide, D. R. (2004). *CRC handbook of chemistry and physics* (Vol. 85). CRC press.

Lidman, F., Boily, Å., Laudon, H., & Köhler, S. J. (2017). From soil water to surface water–how the riparian zone controls element transport from a boreal forest to a stream. *Biogeosciences, 14*(12), 3001-3014.

Ligero, R., Ramos-Lerate, I., Barrera, M., & Casas-Ruiz, M. (2001). Relationships between sea-bed radionuclide activities and some sedimentological variables. *Journal of Environmental Radioactivity, 57*(1), 7-19.

Lin, L., Chaocheng, Z., Qiyou, L., Yunbo, Z., Chunshuang, L., & Jianliang, X. (2014). Optimization for microbial degradation of dibenzothiophene by Pseudomonas

sp. Lky-5 using response surface methodology. *China Petroleum Processing Petrochemical and Technology, 16*, 19-26.

Lindberg, A., Björnberg, K. A., Vahter, M., & Berglund, M. (2004). Exposure to methylmercury in non-fish-eating people in Sweden. *Environmental research, 96*(1), 28-33.

Lindén, O., & Pålsson, J. (2013). Oil contamination in ogoniland, Niger Delta. *Ambio, 42*, 685-701.

Lindsay, W., Sadiq, M., & Porter, L. (1981). Thermodynamics of inorganic nitrogen transformations. *Soil Science Society of America Journal, 45*(1), 61-66.

Littlepage, T. (2013). Mercury in crude oils. *Europe, 198*(3.30), 8.7.

Liu, C.-Q., Li, S.-L., Lang, Y.-C., & Xiao, H.-Y. (2006). Using δ15N-and δ18O-values to identify nitrate sources in karst ground water, Guiyang, Southwest China. *Environmental science & technology, 40*(22), 6928-6933.

Liu, K., Zhang, C., Cheng, Y., Liu, C., Zhang, H., Zhang, G., Sun, X., & Mu, Y. (2015). Serious BTEX pollution in rural area of the North China Plain during winter season. *Journal of Environmental Sciences, 30*, 186-190.

Lokhande, P., Patil, V., & Mujawar, H. (2009). Multivariate statistical study of seasonal variation of BTEX in the surface water of Savitri River. *Environmental monitoring and assessment, 157*, 51-61.

Loomis, D., Guyton, K. Z., Grosse, Y., El Ghissassi, F., Bouvard, V., Benbrahim-Tallaa, L., Guha, N., Vilahur, N., Mattock, H., & Straif, K. (2017). Carcinogenicity of benzene. *The Lancet Oncology, 18*(12), 1574-1575.

López, E., Schuhmacher, M., & Domingo, J. L. (2008). Human health risks of petroleum-contaminated groundwater. *Environmental Science and Pollution Research, 15*, 278-288.

Lowden, R. (1972). Sand consolidation study: Compaction and porosity trends within the Niger Delta Basin. *PED Report, 5*.

Lu, H., Iseley, T., Behbahani, S., & Fu, L. (2020, 2020/04/01/). Leakage detection techniques for oil and gas pipelines: State-of-the-art. *Tunnelling and Underground Space Technology, 98*, 103249. https://doi.org/https://doi.org/10.1016/j.tust.2019.103249

Lu, H., Xu, Z.-D., Song, K., Cheng, Y., Dong, S., Fang, H., Peng, H., Fu, Y., Xi, D., Han, Z., Jiang, X., Dong, Y.-R., Gai, P., Shan, Z., & Shan, Y. (2023, 08/24). Greenhouse gas emissions from U.S. crude oil pipeline accidents: 1968 to 2020. *Scientific Data, 10*. https://doi.org/10.1038/s41597-023-02478-4

Majumdar, D. (2003). The blue baby syndrome: nitrate poisoning in humans. *Resonance, 8*(10), 20-30.

Mao, H., Wang, G., Liao, F., Shi, Z., Rao, Z., Zhang, H., Qiao, Z., Bai, Y., Chen, X., & Yan, X. (2024). Spatiotemporal Variation of Groundwater Nitrate Concentration Controlled by Groundwater Flow in a Large Basin: Evidence From Multi-Isotopes (15N, 11B, 18O, and 2H). *Water Resources Research, 60*(1), e2023WR035299.

Mao, H., Wang, G., Liao, F., Shi, Z., Zhang, H., Chen, X., Qiao, Z., Li, B., & Bai, Y. (2023, 2023/03/05/). Spatial variability of source contributions to nitrate in regional groundwater based on the positive matrix factorization and Bayesian

model. *Journal of Hazardous Materials, 445*, 130569. https://doi.org/https://doi.org/10.1016/j.jhazmat.2022.130569

Margat, J., & Van der Gun, J. (2013). *Groundwater around the world: a geographic synopsis*. Crc Press.

Marić, N., Štrbački, J., Polk, J., Slavković Beškoski, L., Avdalović, J., Lješević, M., Joksimović, K., Žerađanin, A., & Beškoski, V. P. (2022). Spatial–temporal assessment of hydrocarbon biodegradation mechanisms at a contaminated groundwater site in Serbia. *Chemistry and Ecology, 38*(2), 95-107.

Marowsky, G., & Wedepohl, K. (1971). General trends in the behavior of Cd, Hg, Tl and Bi in some major rock forming processes. *Geochimica et Cosmochimica Acta, 35*(12), 1255-1267.

Mashyanov, N. (2021). Mercury in gas and oil deposits: corrosion problem. E3S Web of Conferences,

Maswanganyi, C., Tshilongo, J., Mkhohlakali, A., & Martin, L. (2024). Investigation of BTX Concentrations and Effects of Meteorological Parameters in the Steelpoort Area of Limpopo Province, South Africa. *Atmosphere, 15*(5), 552.

Mayer, B., Boyer, E. W., Goodale, C., Jaworski, N. A., van Breemen, N., Howarth, R. W., Seitzinger, S., Billen, G., Lajtha, K., Nadelhoffer, K., Van Dam, D., Hetling, L. J., Nosal, M., & Paustian, K. (2002, 2002/04/01). Sources of nitrate in rivers draining sixteen watersheds in the northeastern U.S.: Isotopic constraints. *Biogeochemistry, 57*(1), 171-197. https://doi.org/10.1023/A:1015744002496

McAllister, P. M., & Chiang, C. Y. (1994). A practical approach to evaluating natural attenuation of contaminants in ground water. *Groundwater Monitoring & Remediation, 14*(2), 161-173.

McDonough, L. K., Santos, I. R., Andersen, M. S., O'Carroll, D. M., Rutlidge, H., Meredith, K., Oudone, P., Bridgeman, J., Gooddy, D. C., & Sorensen, J. P. (2020). Changes in global groundwater organic carbon driven by climate change and urbanization. *Nature communications, 11*(1), 1-10.

McGuire, J. T., Cozzarelli, I. M., Bekins, B. A., Link, H., & Martinović-Weigelt, D. (2018). Toxicity assessment of groundwater contaminated by petroleum hydrocarbons at a well-characterized, aged, crude oil release site. *Environmental science & technology, 52*(21), 12172-12178.

McLagan, D., Schwab, L., Wiederhold, J., Chen, L., Pietrucha, J., Kraemer, S., & Biester, H. (2022). Demystifying mercury geochemistry in contaminated soil–groundwater systems with complementary mercury stable isotope, concentration, and speciation analyses. *Environmental Science: Processes & Impacts*.

McMahon, P., & Böhlke, J. (2006). Regional patterns in the isotopic composition of natural and anthropogenic nitrate in groundwater, High Plains, USA. *Environmental science & technology, 40*(9), 2965-2970.

Medunić, G., Kuharić, Ž., Krivohlavek, A., Đuroković, M., Dropučić, K., Rađenović, A., Lužar Oberiter, B., Krizmanić, A., & Bajramović, M. (2018). Selenium, sulphur, trace metal, and BTEX levels in soil, water, and lettuce from the Croatian Raša Bay contaminated by superhigh-organic-sulphur coal. *Geosciences, 8*(11), 408.

Melkonian, C., Fillinger, L., Atashgahi, S., da Rocha, U. N., Kuiper, E., Olivier, B., Braster, M., Gottstein, W., Helmus, R., & Parsons, J. R. (2021). High

biodiversity in a benzene-degrading nitrate-reducing culture is sustained by a few primary consumers. *Communications biology, 4*(1), 530.

Meng, M., Sun, R.-y., Liu, H.-w., Yu, B., Yin, Y.-g., Hu, L.-g., Shi, J.-b., & Jiang, G.-b. (2019, 2019/03/05). An Integrated Model for Input and Migration of Mercury in Chinese Coastal Sediments. *Environmental Science & Technology, 53*(5), 2460-2471. https://doi.org/10.1021/acs.est.8b06329

Minet, E., Goodhue, R., Meier-Augenstein, W., Kalin, R., Fenton, O., Richards, K., & Coxon, C. (2017). Combining stable isotopes with contamination indicators: a method for improved investigation of nitrate sources and dynamics in aquifers with mixed nitrogen inputs. *Water research, 124*, 85-96.

Ministry of the Environment. (2009). *The Swedish Government chemicals policy: Sweden will ban the use of mercury on 1 June 2009* https://www.government.se/contentassets/12c4d85c2ca64d05827fc131f1a47ab9/sweden-will-ban-the-use-of-mercury

Miri, M., Rostami Aghdam Shendi, M., Ghaffari, H. R., Ebrahimi Aval, H., Ahmadi, E., Taban, E., Gholizadeh, A., Yazdani Aval, M., Mohammadi, A., & Azari, A. (2016, 2016/11/01/). Investigation of outdoor BTEX: Concentration, variations, sources, spatial distribution, and risk assessment. *Chemosphere, 163*, 601-609. https://doi.org/https://doi.org/10.1016/j.chemosphere.2016.07.088

Mirlean, N., Andrus, V. E., & Baisch, P. (2003). Mercury pollution sources in sediments of Patos Lagoon estuary, Southern Brazil. *Marine pollution bulletin, 46*(3), 331-334.

Mitra, S., & Roy, P. (2011). BTEX: A serious ground-water contaminant. *Research Journal of Environmental Sciences, 5*(5), 394.

Mo, N., Ogwah, C., Ulakpa Eyankware, O. R., & Ulakpa, E. (2020, 01/01). The Study of Sea Water Intrusion in Coastal Aquifer of Niger Delta Region, Nigeria. 369-379. https://doi.org/10.5829/idosi.mejsr.2020.369.379

Mohammadi, L., Rahdar, A., Bazrafshan, E., Dahmardeh, H., Susan, M. A. B. H., & Kyzas, G. Z. (2020). Petroleum hydrocarbon removal from wastewaters: a review. *Processes, 8*(4), 447.

Moore, K. B., Ekwurzel, B., Esser, B. K., Hudson, G. B., & Moran, J. E. (2006). Sources of groundwater nitrate revealed using residence time and isotope methods. *Applied Geochemistry, 21*(6), 1016-1029.

Nambi, I. M., Rajasekhar, B., Loganathan, V., & RaviKrishna, R. (2017). An assessment of subsurface contamination of an urban coastal aquifer due to oil spill. *Environmental monitoring and assessment, 189*, 1-17.

Nanadeinboemi, O. A., Uju, M. L., Christopher, C. N., Hakeem, O. O., & David, D. S. (2024). Environmental and Health Influences of Crude Oil Spills in Niger Delta, Nigeria: Case Study Oporoma Community. *Journal of Health and Environmental Research, 8*(1), 29-40.

National Environmental Regulations. (2011). National Environmental (Surface and Ground Water Quality Control) Regulations of Nigeria. 2011. https://www.nesrea.gov.ng/wp-content/uploads/2020/02/Surface_and_Groundwater_Quality_Control_Regulation%202011.pdf

Navarro, A., Font, X., & Viladevall, M. (2016). Groundwater Contamination by Uranium and Mercury at the Ridaura Aquifer (Girona, NE Spain). *Toxics, 4*(3), 16. https://www.mdpi.com/2305-6304/4/3/16

Nekrasov, I. Y., & Timofeeva, M. (1963). Mercury in rocks and minerals of northwestern Yakutia. *Tr. Yakutskogo Filiala Sibirsk. Otd. Akad. Nauk SSSR, 16*, 23-38.

Newell, C. J. (2002). *Calculation and use of first-order rate constants for monitored natural attenuation studies*. US Environmental Protection Agency, National Risk Management Research Laboratory.

Ngah, S. (1990). Groundwater resource development in the Niger Delta. Problems and prospects. International congress international association of engineering geology. 6,

Ngah, S. (2009). Deep aquifer systems of eastern Niger Delta: Their hydrogeological properties, groundwater chemistry and vulnerability to degradation. *Unpublished Ph. D. Thesis, Rivers State University of Science and Technology. Port Harcourt, Nigeria*.

Ngah, S., & Eze, C. (2017). Typical hydraulic properties of deep aquifers of Niger Delta from pumping test data. *Journal of Geoscience and Environment Protection, 5*(11), 139.

NRC. (2013). *Alternatives for managing the nation's complex contaminated groundwater sites*. National Academies Press. (National Research Council)

Nriagu, J., Udofia, E. A., Ekong, I., & Ebuk, G. (2016). Health risks associated with oil pollution in the Niger Delta, Nigeria. *International journal of environmental research and public health, 13*(3), 346.

NSDWQ. (2015). Nigerian Standard for Drinking Water Quality: Nigerian Industrial Standard NIS 554, Standard Organization of Nigeria. https://africacheck.org/sites/default/files/Nigerian-Standard-for-Drinking-Water-Quality-NIS-554-2015.pdf

Nwajide, C. (2013). Geology of Nigeria's Sedimentary Basins (CSS Bookshops Ltd. Lagos) p 565.

Nwankwoala, H., Okujagu, D., Bolaji, T., Papazotos, P., & Ugbenna, K. (2023). Assessment of groundwater quality for irrigation suitability: a case study of Khana and Gokana LGAs, Rivers State, Nigeria. *Environmental Earth Sciences, 82*(12), 292.

Nwankwoala, H. O., & Omofuophu, E. (2020). Investigation of hydrocarbon contaminant levels and groundwater quality assessment in parts of Bonny Island, Rivers State of Nigeria. *Central Asian Journal of Environmental Science and Technology Innovation, 1*(1), 61-70.

Nwankwoala, H. O., & Walter, I. (2012). Assessment of groundwater quality in shallow coastal aquifers of Okrika Island, Eastern Niger Delta, Nigeria. *Ife Journal of Science, 14*(2), 297-304.

Obaje, N. G. (2009). *Geology and mineral resources of Nigeria* (Vol. 120). Springer.

Obinna, A., Bernard, A., Patience, O., & Eric, M. (2017). Application of Geographic Information System in the Hydrochemical Evaluation of Groundwater in Parts of Eastern Niger Delta Nigeria. *American Journal of Environmental Policy and Management, 3*(6), 39-45. http://www.aascit.org/journal/ajepm

Obrike, S., Aleku, L., & Anudu, G. (2022). Hydro-geochemical characterization and water quality appraisal of groundwater in areas adjoining primordial landfills in the Maastrichtian Lafia Formation, Middle Benue Trough. *International Journal of Energy and Water Resources*, 1-15.

Odesa, G., Gbona, C., & Elozona, O. (2024, 01/05). Assessing the total petroleum hydrocarbon content in groundwater in parts of Eleme, Southern Nigeria. 63-75.

Offodile, M. (2002a). Groundwater Study and Development in Nigeria, Mecon Geology and Eng. *Services Ltd*, 453.

Offodile, M. (2002b). Groundwater Study and Development in Nigeria. 2nd Edition, Mecon Geology and Engineering Services Ltd, Jos., 453.

Ogbe, O., Opatola, O., Idjerhe, W., & Ocheli, A. (2013). Reservoir quality evaluation of sand bodies of K-field, onshore Niger Delta, using wireline logs. *International Journal for Science and Emerging Technologies with Latest Trends, 13*(1), 46-64.

Ogbe, O. B. (2020). Sequence stratigraphic controls on reservoir characterization and architectural analysis: a case study of Tovo field, coastal swamp depobelt, Niger Delta Basin, Nigeria. *Marine and Petroleum Geology, 121*, 104579.

Oh, Y. S., Shareefdeen, Z., Baltzis, B. C., & Bartha, R. (1994). Interactions between benzene, toluene, and p-xylene (BTX) during their biodegradation. *Biotechnology and Bioengineering, 44*(4), 533-538.

Ohwoghere-Asuma, O., Oteng, F. M., & Ophori, D. (2023a). Simulation of Saltwater Intrusion into Coastal Aquifer of the Western Niger Delta. In H. Chenchouni, H. I. Chaminé, Z. Zhang, N. Khelifi, A. Ciner, I. Ali, & M. Chen, *Recent Research on Hydrogeology, Geoecology and Atmospheric Sciences* Cham.

Ohwoghere-Asuma, O., Oteng, F. M., & Ophori, D. (2023b). Simulation of Saltwater Intrusion into Coastal Aquifer of the Western Niger Delta. In H. Chenchouni, H. I. Chaminé, Z. Zhang, N. Khelifi, A. Ciner, I. Ali, & M. Chen (Eds.), Recent Research on Hydrogeology, Geoecology and Atmospheric Sciences - Proceedings of the 1st MedGU, Istanbul 2021 Volume 1 (pp. 135-144). (Advances in Science, Technology and Innovation). Springer Nature. In H. Chenchouni, H. I. Chaminé, Z. Zhang, N. Khelifi, A. Ciner, I. Ali, & M. Chen, *Recent Research on Hydrogeology, Geoecology and Atmospheric Sciences.*

Okechukwu, V. U., Omokpariola, D. O., Onwukeme, V. I., Nweke, E. N., & Omokpariola, P. L. (2021). Pollution investigation and risk assessment of polycyclic aromatic hydrocarbons in soil and water from selected dumpsite locations in rivers and Bayelsa State, Nigeria. *Environmental Analysis, Health and Toxicology, 36*(4).

Ola, I., Drebenstedt, C., Burgess, R. M., Mensah, M., Hoth, N., Okoroafor, P., & Külls, C. (2024). Assessing petroleum contamination in parts of the Niger Delta based on a sub-catchment delineated field assessment. *Environmental Monitoring and Assessment, 196*(6), 585.

Olajire, A., & Essien, J. (2014). Aerobic degradation of petroleum components by microbial consortia. *Journal of Petroleum & Environmental Biotechnology, 5*(5), 1.

Omofonmwan, S. I., & Odia, L. O. (2009). Oil Exploitation and Conflict in the Niger-Delta Region of Nigeria. *Journal of Human Ecology, 26*, 25 - 30.

Omokheyeke, O., Sikoki, F., & Abdelmourhit, L. (2015). *Applying sediment cores and nuclear techniques for pollution assessment in the Bonny/new Calabar River Estuary, Niger Delta, Nigeria*.

Omonona, O. V., & Okogbue, C. O. (2021). Hydrochemical evolution, geospatial groundwater quality and potential health risks associated with intake of nitrate via drinking water: case of Gboko agricultural district, central Nigeria. *Environmental Earth Sciences, 80*(4), 126.

Onyeagocha, A. (1980). Petrography and depositional environment of the Benin Formation. *J. Min. geol, 17*(2), 147-150.

Onyena, A. P., Nkwoji, J. A., Chukwu, L. O., Walker, T. R., & Sam, K. (2023, 2023/08/24). Risk assessment of sediment PAH, BTEX, and emerging contaminants in Chanomi Creek Niger Delta, Nigeria. *Environmental monitoring and assessment, 195*(9), 1080. https://doi.org/10.1007/s10661-023-11703-x

Ordinioha, B., & Brisibe, S. (2013). The human health implications of crude oil spills in the Niger delta, Nigeria: An interpretation of published studies. *Nigerian Medical Journal, 54*(1).

Outridge, Sanei, H., & Goodarzi, F. (2007). Evidence for control of mercury accumulation rates in Canadian High Arctic lake sediments by variations of aquatic primary productivity. *Environmental science & technology, 41*(15), 5259-5265.

Owoyemi, F. B., Oteze, G. E., & Omonona, O. V. (2019, 2019/09/06). Spatial patterns, geochemical evolution and quality of groundwater in Delta State, Niger Delta, Nigeria: implication for groundwater management. *Environmental monitoring and assessment, 191*(10), 617. https://doi.org/10.1007/s10661-019-7788-2

Pacyna, E. G., Pacyna, J. M., Fudala, J., Strzelecka-Jastrzab, E., Hlawiczka, S., & Panasiuk, D. (2006, Oct 15). Mercury emissions to the atmosphere from anthropogenic sources in Europe in 2000 and their scenarios until 2020. *Sci Total Environ, 370*(1), 147-156. https://doi.org/10.1016/j.scitotenv.2006.06.023

Pacyna, J. (1987). Atmospheric emissions of arsenic, cadmium, lead and mercury from high temperature processes in power generation and industry. *Lead, mercury, cadmium and arsenic in the environment, 23*, 69.

Panno, S. V., Kelly, W. R., Martinsek, A. T., & Hackley, K. C. (2006). Estimating background and threshold nitrate concentrations using probability graphs. *Groundwater, 44*(5), 697-709.

Pantazidou, M., & Sitar, N. (1993). Emplacement of nonaqueous liquids in the vadose zone. *Water Resources Research, 29*(3), 705-722.

Paschal, C. C., Okeke, O., Okengwo, N., & Onunkwo, A. (2014). Hydrogeochemical Assessment of Groundwater Quality in Parts of Ohaji Egbema Eastern Niger Delta, Nigeria. *Universal Journal of Environmental Research & Technology, 4*(6).

Patrick, L. (2002). Mercury toxicity and antioxidants: part I: role of glutathione and alpha-lipoic acid in the treatment of mercury toxicity.(Mercury Toxicity). *Alternative Medicine Review, 7*(6), 456-472.

Pavoni, B., Donazzolo, R., Marcomini, A., Degobbis, D., & Orio, A. (1987). Historical development of the Venice Lagoon contamination as recorded in radiodated sediment cores. *Marine Pollution Bulletin, 18*(1), 18-24.

Peña-Fernández, A., González-Muñoz, M. J., & Lobo-Bedmar, M. d. C. (2014). Establishing the importance of human health risk assessment for metals and metalloids in urban environments. *Environment international, 72*, 176-185.

Perović, M., Obradović, V., Zuber-Radenković, V., Knoeller, K., Mitrinović, D., & Čepić, Z. (2024, 2024/05/01). The comprehensive evaluation of nitrate origin and transformation pathways in the oxic alluvial aquifer in Serbia. *Environmental Science and Pollution Research, 31*(22), 33030-33046. https://doi.org/10.1007/s11356-024-33403-w

PHMSA. (2019). Pipeline Failure Causes; Technical Report; U.S. Department of Transportation: Washington, DC, USA. https://www.phmsa.dot.gov/incident-reporting/accident-investigation-division/pipeline-failure-causes

Pinedo, J., Ibáñez, R., Lijzen, J., & Irabien, A. (2013). Assessment of soil pollution based on total petroleum hydrocarbons and individual oil substances. *Journal of environmental management, 130*, 72-79.

Piper, A. M. (1944). A graphic procedure in the geochemical interpretation of water-analyses. *Eos, Transactions American Geophysical Union, 25*(6), 914-928.

Plouffe, A., Hall, G. E., & Pelchat, P. (2001). Leaching of loosely bound elements during wet grain size separation with sodium hexametaphosphate: implications for selective extraction analysis. *Geochemistry: Exploration, Environment, Analysis, 1*(2), 157-162.

Podgorski, D. C., Zito, P., McGuire, J. T., Martinovic-Weigelt, D., Cozzarelli, I. M., Bekins, B. A., & Spencer, R. G. (2018). Examining natural attenuation and acute toxicity of petroleum-derived dissolved organic matter with optical spectroscopy. *Environmental science & technology, 52*(11), 6157-6166.

Postgate, J. R. (1998). *Nitrogen fixation*. Cambridge University Press.

Poursanidis, K., Sharanik, J., & Hadjistassou, C. (2024). World's largest natural gas leak from nord stream pipeline estimated at 478,000 tonnes. *Iscience, 27*(1).

Qin, Y., Zhang, D., & Wang, F. (2019). Using nitrogen and oxygen isotopes to access sources and transformations of nitrogen in the Qinhe Basin, North China. *Environmental Science and Pollution Research, 26*, 738-748.

Rahmawati, S., Juliani, A., Sari, W. P., & Bariroh, A. (2018). Investigation of groundwater pollution by petroleum hydrocarbon from gas stations in Yogyakarta, Indonesia. *Jurnal Sains & Teknologi Lingkungan, 10*(1), 67-76.

Raimi, M. O., Abisoye, O. S., Mcfubara, K. G., Richard, G. T., Iyingiala, A.-A., & Oluwatoyin, O. A. (2023). Geochemical Background and Correlation Study of Ground Water Quality in Ebocha-Obrikom of Rivers State, Nigeria. *Raimi, MO, Oyeyemi, AS, Mcfubara, KG, Richard, GT, Austin-Asomeji, I., Omidiji, AO (2023). Geochemical Background and Correlation Study of Ground Water Quality in Ebocha-Obrikom of Rivers State, Nigeria. Trends Appl. Sci. Res, 18*(1), 149-168.

Rajendiran, T., Sabarathinam, C., Panda, B., & Elumalai, V. (2023). Influence of Dissolved Oxygen, Water Level and Temperature on Dissolved Organic Carbon in Coastal Groundwater. *Hydrology, 10*(4), 85.

Ramesh, R., Subramanian, V., & Van Grieken, R. (1990). Heavy metal distribution in sediments of Krishna river basin, India. *Environmental geology and Water sciences, 15*, 207-216.

Ranjbar, F., & Jalali, M. (2012). Calcium, magnesium, sodium, and potassium release during decomposition of some organic residues. *Communications in soil science and plant analysis, 43*(4), 645-659.

Rao, S. M., Joshua, R. E., & Arkenadan, L. (2017). BTEX contamination of Bengaluru aquifers, Karnataka, India. *Journal of Environmental Engineering and Science, 12*(3), 56-61.

Reddy, K., & D'angelo, E. (1997). Biogeochemical indicators to evaluate pollutant removal efficiency in constructed wetlands. *Water Science and Technology, 35*(5), 1-10.

Reddy, K., Patrick, W., & Broadbent, F. (1984). Nitrogen transformations and loss in flooded soils and sediments. *Critical Reviews in Environmental Science and Technology, 13*(4), 273-309.

Regan, S., Hynds, P., & Flynn, R. (2017). An overview of dissolved organic carbon in groundwater and implications for drinking water safety.

Richard, G., Izah, S. C., Morufu, O. R., & Austin-Asomeji, I. (2023). Public and environmental health implications of artisanal petroleum refining and risk reduction strategies in the Niger Delta region of Nigeria. *Bio-Research, 21*(1), 1896-1910.

Richard, J. (2016). *Mercury contaminated groundwater: Speciation analysis, modeling, and remediation*

Rivett, M. O., Buss, S. R., Morgan, P., Smith, J. W., & Bemment, C. D. (2008). Nitrate attenuation in groundwater: a review of biogeochemical controlling processes. *Water research, 42*(16), 4215-4232.

Rudnick, R. L. (2005). Composition of the continental crust. *The Crust, Treatise on Geochemistry, 3*, 17-18.

Rutkowski, C., Lenz, J., Lang, A., Wolter, J., Mothes, S., Reemtsma, T., Grosse, G., Ulrich, M., Fuchs, M., & Schirrmeister, L. (2021). Mercury in sediment core samples from deep Siberian ice-rich permafrost. *Frontiers in Earth Science, 9*, 718153.

Ryan, J. N., & Gschwend, P. M. (1992). Effect of iron diagenesis on the transport of colloidal clay in an unconfined sand aquifer. *Geochimica et Cosmochimica Acta, 56*(4), 1507-1521.

Rytuba, J. J. (2003). Mercury from mineral deposits and potential environmental impact. *Environmental Geology, 43*, 326-338.

Sack, T. M., Steele, D. H., Hammerstrom, K., & Remmers, J. (1992). A survey of household products for volatile organic compounds. *Atmospheric Environment. Part A. General Topics, 26*(6), 1063-1070.

Saka, D., Adu-Gyamfi, J., Skrzypek, G., Antwi, E. O., Heng, L., & Torres-Martínez, J. A. (2023, 2023/07/01/). Disentangling nitrate pollution sources and apportionment in a tropical agricultural ecosystem using a multi-stable isotope model. *Environmental Pollution, 328*, 121589. https://doi.org/https://doi.org/10.1016/j.envpol.2023.121589

Sam, K. S., Onyena, A. P., Erieegha, O. J., & Eze, F. (2023). Water quality evaluation using water quality index and pollution model in selected communities in Gbaramatu Kingdom, Niger Delta, Nigeria. *African Journal of Environmental Science and Technology, 17*(6), 118-134.

Samaniego, J. O., Gibaga, C. R. L., Tanciongco, A. M., Quierrez, R. N. M., Reyes, R. C. G., & Gervasio, J. H. C. (2024). Distribution of total mercury in coastal sediments of Honda Bay, Palawan Island, the Philippines. *Marine Pollution Bulletin, 207*, 116912.

Sanuade, O. A., Akanji, A. O., Oladunjoye, M. A., Olaojo, A. A., & Fatoba, J. O. (2017). Hydrocarbon reservoir characterization of “AY” field, deep-water Niger Delta using 3D seismic and well logs. *Arabian Journal of Geosciences, 10*, 1-11.

Saxby, J. (1969). Metal-organic chemistry of geochemical cycle. *Reviews of Pure and Applied Chemistry, 19*(JUN), 131-&.

Scanlon, B. R., Reedy, R. C., & Bronson, K. F. (2008). Impacts of land use change on nitrogen cycling archived in semiarid unsaturated zone nitrate profiles, southern High Plains, Texas. *Environmental science & technology, 42*(20), 7566-7572.

Scanu, S., Piazzolla, D., Frattarelli, F. M., Mancini, E., Tiralongo, F., Brundo, M. V., Tibullo, D., Pecoraro, R., Copat, C., & Ferrante, M. (2016). Mercury enrichment in sediments of the coastal area of northern Latium, Italy. *Bulletin of environmental contamination and toxicology, 96*, 630-637.

Schullehner, J., Hansen, B., Thygesen, M., Pedersen, C. B., & Sigsgaard, T. (2018). Nitrate in drinking water and colorectal cancer risk: A nationwide population-based cohort study. *International journal of cancer, 143*(1), 73-79.

Scow, K. M., & Hicks, K. A. (2005). Natural attenuation and enhanced bioremediation of organic contaminants in groundwater. *Current opinion in biotechnology, 16*(3), 246-253.

Seeger, E. M. (2013). *Treatment of groundwater contaminated with benzene, MTBE, and ammonium by constructed wetlands* Dissertation, Tübingen, Universität Tübingen, 2013].

Selin, H., Keane, S. E., Wang, S., Selin, N. E., Davis, K., & Bally, D. (2018). Linking science and policy to support the implementation of the Minamata Convention on Mercury. *Ambio, 47*(2), 198-215.

Shah, K., Filby, R., & Haller, W. (1970). Metals in Crude Oil by Neutron Activation Analysis. *J. Radioanal. Chem, 6*, 413.

Shaw, D. M., Dostal, J., & Keays, R. R. (1976). Additional estimates of continental surface Precambrian shield composition in Canada. *Geochimica et Cosmochimica Acta, 40*(1), 73-83.

Sherris, A. R., Baiocchi, M., Fendorf, S., Luby, S. P., Yang, W., & Shaw, G. M. (2021). Nitrate in drinking water during pregnancy and spontaneous preterm birth: a retrospective within-mother analysis in California. *Environmental health perspectives, 129*(5), 057001.

Shin, W.-J., Jung, Y.-Y., Choi, M., Choi, S.-H., Choi, H.-B., Lee, K.-S., Bong, Y.-S., Song, H., & Koh, D.-C. (2023, 2023/07/01/). National-scale investigation of dual nitrate isotopes and chloride ion in South Korea: Nitrate source apportionment for stream water. *Environmental Research, 228*, 115873. https://doi.org/https://doi.org/10.1016/j.envres.2023.115873

Short, K., & Stäuble, A. (1967). Outline of geology of Niger Delta. *AAPG bulletin, 51*(5), 761-779.

Singh, R., & Celin, S. M. (2010). Biodegradation of BTEX (benzene, toluene, ethyl benzene and xylene) compounds by bacterial strain under aerobic conditions. *Journal of Ecobiotechnology, 2*(4).

Sivasankar, V., & Gopalakrishna, G. (2017). Quantification of benzene in groundwater sources and risk analysis in a popular South Indian Pilgrimage City–a GIS based approach. *Arabian Journal of Chemistry, 10*, S2523-S2533.

Small, G. E., Cotner, J. B., Finlay, J. C., Stark, R. A., & Sterner, R. W. (2014). Nitrogen transformations at the sediment–water interface across redox gradients in the Laurentian Great Lakes. *Hydrobiologia, 731*, 95-108.

Smith, M. R. (1990). The biodegradation of aromatic hydrocarbons by bacteria. *Biodegradation, 1*, 191-206.

Sohrabi, T., Shakiba, M., Mirzaei, F., & Pourbabaee, A. (2022). BTEX biodegradation using Bacillus sp. in a synthetic hypoxic aquatic environment: optimization by Taguchi-based design of experiments. *International Journal of Environmental Science and Technology*, 1-8.

Spyropoulou, A. E., Lazarou, Y. G., Sapalidis, A. A., & Laspidou, C. S. (2022). Geochemical modeling of mercury in coastal groundwater. *Chemosphere, 286*, 131609.

Stark, C. H., & Richards, K. G. (2008). The continuing challenge of nitrogen loss to the environment: Environmental consequences and mitigation strategies. *Dynamic Soil, Dynamic Plant, 2*(2), 41-55.

Stayner, L. T., Jensen, A. S., Schullehner, J., Coffman, V. R., Trabjerg, B. B., Olsen, J., Hansen, B., Pedersen, M., Pedersen, C. B., & Sigsgaard, T. (2022). Nitrate in drinking water and risk of birth defects: Findings from a cohort study of over one million births in Denmark. *The Lancet Regional Health–Europe, 14*.

Stern, G., Sanei, H., Roach, P., Delaronde, J., & Outridge, P. (2009). Historical interrelated variations of mercury and aquatic organic matter in lake sediment cores from a subarctic lake in Yukon, Canada: further evidence toward the algal-mercury scavenging hypothesis. *Environmental science & technology, 43*(20), 7684-7690.

Stumm, W., & Morgan, J. J. (2012). *Aquatic chemistry: chemical equilibria and rates in natural waters* (Vol. 126). John Wiley & Sons.

Stumm, W., Morgan, J. J., & Morgan, J. J. (1981). Aquatic Chemistry. A Wiley-Interscience Publication.

Subirachs Sanchez, G. (2013). *Mercury in extraction and refining process of crude oil and natural gas* Universitat Politècnica de Catalunya]. http://hdl.handle.net/2099.1/22105

Takatert, N., Sanchez-Pérez, J. M., & Trémolières, M. (1999). Spatial and temporal variations of nutrient concentration in the groundwater of a floodplain: effect of hydrology, vegetation and substrate. *Hydrological Processes, 13*(10), 1511-1526.

Taylor, S. R. (1964, 1964/08/01/). Abundance of chemical elements in the continental crust: a new table. *Geochimica et Cosmochimica Acta, 28*(8), 1273-1285. https://doi.org/https://doi.org/10.1016/0016-7037(64)90129-2

Tesoriero, A. J., Wherry, S. A., Dupuy, D. I., & Johnson, T. D. (2024). Predicting Redox Conditions in Groundwater at a National Scale Using Random Forest Classification. *Environmental Science & Technology, 58*(11), 5079-5092.

Thiagalingam, K., & Kanehiro, Y. (1973). Effect of Temperature on Nitrogen Transformation in Hawaiian Soils. *Plant and Soil, 38*(1), 177-189. https://doi.org/Doi 10.1007/Bf00011225

Thorne, L., & Nickless, G. (1981). The relation between heavy metals and particle size fractions within the Severn estuary (UK) inter-tidal sediments. *Science of the total environment, 19*(3), 207-213.

Tian, Z., Lehmann, B., Deng, C., Luo, A., Zhang, X., Moynier, F., & Yin, R. (2023, 2023/11/15/). Mercury abundance and isotopic composition in granitic rocks: Implications for Hg cycling in the upper continental crust. *Geochimica et Cosmochimica Acta, 361*, 200-209. https://doi.org/https://doi.org/10.1016/j.gca.2023.09.019

Torres-Martínez, J. A., Mora, A., Mahlknecht, J., Daesslé, L. W., Cervantes-Avilés, P. A., & Ledesma-Ruiz, R. (2021). Estimation of nitrate pollution sources and transformations in groundwater of an intensive livestock-agricultural area (Comarca Lagunera), combining major ions, stable isotopes and MixSIAR model. *Environmental pollution, 269*, 115445.

Toth, C. R. A., Luo, F., Bawa, N., Webb, J., Guo, S., Dworatzek, S., & Edwards, E. A. (2021, Jun 15). Anaerobic Benzene Biodegradation Linked to the Growth of Highly Specific Bacterial Clades. *Environ Sci Technol, 55*(12), 7970-7980. https://doi.org/10.1021/acs.est.1c00508

Tsao, C.-W., Song, H.-G., & Bartha, R. (1998). Metabolism of benzene, toluene, and xylene hydrocarbons in soil. *Applied and Environmental Microbiology, 64*(12), 4924-4929.

Tseng, C., De Diego, A., Wasserman, J., Amouroux, D., & Donard, O. F. X. (1999). Potential interferences generated during mercury species determination using acid leaching, aqueous ethylation, cryogenic gas chromatography and atomic spectrometry detection techniques. *Chemosphere, 39*(7), 1119-1136.

Tucker, T., & Westerman, R. (1989). Gaseous losses of nitrogen from desert region soils. *Arid Land Research and Management, 3*(2), 267-280.

Tunsaringkarn, T., Siriwong, W., Rungsiyothin, A., & Nopparatbundit, S. (2012). Occupational exposure of gasoline station workers to BTEX compounds in Bangkok, Thailand.

Turekian, K. K., & Wedepohl, K. H. (1961). Distribution of the elements in some major units of the earth's crust. *Geological society of America bulletin, 72*(2), 175-192.

Tuttle, M. L., Charpentier, R. R., & Brownfield, M. E. (1999). *The Niger Delta Petroleum System: Niger Delta Province, Nigeria, Cameroon, and Equatorial Guinea, Africa*. US Department of the Interior, US Geological Survey.

Umar, H., Abdul Khanan, M., Magashi, S., Ja'afar, M., & Sani, M. (2023). Fractal Analysis for Oil Spills Clustering in Ahoada Communities of the Niger Delta Region of Nigeria. *The International Archives of the Photogrammetry, Remote Sensing and Spatial Information Sciences, 48*, 371-377.

UNEP. (2002). *Global Mercury Assessment. United Nations Environment Programme (UNEP), Chemicals, Geneva, Switzerland.*

UNEP. (2011). *Environmental Assessment of Ogoniland, Nigeria* (DEP/1337/GE). U. SMI (Distribution Services) Limited Hertfordshire. www.unep.org/nigeria

UNEP. (2018). UNEP Global Mercury Assessment in Environment; UN Environment Programme, Chemicals and Health Branch: Geneva, Switzerland, 2019. *Google Scholar*.

UNEP. (2022). *Latest draft study report on mercury from oil and gas for consideration by the Global Mercury Partnership Advisory Group at its twelfth meeting*. https://wedocs.unep.org/20.500.11822/38902

UNEP, U. (2013). Global Mercury Assessment 2013: Sources, Emissions, Releases and Environmental Transport. *UNEP Chemicals Branch, Geneva, Switzerland*.

UNEP, U. (2014). *Annual Report 2013*.

Unigwe, C. O., Egbueri, J. C., & Omeka, M. E. (2022, 2022/06/01/). Geospatial and statistical approaches to nitrate health risk and groundwater quality assessment of an alluvial aquifer in SE Nigeria for drinking and irrigation purposes. *Journal of the Indian Chemical Society, 99*(6), 100479. https://doi.org/https://doi.org/10.1016/j.jics.2022.100479

Ünlü, V. S., & Alpar, B. (2018). Spatial distribution and sources of BTEX and TPH contamination in freshwater sediments from Lake İznik, NW Turkey. *International Journal of Environment and Geoinformatics, 5*(3), 304-313.

Unueroh, U., Omonria, G., Efosa, O., & Awotunde, M. (2016). Pipeline corrosion control in oil and gas industry: a case study of NNPC/PPMC system 2A pipeline. *Nigerian Journal of Technology, 35*(2), 317-320.

US EPA Method 1631, R. E. (2002). Mercury in water by oxidation, purge and trap, and cold vapor

811 atomic fluorescence spectrometry, United States Environmental Protection Agency (USEPA), 812 Washington, DC, 2002.

USEPA. (2009). *National Primary Drinking Water Regulations* https://www.nrc.gov/docs/ML1307/ML13078A040.pdf

Vaishnav, D., & Babeu, L. (1987). *Comparison of occurrence and rates of chemical biodegradation in natural waters*.

van Leeuwen, J. A., Gerritse, J., Hartog, N., Ertl, S., Parsons, J. R., & Hassanizadeh, S. M. (2022, 2022/06/01/). Anaerobic degradation of benzene and other aromatic hydrocarbons in a tar-derived plume: Nitrate versus iron reducing conditions. *Journal of Contaminant Hydrology, 248*, 104006. https://doi.org/https://doi.org/10.1016/j.jconhyd.2022.104006

Varona-Torres, E., Carlton Jr, D. D., Payne, B., Hildenbrand, Z. L., & Schug, K. A. (2017). The characterization of BTEX in variable soil compositions near unconventional oil and gas development. In *Advances in Chemical Pollution, Environmental Management and Protection* (Vol. 1, pp. 321-351). Elsevier.

Velis, M., Conti, K. I., & Biermann, F. (2017). Groundwater and human development: synergies and trade-offs within the context of the sustainable development goals. *Sustainability science, 12*, 1007-1017.

Vieira, H., Bordalo, M., Figueroa, A., Soares, A., Morgado, F., Abreu, S., & Rendón-von Osten, J. (2021). Mercury distribution and enrichment in coastal sediments

from different geographical areas in the North Atlantic Ocean. *Marine Pollution Bulletin, 165*, 112153.

Vogt, C., Kleinsteuber, S., & Richnow, H. H. (2011). Anaerobic benzene degradation by bacteria. *Microbial biotechnology, 4*(6), 710-724.

Wadge, A., & Salisbury, J. (1997). Benzene, National Environmental Health Forum Monographs, Air Series No. 2. *South Australian Health Commission*.

Wang, Li, Y., Song, Y., Liu, G., Yin, Y., & Cai, Y. (2022). Effects of physical disturbance of sediment on the cycling of mercury in coastal regions. *Science of the Total Environment, 838*, 156298.

Wang, Shou, Chen, J., Zhang, S., Bai, Y., Zhang, X., Chen, D., & Hu, J. (2024, 2024/04/09). Groundwater hydrochemical signatures, nitrate sources, and potential health risks in a typical karst catchment of North China using hydrochemistry and multiple stable isotopes. *Environmental Geochemistry and Health, 46*(5), 173. https://doi.org/10.1007/s10653-024-01964-x

Wang, H., Yan, Z., Ju, X., Song, X., Zhang, J., Li, S., & Zhu-Barker, X. (2023). Quantifying nitrous oxide production rates from nitrification and denitrification under various moisture conditions in agricultural soils: Laboratory study and literature synthesis. *Frontiers in Microbiology, 13*, 1110151.

Wang, M., Li, Y., Zhao, D., Zhuang, L., Yang, G., & Gong, Y. (2020b). Immobilization of mercury by iron sulfide nanoparticles alters mercury speciation and microbial methylation in contaminated groundwater. *Chemical Engineering Journal, 381*, 122664. https://doi.org/https://doi.org/10.1016/j.cej.2019.122664

Wang, Q., Kim, D., Dionysiou, D. D., Sorial, G. A., & Timberlake, D. (2004). Sources and remediation for mercury contamination in aquatic systems—a literature review. *Environmental pollution, 131*(2), 323-336.

Wang, Y., Liu, J., Liem-Nguyen, V., Tian, S., Zhang, S., Wang, D., & Jiang, T. (2021, 2022/02/10/). Binding strength of mercury (II) to different dissolved organic matter: The roles of DOM properties and sources. *Science of The Total Environment, 807*, 150979. https://doi.org/https://doi.org/10.1016/j.scitotenv.2021.150979

Ward, M. H., Jones, R. R., Brender, J. D., de Kok, T. M., Weyer, P. J., Nolan, B. T., Villanueva, C. M., & van Breda, S. G. (2018, Jul 23). Drinking Water Nitrate and Human Health: An Updated Review. *Int J Environ Res Public Health, 15*(7). https://doi.org/10.3390/ijerph15071557

Wassenaar, L. I. (1994). Evaluation of the origin and fate of nitrate in the Abbotsford aquifer using the isotopes of ^{15}N and ^{18}O in NO_3.

Wedepohl, K. H. (1995). The composition of the continental crust. *Geochimica et cosmochimica Acta, 59*(7), 1217-1232.

Weidemeier, T., Swanson, M., Wilson, J., Kampbell, D., Miller, R., & Hansen, J. (1996). Approximation of biodegradation rate constants for monoaromatic hydrocarbons (BTEX) in ground water. *US Environmental Protection Agency Papers*, 26.

White, A. F. (1990). Heterogeneous electrochemical reactions associated with oxidation of ferrous oxide and silicate surfaces. *Reviews in Mineralogy and Geochemistry, 23*(1), 467-509.

WHO. (2007). World Health Organization: Preventing disease through healthy environments: exposure to mercury: a major public health concern.

WHO. (2011). Guidelines for drinking-water quality. *World Health Organization, 216*, 303-304.

WHO. (2017a). Guidelines for drinking-water quality: first addendum to the fourth edition.

WHO. (2017b). *Ten chemicals of major health concern. World Health Organization* https://www.who.int/teams/environment-climate-change-and-health/chemical-safety-and-health/health-impacts/chemicals/mercury

WHO. (2019). Exposure to benzene: a major public health concern. Article WHO/CED/PHE/EPE/19.4.2. https://www.who.int/publications/i/item/WHO-CED-PHE-EPE-19.4.2

Wiedemeier, T. H., Rifai, H. S., Newell, C. J., & Wilson, J. T. (1999). *Natural attenuation of fuels and chlorinated solvents in the subsurface*. John Wiley & Sons.

Wiley, J. (2008). Sons: Hoboken, NJ, USA. *Google Scholar*.

Wilhelm, S. M. (2001). Estimate of mercury emissions to the atmosphere from petroleum [Article]. *Environmental Science & Technology, 35*(24), 4704-4710. https://doi.org/10.1021/es001804h

Wilhelm, S. M., & Bloom, N. (2000). Mercury in petroleum. *Fuel Processing Technology, 63*(1), 1-27. https://doi.org/10.1016/S0378-3820(99)00068-5

Wilhelm, S. M., & Kirchgessner, D. A. (2001). *Mercury in Petroleum and Natural Gas--estimation of Emissions from Production, Processing, and Combustion*. United States Environmental Protection Agency, National Risk Management ….

Wilson, J. T., Pfeffer, F. M., Weaver, J. W., Kampbell, D. H., Wiedemeier, T. H., Hansen, J. E., & Miller, R. N. (1994). Intrinsic bioremediation of JP-4 jet fuel. Symposium on Intrinsic Bioremediation of Ground Water, EPA/540/R-94/515,

Wu, F., Xu, L., Liao, H., Guo, F., Zhao, X., & Giesy, J. P. (2013). Relationship between mercury and organic carbon in sediment cores from Lakes Qinghai and Chenghai, China. *Journal of Soils and Sediments, 13*, 1084-1092.

Wu, J., Bian, J., Wang, Q., & Ruan, D. (2023). Degradation of benzene in anaerobic groundwater in the typical cold industrial region: Identification, interactions, and optimization of nitrate-/sulfate-reducing assemblages. *Biochemical Engineering Journal, 192*, 108833.

Xia, Y., Li, Y., Zhang, X., & Yan, X. (2017). Nitrate source apportionment using a combined dual isotope, chemical and bacterial property, and Bayesian model approach in river systems. *Journal of Geophysical Research: Biogeosciences, 122*(1), 2-14.

Xue, D., Botte, J., De Baets, B., Accoe, F., Nestler, A., Taylor, P., Van Cleemput, O., Berglund, M., & Boeckx, P. (2009). Present limitations and future prospects of stable isotope methods for nitrate source identification in surface-and groundwater. *Water Research, 43*(5), 1159-1170.

Xue, D., De Baets, B., Van Cleemput, O., Hennessy, C., Berglund, M., & Boeckx, P. (2012). Use of a Bayesian isotope mixing model to estimate proportional contributions of multiple nitrate sources in surface water. *Environmental Pollution, 161*, 43-49.

Yang, Y., Li, J., Lv, N., Wang, H., & Zhang, H. (2023, 2023/04/01). Multiphase migration and transformation of BTEX on groundwater table fluctuation in riparian petrochemical sites. *Environmental Science and Pollution Research, 30*(19), 55756-55767. https://doi.org/10.1007/s11356-023-26393-8

Yu, B., Yuan, Z., Yu, Z., & Xue-song, F. (2022). BTEX in the environment: An update on sources, fate, distribution, pretreatment, analysis, and removal techniques. *Chemical Engineering Journal, 435*, 134825.

Yu, L., Zheng, T., Zheng, X., Hao, Y., & Yuan, R. (2020). Nitrate source apportionment in groundwater using Bayesian isotope mixing model based on nitrogen isotope fractionation. *Science of the Total Environment, 718*, 137242.

Zakaria, N., Gibrilla, A., Owusu-Nimo, F., Adomako, D., Anornu, G. K., Fianko, J. R., & Gyamfi, C. (2023). Quantification of nitrate contamination sources in groundwater from the Anayari catchment using major ions, stable isotopes, and Bayesian mixing model, Ghana. *Environmental Earth Sciences, 82*(16), 381.

Zaryab, A., Alijani, F., Knoeller, K., Minet, E., Musavi, S. F., & Ostadhashemi, Z. (2024, 2024/02/26). Identification of groundwater nitrate sources in an urban aquifer (Alborz Province, Iran) using a multi-parameter approach. *Environmental Geochemistry and Health, 46*(3), 100. https://doi.org/10.1007/s10653-024-01872-0

Zaryab, A., Farahmand, A., & Mack, T. J. (2023). Identification and apportionment of groundwater nitrate sources in Chakari Plain (Afghanistan). *Environmental Geochemistry and Health*, 1-15.

Zhang, D., Kong, H., Wu, D., He, S., Hu, Z., & Dai, L. (2009). Impact of pyrolysis treatment on heavy metals in sediment. *Soil and Sediment Contamination, 18*(6), 754-765.

Zhang, L., Zhang, C., Cheng, Z., Yao, Y., & Chen, J. (2013). Biodegradation of benzene, toluene, ethylbenzene, and o-xylene by the bacterium Mycobacterium cosmeticum byf-4. *Chemosphere, 90*(4), 1340-1347.

Zhang, P., Aagaard, P., Gottschalk, L., . (2010). Water Air Soil Pollution. 1323.

Zhang, Y., Li, F., Zhang, Q., Li, J., & Liu, Q. (2014). Tracing nitrate pollution sources and transformation in surface-and ground-waters using environmental isotopes. *Science of the Total Environment, 490*, 213-222.

Zhang, Z.-Y., Li, G., Yang, L., Wang, X.-J., & Sun, G.-X. (2020). Mercury distribution in the surface soil of China is potentially driven by precipitation, vegetation cover and organic matter. *Environmental Sciences Europe, 32*, 1-10.

Zhao, H., Zhang, D., Lv, X., Song, L., Li, J., Chen, F., & Xie, X. (2024, 01/01). Numerical Simulation of Crude Oil Leakage from Damaged Submarine-Buried Pipeline Keywords: Submarine buried pipeline Crude oil leakage Oil spill Numerical simulation Multiphase flow. *Journal of Applied Fluid Mechanics, 17*. https://doi.org/10.47176/jafm.17.1.2061

Zhao, S., Zhou, N., & Liu, X. (2016). Occurrence and controls on transport and transformation of nitrogen in riparian zones of Dongting Lake, China. *Environmental Science and Pollution Research, 23*, 6483-6496.

Zhou, Z., Ansems, N., & Torfs, P. (2015). A global assessment of nitrate contamination in groundwater. *International Groundwater Resources Assessment Center. Internship report, 4*.

Zhu, A., Chen, J., Gao, L., Shimizu, Y., Liang, D., Yi, M., & Cao, L. (2019). Combined microbial and isotopic signature approach to identify nitrate sources and transformation processes in groundwater. *Chemosphere, 228*, 721-734.

Zoleikha, S., Mirzaei, R., & Roksana, M. (2017). Exposure to chemical hazards in petrol pumps stations in Ahvaz City, Iran. *Archives of Environmental & Occupational Health, 72*(1), 3-9.

Appendix A: Mercury in groundwater – Source, transport and remediation

Dogo Lawrence Aleku [a], Olesya Lazareva [b], Thomas Pichler [a,*]

[a] *Institute of Geosciences, University of Bremen, 28359, Bremen, Germany*

[b] *University of Delaware Environmental Institute, Newark, DE, USA*

*Corresponding author: pichler@uni-bremen.de (T. Pichler).

This appendix corresponds to a manuscript that was published in Applied Geochemistry 170 (2024) 106060. https://doi.org/10.1016/j.apgeochem.2024.106060

Applied Geochemistry 170 (2024) 106060

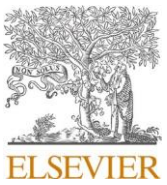

Contents lists available at ScienceDirect

Applied Geochemistry

journal homepage: www.elsevier.com/locate/apgeochem

Invited Review

Mercury in groundwater – Source, transport and remediation

Dogo Lawrence Aleku [a], Olesya Lazareva [b], Thomas Pichler [a,*]

[a] Institute of Geosciences, University of Bremen, 28359, Bremen, Germany
[b] University of Delaware Environmental Institute, Newark, DE, USA

ARTICLE INFO

Editorial handling by: Dr Jiubin Chen

Keywords:
Mercury
Groundwater contamination
Remediation
Source
Mercury speciation
Geogenic
Anthropogenic

ABSTRACT

Mercury (Hg) is one of the most toxic global pollutants of continuing concern, posing a severe threat to human health and wildlife. Due to its mobility, Hg is easily transported through the atmosphere and directly deposited onto water, sediments and soils or incorporated in biota. In groundwater, Hg concentrations can be influenced by either geogenic or anthropogenic sources, causing critical health effects such as damage to the respiratory and nervous systems. The geogenic sources of Hg include rocks and minerals containing Hg (cinnabar, organic-rich shales, and sulfide-rich volcanic) and geothermal fluids. The anthropogenic Hg sources include the combustion of fossil fuels, gold mining, chemical discharges from dental preparation, laboratory activities and legacy sites.

In groundwater, the average background concentration of Hg is < 0.01 μg/L. Mercury can be mobilized into groundwater from geogenic or anthropogenic sources due to changes in redox potential (Eh), with concentrations reaching above the WHO drinking water standard of 1 μg/L. Under reducing conditions, microbial activity facilitates the reductive dissolution of FeOOH, causing the release of sorbed Hg^{2+} into groundwater. The released Hg^{2+} may be reduced to Hg^0 by either dissolved organic matter or Fe^{2+}. The stability of Hg species (Hg^0, Hg_2^{2+}, Hg^{2+}, MeHg) in groundwater is controlled by Eh and pH. While high Eh and low pH conditions can mobilize Hg from the solid into aqueous phases, the soil binding ability can sequestrate the mobilized Hg via adsorption of Hg^{2+} by goethite, hematite, manganese oxides, hydrous ferric oxides, or organic matter restricting it from leaching into groundwater. During groundwater contamination, remediation using nanomaterials such as pumice-supported nanocomposite zero-valent iron, brass shavings, polyaniline-Fe_3O_4-silver diethyldithiocarbamate, and CoMoO/γ-Al_2O_3 has been documented. These promising emerging technologies utilize the principle of adsorption to remove up to 99.98 % of Hg from highly contaminated groundwater. This study presents an overview of groundwater contamination, remediation, complex biogeochemical processes, and a hydrogeochemical conceptual model concerning Hg's mobility, fate, and transport.

1. Introduction

A considerable amount of scientific research focusing on Hg over the past few decades has identified the various geogenic and anthropogenic Hg sources and described its mobility and cycling in the environment (AMAP/UN, 2018; Budianta et al., 2019; Fitzgerald et al., 2007; Gilli et al., 2018; Jernelov, 1973). Environmental impacts, human exposures, and health-related implications of Hg have also been reported (Arrifano et al., 2018; Bravo et al., 2019; Chen, 1997; Feng et al., 2020; Gibi˘car et al., 2009; Lamborg et al., 2002; Li et al., 2012; Outridge et al., 2018). The various studies suggest that Hg is transported globally, primarily via atmospheric pathways. As a result, the United Nations (UN) established the Minamata Convention on Hg, a global program to protect people against direct or indirect consumption or inhalation of Hg. As of 2017, about 128 countries have signed this agreement (Selin et al., 2018). However, even before this UN initiative, Hg was already regulated in several developed and developing countries. In 2007, the European Union (EU) banned Hg-containing batteries, thermometers, barometers, blood pressure monitors, and the production of Hg-containing electronics. In 2008, the United States (US) signed a law banning exports of elemental Hg effective from 2013, and in 2009, Sweden prohibited Hg-containing products (Ministry of the Environment, 2009). Denmark banned the use of Hg for dental amalgam. However, its application for molar mastication of surface fillings in permanent teeth treatment for adults is allowed (Edlich et al., 2010).

In January 2008, Norway also enacted a law banning Hg in the manufacturing and import/export of Hg products while providing satisfactory alternatives to Hg products (Edlich et al., 2010). The ban

* Corresponding author.
E-mail address: pichler@uni-bremen.de (T. Pichler).

https://doi.org/10.1016/j.apgeochem.2024.106060
Received 25 March 2024; Received in revised form 30 May 2024; Accepted 1 June 2024
Available online 8 June 2024

resulted from the reported Hg contamination in several lakes and sediments in Norway (Berg et al., 2006). In 2018, the mining and export of Hg were also banned, and the utilization of Hg dental amalgam on vulnerable patients was restricted. Beginning in 2021, China restricted the manufacturing and importation of Hg-containing batteries, switches and relays, compact fluorescent lamps, high-pressure Hg vapor lamps, pesticides, biocides, topical antiseptics, and cosmetics. By 2026, Hg-containing thermometers and Hg sphygmomanometers will be banned (CIRS, 2017). Furthermore, the World Health Organization (WHO), United Nations Environment Programme (UNEP), European Union (EU), and Chemical Inspection and Regulation Service (CIRS) China established drinking water guidelines for Hg at 1 μg/L (Jin et al., 2006; Rhee, 2015; UNEP, 2013). In comparison, the United States Environmental Protection Agency (USEPA) set the Hg limit at 2 μg/L (USEPA, 2009).

The continuous study of Hg in groundwater remains vital to the global effort to manage contamination risks to human health. Recent studies on Hg in groundwater focused on its occurrence and mobility (Amiri et al., 2021; Barringer et al., 2013; Díaz et al., 2006; Gonza´lez-Ferna´ndez et al., 2014), local distribution, contamination incidences, biogeochemical cycling (Amiri et al., 2021; Barringer et al., 2005; Bollen et al., 2008; Ganguli et al., 2012; Gonz´alez-Ferna´ndez et al., 2014; Khattak et al., 2021; Lamborg et al., 2013; Magi et al., 2019; McLagan et al., 2022; Moussa and Yahia, 2012; Nevondo et al., 2019; Sharma et al., 2021; Tran et al., 2020), speciation (Bollen et al., 2008; Wang et al., 2020b), and existing and emerging remediation technologies (Agyapong et al., 2018; Huang et al., 2020; Marotte, 2002; Richard and Biester, 2016; Weisener et al., 2005). Other studies investigated environmental monitoring strategies for detecting Hg contamination using biological methods (Huang et al., 2015), groundwater discharge and biogeochemical cycling (Schmitt et al., 2020), mercu-ry–thermal/microbe/mineral interactions (Mishra, 2017; Zhao, 2005), and the modeling of Hg-contaminated groundwater (Richard et al., 2016). Nevertheless, studies on Hg contamination in groundwater are generally scarce (Barringer et al., 2013) because the scientific focus is primarily on atmospheric Hg pollution, remediation, cycling, and sources (Engstrom et al., 2007; Kumari et al., 2015; Pacyna et al., 2006; Schuster et al., 2002; Zhong et al., 2019), Hg contamination, speciation, mobility and transport in soils, sediments, lakes and the ocean (Fitzgerald et al., 2007; Gębka et al., 2020; Gilli et al., 2018; Grigal, 2002; Hammerschmidt et al., 2004; Lamborg et al., 2002; Liao et al., 2009; O'Connor et al., 2019), and bioaccumulation in food chains with emphasis on human health effects (Feng et al., 2018; Lawson and Mason, 1998; Nogara et al., 2019; Renzoni et al., 1998; Xu et al., 2018; Yan et al., 2019).

This review discusses and summarizes an up-to-date overview of Hg sources and concentrations in groundwater, emerging remediation technologies, complex biogeochemical processes, and conceptual modeling for processes influencing the mobility, fate, and transport mechanisms of Hg in groundwater.

2. Groundwater Hg sources and fluxes

2.1. Geogenic Hg sources

There are several naturally occurring Hg-bearing minerals found in crustal rocks (Kozin and Hansen, 2013). The commonest are cinnabar (HgS), *meta*-cinnabar (β-HgS) and native Hg. HgS is usually formed from igneous activity at temperatures <300 °C and is mainly found in mineral veins or fractures. It can contain up to 86 % of Hg by weight (Navarro, 2008; Rytuba, 2003; USGS, 2000). Also, Hg is present in other minerals (Table 1). While concentrations in these deposits are usually high, up to 1,198,000 μg/kg (Schwartz, 1997), mine wastes derived from ore processing can contain even higher Hg concentrations, up to 1,500,000 μg/kg (Gray et al., 2000; Rytuba, 2000, 2003).

In igneous rocks, Hg was found in basalts, gabbros, diabases, andesites, dacites, and rhyolitic, mafic, ultramafic, alkalic and silicic rocks in substantial concentrations, with averages of 80 to less than 100 μg/kg (Taylor, 1964; USGS, 2000). In a Metamorphic Complex, Hg was associated with pyrites in quartz gangue, carbonatic chloritic phyllites and calc-alkaline metabasites, formed from hydrothermal fluids circulation and ore deposition (Dini et al., 2001). Similarly, Hg was found in sandstones and limestones, sedimentary clays, coals associated with pyrites, organic-rich shales, and sulfide-rich volcanic and sedimentary deposits, with concentrations averaging 30 to 50 μg/kg. Nevertheless, considerable variations exist, especially when rocks (e.g., shales and clays) were enriched in Hg by an accumulation of the exhalations of mud volcanoes as observed in Crimea, the Donets Basin, and the Kerch Peninsula (Barringer et al., 2013; USGS, 2000). Also, Hg can be enriched in sedimentary Fe and Mn ores, possibly by adsorption or co-precipitation, or in shales when organic complexes form (USGS, 2000). Nevertheless, Hg is one of the least abundant elements in the upper continental Earth's crust, with an estimated concentration ranging from 12.3 to 96 μg/kg (Gao et al., 1998; Rudnick, 2005; Shaw et al., 1976; Taylor, 1964; Tian et al., 2023; Wedepohl, 1995). Water-rock interaction with these crustal rocks, ore deposits and mine wastes containing Hg (Fleischer, 1970; Marowsky and Wedepohl, 1971) can release Hg directly into groundwater (Gonza´lez-Ferna´ndez et al., 2014; Navarro, 2008). However, the contribution of Hg from crustal rocks to groundwater is considered low (Barringer et al., 2013; Fleischer, 1970).

The principal geogenic sources of Hg in groundwater are sulfide deposits of volcanic origin containing HgS (Barringer et al., 2013). Other geogenic groundwater sources of Hg can include geothermal fluids, as demonstrated for locations in Russia (Kamchatka Peninsula) with concentrations up to 110 μg/L (Yudovich and Ketris, 2005), Russia (Uzon Caldera, Kamchatka) with up to 700 μg/g (Migdisov and Bychkov, 1998), Japan with up to 400,000 ng/kg (Yudovich and Ketris, 2005), the USA with up to 0.6 μg/L (Ball et al., 2006), and New Zealand with up to 276 μg/L (Davey and van Moort, 1986). In addition, Hg can be introduced indirectly into groundwater due to volcanic emissions, forest fires (Ermolin et al., 2018), and degassing from Hg-containing rocks, soils, and sediments. Mercury released from such sources is usually gaseous and transported into the atmosphere. Following atmospheric deposition and accumulation on the Earth's surface, Hg can enter an aquifer during

Table 1
Hg-bearing mineral deposits.

Ore deposits	Chemical Formula	Hg (wt%)
Schwatzite[a]	$(HgCuFe)_{12}Sb_4S_{13}$	17.6
Wurtzite[a]	(Zn,Fe)S	0.3
Celestites, barites[a]	$SrSO_4$, $BaSO_4$	–
Corderoite[b]	$Hg_3S_2Cl_2$	–
Volcanogenic manganese[b]	absorbed on Fe-Mn oxides	–
Sphalerite[c]	ZnS	41.1
Timanite[d]	HgSe	71.8
Petrovicite[d]	$Cu_3PbHgBiSe_5$	16.7
Gruzdevite[d]	$Cu_6Hg_3Sb_4S_{12}$	32.4
Tvalchrelidzeite[d]	$Hg_{12}(Sb,As)_8S_{15}$	69.0
Laffittite[d]	$AgHgAsS_3$	41.8
Velikite[d]	Cu_2HgSnS_4	34.9
Galkhaite[d]	$Tl(Cu,Hg,Zn)_{12}As_8S_{24}$	60.5
Temagamite[d]	Pd_3HgTe_3	22.2
Lorodaite[d]	HgTe	61.1
Khakite[d]	$(Cu,Hg)_3SbSe_3$	62.9
Balkanite[d]	$Ag_5Cu_9HgS_8$	12.8
Aktashite[d]	$Cu_6Hg_3As_5S_{12}$	34.5
Livingstonite[d]	$HgSb_4S_8$	21.3
Christite[d]	$TlHgAsS_3$	34.8

Reference.
[a] USGS (2000).
[b] Rytuba (2003).
[c] Tauson and Abramovich (1980).
[d] Kozin and Hansen (2013).

groundwater recharge (Barringer and Szabo, 2006; Bradley et al., 2012; Gonza´lez-Ferna´ndez et al., 2014; Wang et al., 2004). Although Hg released from volcanic emissions can cause local contamination of soils and surface waters, the impact on groundwater is typically low, as shown at Mt. Etna (Sicily). There, Hg in groundwater was <0.01 μg/L. In contrast, Hg in soils and Castanea sativa (sweet chestnut) leaves ranged from 4.6 to 73 μg/kg and 19 to 190 μg/kg, suggesting that the emitted Hg was not easily mobilized into groundwater (Martin et al., 2012).

2.2. Anthropogenic Hg sources

Anthropogenic activities such as industrial processes and burning fossil fuels are arguably the most significant Hg contributors to the environment (e.g., Fitzgerald and Lamborg, 2003). Once released into the atmosphere, Hg can travel great distances before being deposited on land or water surfaces, contaminating areas without any apparent direct source of anthropogenic emissions (e.g., Beckers and Rinklebe, 2017).

On the other hand, artisanal and small-scale gold mining, landfill wastes, chemical discharge from dental preparations and laboratory activities, discharge of energy-efficient lamps and batteries, manufacturing of non-ferrous and alkali metals, and chloralkali and caustic soda using Hg-cells are known to release Hg into groundwater directly. Minor direct sources are the production of chloralkali, cement, electrical materials, vinyl chloride monomer, refining petroleum products and cremation (Bigham et al., 1964; Futsaeter and Wilson, 2013; Gupta et al., 2018; UNEP, 2019). However, reported Hg contamination from these sources was low in most locations. For instance, at a site in Trondheim, Norway, the soil-Hg binding ability attenuated the mobilized Hg, preventing it from leaching into groundwater (Saether et al., 1997). Specifically, Hg^{2+} adsorption by clay, manganese oxides (Farrell et al., 1998), hydrous ferric oxides (HFO), or Fe-rich geological formations (Andersson and Nriagu, 1979), and organic matter (Skyllberg et al., 2006) act as a Hg attenuation mechanism. This can prevent Hg addition to groundwater as observed in Zimbabwe, Tanzania (VanStraaten, 2000), Sierra Nevada gold mines, USA (Domagalski, 1998), Idrija Hg mine, Slovenia (Covelli et al., 2007), and mining sites in Spain (Navarro, 2008).

On the other hand, in the Madras surficial alluvial aquifer, India, where the attenuation effects were minimal, groundwater Hg contamination suspected from industrial and wastewater discharge was up to 18 μg/L, exceeding the Indian 1 μg/L drinking water limit (Somasundaram et al., 1993). Orica (2013) reported elevated groundwater Hg at a site in Sydney, Australia, due to chloralkali manufacturing and applying Hg-cell technology. In Canada, oxidation of gold and silver mine tailings containing accessory HgS facilitated the leaching of Hg into groundwater as Hg^{2+}-cyanide complexes and raising its concentration to 151 μg/L (Foucher et al., 2013). Koski et al. (2008) reported a waste disposal incidence along the Alaskan coast, while Gemici (2008) documented extended mining activities in Turkey that elevated Hg in groundwater up to 4.1 μg/L and 0.274 μg/L, respectively. Case studies for Hg sources and concentrations in groundwater are discussed in Section 4.0. An overview of Hg cycling in the environment is given in Fig. 1.

3. Biogeochemical cycling of Hg

Mercury exists in three stable oxidation states in the environment, i. e., Hg^0 (metallic), Hg^+ (mercurous), and Hg^{2+} (mercuric). The stability of these species is controlled by redox potential (Eh) and pH (Fig. 2). In groundwater systems, Hg undergoes complexation, reduction-oxidation (redox), precipitation-dissolution, aqueous and adsorption-desorption reactions. These reactions are critical for Hg transformation and mobility in groundwater (Barringer et al., 2013). For instance, complexation can cause Hg^{2+} to exist as $Hg(OH)_2$, $HgCl_2$ or OH^- and Cl^- complexes depending on pH, Eh, dissolved organic matter (DOM), and Cl^- concentration (Reimers and Krenkel, 1974; Stumm et al., 1981). This was shown in a study carried out by Spyropoulou et al. (2022) where Hg contamination was associated with elevated Cl^- concentrations in the coastal groundwater of the Greek island, Skiathos. Based on

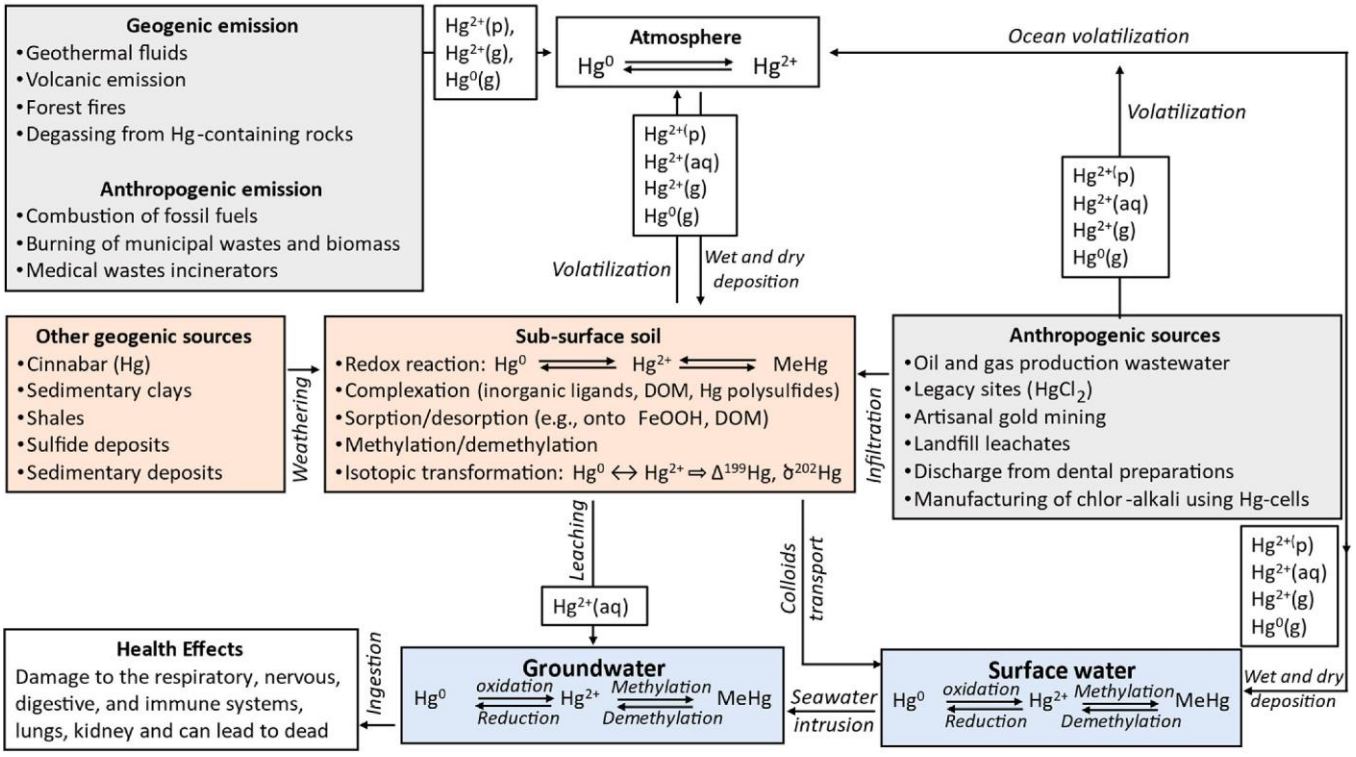

Fig. 1. An overview of Hg sources and mechanisms controlling its release into groundwater (Broczа et al., 2019; Fleischer, 1970; Gibi˘car et al., 2009; Gue´rin et al., 2014; Ignatavi˘cius et al., 2022; Lamborg et al., 2002; Obrist et al., 2018; UNEP, 2019).

the geochemical equilibrium modeling, $HgCl_2$, $HgClOH$, $HgCl_3^-$ and $HgCl_4^{2-}$ were predicted as the dominant species in the groundwater at the normal pH range of groundwater under oxidizing conditions. Controlling factors were seawater intrusion into the aquifer, an Hg—rich (HgS) bedrock, and $Hg(OH)_2$ adsorption onto $Fe_2O_3{\cdot}H_2O$ surfaces. A Pourbaix diagram for the aqueous Hg–O–S–Cl-containing system is shown in Fig. 2. During groundwater salinization, the high affinity of Hg^{2+} with Cl^- was considered the driving force of Hg transport in the presence of Hg-containing minerals (Grassi and Netti, 2000; Kozin and Hansen, 2013).

Furthermore, Nriagu (1979) showed that in oxidized solutions, Hg^{2+} reacts with Cl^- to form aqueous $HgCl^0_2$ complexes (eq. (1)), the predominant dissolved form of Hg in most oxidized waters. Under reducing conditions, however, sulfur plays a crucial role in Hg complexation, more than any other inorganic ligands (Coulibaly et al., 2016), and thus controls Hg speciation in anaerobic environments to form complexes such as dissolved HgS, HgS_2^{2-}, $Hg(SH)_2$, $HgSH^+$, HgOHSH, and HgClSH (Gabriel and Williamson, 2004).

$$Hg^{2+} + 2Cl^- \rightarrow HgCl^0_{2(aq)} \quad (1)$$

Similarly, redox reactions will strongly influence Hg fate and transport in groundwater. Under reducing conditions, Hg^{2+} released from the reductive dissolution of FeOOH can be reduced to Hg^0 by either DOM or Fe^{2+} (or other metals such as tin) or undergo complexation with different ligands (Barringer, 2001; Biester et al., 2000; Charlet et al., 2002; Gu et al., 2011). Microbially facilitated redox reactions involving a Pseudomonas strain (Baldi et al., 1993) or Bradyrhizobium bacterium (Wang et al., 2013) can reduce Hg^{2+} to Hg^0.

Although several scientific publications reported on the cycling of Hg in continental aquifers (Bradley, 2012; Bradley et al., 2011; Gue´dron et al., 2014; Johannesson and Neumann, 2013; Lamborg et al., 2013), our understanding related to groundwater Hg biogeochemistry, its bioavailability, speciation (i.e., methylation, demethylation, and reduction) and mobility in groundwater remains relatively limited. In general, dissolved Hg^{2+} complexes in the aqueous phase have a higher bioavailability to methylating bacteria than Hg in the solid phase (Hsu-Kim et al., 2013; Schartup et al., 2014). In addition, Hg derived from nanoparticulate HgS is more bioavailable for methylation than bulk minerals (or metacinnabar) (Zhang et al., 2012). The partitioning of Hg^{2+} in dissolved and particulate forms will control the general transport of Hg in groundwater systems and Hg bioavailability to methylating bacteria in an anaerobic environment (Hsu-Kim et al., 2013). Changing redox conditions in an aqueous environment impact the formation and mobilization of organomercury compounds, including methylmercury (MeHg), the leading neurotoxic form of Hg, which is highly bioaccumulative in the aquatic and terrestrial food chain (Hintelmann, 2010, 2010i˘zek et al., 2007). Under anoxic conditions, the formation of MeHg critically depends on factors such as the concentration of labile organic carbon (OC), bioavailable inorganic Hg, supply of Fe^{3+}, SO_4^{2-} or other electron-accepting groups, and the activity of Hg^{2+}-methylating microbial communities (Marvin-DiPasquale et al., 2009; Zhang et al., 2014). Production of MeHg is not always associated with the THg amount (Fitzgerald and Lamborg, 2003). Notably, the quality or composition of DOM rather than total OC concentration is critical. The main components of DOM contain protein-like material and humic and fulvic acids (Hansen et al., 2016). DOM composed of sugars, starches and simple proteins is more bioavailable for microbial uptake than larger DOM (Bravo et al., 2017). It can considerably influence the availability and transport (or sorption) of inorganic Hg, biological uptake, transformation, Hg methylation, and microbial potential mediating MeHg production (Burns et al., 2013; Dong et al., 2010; Eckley et al., 2021; Marvin-DiPasquale et al., 2009; Noh et al., 2018; Schuster et al., 2008). Waples et al. (2005) observed that the dissolution of HgS was controlled by DOM interaction with the HgS surface. Moreover, in most aquatic environments, the speciation of Hg is governed by DOM through forming strong MeHg-DOM and Hg-DOM complexes via the reactive sulfur and thiol-like functional groups (Dittman et al., 2010; Dong et al., 2010; Kneer et al., 2020; Schuster et al., 2008). Therefore, Hg mobilization tends to be less in environments with a high OC binding of Hg in the aquifer matrix and greater in sandy, low OC conditions (Eckley et al., 2020; Lamborg et al., 2013).

Mercury is methylated and demethylated by iron-reducing bacteria (IRB) (Fleming et al., 2006; Kerin et al., 2006; Si et al., 2015), sulfate-reducing bacteria (SRB) (Gilmour et al., 2011; Jones et al., 2020; Lin et al., 2012; Vishnivetskaya et al., 2011), and methanogenic, fermentative, cellulolytic, and acetogenic microorganisms (Gilmour et al., 2013; Hamelin et al., 2011; Parks et al., 2013; Podar et al., 2015; Wang et al., 2020; Yu et al., 2013). Some publications reported on the role of microorganisms in the formation of MeHg in contaminated groundwaters (Brooks and Southworth, 2011; Podar et al., 2015; Vishnivetskaya et al., 2011). For example, IRB *Geobacter sulphurreducens* PCA and SRB *Desulfovibrio desulfuricans* ND132 can mediate oxidation and methylation of Hg^0 under anaerobic conditions (Hsu-Kim et al., 2013). The SRB *Desulfovibrio desulfuricans* and *Desulfobulbus propionicus* may facilitate the methylation of Hg at much higher rates when subjected to nanoparticulate rather than microcrystalline HgS (Zhang et al., 2014).

A column study by Hellal et al. (2015) was set up to simulate aquifer conditions where two equal glass columns containing Fe oxides were spiked with Hg^{2+} and exposed to (1) direct Fe reduction by IRB and (2) indirect Fe reduction by sulfides induced by SRB. In the first column, where IRB was dominant, the leaching and methylation of Hg were connected to the bacterial reduction of Fe. In the second column governed by SRB, sulfide formation caused the precipitation of HgS or indirect reduction of Fe oxides with rapid adsorption of leached Hg or MeHg on neoformed mackinawite. Those experiments confirmed that mobilization and methylation of Hg were during the peak of bacterial activity and that Hg bound to FeS colloids could be a prominent process for aqueous Hg transport in groundwater.

Johannesson and Neumann (2013) modeled the cycling of Hg in the confined Carrizo Sand aquifer in southeastern Texas, USA, through *in-situ* observations and reactive transport modeling. The authors concluded that dissolved sulfide rather than organic phases mainly complexed Hg. The modeling implied that Hg was released from the aquifer matrix to groundwater by dissimilatory Fe_2O_3/FeO(OH) reduction and subsequently eliminated along the flow path by adsorption onto hematite and goethite. Also, co-precipitation with or adsorption onto mackinawite or HgS may play an essential role in Hg removal from groundwater. (Jacobson et al., 2012) analyzed a 17-m-long sediment

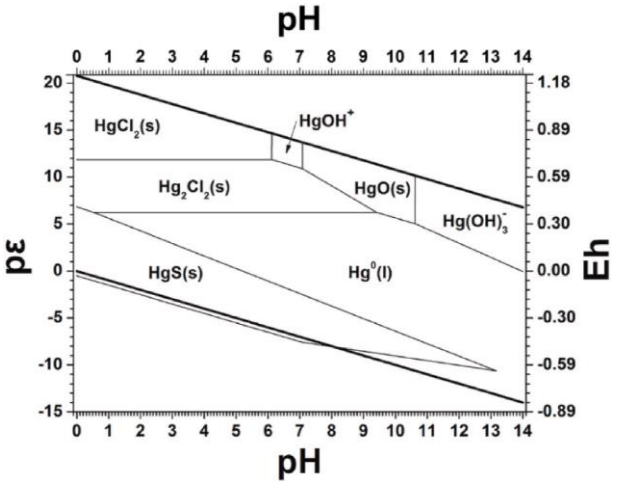

Fig. 2. Pourbaix diagram for the aqueous system Hg–O–S–Cl with a concentration of Hg, Cl^- and SO_4^{2-} of 10 nM, 20 mM and 1 mM, respectively, characteristic for saline groundwater. Note: the two thicker lines constrain the water stability region (Spyropoulou et al., 2022).

core from Lake Tulane (Florida), reporting a drastic increase in Hg flux during the last deglaciation due to global sea-level rise and the associated increase of the groundwater level. Flooding of the oxidized soils near the lake triggered the reductive dissolution of FeO(OH) and the mobilization of the adsorbed Hg.

4. Field studies

The wide range of field studies on groundwater Hg contamination worldwide are presented below and separated into subchapters based on the pristine, geogenic and anthropogenically influenced groundwater locations.

4.1. Hg in pristine (uncontaminated) groundwater

4.1.1. Allequash Creek Watershed, Northern Wisconsin, USA

Krabbenhoft et al. (1995) assessed Hg cycling in the Allequash Creek Watershed, Northern Wisconsin, USA. That study investigated the spatial and temporal distribution of THg and MeHg within the different watershed compartments (i.e., upland soils, groundwater, wetlands, streams, and lakes). THg ranged from 0.0011 to 0.0033 μg/L in the groundwater, while MeHg was less than 0.00002 μg/L. The study observed an increase in THg and MeHg as groundwater discharged through peat-forming springs or when rivulets drained across the wetland surface. Elevated DOC accompanied those increases. Notably, the contributing groundwater basin for the Allequash Creek watershed is approximately 50 % larger than the topographic drainage basin. Considering total Hg concentrations in groundwater, the area of the groundwater basin, and annual stream flow data, the calculated watershed yield rate was determined to be 1.2 mg/km^2/d, reflecting a retention rate of 96 %. On the other hand, the estimated MeHg yield rate for the wetland area ranged from 0.6 to 1.5 mg/km^2/d, up to six times higher than the atmospheric deposition rate.

4.1.2. Poznan´, Poland

Kowalski et al. (2007) studied Hg occurrence in the surface and groundwater of Poznan´, a city in Poland with over 500,000 inhabitants. The groundwater Hg concentrations in 26 wells were low, ranging from 0.0008 to 0.0041 μg/L. Surface waters, including ponds, lakes, streams, and rivers, ranged from 0.008 to 0.04 μg/L. According to the author, low Hg concentrations in the groundwater were typical for background values for marine and freshwater environments. Groundwater appears unaffected by the previously reported Hg levels from 29 to 283 μg/kg in the sediments and from 17 to 746 μg/kg in the soils (Boszke and Kowalski, 2006). However, leaching of Hg from the soils could potentially contribute to the groundwater when the buffering property of the soil is exceeded.

4.2. Geogenic effects on groundwater Hg concentrations

4.2.1. Southern Tuscany, Italy

Grassi and Netti (2000) examined the influence of seawater intrusion on the Hg content of coastal aquifers in Grosseto, Southern Tuscany, Italy. The subsurface of the Grosseto province is mineralized with pyrite, barite, Fe, Cu-Pb-Zn, Sb, and Hg (occurring as cinnabar). According to the authors, the interaction of Hg-bearing minerals in the aquifer matrix with Cl^- in groundwater produced Hg-Cl complexes, increasing the Hg concentration in the aqueous phase. Analyzed groundwater samples had Hg concentrations ranging from 0.5 to 11.2 μg/L and salinity between 0.7 and 34 g/L. The $\delta^{18}O$ data and the Ca^{2+}–Mg^{2+}/HCO^-_3 to Na^+/Cl^- water type suggest mixing between groundwater and seawater in all investigated aquifers. The data showed a close relationship between Hg and Cl^-, where higher Hg corresponded to higher Cl^-. The PHREEQC code suggested that high Cl^- concentration in mixed water forms stable complexes with Hg (e.g., $HgCl^-_3$, $HgCl^-_2$, $HgCl^{2-}_4$, and $HgBrCl^-$), leading to increased dissolution of solid phase Hg. Similarly, Protano et al. (2023) found that the Hg levels in Southern Tuscany groundwater ranged from <0.1 to 11 μg/L. The authors showed that the circulating water within the Quaternary continental sediments overlying the carbonate aquifer dissolves the solid Hg-bearing constituents, mobilizing Hg mainly as Cl^- complexes.

Seawater incursion may be even more detrimental to groundwater quality if it happens in areas with coastal (nearshore) hydrothermal activity. There, hydrothermally influenced seawater with elevated Hg concentrations can migrate landwards (e.g., Pichler, 2024; Roberts et al., 2021).

4.2.2. Volcanic aquifers: Italy and Guadeloupe (Lesser Antilles)

Bagnato et al. (2009) investigated Hg concentration, speciation, and budget in various volcanic aquifers of Italy and Guadeloupe (Lesser Antilles). Concentrations of THg in groundwater were up to 0.5 μg/L and positively correlated with SO^{2-}_4. This Hg-SO_4-rich acid groundwater indicated a direct input of Hg-bearing fluids of magmatic origin into groundwater potentially before a volcanic eruption. The final concentration of Hg is controlled by direct input of Hg as Hg^0(gas) from the magmatic/hydrothermal gases, water-rock interaction within the hot and acidic hydrothermal aquifer, the rise of hydrothermal steam from a deep reservoir of hydrothermal fluid, as well as aquifer mineralogy, T, pH, and Eh. Speciation analysis was carried out further to understand the complex behavior of Hg in volcanic aquifers. The data revealed the dominance of dissolved elemental Hg^0(aq) and particulate-bound Hg (HgP) in the aquifer, demonstrating the efficiency of Hg adsorption onto colloidal particles. The authors observed a coexistence of dissolved Hg^0(aq) and Hg^{2+} forms in nearly equal amounts across most of the water samples, contradicting the expectations of thermodynamic equilibrium modeling. Therefore, a chemical equilibrium involving dissolved mercury species in volcanic waters could either be prevented by natural kinetic effects in the aquifer or may not be preserved during sampling or storage artifacts.

4.2.3. Azzaba, northeast Algeria

Moussa and Yahia (2012) investigated the elevated Hg groundwater concentration in the Azzaba region (North-East Algeria) and the effects of Hg on the community's residents. The hydrogeological stratigraphy consists of a confined lower Paleocene-Eocene aquifer overlain by an Oligocene phreatic aquifer (Benhamza, 1996). The aquifers are separated by impermeable Palaeozoic and Lutetian-Priabonian layers. Hg-bearing cinnabar is present in the matrix of the Paleocene-Eocene deep aquifer. The Hg content in the Oligocene aquifer was up to 80 μg/L, whereas, in the deep aquifer, the maximum Hg concentration was up to 7 μg/L, exceeding the 1 μg/L drinking water recommendation (WHO, 2004, 2011). According to Benhamza (1996), Hg in Azzaba has a medium migration coefficient and, therefore, has a limited chance of mobilization into the Oligocene aquifer. Hence, Hg contamination was not related to the leaching of HgS. Ultimately, Hg in the Azzaba groundwater was attributed to the atmospheric and hydric pollution from a Hg plant and atmospheric Hg recycling by rainfall.

4.2.4. District Swabi, Pakistan

Khattak et al. (2021) reported on the potential risks and sources of Hg in groundwater in four communities (Naranji, Sher Dara, Parmoli, and Mirali) in the District of Swabi, Pakistan. Samples from shallower (10–20 m), middle (25–45 m), and deep (50–90 m) aquifers were collected for this investigation. The THg concentration ranged from 0.9 to 2 μg/L in the shallower, 0.3 to 1.9 μg/L in the middle, and 0.2 to 1.8 μg/L in the deep aquifer. According to the authors, the mobilization of Hg into groundwater was due to the long-term water-rock interaction affecting HgS and clay minerals in the shallow aquifer. The deeper aquifer is contaminated due to the inter-mixing of groundwater sources in the vadose zone. Furthermore, the authors demonstrated that 81.5 % of the investigated groundwater was unfit for drinking or domestic use, although the health-related risk was considered moderate.

4.2.5. Girona, NE Spain

Navarro et al. (2016) investigated the geochemical behavior of Hg in the alluvial and granitic matrix of the Ridaura Aquifer, Girona, NE, Spain. The aquifers are categorized into three (3) units: (i) deep regional aquifer in the fractured basement composed of granitic materials, (ii) aquifer associated with the weathered granitic materials, and (iii) shallow unconsolidated aquifers composed of recent colluvial/alluvial sediments derived from the Ridaura River. The authors concluded that the intermediate aquifer is the likely groundwater source for the deep regional and shallow aquifers. THg ranged from 0.2 to 4.2 μg/L in the alluvial groundwater, 0.2 μg/L in groundwater from the granite border and 1.1 μg/L in Ridaura river water. Concentration in streambed sediments ranged from 13 to 103 μg/kg. Elevated Hg in the sediments and groundwater were traced to two sources: Hg migrating from weathered granitic materials and agricultural practices such as using fungicides and fertilizers.

4.3. Hg in affected (contaminated) groundwater

4.3.1. Black Forest, south Germany

Bollen et al. (2008) investigated $HgCl_2$-contaminated soils and groundwater at a site of a former wood impregnation facility in the Black Forest, South Germany. Within a 1.3 km distance, THg in groundwater ranged from 0.5 to 230 μg/L. Studies showed that most $HgCl_2$ is bound to inorganic soil components in soils low in organic matter. In groundwater, the redox conditions support the secondary formation of Hg^0 from Hg^{2+}. The occurrence of Hg^0 in groundwater suggested that the formation and degassing of Hg^0 and dilution could have been essential in decreasing Hg concentrations in the aquifer. Yet, the high percentage of mobile Hg (3–26 %) and low seepage in the area could influence the continuous release of Hg into groundwater over a long period. The study revealed that a part of the affected aquifer had an elevated organic matter (peat) content, facilitating oxygen depletion and periodic anoxic conditions. Variable groundwater levels and oxidation contributed to the formation of HFO colloids. The authors reported that reduction of Hg^{2+} to Hg^0, co-precipitation with HFO, and subsequent retention in $HgCl_2$-contaminated aquifers are critical in environments with oscillating redox conditions. A further study by McLagan et al. (2022) using stable Hg isotopes showed that Hg enrichment at this site may not primarily result from the reduction of Hg^{2+}(i.e., $HgCl_2$) exchangeable by water to Hg^0, but the preferential sorption of lighter Hg^{2+} isotopes from the liquid-phase to the solid-phase (likely Fe and Mn oxides).

4.3.2. New Jersey, USA

Field-scale studies in the upper Great Egg Harbor River watershed in New Jersey's Coastal Plain, USA, were designed to investigate the dynamics of Hg and MeHg in an unconfined quartz sand aquifer impacting a first-order urban coastal plain stream (Barringer et al., 2005, 2010, 2013a). It was proposed that mobilization of Hg to shallow groundwater occurred as narrow plumelets due to soil disturbances (i.e., stream tributaries). The authors showed that in effluent-tainted groundwater, the reductive dissolution of FeO(OH) in the aquifer matrix caused the mobilization of sorbed Hg^{2+} during suboxic to anoxic conditions. Notably, high Hg concentrations similar to those detected in deeper domestic well waters appeared in shallow groundwaters, indicating Hg mobilization at or near the land surface. Furthermore, other regions of similar coastal aquifers, hydrogeology and land use might be susceptible to the contamination of Hg from shallow groundwater and related surface water environments (Barringer et al., 2013a). Bradley et al. (2012) showed the significance of floodplain/riparian wetland zones for Hg mobilization and sources of fluvial MeHg as a significant control of Hg supply to coastal plain streams. The authors stated that under non-flood conditions, shallow groundwater discharge instead of atmospheric Hg deposition, in-stream MeHg production, or tributary transport from wetlands were the primary pathways for MeHg between the local stream and the wetland/floodplain environment, and, therefore, a substantial impact on fluvial MeHg concentrations. Barringer et al. (2010) reported a predominance of groundwater discharge for this area under flood conditions. In addition, other studies demonstrated that Coastal Plain streams in the southeastern U.S. are particularly susceptible to a strong wetland-stream hydraulic connectivity, which is essential for Hg distribution and mobilization in shallow groundwaters (Bradley et al., 2010, 2011; Warner et al., 2005).

4.3.3. Dumasi, Ghana

Babut et al. (2003) investigated Hg mobilization to rivers, soil systems, and groundwater due to small-scale gold mining operations carried out by Bogoso Ltd in Dumasi, Ghana. The Dumasi village is home to about 2000 people, of whom 25 % of the adult population is involved in the local artisanal production of gold. The authors observed significant Hg transfers from gold extraction processes (i.e., amalgamation and distillation) to marsh sediments in the 'sump' (i.e., an artificially constructed wetland connected to river Dumasi) and eventually downstream into the river sediments and fish. Concentrations ranged from 0.2 to 0.8 μg/L in surface water, 0.6 to 93.1 μg/g in sediments and 0.1 to 0.3 μg/L in groundwater. While this transfer was mainly evident in soils and sediments throughout the host village, groundwater was not contaminated.

4.3.4. Abakaliki, Nigeria

Obasi and Akudinobi (2020) assessed the abundance of Hg and other heavy metals in surface water and groundwater in the Abakaliki state (Nigeria). The water resources in this location were affected by Pb-Zn mining activities. The impacted communities include Enyigba, Mkpuma Akpatakpa, Ameka, Amorie, Amanchara, and Alibaruhu. The samples were collected during the pre-monsoon and post-monsoon seasons. The concentration of THg in the surface water was up to 2600 μg/L and 1000 μg/L in pre-monsoon and post-monsoon seasons, respectively. In the corresponding groundwater, Hg was generally lower in the pre-monsoon season (up to 2300 μg/L) and about 400 μg/L in the post-monsoon high precipitation season due to dilution.

4.3.5. West Nusa Tenggara Province, Indonesia

Johari and Rahmawati (2020) assessed Hg contamination in groundwater due to artisanal and small-scale gold mining activities on the Southern Lombok Coast, West Nusa Tenggara Province, Indonesia. Gold extracting at this location involves the use of Hg for amalgamation. One amalgamation process requires 0.5–1 kg of Hg in about 20 L of water to process 7.5 kg of rocks for Au extraction. This produces amalgamation residues and tailings, usually disposed of in ponds or surrounding rivers, leading to Hg contamination of the environment. Surprisingly, the concentration of Hg in groundwater was <0.1 μg/L. According to the authors, such a low concentration was only possible because (i) the tailing ponds and the amalgamation procedure sites were designed to prevent possible water seepage, and (ii) groundwater flowed in the opposite direction. That study, however, did not analyze the tailings, river sediments, and surface water for Hg.

4.3.6. Puerto Princesa, Philippines

Samaniego et al. (2020) analyzed Hg and other heavy metals (As, Ba, Cr, Mn, and Ni) in the groundwater of an abandoned Hg mine (cinnabar hosted by opalite bodies) in Puerto Princesa City, Philippines (Irving, 1954; Williams et al., 1999). The mining was carried out by Palawan Quicksilver Mines, Inc. (PQMI) from 1953 to 1976. The open-pit mine has yet to be reclaimed since it was abandoned. The analysis of groundwater samples near the PQMI pit lake showed that THg was up to 0.2 μg/L, Ni from 0.3 to 1.5 mg/L, Mn from 0.6 to 1.4 mg/L, Cr from 0.1 to 0.3 mg/L, Ba up to 0.1 mg/L, and As below the detection limit. The authors reported that the presence of Hg in the groundwater of the PQMI region is minimal, highlighting the low solubility potential of Hg-bearing compounds like cinnabar. Those results correspond to the study by Williams et al. (1996) who reported less than 0.04 μg/L Hg in

the surface and groundwaters despite 340,000 μg/kg of Hg measured in the PQMI mine wastes.

4.3.7. South River, Virginia, USA

Lazareva et al. (2019) investigated the legacy industrial Hg contamination from the former DuPont plant in floodplain soils of South River, Virginia, USA. Sequential chemical extraction analysis showed that Hg in soils primarily existed as meta-cinnabar (β-HgS) followed by thiol-bound Hg, Hg^0 and organo-chelated Hg, Hg_2Cl_2 fractions. Dynamic seasonal fluctuations and oscillating redox potentials due to the intermittent soil flooding at the study site were critical for leaching redox-sensitive minerals and mobilizing Hg, Fe, and Mn, triggering the anoxic response for MeHg production. In groundwater, THg varied between 0.03 and 0.54 μg/L, and MeHg ranged between 0.001 and 0.14 μg/L. During storms, the highest MeHg in shallow groundwater was connected to the highest concentrations of Fe^{2+}, Mn^{2+}, SO_4^{2-}, conductivity, and total alkalinity due to the leaching and dissolution of Hg-enriched floodplain soils. Importantly, the intensity and duration of the storms impacted the magnitude of redox gradients, causing the formation of MeHg via the competition between Fe or Mn in a more oxidizing environment versus SO_4^{2-} reduction during sustained flooding conditions.

4.3.8. Bhopal and Ganga, India

Kabir et al. (2002) investigated the extent of groundwater Hg contamination in communities surrounding the Union Carbide India Limited (UCIL) factory in Bhopal, India. The investigation was carried out following an accidental escape of methyl isocyanate gas from the factory in 1984, which killed more than 1000 and left more than 500, 000 people with health problems during 1985–1994 (Sriramachari, 2004). The incident resulted in the factory's closure, where nearly one metric ton of Hg was abandoned. Groundwater was collected from 20 communities surrounding the UCIL factory during pre-monsoon and post-monsoon seasons. Results showed elevated Hg ranging from 2 to 70 μg/L in pre-monsoon and 1–24 μg/L in post-monsoon seasons, respectively. As expected, the concentration decreased with distance from the UCIL plant along the groundwater flow path. Similarly, Devi et al. (2022) examined the sources and transport of Hg in the rain-water–groundwater–river interaction system in the Ganga Alluvial Plain (northern India). Here, in a global Hg hotspot region, the impacts of atmospheric deposition of Hg from coal-based thermal power plants and brick kilns combined with the intense monsoon precipitation were critical for the passage of Hg into the unconfined alluvial aquifer with up to 1.4 μg/L of measured Hg.

4.3.9. Rio Grande, Brazil

Quintana and Mirlean (2018) studied the environmental impact of carroting, the chemical treatment of animal fur, in Rio Grande, Brazil. The carroting industry caused Hg contamination of urban soils and groundwater between the 18th and 20th centuries. The concentration of Hg in the soil cores of Rio Grande was up to 27,000 μg/kg, about 90 times higher than the control sample. Soil pollution was attributed to Hg-containing felts, cement and debris materials from construction and demolition wastes, which were discarded or used to fill "man-made grounds" (Pimentel, 1944; Quintana and Mirlean, 2018). Maximum groundwater Hg concentration at this contaminated site was 0.253 μg/L, about 13 times higher than the control site value of 0.019 μg/L but still below the limit of 1 μg/L for Hg in potable water (WHO, 2004, 2011).

4.3.10. West Gijón (Asturias, NW Spain)

González-Fernández et al. (2014) reported that groundwater Hg concentrations in the unconfined aquifer system of the Barrios (*Palaeozoic)*, La Ñora, and Vega (*Jurassic)* formations in Gijón were 10 times higher than the maximum concentration allowed in drinking water (1 μg/L) (Del Estado, 2003). The authors sampled 52 springs from different lithologies between 2010 and 2013 to investigate the sources of Hg contamination. Minimal to no Hg was found in the sediments and rock samples. Although Hg mineralization occurs about 30 km south of Gijón, it is not likely the source of the elevated concentration observed at the contaminated site in the West of the Gijón area. High Hg, ranging from 236 μg/kg to 856 μg/kg, were detected in soil samples from the recharge area. According to the authors, total atmospheric emissions from a nearby coal-fired power plant and cement factory were the major controlling factor in Gijón, which were widely dispersed throughout the atmosphere, oxidized to reactive gaseous Hg, or converted to aerosol Hg. Consequently, Hg^0 accumulated in soils via wet and dry deposition and eventually mobilized into groundwater (Dvonch et al., 1998).

4.3.11. Western Cape Cod, Massachusetts, USA

Lamborg et al. (2013) assessed the concentration and speciation of Hg in a wastewater-contaminated groundwater plume in Western Cape Cod, Massachusetts. The authors observed the dominance of MeHg in the nitrate/ammonium groundwater zone and the reduction of Hg^{2+} to Hg^0 in the Fe reduction anoxic zone. Moreover, Hg mobility in groundwater might be governed in the regions where the redox conditions stimulate the transformation of oxidized Hg to Hg^0 or MeHg, which are less susceptible to solid-phase sorption. They suggested that eutro-phication and anoxia in groundwaters regulate the leaching and transport of anthropogenic and natural Hg from watersheds to coastal areas. In addition, in those areas where Hg^0 spills occurred, Hg might be present as an immiscible dense non-aqueous phase liquid able to percolate deep into the aquifer due to the low residual saturation, high density and surface tension (Sweijen et al., 2014).

4.3.12. Tianjin, China

Wu and Cao (2010) studied the concentration of Hg and Cd in irrigation water, sediment, soil, and shallow groundwater of a wastewater-irrigated field near Tianjin City in Northern China. The Beitang Wastewater Drainage River (BWDR) receives wastewater from several urban areas of Tianjin and serves as an irrigation source. The use of treated wastewater from the BWDR was instigated due to a shortage of freshwater within the region. According to the authors, this practice lasted 45 years before their study. Analyses showed that Hg concentration ranged from 0.1 to 2.1 μg/L in irrigation water, up to 0.1 μg/L in groundwater, up to 1900 μg/kg in soils, and 2700 to 3000 μg/kg in sediments. Although the soils irrigated with wastewater have a high concentration of Hg, the shallow groundwater within the area remained uncontaminated. However, the geo-accumulation index showed a substantial Hg buildup in the river sediments (I_{geo} = 5.24) and wastewater-irrigated soils (I_{geo} = 2.5). The authors noted that using wastewater for irrigation had altered the soil quality in Tianjin. With time, the practice will elevate the concentration of Hg and other trace metals, including Cd, Pb, and As, through vertical infiltration-induced leaching into groundwater.

4.3.13. Thohoyandou, South Africa

Nevondo et al. (2019) measured THg concentrations in leachate, sediments, and groundwater from four landfill sites in Gauteng and Limpopo Province – Thohoyandou, South Africa. The landfills comprised unseparated municipal solid waste, including discarded electrical switches, batteries, dental amalgam fillings, light bulbs, biocides, pesticides, etc. The authors found that Hg from these products leached from the waste and the THg in the landfill leachate, sediments, and groundwater ranged from 0.1 to 2.4 μg/L, up to 0.8 μg/L, and 0.1–2.4 μg/L, respectively. It was observed that the concentrations varied during summer and winter periods due to a dilution effect from the rainfall.

4.3.14. Migori County, Kenya

The use of Hg during the amalgamation process at the Migori County artisanal and small-scale gold mine site has become an increasing cause of concern. Omondi et al. (2023) investigated the concentration of Hg in

the groundwater of five mine sites (i.e., Masara, Osiri Matanda, Mac-alder, Kitere and Kehancha) in Migori County. They reported that it ranged from 80 to 760 μg/L within 6 km from the mines during the dry season. Along the flow direction, Hg decreased with increasing distance from the mine (mean values = 292 μg/L at < 1 km, 258 μg/L at 1 to < 2 km, and 234 μg/L at 3–6 km). In contrast, the concentration of Hg in the samples collected during the wet season was below the detection limit due to increased groundwater recharge from rainfall. The seasonal variation and distance play important roles in the distribution and concentration of Hg in Migori County. Table 2 summarizes the reported investigations of Hg in groundwater from different locations.

5. Fate and transport of Hg in groundwater – conceptual model

Understanding the complex Hg biogeochemistry is essential to estimate how existing research applies to the transport and fate of anthropogenic and geogenic Hg in groundwater systems. Precipitation-dissolution, oxidation-reduction, adsorption-desorption, and aqueous complexation reactions control Hg transport and fate in groundwater. Adsorption of Hg^{2+} onto goethite and hematite or co-precipitation with/or adsorption onto mackinawite or HgS along the flow path (Johannesson and Neumann, 2013) can restrict Hg mobility unless Hg is bound to colloids (particles <1 μm). A colloidal component is vital for transporting Hg in groundwater (Kretzschmar and Schafer, 2005). Colloids of Hg can be formed by hydr(oxides) of Fe, Al, and Mn, clay minerals, Si, carbonates, phosphates, humic and fulvic acids, bacteria, and viruses. They are susceptible to water table fluctuations triggered by groundwater pumping, pH and redox alterations.

Table 2
Global overview of groundwater Hg investigations.

Study	Location	THg (μg/L)	Hg source
Hg in pristine groundwater			
Krabbenhoft et al. (1995)	Northern Wisconsin, USA	0.0011 to 0.0033	Geogenic
Barringer and Szabo (2006)	New Jersey, USA	0.0002 to 0.005	Geogenic
Kowalski et al. (2007)	Poznan´, Poland	0.0008 to 0.004	Geogenic
Hg from geogenic sources			
Moussa and Yahia (2012)	Azzaba, Algeria	1 to 80	Hg ore deposit
Khattak et al. (2021)	District Swabi, Pakistan	0.2 to 2	Cinnabar from granitic rocks
Grassi and Netti (2000) and Protano et al. (2023)	Southern Tuscany, Italy	0.5 to 11.2	Dissolution of naturally occurring Hg minerals caused by seawater intrusion
Bagnato et al. (2009)	Italy and Guadeloupe Island	0.01 to 0.5	Volcanic water
Navarro et al. (2016)	Girona, Spain	0.2 to 3	Granitic materials
Amiri et al. (2021)	Urmia, Iran	2.2 to 6.3	Weathering of geological materials
Hg from anthropogenic sources			
Gonz´alez-Fema´ndez et al. (2014)	West Gijo´n (Asturias, NW Spain)	<0.01 to 10.2	Atmospheric deposition from industrial activities
Babut et al. (2003)	Dumasi, Ghana	0.1 to 0.3	Hg emissions from the small-scale gold mining operations
Obasi and Akudinobi (2020)	Abakaliki, Nigeria	0 to 2300	Lead-Zinc mining activities
Nevondo et al. (2019)	South Africa	0.1 to 2.4	Landfill leachate
Wu and Cao (2010)	Tianjin, China	0.1	Field irrigated with wastewater
Kabir et al. (2002)	Bhopal, India	1 to 70	UCIL Factory
Ezeabasili et al. (2015)	Anambra State, Nigeria	0 to 7	Plastic industries, medical and electronic wastes
Johari and Rahmawati (2020)	West Nusa Tenggara Province, Indonesia	0.1	Artisanal mining operations
Samaniego et al. (2020)	Puerto Princesa, Philippines	0.2	PQMI
Quintana and Mirlean (2018)	Rio Grande, Brazil	0.3	Wastes from the carroting industry
Omondi et al. (2023)	Migori County, Kenya	80 to 760	Using Hg for artisanal and small-scale gold mining

Hydrodynamic dispersion can influence groundwater Hg transport and fate. Here, in an inferred groundwater-seawater mixing scenario, Hg and MMHg (i.e., monomethylmercury) transport was associated with increased submarine groundwater discharge (SDG) to coastal waters. At low tide, MMHg and filtered Hg concentrations increased, suggesting that inputs from SDG altered Hg partitioning and/or solubility in the ocean (Ganguli et al., 2020). Typically, the mixing zone between groundwater and seawater is characterized by different redox conditions and OM gradients, which potentially support methylation and transport of biologically available Hg to nearshore coastal waters (Ganguli et al., 2020; Moore, 2010). However, where hydrodynamic dispersion involves Hg transport within contaminated sediment, aquifer capillary fringe and the aquifer, soluble Hg transport is largely controlled by water table fluctuations. Here, when the soluble Hg (e.g., $HgCl_2$) is eventually transported away from the most contaminated part of the aquifer, the groundwater becomes progressively more enriched in heavier Hg isotopes (McLagan et al., 2022).

The quality and quantity of dissolved organic matter (DOM) can also control the aqueous transport and the formation of toxic MeHg under various environmental conditions (Shanley et al., 2022). Mercury mobilization by DOM is related to the strong attraction of Hg^{2+} with anionic thiol groups in the DOM molecules (Liu et al., 2019). The formation of MeHg has been correlated to protein-like DOM, but its transport was associated with humic-like DOM (Shanley et al., 2022). High aromatic OM and low HS^- result in Hg association with nanoparticulate β-HgS (Graham et al., 2012; Poulin et al., 2017), which is highly available for Hg-methylating bacteria.

Additionally, the exposure of Hg-containing natural waters to ambient sunlight can also influence the redox chemistry of Hg, causing a simultaneous occurrence of both Hg^{2+} photo-reduction and Hg^0 photo-oxidation (Whalin et al., 2007; Whalin and Mason, 2006; Zhijia et al., 2016). In addition to the impact of DOM structure, this process is significantly influenced by sunlight wavelength and intensity, pH, DO and Cl^- concentrations in waters (Si et al., 2022). These dynamic redox conditions, including the presence of hydroxyl (OH^-) or carbonate (CO_3^-) radicals during the photo-redox reactions, affect mercury mobility due to the formation of Hg^0 (Jardim et al., 2010).

5.1. Conceptual model of Hg in groundwater

The critical factors to be considered for a conceptual model should include the following: (1) Hg sources such as geogenic, anthropogenic, or atmospheric deposition; (2) transport pathways including floodplain/riparian wetland zones, erosion or leaching of Hg-contaminated streambanks or soils followed by the influx of Hg to shallow groundwater, fluvial Hg or MeHg, as well as input to deep groundwater, storm drain systems or coastal plain streams; and (3) fluxes (i.e., quantification of Hg) using seasonally collected samples during varied flow regimes (e.g., pre- and post-monsoon).

Other factors to consider in obtaining an improved picture of Hg fate and behavior in groundwater systems also include the understanding of the following:

- The isotopic transformation of Hg source materials (e.g., $HgCl_2$, Hg_2Cl_2, HgS) in the subsurface and the isotopic signatures in the corresponding groundwaters (Brocza et al. (2020). These signatures

carry vital information on the initial Hg source and the potentially occurring transformation processes. McLagan et al. (2022) showed the advantage of combining Hg stable isotope analyses, concentration, and speciation to estimate the fate of Hg in $HgCl_2$-contaminated soil–groundwater systems. The authors characterized *in situ* processes of Hg^{2+} speciation dynamics associated with groundwater level changes and redox conditions, Hg^{2+} sorption to the solid phase, and Hg^{2+} reduction to Hg^0;

- Site-specific sorption of DOM or FeOOH onto Hg under varying redox conditions;
- Quantifying the *in situ* dynamics of Hg redox cycling via microbial activity in groundwater systems (Colombo et al., 2014) and
- Site-specific Hg speciation within legacy sites.

In addition, the factors that could impact bacterial methylation rates (Babiarz et al., 2001; Benoit et al., 2003; EPA, 2006; Fitzgerald and Lamborg, 2003; Lamborg et al., 2003; Zhou, 2003) might include the following:

- Higher seasonal temperatures increase the MeHg formation. 35 °C was reported as the optimal temperature for MeHg formation;
- Increasing SO_4^{2-} concentrations boost methylation in SO_4^{2-}-deficient systems. 0.2–0.5 mmol/L is the optimal range of SO_4^{2-} concentration for methylation;
- Higher concentration of inorganic Hg^{2+} increases methylation rates;
- The redox potential (Eh) influences the formation of MeHg (Wang et al., 2021). At an Eh between −300 and −100 mV, high MeHg and dissolved THg were found due to the activity of Hg-methylating bacteria (FeRB, SRB), acidification, and reductive dissolution of Fe oxy(hydroxides). Net MeHg production reaches an optimum at suboxic to low anoxic conditions when $HgCl^0_2$is preferentially taken up by bacteria instead of the negatively charged Hg-chloride and Hg-DOC complexes (Barkay et al., 1997). At Eh from 0 to +200 mV, there are the processes of colloidal growth, adsorption of Hg and increase of colloidal Hg.

Moreover, these factors would be critical for Hg fate conceptual models (EPA, 2006):

- Increasing the concentration of OM reduces the amount of MeHg due to the formation of Hg^{2+}-DOM complexes inaccessible for Hg-methylating bacteria;
- The concentration of sulfide due to the formation of neutrally charged Hg-sulfide complexes enhances methylation, while charged complexes are detrimental to methylation;
- The binding of Hg^{2+} to particulate matter and sediment decreases Hg methylation;
- Mixing redox-susceptible zones are more accessible for methylation;
- Hg formed *de novo* is more available for methylation than "older" Hg.

Since precise information on the hydraulic parameters of aquifers (e.g., hydraulic conductivity, porosity, transmissivity, and specific yield) is essential in designing a reliable groundwater flow and transport model (Li et al., 2023; Ro¨mhild et al., 2022), it is, therefore, also important to consider the roles of these parameters when modeling the fate and behavior of Hg in groundwater systems. For instance, cone of depression enhanced by intense groundwater pumping (up to $48{\cdot}10^6$ m^3/yr) in carbonate aquifers could increase groundwater Hg concentration due to possible upwelling of Hg^0. (Protano et al., 2000, 2023). Similarly, the mobility of particulate-bound Hg is controlled by forces exerted by groundwater pumping (Szabo et al., 2010). Site-specific hydraulic parameters of aquifers, therefore, might play a critical role in Hg mobility.

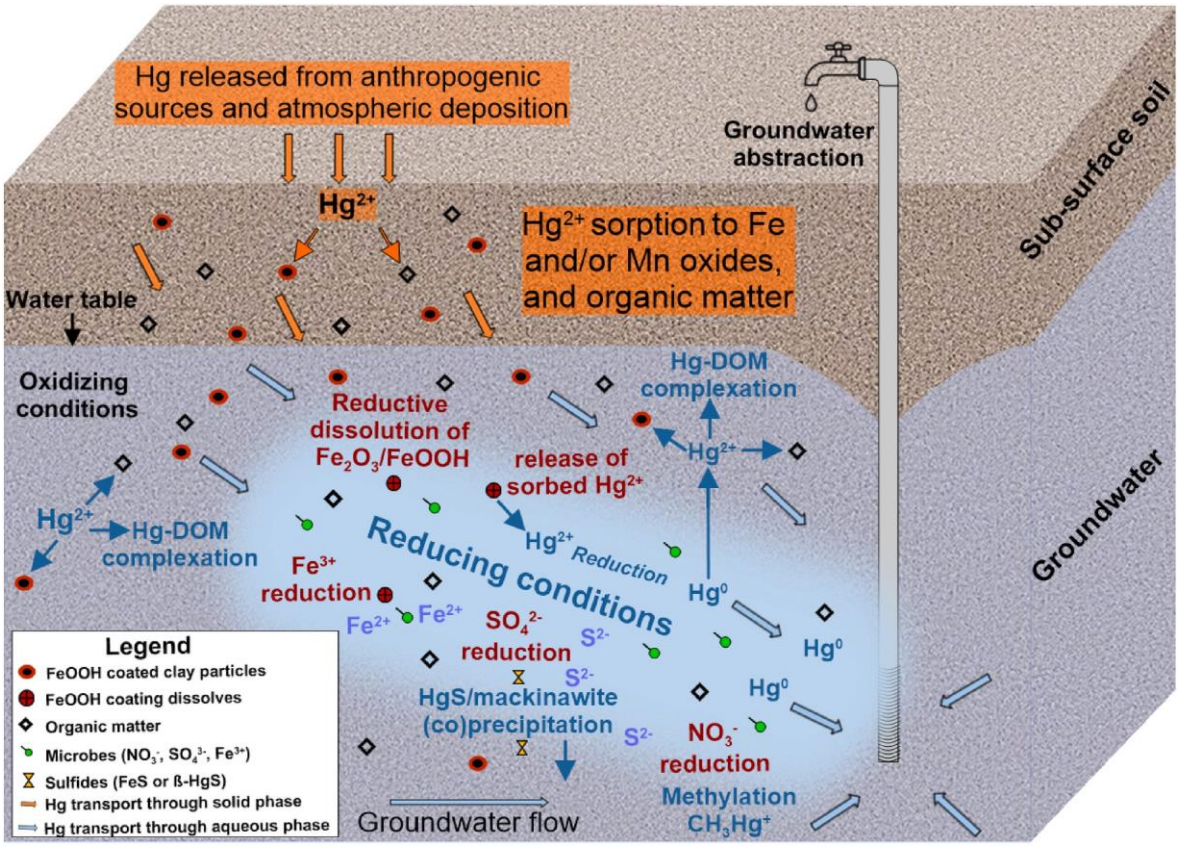

Fig. 3. Transport of Hg from the land surface to groundwater in an unconsolidated sandy, acidic aquifer (Based on Barringer et al., 2013; Lamborg et al., 2013; Reilly et al., 2012).

Fig. 3 shows a suggested conceptual model to illustrate the fate, transport, and biogeochemical transformations of Hg along flow paths from the contaminated site at the land surface to groundwater in an unconsolidated sandy and acidic aquifer (Adapted from Barringer et al., 2013; Reilly et al., 2012). It is assumed that Hg^{2+} can be mobilized to the water table from anthropogenic (e.g., septic-system effluent, fertilizers, or road salt) and geogenic sources. Under oxidizing conditions, Hg^{2+} can be sorbed to FeOOH-coated clay particles and DOM complexes dissolved THg. Once the redox potential changes to reducing conditions, SO_4^{2-} reduction, S^{2-} formation, Fe^{3+} reduction, NO_3^- reduction, methylation and elimination of Fe and Hg from the aqueous phase can form Fe and Hg-sulfide particles. Finally, Hg^0 can be re-oxidized to Hg^{2+}, sorbed again or complexed with FeOOH and DOM and transported down the groundwater flow path.

6. Nanomaterials (NMs) as emerging technologies for remediation of Hg-contaminated groundwater

Adsorption (Jeon and Park, 2005; Sumesh et al., 2011), ion exchange (Chiarle et al., 2000), chemical precipitation (Brown et al., 1979), amalgamation, coagulation (Anirudhan et al., 2008), bio-absorption/biological methods (Inbaraj et al., 2009), and complexation (Jiskra et al., 2012) are widely used to remove Hg from contaminated water. At the same time, applying nanomaterials (NMs, e.g., nanoparticles and nanotubes) using principles of adsorption (Xia et al., 2019) is a promising emerging technology (Faraji et al., 2010; Huang and Hu, 2008). Nanomaterials have proven effective, cost-friendly, easy to use and regenerate, demand low energy, work for *in-situ* treatment, and have a high adsorption capacity per unit volume. They possess unique electrical, mechanical, and chemical properties suitable for Hg removal from water (Alijani and Shariatinia, 2018; Wang et al., 2019) and can potentially reduce contamination levels to "nearly zero" (Bardos et al., 2018).

According to Mukhopadhyay et al. (2021) and Guerra et al. (2018), NMs are grouped into (a) inorganic or metal-based nanomaterials (e.g., Fe- and Cu-based nanoparticles), (b) carbon-based nanomaterials (e.g., graphene), (c) polymer-based nanomaterials (e.g., alginate, chitosan), and (d) composite nanomaterials (e.g., clay polymer nanocomposites, biochar, and zeolite-supported nanocomposites). Wang et al. (2020a) grouped the nanomaterials into (a) nanoparticles, (b) nanosheets, and (c) nanocomposites. Nanosheets have received less practical application than nanoparticles and nanocomposites, except for MoS_2 nanosheets, which have a high adsorption capacity for removing Hg^0 (Zhao et al., 2016, 2018) and Hg^{2+} (Ai et al., 2016; Song et al., 2018) at low temperatures.

Pumice-supported nanocomposite zero-valent iron (p-nZVI) was used in a laboratory experiment to remove Hg from groundwater (Qasim et al., 2018). It removed 6.1 mg/g of Hg^{2+} under oxic and 1.5 mg/g under anoxic conditions from aqueous solutions (Qasim et al., 2018). Blue et al. (2008) investigated the effectiveness of a synthetic chelating ligand (K_2BDET) as a precipitant to remove low-level Hg irreversibly and permanently from contaminated groundwater. After producing a stable precipitate, K_2BDET reduced the Hg concentration to less than a detection limit of 0.05 μg/L. In a sequence of 11 laboratory studies and pilot-scale field tests, Barkley (1991) evaluated immobilized algae in contaminated groundwater and concluded that AlgaSORB effectively removed Hg from groundwater.

Since adsorption is emerging as the most promising Hg removal technology for NMs (Kabiri et al., 2015), the current focus is to develop adsorbent NMs. Such NMs include graphene (Kabiri et al., 2015; Zhou et al., 2017), activated carbon (Gai et al., 2019), ion exchange resins (Zhou et al., 2017), carbon nanotubes (Gai et al., 2019), layered double hydroxides, chitosan (Zhuang et al., 2018) and certain minerals due to their high-efficiency level, economy, flexibility and easy operation (Xia et al., 2019).

6.1. Graphene

Graphene, derived from the mineral graphite, is a carbon-based nanomaterial (i.e., carbon nanotubes, graphene oxide (GO) and nano-porous graphene) that has unique and structural, electrical, thermal, and mechanical properties as well as a high adsorption capacity (Bodzek et al., 2020; Cui et al., 2015; Kabiri et al., 2015). These properties, along with its surface area of more than 1000 m^2/g, low density (1 m^2 sheet = 0.77 mg) and tailorable functionalities, have proven its efficiency for superior removal of Hg compared to other nanomaterials (Bai et al., 2011; Stoller et al., 2008). Graphene aerogel sheets and diatomaceous earth (DE) particles decorated with αFeOOH nanoparticles showed a remarkable adsorption capacity for Hg of more than 500 mg/g (at 400 mg/L Hg^{2+}). This adsorption capacity exceeds many competing adsorbents, suggesting graphene as the most promising material for developing effective and cost-friendly adsorbents to remove Hg from contaminated groundwater (Kabiri et al., 2015). Similarly, Khorshidi et al. (2020) demonstrated the adsorption efficiency of graphene oxide nanosheets with functionalized glutathione nickel ferrite (GSH-$NiFe_2O_4$) magnetic particles to eliminate Hg^{2+}. The adsorption capacity was as high as 272.94 mg/g, demonstrating an excellent adsorption and metal removal efficiency of >94 %. That study also demonstrated the applicability of GSH-$NiFe_2O_4$/GO for Hg removal from groundwater. Graphene was more effective in removing Hg when combined with other NMs like carbon nanotubes, nanoparticles, and polymers.

6.2. Minerals

Adsorption by minerals has proven to be effective in removing Hg^{2+} from groundwater. Pyrite (FeS_2), for instance, is an emerging cost-effective Hg^0 and Hg^{2+} absorbent (Duan et al., 2016; Yang et al., 2018). Duan et al. (2016) used synthesized nanoscale FeS_2 particles for Hg^{2+} removal via surface precipitation and adsorption. Similarly, FeS nanoparticles are also commonly applied to immobilize Hg (Sun et al., 2017, 2018). Zeolites and clay minerals are also effective adsorbers of Hg, mainly when modified chemically. Such chemical modification is achieved by dissolving 1.25 g of cornstarch in 100 mL of acetic acid (5 % v/v), adding 50 g of bentonite, and storing the mixture in a thermostat water bath at 50 °C for 10 h under constant stirring. The mixture is then dried at 105 °C for 24 h, ground and sieved to 150 mesh size (Shao et al., 2016). Large-scale applications are possible since their use is cost-friendly (Saleh et al., 2018). Vermiculite, montmorillonite, and palygorskite absorb Hg through an ion exchange mechanism (Chen et al., 2015; Tran et al., 2015), while Na-montmorillonite absorbs Hg through precipitation (Chen et al., 2015). Other minerals, including diatomite and zeolite, only take up Hg when functionalized with hexadecyltrimethylammonium bromide (Shirzadi and Nezamzadeh-Ejhieh, 2017), thiosemicarbazones (Abbas et al., 2018), $CuBr_2$ (Liu et al., 2019a) or other supporting nanocomposite materials. This is attributed to the porous structure of diatomite and zeolite minerals.

6.3. Carbon nanotubes (CNTs)

Carbon nanotubes (CNTs) are nanostructured allotropes of carbon intermediate between fullerene cages and flat graphene (Zhang et al., 2017). CNTs have unique properties, i.e., structure, high mechanical strength, high thermal and electrical stability, high adsorption capacity, porous/hollow structure, and large surface area (Mallakpour and Khadem, 2016; Sarkar et al., 2018; Zhang et al., 2017). Due to their excellent contaminant removal efficiency, CNTs can act as adsorbents, sensors, membranes, or catalysts to remove organic, inorganic Hg, and biological contaminants from water (Sarkar et al., 2018). They can also facilitate the recovery and regeneration of nanomaterials (Sarkar et al., 2018). CNTs ability to efficiently absorb Hg^{2+} depends on pH, ionic strength, and presence of organic matter (Pandey and Dahiya, 2016; Tawabini et al., 2010; Zhang et al., 2017).

Pandey and Dahiya (2016) reported that CNTs exist as single-walled (SWNTs) and multi-walled (MWNTs) structures. SWCNTs have been experimentally proven to consist of a single-cylindrical carbon layer with a strong ability to absorb Hg^{2+} from aqueous solutions (Shadbad et al., 2011). MWCNTs, on the other hand, consist of multiple coaxial cylinders made of micro-crystals of graphite around a hollow core and can absorb Hg^{2+} (Zhang et al., 2017) as SWCNTs. Both are widely used as an absorbent for Hg, but SWCNTs are considered more efficient due to their ultra-high surface area (Pandey and Dahiya, 2016).

AlOmar et al. (2017) used CNTs functionalized with deep eutectic solvents (DES) to study their efficiency as adsorbents for Hg removal from water. Below a pH of 5.5, CNTs achieved a maximum adsorption capacity of 186.97 mg/g. Using multiwalled carbon nanotubes (MWCNTs), Tawabini et al. (2010) investigated the efficiency of MWCNTs in removing Hg^{2+} from contaminated water by adsorption and found that up to 1.0 mg/L of Hg^{2+} was effectively removed. With the increase in pH from pH 4 to 8, MWCNTs showed an increased (100 %) ability to remove Hg. Also, a higher amount of MWCNTs eliminated more Hg^{2+}. Corps et al. (2018) coated Fe_3O_4 magnetic nanoparticles (MNPs) with different types of CNTs as sorbent materials for pre-concentration analysis of monomethylmercury (MMHg) in water using adsorption and desorption.

Interestingly, the removal of inorganic Hg was simultaneously achieved during the desorption stage of the experiment. This shows that even without functionalizing CNTs, they can efficiently remove Hg from groundwater. Although CNTs are highly effective in absorbing Hg, they have not yet been widely applied to remediate Hg contamination, nor are they accepted for commercial use. They are expensive to use (Sarkar et al., 2018). Therefore, further research is needed to develop CNT-based technologies to gain wider acceptability and applications for *in situ* treatment of Hg contamination in groundwater.

6.4. Biochar

Biochar (BC) is a porous carbon-rich solid with a fine-grained texture produced by the thermal decomposition of organic material under anaerobic conditions (Gąsior and Tic, 2016). Its internal pore structure has a large surface area, capable of serving as an adsorbent. BC is regarded as a promising emerging technology suitable for removing Hg from water because it is inexpensive and highly effective (Boutsika et al., 2014; Faheem et al., 2018; Gąsior and Tic, 2016; Hanandeh et al., 2016). Feng et al. (2020) investigated the efficiency of unmodified, $FeCl_3$-modified, and $FeSO_4$-modified biochars to remove Hg^{2+} from groundwater. They discovered that pyrolyzation of BC at 300, 600, and 900 °C and a contact time of 16 h removed up to 99 % of Hg from contaminated groundwater. BC efficiency and effectiveness in eliminating Hg^{2+} depends on the pyrolytic temperature and the nature of Fe-modification. Fe, S, and Cl species in Fe-modified biochar improved surface characteristics, making the modified BC ideal for Hg^{2+} removal. Gąsior and Tic (2016) investigated the adsorption of Hg ions from aqueous solutions by BC. Its efficiency depended on the type of BC used, raw materials used for its production, pH of the aqueous solution, and the duration of contact between BC and Hg ions in the contaminated water. Adding thiol or amino groups to its surface further enhances its adsorption capacity (Huang et al., 2019) because chemical bonding happens between Hg^{2+} and surface-active sites (e.g., SH, – NH_2, – OH, – COOH) (Huang et al., 2019; Liu, 2016). In a batch experiment, Liu et al. (2019) evaluated the BC potential to remove Hg from an aqueous solution using 36 feedstock biochars. Results showed that high-temperature biochars (600–700 °C) removed >90 % of Hg, whereas BC produced at 300 °C removed only between 40 and 90 %. Although manure-based BC has proven effective for Hg removal, the possible release of up to 1000 mg/L SO_4^{2-} into groundwater has become a significant concern. This may affect the wide acceptability of the use of BC for Hg removal from groundwater.

6.5. Metal-based nanomaterials

6.5.1. Selenium nanoparticles (SeNPs)

SeNPs are newly discovered metal-based nanomaterials with unique properties, i.e., high photoconductivity, nonlinear-optical response, thermoelectric response, and the anisotropy of thermo-conductivity (Berger, 1996; Zhang et al., 2011). These properties play essential roles during Hg removal. Wang et al. (2017) investigated the homo-aggregation and hetero-aggregation of SeNPs with goethite and their remediation potential for Hg-contaminated groundwater. First, SeNPs were produced by reducing Na_2SeO_3 with a selenite-reducing bacterium, Citrobacter freundii Y9 (Wang et al., 2017). Goethite (α-FeOOH) was synthesized following the procedure of Schwertmann and Cornell (2008). The zeta potentials of SeNPs and goethite particles were measured by a Zetasizer and calculated based on the Smoluchowski approximation. Hg^0-contaminated groundwater collected from Urumqi, Xinjiang, China, was used for this investigation. Aggregation and column experiments were employed to investigate the effect of goethite on the transport of SeNPs through a quartz sand column. The study showed that SeNPs remove Hg^0 from groundwater by forming HgSe. However, the remediation efficiency of Hg^0 by SeNPs was inhibited by goethite. The study further revealed that the hetero-aggregation of SeNPs with goethite in groundwater is stronger than the homo-aggregation of SeNPs. When an extracellular polymeric substance (EPS) was added, a slight decrease in homo-aggregation of SeNPs and a significant reduction in hetero-aggregation of SeNPs was observed.

On the other hand, the column transport experiments showed that the goethite-coated quartz sand could retain significantly more SeNPs than the uncoated quartz sand. However, remediation of Hg^0 by SeNPs can be inhibited by SeNPs hetero-aggregation with goethite; EPS can efficiently mitigate this inhibitory effect. It was observed that Hg^0 removal decreased from 71.6 to 66.9 % in the presence of 20 and 100 mg/L goethite, respectively. However, adding 200 mg/L of EPS in the presence of 100 mg/L of goethite increased Hg^0 removal efficiency to 81.2 %. This shows that although crucial for the remediation of Hg^0-contaminated groundwater, goethite can significantly reduce the remediation efficiency of SeNPs. On the other hand, adding an extracellular polymeric substance can mitigate the adverse effect of goethite.

6.5.2. Gold nanoparticles (AuNPs)

Lisha et al. (2009) developed a gold nanoparticle supported on alumina at a capacity of 738,000 μg/kg alumina to remove Hg^0 from drinking water. The adsorption capacity of 4.065 g per g of gold nanoparticles for Hg^0 was observed. However, this method released up to 3.5 mg/L of boron (B) into a solution, which initially had less than 0.5 mg/L. However, adding magnesia ($MgCO_3$) lowered the concentration of B to 0.5 mg/L after 1 h and 0.25 mg/L after 2 h of treatment. Although the author described AuNPs as an excellent Hg^0 adsorbent, the need to introduce additional reagents during treatment remains a limitation. Similarly, Lo et al. (2012) used AuNPs supported on aluminum oxide (Au NPs-Al_2O_3) to remove different Hg species (Hg^{2+}, $MeHg^+$, and $EtHg^+$) in aqueous solutions. It was observed that Au NPs-Al_2O_3 adsorbent has an efficiency of >97 % for Hg^{2+} and $MeHg^+$ removal in lake water, groundwater, and seawater. The low-cost but effective Au NPs-Al_2O_3 Hg adsorbent is a promising method for removing various Hg species from groundwater.

6.5.3. Brass shavings

Richard and Biester (2016) tested the efficiency of brass shavings (Cu/Zn) as a long-term in-situ treatment for Hg-contaminated groundwater. The method showed remarkable efficiency in removing >99.95 % of Hg from highly contaminated groundwater (up to 870 μg/L Hg) at a pH range between 6.3 and 6.7. Regardless of pH, the method removed 60–80 % of Hg in the first few millimeters of the filter bed. While the method's removal rates, reaction kinetics, and loading capacities

exceeded those of the tested conventional filter materials (Hg-specific organic resin and sulfurized mineral adsorber), it has limitations. These include the introduction of Zn into the treated groundwater and the lowering of groundwater pH. Similarly, Huttenloch et al. (2003) tested the efficiency of copper shavings (Cu^0) for Hg^{2+} removal from an aqueous solution. The batch sorption experiment showed that Cu^0 could remove 96–98 % of Hg^{2+} within 2 h in contaminated water with up to 10,000 μg/L Hg^{2+}. According to the author, this method appears to be an approach for field application due to its high Hg^{2+} retardation coefficient and fast reaction kinetics. Because this method can release up to 0.6 mg/L Cu^{2+} into the treated water, the author suggested using a reactive material, e.g., zeolite, to remove the mobilized Cu^{2+} from the treated water via ion exchange.

6.5.4. Molybdenum disulfide (MoS_2)

Hg removal by nanofibrous mats coated with MoS_2 was tested recently by Fausey et al. (2020). The nanocomposite demonstrated a high (0.436 min/mg) and fast (6258.7 mg/g) capacity for Hg removal. The use of poly(vinylpyrrolidone) to increase the MoS_2 interlayer distance from the initial 0.68 nm to > 0.90 nm further optimized removal. The optimized MoS_2 could adsorb 70 % of Hg in water, five times higher than the initial non-optimized MoS_2. Similarly, Ai et al. (2016) recorded close to 2506 mg/g Hg removal capacity using a non-optimized MoS_2 method. Song et al. (2018) applied a different approach with MoS_2, i.e., using the decoration of defective MoS_2 (d-MoS_2) nanosheets with Fe_3O_4 nanoparticles for Hg^{2+} removal in an aqueous solution. This method reduces the initial 10 mg/L of Hg^{2+} to 1.7 μg/L within 20 min. However, the MoS_2/Fe_3O_4 nanohybrids method can reach the adsorption capacity of 452.5 mg/g for Hg^{2+}. A summary of emerging nanomaterials, supporting media, chemical processes and adsorption capacity is given in Table 3.

Table 3
Emerging technologies for removal of mercury in contaminated groundwater.

Reference	Nanomaterials	Chemical Process	Adsorption Capacity (%)
Richard and Biester (2016)	Cu/Zn	Filtration	99
(Lisha et al., 2009; Lo et al., 2012)	Au	Absorption	97
Wang et al. (2017).	SeNPs	–	81
Fausey et al. (2020)	MoS_2	Adsorption	70
Feng et al. (2020)	BC	Pyrolyzation	99
Khorshidi et al. (2020)	GO	Adsorption	94
Asare et al. (2018)	Bacillus thuringiensis MC28	–	99
Huttenloch et al. (2003)	CuO	Ion exchange	98
Hashemi et al. (2019)	Polyaniline-Fe_3O_4-silver diethyldithiocarbamate	Chemisorption	99
Nasirimoghaddam et al. (2015)	Chitosan-coated magnetic nanoparticles	Desorption	90
Jackson Jr (2008)	Stannous chloride	Chemical reduction	95
Han et al. (2014)	Reactive FeS-supported ultrafiltration	Desorption	99
Chiarle et al. (2000)	Resin	Adsorption	40
Weisener et al. (2005)	Zerovalent Iron	Absorption	50

7. Summary and conclusion

Mercury (Hg) is one of the groundwater's most toxic, mobile, and persistent contaminants, released from geogenic or anthropogenic sources. It accumulates in soils and sediments from legacy sites, artisanal and small-scale gold mining, chloralkali (using Hg cells) manufacturing, oil and gas production wastewaters, or atmospheric deposition. Once in the soil, Hg undergoes various biogeochemical reactions, including complexation, oxidation-reduction, adsorption-desorption, and precipitation-dissolution, which are critical to its fate and transport. Soil pH, soil organic matter (SOM), texture, slope, and clay properties are crucial to Hg retention and transport. These parameters determine whether Hg from soils and sediments in the vadose zone migrates into the corresponding groundwater. Typically, the low solubility of Hg^0 and Hg^{2+} and sorption onto FeOOH, clays, manganese oxides and SOM can mitigate its impact on groundwater quality. However, under oxidizing conditions, Hg sorbed on FeOOH particulates could become mobilized in groundwater systems.

Several investigations revealed that mobilization, transport, and fate of Hg in groundwater are strongly controlled by (1) redox processes that support precipitation-dissolution and microbial activity (including methylation of Hg^{2+}) within the aquifer; (2) a pH condition favorable to adsorption-desorption and the availability of Fe and DOM in the groundwater. However, these studies need to identify the critical factors for designing a conceptual model on the transport and fate of anthropogenic and geogenic Hg in groundwater systems. Given the results of recent investigations on (1) combining isotopic signatures of Hg, concentration, and speciation to improve our understanding of the complex Hg biogeochemistry of Hg-contaminated soil–groundwater systems and (2) factors that could influence groundwater methylation rates, further investigation into Hg transport in groundwater and the application of promising emerging nanotechnologies for complete removal of Hg removal from contaminated groundwater is needed.

Studies on applying promising emerging NMs using various principles (e.g., adsorption, coagulation and complexation) for the complete remediation of Hg-contaminated groundwater show that adsorption-based emerging NMs are the most promising and effective Hg removal technology. Here, Cu/Zn, BC, bacillus thuringiensis MC28, polyaniline-Fe_3O_4-silver diethyldithiocarbamate, and reactive FeS-supported ultrafiltration are the most effective, having a high Hg adsorption capacity of >99 %. Although they are effective, economical, and suitable for *in situ* remediation, the (1) potential release of chemical parameters and (2) application of species-based NMs for Hg removal still needs to be better understood. The research discussed here is intended to aid readers in understanding groundwater Hg transport and the various effective remediation options for Hg contamination.

CRediT authorship contribution statement

Dogo Lawrence Aleku: Writing – original draft, Methodology, Investigation. **Olesya Lazareva:** Writing – review & editing, Methodology, Investigation. **Thomas Pichler:** Writing – review & editing, Supervision, Project administration, Funding acquisition, Conceptualization.

Declaration of competing interest

The authors declare the following financial interests/personal relationships which may be considered as potential competing interests:

Thomas Pichler reports financial support was provided by German Research Foundation. Dogo Lawrence Aleku reports a relationship with Petroleum Technology Development Fund that includes: funding grants.

Data availability

No data was used for the research described in the article.

Acknowledgments

This work was partly funded by the Deutsche Forschungsgemeinschaft (DFG) grant PI 746/19-1 to Pichler and by a Nigerian Petroleum Technology Development Fund to Dogo.

References

Abbas, K., Znad, H., Awual, M.R., 2018. A ligand anchored conjugate adsorbent for effective mercury(II) detection and removal from aqueous media. Chem. Eng. J. 334, 432–443. https://doi.org/10.1016/j.cej.2017.10.054.

Agyapong, A.E., Essumang, D., Dodoo, D., Tagoe, S., 2018. Utilization of Bacillus thuringiensis MC28 as a biosorbent for mercury in groundwaters from some selected gold mining communities in the Wassa West District of the Western Region of Ghana. Environ. Nanotechnol. Monit. Manag. 9, 95–106. https://doi.org/10.1016/j.enmm.2017.12.005.

Ai, K., Ruan, C., Shen, M., Lu, L., 2016. MoS 2 nanosheets with Widened interlayer spacing for high-efficiency removal of mercury in aquatic systems. Adv. Funct. Mater. 26 https://doi.org/10.1002/adfm.201601338.

Alijani, H., Shariatinia, Z., 2018. Synthesis of high growth rate SWCNTs and their magnetite cobalt sulfide nanohybrid as super-adsorbent for mercury removal. Chem. Eng. Res. Des. 129, 132–149. https://doi.org/10.1016/j.cherd.2017.11.014.

AlOmar, M.K., Alsaadi, M.A., Hayyan, M., Akib, S., Ibrahim, M., Hashim, M.A., 2017. Allyl triphenyl phosphonium bromide based DES-functionalized carbon nanotubes for the removal of mercury from water. Chemosphere 167, 44–52. https://doi.org/10.1016/j.chemosphere.2016.09.133.

AMAP/UN, 2018. *Technical Background Report to the Global Mercury Assessment 2018. Arctic Monitoring and Assessment Programme* (978-82-7971-108-7). (Arctic Monitoring and Assessment Programme, Oslo, Norway/UN Environment Programme, Issue. https://www.unep.org/resources/publication/global-mercury-assessment-2018.

Amiri, V., Li, P., Bhattacharya, P., Nakhaei, M., 2021. Mercury pollution in the coastal Urmia aquifer in northwestern Iran: potential sources, mobility, and toxicity. Environ. Sci. Pollut. Control Ser. 1–17. https://doi.org/10.1007/s11356-020-11865-y.

Andersson, A., Nriagu, J., 1979. The Biogeochemistry of Mercury in the Environment, 79. Eisevier/North-Hoiland Biomedical Press, New York.

Anirudhan, T.S., Divya, L., Ramachandran, M., 2008. Mercury(II) removal from aqueous solutions and wastewaters using a novel cation exchanger derived from coconut coir pith and its recovery. J. Hazard Mater. 157 (2), 620–627. https://doi.org/10.1016/j.jhazmat.2008.01.030.

Arrifano, G.P., Martín-Doimeadios, R.C.R., Jime´nez-Moreno, M., Ramírez-Mateos, V., da Silva, N.F., Souza-Monteiro, J.R., Augusto-Oliveira, M., Paraense, R.S., Macchi, B.M., do Nascimento, J.L.M., 2018. Large-scale projects in the amazon and human exposure to mercury: the case-study of the Tucuruí Dam. Ecotoxicol. Environ. Saf. 147, 299–305.

Asare, E.A., Essumang, D.K., Dodoo, D.K., Tagoe, S., 2018. Utilization of Bacillus thuringiensis MC28 as a biosorbent for mercury in groundwaters from some selected gold mining communities in the Wassa West District of the Western Region of Ghana. Environ. Nanotechnol. Monit. Manag. 9, 95–106. https://doi.org/10.1016/j.enmm.2017.12.005.

Babiarz, C.L., Hurley, J.P., Hoffmann, S.R., Andren, A.W., Shafer, M.M., Armstrong, D.E., 2001. Partitioning of total mercury and methylmercury to the colloidal phase in freshwaters. Environ. Sci. Technol. 35 (24), 4773–4782.

Babut, M., Sekyi, R., Rambaud, A., Potin-Gautier, M., Tellier, S., Bannerman, W., Beinhoff, C., 2003. Improving the environmental management of small-scale gold mining in Ghana: a case study of Dumasi. J. Clean. Prod. 11 (2), 215–221. https://doi.org/10.1016/S0959-6526(02)00042-2.

Bagnato, E., Aiuppa, A., Parello, F., D'alessandro, W., Allard, P., Calabrese, S., 2009. Mercury concentration, speciation and budget in volcanic aquifers: Italy and Guadeloupe (Lesser Antilles). J. Volcanol. Geoth. Res. 179 (1–2), 96–106.

Bai, H., Li, C., Shi, G., 2011. Functional composite materials based on chemically converted graphene. Adv. Mater. 23 (9), 1089–1115.

Baldi, F., Parati, F., Semplici, F., Tandoi, V., 1993. Biological removal of inorganic Hg (II) as gaseous elemental Hg (0) by continuous culture of a Hg-resistant Pseudomonas putida strain FB-1. World J. Microbiol. Biotechnol. 9, 275–279.

Ball, J.W., McCleskey, R.B., Nordstrom, D.K., Holloway, J.M., 2006. Water-Chemistry Data for Selected Springs, Geysers, and Streams in Yellowstone National Park. Wyoming.

Bardos, P., Merly, C., Kvapil, P., Koschitzky, H.-P., 2018. Status of nanoremediation and its potential for future deployment: risk-benefit and benchmarking appraisals. Remed. J. 28 (3), 43–56. https://doi.org/10.1002/rem.21559.

Barkay, T., Gillman, M., Turner, R.R., 1997. Effects of dissolved organic carbon and salinity on bioavailability of mercury. Appl. Environ. Microbiol. 63 (11), 4267–4271.

Barkley, N.P., 1991. Extraction of mercury from groundwater using immobilized algae. J. Air Waste Manag. Assoc. 41 (10), 1387–1393. https://doi.org/10.1080/10473289.1991.10466935.

Barringer, J.L., 2001. Relation of mercury to other chemical constituents in ground water in the Kirkwood-Cohansey aquifer system, New Jersey Coastal Plain, and mechanisms for mobilization of mercury from sediments to ground water [electronic resource]. In: Barringer, Julia L., MacLeod, Cecilia L. (Eds.), Prepared in Cooperation with the New Jersey Department of Environmental Protection. U.S. Dept. of the Interior, U.S. Geological Survey.

Barringer, J.L., Riskin, M.L., Szabo, Z., Reilly, P.A., Rosman, R., Bonin, J.L., Fischer, J.M., Heckathorn, H.A., 2010. Mercury and methylmercury dynamics in a coastal plain watershed, New Jersey, USA. Water, Air, Soil Pollut. 212 (1), 251–273.

Barringer, J.L., Szabo, Z., 2006. Overview of investigations into mercury in ground water, soils, and septage, New Jersey coastal plain. Water, Air, Soil Pollut. 175 (1–4), 193–221. https://doi.org/10.1007/s11270-006-9130-1.

Barringer, J.L., Szabo, Z., Kauffman, L.J., Barringer, T.H., Stackelberg, P.E., Ivahnenko, T., Rajagopalan, S., Krabbenhoft, D.P., 2005. Mercury concentrations in water from an unconfined aquifer system, New Jersey coastal plain. Sci. Total Environ. 346 (1–3), 169–183. https://doi.org/10.1016/j.scitotenv.2004.11.013.

Barringer, J.L., Szabo, Z., Reilly, P.A., 2013. Occurrence and mobility of mercury in groundwater. In: Current Perspectives in Contaminant Hydrology and Water Resources Sustainability. https://doi.org/10.5772/55487.

Barringer, J.L., Szabo, Z., Reilly, P.A., Riskin, M.L., 2013a. Variable contributions of mercury from groundwater to a first-order urban coastal plain stream in New Jersey, USA. Water, Air, Soil Pollut. 224 (4), 1–25.

Beckers, F., Rinklebe, J., 2017. Cycling of mercury in the environment: sources, fate, and human health implications: a review. Crit. Rev. Environ. Sci. Technol. 47 (9), 693–794.

Benhamza, M., 1996. Etude hydroge´ologique de la zone mercurielle de Fendek (AZZABA)-Cons´equences de l'exploitation sur l'environnement Annaba].

Benoit, J., Gilmour, C.C., Heyes, A., Mason, R., Miller, C., 2003. Geochemical and Biological Controls over Methylmercury Production and Degradation in Aquatic Ecosystems. Biogeochemistry of Environmentally Important Trace Elements.

Berg, T., Fjeld, E., Steinnes, E., 2006. Atmospheric mercury in Norway: contributions from different sources. Sci. Total Environ. 368 (1), 3–9. https://doi.org/10.1016/j.scitotenv.2005.09.059.

Berger, L.I., 1996. Semiconductor Materials. CRC press.

Biester, H., P, S., Müller, G., 2000. Effectiveness of mossy tin filters to remove mercury from aqueous solution by Hg (II) reduction and Hg (0) amalgamation. Water Res. 34 (7), 2031–2036.

Bigham, G.N., Henry, B., Bessinger, B., 1964. 1 - mercury. In: Morrison, R.D., Murphy, B. L. (Eds.), Environmental Forensics. Academic Press, pp. 1–17. https://doi.org/10.1016/B978-012507751-4/50023-9.

Blue, L.Y., Van Aelstyn, M.A., Matlock, M., Atwood, D.A., 2008. Low-level mercury removal from groundwater using a synthetic chelating ligand. Water Res. 42 (8), 2025–2028. https://doi.org/10.1016/j.watres.2007.12.010.

Bodzek, M., Konieczny, K., Kwiecin´ska-Mydlak, A., 2020. Nanotechnology in water and wastewater treatment. Graphene – the nanomaterial for next generation of semipermeable membranes. Crit. Rev. Environ. Sci. Technol. 50 (15), 1515–1579. https://doi.org/10.1080/10643389.2019.1664258.

Bollen, A., Wenke, A., Biester, H., 2008. Mercury speciation analyses in HgCl2-contaminated soils and groundwater - implications for risk assessment and remediation strategies [Article]. Water Res. 42 (1–2), 91–100. https://doi.org/10.1016/j.watres.2007.07.011.

Boszke, L., Kowalski, A., 2006. Spatial distribution of mercury in bottom sediments and soils from Poznan´, Poland. Pol. J. Environ. Stud. 15 (2).

Boutsika, L.G., Karapanagioti, H.K., Manariotis, I.D., 2014. Aqueous mercury sorption by biochar from malt spent rootlets. Water, Air, Soil Pollut. 225 (1), 1–10.

Bradley, P.J.C., 2012. Hydrology and methylmercury availability in Coastal Plain streams. Chapter 8. In: Nayak, P. (Ed.), Water Resources Management and Modeling, 8, pp. 169–190. https://cdn.intechopen.com/pdfs/32914/InTech-Hydrology_and_methylmercury_availability_in_coastal_plain_streams.pdf.

Bradley, P.M., Burns, D.A., Murray, K.R.-., Brigham, M.E., Button, D.T., Chasar, L.C., Marvin-DiPasquale, M., Lowery, M.A., Journey, C.A., 2011. Spatial and seasonal variability of dissolved methylmercury in two stream basins in the eastern United States. Environ. Sci. Technol. 45 (6), 2048–2055.

Bradley, P.M., Journey, C.A., Chapelle, F.H., Lowery, M.A., Conrads, P.A., 2010. Flood hydrology and methylmercury availability in Coastal Plain rivers. Environ. Sci. Technol. 44 (24), 9285–9290.

Bradley, P.M., Journey, C.A., Lowery, M.A., Brigham, M.E., Burns, D.A., Button, D.T., Chapelle, F.H., Lutz, M.A., Marvin-DiPasquale, M.C., Riva-Murray, K., 2012. Shallow groundwater mercury supply in a Coastal Plain stream. Environ. Sci. Technol. 46 (14), 7503–7511.

Bravo, A.G., Bouchet, S., Tolu, J., Bjo¨rn, E., Mateos-Rivera, A., Bertilsson, S., 2017. Molecular composition of organic matter controls methylmercury formation in boreal lakes. Nat. Commun. 8 (1), 1–9.

Bravo, M.A., Parra, S., Quiroz, W., Neaman, A., 2019. Human exposure assessment to mercury through hair analysis in coastal villages of the valparaiso region (Chile). J. Chil. Chem. Soc. 64, 4480–4483. http://www.scielo.cl/scielo.php?script=sci_arttext&pid=S0717-97072019000204480&nrm=iso.

Brocza, F.M., Biester, H., Richard, J.-H., Kraemer, S.M., Wiederhold, J.G., 2019. Mercury isotope fractionation in the subsurface of a Hg(II) chloride-contaminated industrial legacy site. Environ. Sci. Technol. 53 (13), 7296–7305. https://doi.org/10.1021/acs.est.9b00619.

Brooks, S.C., Southworth, G.R., 2011. History of mercury use and environmental contamination at the Oak Ridge Y-12 Plant. Environ. Pollut. 159 (1), 219–228.

Brown, J.R., Bancroft, G.M., Fyfe, W.S., McLean, R.A., 1979. Mercury removal from water by iron sulfide minerals. An electron spectroscopy for chemical analysis (ESCA) study. Environ. Sci. Technol. 13 (9), 1142–1144.

Budianta, W., Fahmi, F.L., Arifudin, Warmada, I.W., 2019. The distribution and mobility of mercury from artisanal gold mining in river sediments and water, Banyumas, Central Java, Indonesia. Environ. Earth Sci. 78 (3), 90. https://doi.org/10.1007/s12665-019-8108-4.

Burns, D.A., Aiken, G.R., Bradley, P.M., Journey, C.A., Schelker, J., 2013. Specific ultraviolet absorbance as an indicator of mercury sources in an Adirondack River basin. Biogeochemistry 113 (1), 451–466.

Charlet, L., Bosbach, D., Peretyashko, T., 2002. Natural attenuation of TCE, As, Hg linked to the heterogeneous oxidation of Fe (II): an AFM study. Chem. Geol. 190 (1–4), 303–319.

Chen, C., Liu, H., Chen, T., Chen, D., Frost, R.L., 2015. An insight into the removal of Pb (II), Cu(II), Co(II), Cd(II), Zn(II), Ag(I), Hg(I), Cr(VI) by Na(I)-montmorillonite and Ca(II)-montmorillonite. Appl. Clay Sci. 118, 239–247. https://doi.org/10.1016/j.clay.2015.09.004.

Chen, Y., 1997. Environmental Impacts of Mercury Contamination Associated with Mining. University of Nevada, Reno.

Chiarle, S., Ratto, M., Rovatti, M., 2000. Mercury removal from water by ion exchange resins adsorption. Water Res. 34 (11), 2971–2978. https://doi.org/10.1016/S0043-1354(00)00044-0.

CIRS, 2017. China enforcing mercury convention. http://www.cirs-reach.com/news-and-articles/China-Enforcing-Mercury-Convention.html#:~:text=From%201%20January%202021%2C%20the,with%20mercury%20less%20than%202%25.

Colombo, M., Ha, J., Reinfelder, J., Yee, N., 2014. Oxidation of Hg(0) to Hg(II) by diverse anaerobic bacteria. Chem. Geol. 363, 334–340. https://doi.org/10.1016/j.chemgeo.2013.11.020.

Corps, R.A.I., S´anchez-Cachero, A., Jim´enez-Moreno, M., Guzma´n Bernardo, F.J., Rodríguez Martín-Doimeadios, R.C., Ríos, A´., 2018. Carbon nanotubes magnetic hybrid nanocomposites for a rapid and selective preconcentration and clean-up of mercury species in water samples. Talanta 179, 442–447. https://doi.org/10.1016/j.talanta.2017.11.024.

Coulibaly, M., Bamba, D., Yao, N.G.A., Zoro, E.G., El Rhazi, M., 2016. Some aspects of speciation and reactivity of mercury in various matrices. Compt. Rendus Chem. 19 (7), 832–840. https://doi.org/10.1016/j.crci.2016.02.005.

Covelli, S., Piani, R., Acquavita, A., Predonzani, S., Faganeli, J., 2007. Transport and dispersion of particulate Hg associated with a river plume in coastal Northern Adriatic environments. Mar. Pollut. Bull. 55 (10–12), 436–450.

Cui, L., Guo, X., Wei, Q., Wang, Y., Gao, L., Yan, L., Yan, T., Du, B., 2015. Removal of mercury and methylene blue from aqueous solution by xanthate functionalized magnetic graphene oxide: sorption kinetic and uptake mechanism. J. Colloid Interface Sci. 439, 112–120. https://doi.org/10.1016/j.jcis.2014.10.019.

Davey, H.A., van Moort, J.C., 1986. Current mercury deposition at ngawha springs, New Zealand. Appl. Geochem. 1 (1), 75–93. https://doi.org/10.1016/0883-2927(86)90039-9, 1986/01/01/.

Del Estado, B.O., 2003. Real Decreto, de 7 de febrero, por el que se establecen los criterios sanitarios de la calidad del agua de consumo humano. BOE 45, 7228–7245.

Devi, V., Atique, M., Raju, A., Upreti, G., Jigyasu, D., Yadav, J., Singh, S., Kar, R., Singh, M., 2022. Mercury transportation dynamics in the Ganga Alluvial Plain, India: rainwater–groundwater–river water interaction study from hotspot region. Int. J. Environ. Sci. Technol. 19 (6), 4891–4900.

Díaz, L.E., Gutie´rrez, J., García-Men´endez, O., Ballesteros, B., 2006. About the presence of mercury in groundwater of La Plana de Castello´n aquifer (east Spain). Bol. Geol. Min. 117, 621–625.

Dini, A., Benvenuti, M., Costagliola, P., Lattanzi, P., 2001. Mercury deposits in metamorphic settings: the example of levigliani and ripa mines, apuane alps (Tuscany, Italy). Ore Geol. Rev. 18 (3), 149–167. https://doi.org/10.1016/S0169-1368(01)00026-9, 2001/10/01/.

Dittman, J.A., Shanley, J.B., Driscoll, C.T., Aiken, G.R., Chalmers, A.T., Towse, J.E., Selvendiran, P., 2010. Mercury dynamics in relation to dissolved organic carbon concentration and quality during high flow events in three northeastern US streams. Water Resour. Res. 46 (7).

Domagalski, J., 1998. Occurrence and transport of total mercury and methyl mercury in the Sacramento River Basin, California. J. Geochem. Explor. 64 (1–3), 277–291.

Dong, W., Liang, L., Brooks, S., Southworth, G., Gu, B., 2010. Roles of dissolved organic matter in the speciation of mercury and methylmercury in a contaminated ecosystem in Oak Ridge, Tennessee. Environ. Chem. 7 (1), 94–102.

Duan, Y., Han, D.S., Batchelor, B., Abdel-Wahab, A., 2016. Synthesis, characterization, and application of pyrite for removal of mercury. Colloids Surf. A Physicochem. Eng. Asp. 490, 326–335. https://doi.org/10.1016/j.colsurfa.2015.11.057.

Dvonch, J., Graney, J., Marsik, F., Keeler, G., Stevens, R., 1998. An investigation of source–receptor relationships for mercury in south Florida using event precipitation data. Sci. Total Environ. 213 (1–3), 95–108.

Eckley, C.S., Gilmour, C.C., Janssen, S., Luxton, T.P., Randall, P.M., Whalin, L., Austin, C., 2020. The assessment and remediation of mercury contaminated sites: a review of current approaches. Sci. Total Environ. 707, 136031.

Eckley, C.S., Luxton, T.P., Stanfield, B., Baldwin, A., Holloway, J., McKernan, J., Johnson, M.G., 2021. Effect of organic matter concentration and characteristics on mercury mobilization and methylmercury production at an abandoned mine site. Environ. Pollut. 271, 116369.

Edlich, R.F., Rhoads, S.K., Cantrell, H.S., Azavedo, S.M., Newkirk, A.T., 2010. Banning Mercury Amalgam. Meeting Materials of the Dental Products Panel. Food and Drug Administration, Washington DC.

Engstrom, D.R., Balogh, S.J., Swain, E.B., 2007. History of mercury inputs to Minnesota lakes: influences of watershed disturbance and localized atmospheric deposition. Limnol. Oceanogr. 52 (6), 2467–2483.

EPA, 2006. Mercury Transport and Fate through a Watershed. Synthesis Report of Research from EPA's Science to Achieve Results (STAR) Grant Program.

Ermolin, M.S., Fedotov, P.S., Malik, N.A., Karandashev, V.K., 2018. Nanoparticles of volcanic ash as a carrier for toxic elements on the global scale. Chemosphere 200, 16–22.

Ezeabasili, A., Anike, O., Okoro, B., 2015. Accumulation of mercury in surface and groundwater of anambra state, Nigeria. Global Journal of Engineering Science and Researches 2.

Faheem, Bao, J., Zheng, H., Tufail, H., Irshad, S., Du, J., 2018. Adsorption-assisted decontamination of Hg(ii) from aqueous solution by multi-functionalized corncob-derived biochar [10.1039/C8RA06622A]. RSC Adv. 8 (67), 38425–38435. https://doi.org/10.1039/C8RA06622A.

Faraji, M., Yamini, Y., Saleh, A., Rezaee, M., Ghambarian, M., Hassani, R., 2010. A nanoparticle-based solid-phase extraction procedure followed by flow injection inductively coupled plasma-optical emission spectrometry to determine some heavy metal ions in water samples. Anal. Chim. Acta 659 (1), 172–177. https://doi.org/10.1016/j.aca.2009.11.053.

Farrell, R., Huang, P., Germida, J., 1998. Biomethylation of mercury (II) adsorbed on mineral colloids common in freshwater sediments. Appl. Organomet. Chem. 12 (8-9), 613–620.

Fausey, C.L., Zucker, I., Lee, D.E., Shaulsky, E., Zimmerman, J.B., Elimelech, M., 2020. Tunable molybdenum disulfide-enabled fiber mats for high-efficiency removal of mercury from water. ACS Appl. Mater. Interfaces 12 (16), 18446–18456. https://doi.org/10.1021/acsami.9b22823.

Feng, X., Meng, B., Yan, H., Fu, X., Yao, H., Shang, L., 2018. Bioaccumulation of mercury in aquatic food chains. In: Biogeochemical Cycle of Mercury in Reservoir Systems in Wujiang River Basin, Southwest China. Springer, pp. 339–389.

Feng, Y., Liu, P., Wang, Y., Liu, W., Liu, Y., Finfrock, Y.Z., 2020. Mechanistic investigation of mercury removal by unmodified and Fe-modified biochars based on synchrotron-based methods. Sci. Total Environ. 719, 137435 https://doi.org/10.1016/j.scitotenv.2020.137435.

Fitzgerald, W., Lamborg, C., 2003. Geochemistry of mercury in the environment. Treatise on Geochemistry 9, 612.

Fitzgerald, W.F., Lamborg, C.H., Hammerschmidt, C.R., 2007. Marine biogeochemical cycling of mercury [Review]. Chem. Rev. 107 (2), 641–662. https://doi.org/10.1021/cr050353m.

Fleischer, M., 1970. Summary of the Literature on the Inorganic Geochemistry of Mercury. Mercury in the Environment, pp. 6–13.

Fleming, E.J., Mack, E.E., Green, P.G., Nelson, D.C., 2006. Mercury methylation from unexpected sources: molybdate-inhibited freshwater sediments and an iron-reducing bacterium. Appl. Environ. Microbiol. 72 (1), 457–464.

Foucher, D., Hintelmann, H., Al, T.A., MacQuarrie, K.T., 2013. Mercury isotope fractionation in waters and sediments of the Murray Brook mine watershed (New Brunswick, Canada): tracing mercury contamination and transformation. Chem. Geol. 336, 87–95.

Futsaeter, G., Wilson, S., 2013. The UNEP global mercury assessment: sources, emissions and transport. E3S Web of Conferences 1, 36001. https://doi.org/10.1051/e3sconf/20130136001.

Gabriel, M.C., Williamson, D.G., 2004. Principal biogeochemical factors affecting the speciation and transport of mercury through the terrestrial environment. Environ. Geochem. Health 26 (3), 421–434.

Gai, K., Avellan, A., Hoelen, T.P., Lopez-Linares, F., Hatakeyama, E.S., Lowry, G.V., 2019. Impact of mercury speciation on its removal from water by activated carbon and organoclay. Water Res. 157, 600–609. https://doi.org/10.1016/j.watres.2019.04.006.

Ganguli, P.M., Conaway, C.H., Swarzenski, P.W., Izbicki, J.A., Flegal, A.R., 2012. Mercury speciation and transport via submarine groundwater discharge at a southern California coastal lagoon system. Environ. Sci. Technol. 46 (3), 1480–1488. https://doi.org/10.1021/es202783u.

Gao, S., Luo, T.-C., Zhang, B.-R., Zhang, H.-F., Han, Y.-w., Zhao, Z.-D., Hu, Y.-K., 1998. Chemical composition of the continental crust as revealed by studies in East China. Geochem. Cosmochim. Acta 62 (11), 1959–1975.

Gąsior, D., Tic, W., 2016. Biochar application in the mercury ions adsorption from aqueous solutions. Economic and Environmental Studies 16, 803–818.

Gębka, K., Saniewska, D., Bełdowska, M., 2020. Mobility of mercury in soil and its transport into the sea. Environ. Sci. Pollut. Control Ser. 27 (8), 8492–8506.

Gemici, Ü., 2008. Evaluation of the water quality related to the acid mine drainage of an abandoned mercury mine (Alas¸ehir, Turkey). Environ. Monit. Assess. 147 (1), 93–106.

Gibi˘car, D., Horvat, M., Logar, M., Fajon, V., Falnoga, I., Ferrara, R., Lanzillotta, E., Ceccarini, C., Mazzolai, B., Denby, B., 2009. Human exposure to mercury in the vicinity of chlor-alkali plant. Environ. Res. 109 (4), 355–367.

Gilli, R.S., Karlen, C., Weber, M., Rüegg, J., Barmettler, K., Biester, H., Boivin, P., Kretzschmar, R., 2018. Speciation and mobility of mercury in soils contaminated by legacy emissions from a chemical factory in the Rhoˆne valley in canton of Valais, Switzerland. Soil Systems 2 (3), 44.

Gilmour, C.C., Elias, D.A., Kucken, A.M., Brown, S.D., Palumbo, A.V., Schadt, C.W., Wall, J.D., 2011. Sulfate-reducing bacterium Desulfovibrio desulfuricans ND132 as a model for understanding bacterial mercury methylation. Appl. Environ. Microbiol. 77 (12), 3938–3951.

Gilmour, C.C., Podar, M., Bullock, A.L., Graham, A.M., Brown, S.D., Somenahally, A.C., Johs, A., Hurt Jr, R.A., Bailey, K.L., Elias, D.A., 2013. Mercury methylation by novel microorganisms from new environments. Environ. Sci. Technol. 47 (20), 11810–11820.

Gonza´lez-Fern´andez, B., Men´endez-Casares, E., Asensio, M., Fern´andez, S., Ramos-Mun˜iz, F., Cruz-Herna´ndez, P., Gonza´lez Quiro´s, A., 2014. Sources of mercury in groundwater and soils of west Gijo´n (Asturias, NW Spain). Sci. Total Environ. 481, 217–231. https://doi.org/10.1016/j.scitotenv.2014.02.034.

Graham, A.M., Aiken, G.R., Gilmour, C.C., 2012. Dissolved organic matter enhances microbial mercury methylation under sulfidic conditions. Environ. Sci. Technol. 46 (5), 2715–2723.

Grassi, S., Netti, R., 2000. Sea water intrusion and mercury pollution of some coastal aquifers in the province of Grosseto (Southern Tuscany — Italy). J. Hydrol. 237 (3), 198–211. https://doi.org/10.1016/S0022-1694(00)00307-3.

Gray, J.E., Theodorakos, P.M., Bailey, E.A., Turner, R.R., 2000. Distribution, speciation, and transport of mercury in stream-sediment, stream-water, and fish collected near abandoned mercury mines in southwestern Alaska, USA. Sci. Total Environ. 260 (1–3), 21–33.

Grigal, D., 2002. Inputs and outputs of mercury from terrestrial watersheds: a review. Environ. Rev. 10 (1), 1–39.

Gu, B., Bian, Y., Miller, C.L., Dong, W., Jiang, X., Liang, L., 2011. Mercury reduction and complexation by natural organic matter in anoxic environments. Proc. Natl. Acad. Sci. USA 108 (4), 1479–1483.

Gu´edron, S., Duwig, C., Prado, B.L., Point, D., Flores, M.G., Siebe, C., 2014. (Methyl) mercury, arsenic, and lead contamination of the world's largest wastewater irrigation system: the mezquital valley (hidalgo state—Mexico). Water, Air, Soil Pollut. 225 (8), 1–19.

Gu´erin, V., Merly, C., Ohlsson, Y., Sweenay, R., Jacques, D., 2014. ImaHg- Enhanced Knowledge in Mercury Fate and Transport for Improved Management of Hg Soil Contamination. Brief Note. Project No. SN-03/08.

Guerra, F.D., Attia, M.F., Whitehead, D.C., Alexis, F., 2018. Nanotechnology for environmental remediation: materials and applications. Molecules 23 (7), 1760. https://www.mdpi.com/1420-3049/23/7/1760.

Gupta, R.C., Milatovic, D., Lall, R., Srivastava, A., 2018. Chapter 31 - mercury. In: Gupta, R.C. (Ed.), Veterinary Toxicology, third ed. Academic Press, pp. 455–462. https://doi.org/10.1016/B978-0-12-811410-0.00031-3.

Hamelin, S., Amyot, M., Barkay, T., Wang, Y., Planas, D., 2011. Methanogens: principal methylators of mercury in lake periphyton. Environ. Sci. Technol. 45 (18), 7693–7700.

Hammerschmidt, C.R., Fitzgerald, W.F., Lamborg, C.H., Balcom, P.H., Visscher, P.T., 2004. Biogeochemistry of methylmercury in sediments of long island sound. Mar. Chem. 90 (1–4), 31–52.

Han, D.S., Orillano, M., Khodary, A., Duan, Y., Batchelor, B., Abdel-Wahab, A., 2014. Reactive iron sulfide (FeS)-supported ultrafiltration for removal of mercury (Hg(II)) from water. Water Res. 53, 310–321. https://doi.org/10.1016/j.watres.2014.01.033.

Hanandeh, A.E., Abu-Zurayk, R.A., Hamadneh, I., Al-Dujaili, A.H., 2016. Characterization of biochar prepared from slow pyrolysis of Jordanian olive oil processing solid waste and adsorption efficiency of Hg2+ ions in aqueous solutions. Water Sci. Technol. 74 (8), 1899–1910.

Hansen, A.M., Kraus, T.E., Pellerin, B.A., Fleck, J.A., Downing, B.D., Bergamaschi, B.A., 2016. Optical properties of dissolved organic matter (DOM): effects of biological and photolytic degradation. Limnol. Oceanogr. 61 (3), 1015–1032.

Hashemi, S.A., Mousavi, S.M., Ramakrishna, S., 2019. Effective removal of mercury, arsenic and lead from aqueous media using Polyaniline-Fe3O4-silver diethyldithiocarbamate nanostructures. J. Clean. Prod. 239, 118023 https://doi.org/10.1016/j.jclepro.2019.118023.

Hellal, J., Gu´edron, S., Huguet, L., Sch¨afer, J., Laperche, V., Joulian, C., Lanceleur, L., Burnol, A., Ghestem, J.-P., Garrido, F., 2015. Mercury mobilization and speciation linked to bacterial iron oxide and sulfate reduction: a column study to mimic reactive transfer in an anoxic aquifer. J. Contam. Hydrol. 180, 56–68.

Hintelmann, H., 2010. Organomercurials. Their formation and pathways in the environment. Met Ions Life Sci 7 (7), 365–401.

Hsu-Kim, H., Kucharzyk, K.H., Zhang, T., Deshusses, M.A., 2013. Mechanisms regulating mercury bioavailability for methylating microorganisms in the aquatic environment: a critical review. Environ. Sci. Technol. 47 (6), 2441–2456.

Huang, C.-W., Yang, S.-H., Sun, M.-W., Liao, V., 2015. Development of a set of bacterial biosensors for simultaneously detecting arsenic and mercury in groundwater. Environ. Sci. Pollut. Res. Int. 22 https://doi.org/10.1007/s11356-015-4216-1.

Huang, C., Hu, B., 2008. Silica-coated magnetic nanoparticles modified with γ-mercaptopropyltrimethoxysilane for fast and selective solid phase extraction of trace amounts of Cd, Cu, Hg, and Pb in environmental and biological samples prior to their determination by inductively coupled plasma mass spectrometry. Spectrochim. Acta B Atom Spectrosc. 63 (3), 437–444. https://doi.org/10.1016/j.sab.2007.12.010.

Huang, Y., Wang, M., Gong, Y., Zeng, E., 2020. Efficient removal of mercury from simulated groundwater using thiol-modified graphene oxide/Fe–Mn composite in fixed-bed columns: experimental performance and mathematical modeling. Sci. Total Environ. 714, 136636 https://doi.org/10.1016/j.scitotenv.2020.136636.

Huang, Y., Xia, S., Lyu, J., Tang, J., 2019. Highly efficient removal of aqueous Hg2+ and CH3Hg+ by selective modification of biochar with 3-mercaptopropyltrimethoxysilane. Chem. Eng. J. 360, 1646–1655. https://doi.org/10.1016/j.cej.2018.10.231.

Huttenloch, P., Roehl, K.E., Czurda, K., 2003. Use of copper shavings to remove mercury from contaminated groundwater or wastewater by amalgamation [journal article]. Environ. Sci. Technol. 37 (18), 4269–4273.

Ignatavi˘cius, G., Unsal, M.H., Busher, P., Wołkowicz, S., Satku¯nas, J., S˘ulijiene˙, G., Valskys, V., 2022. Geochemistry of mercury in soils and water sediments. AIMS environmental science 9 (3), 261–281.

Inbaraj, B.S., Wang, J., Lu, J., Siao, F., Chen, B., 2009. Adsorption of toxic mercury (II) by an extracellular biopolymer poly (γ-glutamic acid). Bioresour. Technol. 100 (1), 200–207.

Irving, E., 1954. Note on the first discovery of commercial mercury in the Philippines. Philippine Geol. 9, 1–8.

Jackson, Jr D.G., 2008. Removal of Mercury in Groundwater via Chemical Reduction.

Jacobson, G., Norton, S., Grimm, E., Edgar, T., 2012. Changing climate and sea level alter Hg mobility at Lake Tulane, Florida, US. Environ. Sci. Technol. 46 (21), 11710–11717.

Jardim, W.F., Bisinoti, M.C., Fadini, P.S., da Silva, G.S., 2010. 2010/03/01). Mercury redox chemistry in the negro river basin, amazon: the role of organic matter and solar light. Aquat. Geochem. 16 (2), 267–278. https://doi.org/10.1007/s10498-009-9086-z.

Jeon, C., Park, K.H., 2005. Adsorption and desorption characteristics of mercury (II) ions using aminated chitosan bead. Water Res. 39 (16), 3938–3944.

Jernelov, A., 1973. Cycling of mercury in the environment. Swed Water Air Pollut Res Lab, Ivl Publ Ser B;(Sweden) 182.

Jin, Y., Chen, E., Chen, C., Zhang, X., Chen, L., 2006. Standards for Drinking Water Quality (GB-5749-2006). Beijing Ministry of Health of the People's Republic of China.

Jiskra, M., Wiederhold, J.G., Bourdon, B., Kretzschmar, R., 2012. Solution speciation controls mercury isotope fractionation of Hg (II) sorption to goethite. Environ. Sci. Technol. 46 (12), 6654–6662.

Johannesson, K.H., Neumann, K., 2013. Geochemical cycling of mercury in a deep, confined aquifer: insights from biogeochemical reactive transport modeling. Geochem. Cosmochim. Acta 106, 25–43.

Johari, H., Rahmawati, D., 2020. Mercury contamination in groundwater from artisanal and small scale gold mining activities: a case study of Southern Lombok Coast, West Nusa Tenggara Province. IOP Conf. Ser. Earth Environ. Sci. 413–012016. https://doi.org/10.1088/1755-1315/413/1/012016.

Jones, D.S., Johnson, N.W., Mitchell, C.P., Walker, G.M., Bailey, J.V., Pastor, J., Swain, E. B., 2020. Diverse communities of hgcAB+ microorganisms methylate mercury in freshwater sediments subjected to experimental sulfate loading. Environ. Sci. Technol. 54 (22), 14265–14274.

Kabir, Y., Sengupta, R., Agrawal, G.D., Chopra, R., 2002. Mercury Contamination of the Groundwater in Bhopal, 1 – 8. https://peoplesscienceinstitute.org/PDF%27s/EQMG/mercury%20in%20bhopal.pdf.

Kabiri, S., Tran, D.N.H., Azari, S., Losic, D., 2015. Graphene-diatom silica aerogels for efficient removal of mercury ions from water. ACS Appl. Mater. Interfaces 7 (22), 11815–11823. https://doi.org/10.1021/acsami.5b01159.

Kerin, E.J., Gilmour, C.C., Roden, E., Suzuki, M., Coates, J., Mason, R., 2006. Mercury methylation by dissimilatory iron-reducing bacteria. Appl. Environ. Microbiol. 72 (12), 7919–7921.

Khattak, S.A., Rashid, A., Tariq, M., Ali, L., Gao, X., Ayub, M., Javed, A., 2021. Potential risk and source distribution of groundwater contamination by mercury in district Swabi, Pakistan: application of multivariate study. Environ. Dev. Sustain. 23 (2), 2279–2297. https://doi.org/10.1007/s10668-020-00674-5.

Khorshidi, P., Shirazi, R.H.S.M., Miralinaghi, M., Moniri, E., Saadi, S., 2020. Adsorptive removal of mercury (II), copper (II), and lead (II) ions from aqueous solutions using glutathione-functionalized NiFe2O4/graphene oxide composite. Res. Chem. Intermed. 46 (7), 3607–3627. https://doi.org/10.1007/s11164-020-04164-1.

Kneer, M.L., White, A., Rolfhus, K.R., Jeremiason, J.D., Johnson, N.W., Ginder-Vogel, M., 2020. Impact of dissolved organic matter on porewater Hg and MeHg concentrations in St. Louis river estuary sediments. ACS Earth Space Chem. 4 (8), 1386–1397.

Koski, R.A., Munk, L., Foster, A.L., Shanks III, W.C., Stillings, L.L., 2008. Sulfide oxidation and distribution of metals near abandoned copper mines in coastal environments, Prince William Sound, Alaska, USA. Appl. Geochem. 23 (2), 227–254.

Kowalski, A., Siepak, M., Boszke, L., 2007. Mercury contamination of surface and ground waters of Poznan´, Poland. Pol. J. Environ. Stud. 16 (1).

Kozin, L.F., Hansen, S.C., 2013. Mercury Handbook: Chemistry, Applications and Environmental Impact. Royal society of chemistry.

Krabbenhoft, D.P., Benoit, J.M., Babiarz, C.L., Hurley, J.P., Andren, A.W., 1995. Mercury cycling in the Allequash Creek watershed, northern Wisconsin. Water Air Soil Pollut. 80, 425–433.

Kretzschmar, R., Schafer, T., 2005. Metal retention and transport on colloidal particles in the environment. Elements 1 (4), 205–210.

Kumari, A., Kumar, B., Manzoor, S., Kulshrestha, U., 2015. Status of atmospheric mercury research in south asia: a review. Aerosol Air Qual. Res. https://doi.org/10.4209/aaqr.2014.05.0098, 2015.

Lamborg, C., Fitzgerald, W., Damman, A., Benoit, J., Balcom, P., Engstrom, D., 2002. Modern and historic atmospheric mercury fluxes in both hemispheres: global and regional mercury cycling implications. Global Biogeochem. Cycles 16 (4), 51-51-51-11.

Lamborg, C.H., Kent, D.B., Swarr, G.J., Munson, K.M., Kading, T., O'Connor, A.E., Fairchild, G.M., LeBlanc, D.R., Wiatrowski, H.A., 2013. Mercury speciation and mobilization in a wastewater-contaminated groundwater plume. Environ. Sci. Technol. 47 (23), 13239–13249.

Lamborg, C.H., Tseng, C.-M., Fitzgerald, W.F., Balcom, P.H., Hammerschmidt, C.R., 2003. Determination of the mercury complexation characteristics of dissolved organic matter in natural waters with "reducible Hg" titrations. Environ. Sci. Technol. 37 (15), 3316–3322.

Lawson, N.M., Mason, R.P., 1998. Accumulation of mercury in estuarine food chains. Biogeochemistry 40 (2), 235–247.

Li, P., Feng, X., Qiu, G., Shang, L., Wang, S., 2012. Mercury pollution in Wuchuan mercury mining area, Guizhou, Southwestern China: the impacts from large scale and artisanal mercury mining. Environ. Int. 42, 59–66.

Li, Y., Zhou, Z., Zhuang, C., Dou, Z., 2023. Estimating hydraulic parameters of aquifers using type curve analysis of pumping tests with piecewise-constant rates. Water 15 (9), 1661.

Liao, L., Selim, H., DeLaune, R., 2009. Mercury adsorption-desorption and transport in soils. J. Environ. Qual. 38 (4), 1608–1616.

Lin, C., Yee, N., Barkay, T., 2012. Microbial transformations in the mercury cycle. Environmental chemistry and toxicology of mercury 155–191.

Lisha, K.P., Anshup, Pradeep, T., 2009. Towards a practical solution for removing inorganic mercury from drinking water using gold nanoparticles. Gold Bull. 42 (2), 144–152. https://doi.org/10.1007/BF03214924.

Liu, H., Zhao, Y., Zhou, Y., Chang, L., Zhang, J., 2019a. Removal of gaseous elemental mercury by modified diatomite. Sci. Total Environ. 652, 651–659. https://doi.org/10.1016/j.scitotenv.2018.10.291.

Liu, P., 2016. Stabilization of Mercury in River Water and Sediment Using Biochars.

Liu, P., Ptacek, C.J., Blowes, D.W., 2019. Mercury complexation with dissolved organic matter released from thirty-six types of biochar. Bull. Environ. Contam. Toxicol. 103 (1), 175–180.

Lo, S.-I., Chen, P.-C., Huang, C.-C., Chang, H.-T., 2012. Gold nanoparticle–aluminum oxide adsorbent for efficient removal of mercury species from natural waters. Environ. Sci. Technol. 46 (5), 2724–2730. https://doi.org/10.1021/es203678v.

Magi, F., Cabassi, J., Capecchiacci, F., Giannini, L., Nisi, B., Pandeli, E., Rappuoli, D., Tassi, F., Venturi, S., Vaselli, O., 2019. Mercury in Groundwater from the Mt. Amiata Area (Central Italy).

Mallakpour, S., Khadem, E., 2016. Carbon nanotube–metal oxide nanocomposites: fabrication, properties and applications. Chem. Eng. J. 302, 344–367. https://doi.org/10.1016/j.cej.2016.05.038.

Marotte, F., 2002. Innovative hydroxide slurry processing system reclaims mercury from groundwater (A case study). In: Proceedings of the Water Environment Federation, pp. 395–402. https://doi.org/10.2175/193864702784162480, 2002.

Marowsky, G., Wedepohl, K., 1971. General trends in the behavior of Cd, Hg, Tl and Bi in some major rock forming processes. Geochem. Cosmochim. Acta 35 (12), 1255–1267.

Martin, R., Witt, M., Sawyer, G., Thomas, H., Watt, S., Bagnato, E., Calabrese, S., Aiuppa, A., Delmelle, P., Pyle, D., 2012. Bioindication of volcanic mercury (Hg) deposition around Mt. Etna (Sicily). Chem. Geol. 310, 12–22.

Marvin-DiPasquale, M., Lutz, M.A., Brigham, M.E., Krabbenhoft, D.P., Aiken, G.R., Orem, W.H., Hall, B.D., 2009. Mercury cycling in stream ecosystems. 2. Benthic methylmercury production and bed sediment— pore water partitioning. Environ. Sci. Technol. 43 (8), 2726–2732.

McLagan, D., Schwab, L., Wiederhold, J., Chen, L., Pietrucha, J., Kraemer, S., Biester, H., 2022. Demystifying mercury geochemistry in contaminated soil–groundwater systems with complementary mercury stable isotope, concentration, and speciation analyses. Environ. Sci. J. Integr. Environ. Res.: Process. Impacts.

Migdisov, A.A., Bychkov, A.Y., 1998. The behaviour of metals and sulphur during the formation of hydrothermal mercury–antimony–arsenic mineralization, Uzon caldera, Kamchatka, Russia. J. Volcanol. Geoth. Res. 84 (1–2), 153–171.

Ministry of the Environment, 2009. The Swedish Government chemicals policy: Sweden will ban the use of mercury on 1 June 2009. https://www.government.se/content assets/12c4d85c2ca64d05827fc131f1a47ab9/sweden-will-ban-the-use-of-mercury.

Mishra, B., 2017. Towards a mechanistic understanding of mercury–microbe/mineral interactions. Acta Crystallographica Section A Foundations and Advances 73, C333. https://doi.org/10.1107/S2053273317092403. C333.

Moore, W.S., 2010. The effect of submarine groundwater discharge on the ocean. Ann. Rev. Mar. Sci 2, 59–88.

Moussa, B., Yahia, H., 2012. Contamination by mercury of groundwater of the North Numidian zone of Azzaba, North East Algeria. Effect of inorganic mercury contamination of population. Int. J. Environ. Waste Manag. 9, 347–357. https://doi.org/10.1504/IJEWM.2012.046397.

Mukhopadhyay, R., Sarkar, B., Khan, E., Alessi, D.S., Biswas, J.K., Manjaiah, K., Eguchi, M., Wu, K.C., Yamauchi, Y., Ok, Y.S., 2021. Nanomaterials for sustainable remediation of chemical contaminants in water and soil. Crit. Rev. Environ. Sci. Technol. 1–50.

Nasirimoghaddam, S., Zeinali, S., Sabbaghi, S., 2015. Chitosan coated magnetic nanoparticles as nano-adsorbent for efficient removal of mercury contents from industrial aqueous and oily samples. J. Ind. Eng. Chem. 27, 79–87. https://doi.org/10.1016/j.jiec.2014.12.020.

Navarro, A., 2008. Review of characteristics of mercury speciation and mobility from areas of mercury mining in semi-arid environments. Rev. Environ. Sci. Biotechnol. 7 (4), 287–306.

Navarro, A., Font, X., Viladevall, M., 2016. Groundwater contamination by uranium and mercury at the Ridaura aquifer (Girona, NE Spain). Toxics 4 (3), 16. https://www.mdpi.com/2305-6304/4/3/16.

Nevondo, V., Malehase, T., Daso, A.P., Okonkwo, O., 2019. Leachate seepage from landfill: a source of groundwater mercury contamination in South Africa. WaterSA 45, 225. https://doi.org/10.4314/wsa.v45i2.09.

Nogara, P.A., Farina, M., Aschner, M., Rocha, J.B., 2019. Mercury in Our Food, 0893–228X.

Noh, S., Kim, J., Hur, J., Hong, Y., Han, S., 2018. Potential contributions of dissolved organic matter to monomethylmercury distributions in temperate reservoirs as revealed by fluorescence spectroscopy. Environ. Sci. Pollut. Control Ser. 25 (7), 6474–6486.

Nriagu, J.O., 1979. The Biogeochemistry of Mercury in the Environment.

O'Connor, D., Hou, D., Ok, Y.S., Mulder, J., Duan, L., Wu, Q., Wang, S., Tack, F.M., Rinklebe, J., 2019. Mercury speciation, transformation, and transportation in soils, atmospheric flux, and implications for risk management: a critical review. Environ. Int. 126, 747–761.

Obasi, P.N., Akudinobi, B.B., 2020. Potential health risk and levels of heavy metals in water resources of lead–zinc mining communities of Abakaliki, southeast Nigeria. Appl. Water Sci. 10 (7), 184. https://doi.org/10.1007/s13201-020-01233-z.

Obrist, D., Kirk, J.L., Zhang, L., Sunderland, E.M., Jiskra, M., Selin, N.E., 2018. A review of global environmental mercury processes in response to human and natural perturbations: changes of emissions, climate, and land use. Ambio 47 (2), 116–140.

Omondi, G.Z.O., Nyamari, J., Mugo, J., 2023. Mercury levels in groundwater near artisanal small-scale gold mines in Migori county, Kenya. East African Journal of Environment and Natural Resources 6 (1), 421–431.

Orica, L., 2013. Former ChlorAlkali plant, human health and environmental risk assessment. Article O/13/CAPR001-A. https://www.orica.com/ArticleDocuments/857/20130620_HHREA_FCAP.pdf.aspx.

Outridge, P.M., Mason, R., Wang, F., Guerrero, S., Heimburger-Boavida, L., 2018. Updated global and oceanic mercury budgets for the united Nations global mercury assessment 2018. Environ. Sci. Technol. 52 (20), 11466–11477.

Pacyna, E.G., Pacyna, J.M., Fudala, J., Strzelecka-Jastrzab, E., Hlawiczka, S., Panasiuk, D., 2006. Mercury emissions to the atmosphere from anthropogenic sources in Europe in 2000 and their scenarios until 2020. Sci. Total Environ. 370 (1), 147–156. https://doi.org/10.1016/j.scitotenv.2006.06.023.

Pandey, P., Dahiya, M., 2016. Carbon nanotubes: types, methods of preparation and applications. Int. J. Pharmaceut. Sci. Res. 1, 15–21.

Parks, J.M., Johs, A., Podar, M., Bridou, R., Hurt, R.A., Smith, S.D., Tomanicek, S.J., Qian, Y., Brown, S.D., Brandt, C.C., 2013. The genetic basis for bacterial mercury methylation. Science 339 (6125), 1332–1335.

Pichler, T., 2024. Environmental inventory of mercury (Hg) for the marine shallow water hydrothermal system at Panarea, Italy. Sci. Total Environ. 911, 168575 https://doi.org/10.1016/j.scitotenv.2023.168575.

Pimentel, F., 1944. Aspectos gerais do município de Rio Grande.

Podar, M., Gilmour, C.C., Brandt, C.C., Soren, A., Brown, S.D., Crable, B.R., Palumbo, A.V., Somenahally, A.C., Elias, D.A., 2015. Global prevalence and distribution of genes and microorganisms involved in mercury methylation. Sci. Adv. 1 (9), e1500675.

Poulin, B.A., Gerbig, C.A., Kim, C.S., Stegemeier, J.P., Ryan, J.N., Aiken, G.R., 2017. Effects of sulfide concentration and dissolved organic matter characteristics on the structure of nanocolloidal metacinnabar. Environ. Sci. Technol. 51 (22), 13133–13142.

Protano, G., Bianchi, S., De Santis, M., Di Lella, L.A., Nannoni, F., Salleolini, M., 2023. New geochemical data for defining origin and distribution of mercury in groundwater of a coastal area in southern Tuscany (Italy). Environ. Sci. Pollut. Control Ser. 30 (17), 50920–50937.

Protano, G., Riccobono, F., Sabatini, G., 2000. Does salt water intrusion constitute a mercury contamination risk for coastal fresh water aquifers? Environ. Pollut. 110 (3), 451–458.

Qasim, G.H., Lee, S., Lee, G., Lee, W., Hong, Y., Han, S., 2018. Dissolved oxygen and nitrate effects on the reduction and removal of divalent mercury by pumice supported nanoscale zero-valent iron [10.1039/C8EW00326B]. Environ. Sci. J. Integr. Environ. Res.: Water Research & Technology 4 (10), 1651–1661. https://doi.org/10.1039/C8EW00326B.

Quintana, G.C., Mirlean, N., 2018. Groundwater contamination by mercury from the aforetime carroting practice. Bull. Environ. Contam. Toxicol. 100 (6), 839–842. https://doi.org/10.1007/s00128-018-2333-5.

Reilly, P.A., Barringer, J.L., Szabo, Z., 2012. MOBILITY OF MERCURY IN DISTURBED SOILS WITHIN THE NEW JERSEY COASTAL PLAIN.

Reimers, R.S., Krenkel, P.A., 1974. Kinetics of mercury adsorption and desorption in sediments. Journal (Water Pollution Control Federation) 352–365.

Renzoni, A., Zino, F., Franchi, E., 1998. Mercury levels along the food chain and risk for exposed populations. Environ. Res. 77 (2), 68–72.

Rhee, S.-W., 2015. Control of mercury emissions: policies, technologies, and future trends. Energy Emiss. Control Technol. 1 https://doi.org/10.2147/EECT.S73403.

Richard, J., Biester, H., 2016. Mercury removal from contaminated groundwater: performance and limitations of amalgamation through brass shavings. Water Res. 99, 272–280. https://doi.org/10.1016/j.watres.2016.05.007.

Richard, J., Bischoff, C., Biester, H., 2016. Comparing modeled and measured mercury speciation in contaminated groundwater: importance of dissolved organic matter composition. Environ. Sci. Technol. 50 (14), 7508–7516.

Ro¨mhild, L., Fiandaca, G., Hu, L., Meyer, L., Bayer, P., 2022. Imaging hydraulic conductivity in near-surface aquifers by complementing cross-borehole induced polarization with hydraulic experiments. Adv. Water Resour. 170, 104322.

Roberts, H., Price, R., Brombach, C.-C., Pichler, T., 2021. Mercury in the hydrothermal fluids and gases in paleochori bay, milos, Greece. Mar. Chem. 233, 103984.

Rudnick, R.L., 2005. Composition of the continental crust. The Crust, Treatise on Geochemistry 3, 17–18.

Rytuba, J.J., 2000. Mercury mine drainage and processes that control its environmental impact. Sci. Total Environ. 260 (1–3), 57–71.

Rytuba, J.J., 2003. Mercury from mineral deposits and potential environmental impact. Environ. Geol. 43, 326–338.

Saether, O.M., Storroe, G., Segar, D., Krog, R., 1997. Contamination of soil and groundwater at a former industrial site in Trondheim, Norway. Appl. Geochem. 12 (3), 327–332.

Saleh, T.A., Tuzen, M., Sarı, A., 2018. Polyamide magnetic palygorskite for the simultaneous removal of Hg(II) and methyl mercury; with factorial design analysis. J. Environ. Manag. 211, 323–333. https://doi.org/10.1016/j.jenvman.2018.01.050.

Samaniego, J., Gibaga, C.R., Mendoza, N., Racadio, C.D., Tanciongco, A., Rastrullo, R., 2020. Mercury and other heavy metals in groundwater in the abandoned mercury mine in Puerto Princesa city, Philippines. Philipp. J. Sci. 149, 897–901.

Sarkar, B., Mandal, S., Tsang, Y.F., Kumar, P., Kim, K.-H., Ok, Y.S., 2018. Designer carbon nanotubes for contaminant removal in water and wastewater: a critical review. Sci. Total Environ. 612, 561–581. https://doi.org/10.1016/j.scitotenv.2017.08.132.

Schartup, A.T., Balcom, P.H., Mason, R.P., 2014. Sediment-porewater partitioning, total sulfur, and methylmercury production in estuaries. Environ. Sci. Technol. 48 (2), 954–960.

Schmitt, E., Swarzenski, P., Kroeger, K., Smith, C., Hauswirth, S., Lamborg, C., Beutel, M., Flegal, A., Ganguli, P., 2020. Linking submarine groundwater discharge to mercury biogeochemical cycling at the coastal margin. https://doi.org/10.1130/abs/2020AM-359118.

Schuster, P., Shanley, J., Marvin-Dipasquale, M., Reddy, M., Aiken, G., Roth, D., Taylor, H.E., Krabbenhoft, D., DeWild, J., 2008. Mercury and organic carbon dynamics during runoff episodes from a northeastern USA watershed. Water Air Soil Pollut. 187 (1), 89–108.

Schuster, P.F., Krabbenhoft, D.P., Naftz, D.L., Cecil, L.D., Olson, M.L., Dewild, J.F., Susong, D.D., Green, J.R., Abbott, M.L., 2002. Atmospherc mercury deposition during the last 270 years: a glacial ice core record of natural and anthropogenic

sources. Environ. Sci. Technol. 36 (11), 2303–2310. https://doi.org/10.1021/es0157503.
Schwartz, M.O., 1997. Mercury in zinc deposits: economic geology of a polluting element. Int. Geol. Rev. 39 (10), 905–923.
Schwertmann, U., Cornell, R.M., 2008. Iron Oxides in the Laboratory: Preparation and Characterization. John Wiley & Sons.
Selin, H., Keane, S.E., Wang, S., Selin, N.E., Davis, K., Bally, D., 2018. Linking science and policy to support the implementation of the Minamata Convention on Mercury. Ambio 47 (2), 198–215.
Shadbad, M.J., Mohebbi, A., Soltani, A., 2011. Mercury(II) removal from aqueous solutions by adsorption on multi-walled carbon nanotubes. Kor. J. Chem. Eng. 28 (4), 1029–1034. https://doi.org/10.1007/s11814-010-0463-5.
Shanley, J.B., Taylor, V.F., Ryan, K.A., Chalmers, A.T., Perdrial, J., Stubbins, A., 2022. Using dissolved organic matter fluorescence to predict total mercury and methylmercury in forested headwater streams, Sleepers River, Vermont USA. Hydrol. Process. 36 (5), e14572.
Shao, H., Liu, X., Zhou, Z., Zhao, B., Chen, Z., Xu, M., 2016. Elemental mercury removal using a novel KI modified bentonite supported by starch sorbent. Chem. Eng. J. 291, 306–316. https://doi.org/10.1016/j.cej.2016.01.090.
Sharma, T., Bajwa, B., Kaur, I., 2021. Contamination of groundwater by potentially toxic elements in groundwater and potential risk to groundwater users in the Bathinda and Faridkot districts of Punjab, India. Environ. Earth Sci. 80 https://doi.org/10.1007/s12665-021-09560-3.
Shaw, D.M., Dostal, J., Keays, R.R., 1976. Additional estimates of continental surface Precambrian shield composition in Canada. Geochem. Cosmochim. Acta 40 (1), 73–83.
Shirzadi, H., Nezamzadeh-Ejhieh, A., 2017. An efficient modified zeolite for simultaneous removal of Pb(II) and Hg(II) from aqueous solution. J. Mol. Liq. 230, 221–229. https://doi.org/10.1016/j.molliq.2017.01.029.
Si, L., Branfireun, B.A., Fierro, J., 2022. Chemical oxidation and reduction pathways of mercury relevant to natural waters: a review. Water 14 (12), 1891.
Si, Y., Zou, Y., Liu, X., Si, X., Mao, J., 2015. Mercury methylation coupled to iron reduction by dissimilatory iron-reducing bacteria. Chemosphere 122, 206–212. https://doi.org/10.1016/j.chemosphere.2014.11.054.
Skyllberg, U., Bloom, P.R., Qian, J., Lin, C.-M., Bleam, W.F., 2006. Complexation of mercury (II) in soil organic matter: EXAFS evidence for linear two-coordination with reduced sulfur groups. Environ. Sci. Technol. 40 (13), 4174–4180.
Somasundaram, M.V., Ravindran, G., Tellam, J.H., 1993. Groundwater pollution of the Madras urban aquifer, India [article]. Ground Water 31 (1), 4–11. https://doi.org/10.1111/j.1745-6584.1993.tb00821.x.
Song, Y., Lu, M., Huang, B., Wang, D., Wang, G., Zhou, L., 2018. Decoration of defective MoS2 nanosheets with Fe3O4 nanoparticles as superior magnetic adsorbent for highly selective and efficient mercury ions (Hg2+) removal. J. Alloys Compd. 737, 113–121. https://doi.org/10.1016/j.jallcom.2017.12.087.
Spyropoulou, A.E., Lazarou, Y.G., Sapalidis, A.A., Laspidou, C.S., 2022. Geochemical modeling of mercury in coastal groundwater. Chemosphere 286, 131609.
Sriramachari, S., 2004. Health Effects of the Toxic Gas Leak from the Union Carbide Methyl Isocyanate Plant in Bhopal. Indian Council for Medical Research, New Delhi, pp. 1988–2003.
Stoller, M.D., Park, S., Zhu, Y., An, J., Ruoff, R.S., 2008. Graphene-based ultracapacitors. Nano Lett. 8 (10), 3498–3502.
Stumm, W., Morgan, J.J., Morgan, J.J., 1981. Aquatic Chemistry. A Wiley-Interscience Publication.
Sumesh, E., Bootharaju, M.S., Anshup, Pradeep, T., 2011. A practical silver nanoparticle-based adsorbent for the removal of Hg2+ from water. J. Hazard Mater. 189 (1), 450–457. https://doi.org/10.1016/j.jhazmat.2011.02.061.
Sun, M., Cheng, G., Ge, X., Chen, M., Wang, C., Lou, L., Xu, X., 2018. Aqueous Hg (II) immobilization by chitosan stabilized magnetic iron sulfide nanoparticles. Sci. Total Environ. 621, 1074–1083.
Sun, Y., Lou, Z., Yu, J., Zhou, X., Lv, D., Zhou, J., Baig, S.A., Xu, X., 2017. Immobilization of mercury (II) from aqueous solution using Al2O3-supported nanoscale FeS. Chem. Eng. J. 323, 483–491.
Sweijen, T., Hartog, N., Marsman, A., Keijzer, T.J., 2014. The transport behaviour of elemental mercury DNAPL in saturated porous media: analysis of field observations and two-phase flow modelling. J. Contam. Hydrol. 161, 24–34.
Szabo, Z., Barringer, J.L., Jacobsen, E., Smith, N.P., Gallagher, R.A., Sites, A., 2010. Variability of mercury concentrations in domestic well water, New Jersey Coastal Plain. In: Northeastern Section (45th Annual) and Southeastern Section (59th Annual) Joint Meeting.
Tauson, V., Abramovich, M., 1980. Hydrothermal Study of the ZnS-HgS System.
Tawabini, B., Al-Khaldi, S., Atieh, M., Khaled, M., 2010. Removal of mercury from water by multi-walled carbon nanotubes. Water Sci. Technol. 61 (3), 591–598. https://doi.org/10.2166/wst.2010.897.
Taylor, S.R., 1964. Abundance of chemical elements in the continental crust: a new table. Geochem. Cosmochim. Acta 28 (8), 1273–1285. https://doi.org/10.1016/0016-7037(64)90129-2, 1964/08/01/.
Tian, Z., Lehmann, B., Deng, C., Luo, A., Zhang, X., Moynier, F., Yin, R., 2023. Mercury abundance and isotopic composition in granitic rocks: implications for Hg cycling in the upper continental crust. Geochem. Cosmochim. Acta 361, 200–209. https://doi.org/10.1016/j.gca.2023.09.019, 2023/11/15/.
Tran, L., Wu, P., Zhu, Y., Yang, L., Zhu, N., 2015. Highly enhanced adsorption for the removal of Hg(II) from aqueous solution by Mercaptoethylamine/Mercaptopropyltrimethoxysilane functionalized vermiculites. J. Colloid Interface Sci. 445, 348–356. https://doi.org/10.1016/j.jcis.2015.01.006.
Tran, V., Nguyet, T., Quốc, T., Trung, T., Huy, H., Nie, H., Minh, T., Pham Hong, N., 2020. Heavy metals contamination in groundwater resource in dak nong province, Viet Nam. Vietnam Journal of Science and Technology 58, 42–49. https://doi.org/10.15625/2525-2518/58/3A/14247.
UNEP, 2019. Technical Background Report to the Global Mercury Assessment 2018 [Preprint].
UNEP, U., 2013. Global Mercury Assessment 2013: Sources, Emissions, Releases and Environmental Transport. UNEP Chemicals Branch, Geneva, Switzerland.
USEPA, 2009. National primary drinking water regulations. https://www.nrc.gov/docs/ML1307/ML13078A040.pdf.
USGS, 2000. Mercury in the environment. https://www2.usgs.gov/themes/factsheet/146-00/.
VanStraaten, P., 2000. Mercury contamination associated with small-scale gold mining in Tanzania and Zimbabwe. Sci. Total Environ. 259 (1–3), 105–113.
Vishnivetskaya, T.A., Mosher, J.J., Palumbo, A.V., Yang, Z.K., Podar, M., Brown, S.D., Brooks, S.C., Gu, B., Southworth, G.R., Drake, M.M., 2011. Mercury and other heavy metals influence bacterial community structure in contaminated Tennessee streams. Appl. Environ. Microbiol. 77 (1), 302–311.
Wang, J., Shaheen, S.M., Jing, M., Anderson, C.W., Swertz, A.-C., Wang, S.-L., Feng, X., Rinklebe, J., 2021. Mobilization, methylation, and demethylation of mercury in a paddy soil under systematic redox changes. Environ. Sci. Technol. 55 (14), 10133–10141.
Wang, L., Hou, D., Cao, Y., Ok, Y.S., Tack, F.M.G., Rinklebe, J., O'Connor, D., 2020a. Remediation of mercury contaminated soil, water, and air: a review of emerging materials and innovative technologies. Environ. Int. 134, 105281 https://doi.org/10.1016/j.envint.2019.105281, 2020/01/01/).
Wang, M., Li, Y., Zhao, D., Zhuang, L., Yang, G., Gong, Y., 2020b. Immobilization of mercury by iron sulfide nanoparticles alters mercury speciation and microbial methylation in contaminated groundwater. Chem. Eng. J. 381, 122664 https://doi.org/10.1016/j.cej.2019.122664.
Wang, Q., Kim, D., Dionysiou, D.D., Sorial, G.A., Timberlake, D., 2004. Sources and remediation for mercury contamination in aquatic systems—a literature review. Environ. Pollut. 131 (2), 323–336.
Wang, X., Zhang, D., Qian, H., Liang, Y., Pan, X., Gadd, G.M., 2017. Interaction of Biogenic Selenium Nanoparticles and Goethite Colloids and its Impact on Remediation of Elemental Mercury Contaminated Groundwater.
Wang, Y., O'Connor, D., Shen, Z., Lo, I.M.C., Tsang, D.C.W., Pehkonen, S., Pu, S., Hou, D., 2019. Green synthesis of nanoparticles for the remediation of contaminated waters and soils: constituents, synthesizing methods, and influencing factors. J. Clean. Prod. 226, 540–549. https://doi.org/10.1016/j.jclepro.2019.04.128.
Wang, Y., Roth, S., Schaefer, J.K., Reinfelder, J.R., Yee, N., 2020. Production of methylmercury by methanogens in mercury contaminated estuarine sediments. FEMS (Fed. Eur. Microbiol. Soc.) Microbiol. Lett. 367 (23), fnaa196.
Wang, Y., Wiatrowski, H.A., John, R., Lin, C.-C., Young, L.Y., Kerkhof, L.J., Yee, N., Barkay, T., 2013. Impact of mercury on denitrification and denitrifying microbial communities in nitrate enrichments of subsurface sediments. Biodegradation 24, 33–46.
Waples, J.S., Nagy, K.L., Aiken, G.R., Ryan, J.N., 2005. Dissolution of cinnabar (HgS) in the presence of natural organic matter. Geochem. Cosmochim. Acta 69 (6), 1575–1588.
Warner, K.A., Bonzongo, J.-C.J., Roden, E.E., Ward, G.M., Green, A.C., Chaubey, I., Lyons, W.B., Arrington, D.A., 2005. Effect of watershed parameters on mercury distribution in different environmental compartments in the Mobile Alabama River Basin, USA. Sci. Total Environ. 347 (1–3), 187–207.
Wedepohl, K.H., 1995. The composition of the continental crust. Geochem. Cosmochim. Acta 59 (7), 1217–1232.
Weisener, C.G., Sale, K.S., Smyth, D.J.A., Blowes, D.W., 2005. Field column study using zerovalent iron for mercury removal from contaminated groundwater. Environ. Sci. Technol. 39 (16), 6306–6312. https://doi.org/10.1021/es050092y.
Whalin, L., Kim, E.-H., Mason, R., 2007. Factors influencing the oxidation, reduction, methylation and demethylation of mercury species in coastal waters. Mar. Chem. 107 (3), 278–294.
Whalin, L.M., Mason, R.P., 2006. A new method for the investigation of mercury redox chemistry in natural waters utilizing deflatable Teflon® bags and additions of isotopically labeled mercury. Anal. Chim. Acta 558 (1–2), 211–221.
WHO, 2004. Guidelines for Drinking-Water Quality, 1. Recommendations.
WHO, 2011. Guidelines for drinking-water quality. World Health Organization 216, 303–304.
Williams, T., Weeks, J., Apostol, A., Miranda, C., 1996. Assessment of mercury toxicity hazard associated with former cinnabar mining and tailings disposal in honda bay, palawan, Philippines. British geological survey overseas geology series technical report WC. Overseas Geology Series Technical Report WC 96, 31.
Williams, T., Weeks, J., Miranda, C., 1999. Assessment of mercury contamination and human exposure associated with coastal disposal of waste from a cinnabar mining operation, Palawan, Philippines. Environ. Geol. 39 (1), 51–60.
Wu, G.-H., Cao, S.-S., 2010. Mercury and cadmium contamination of irrigation water, sediment, soil and shallow groundwater in a wastewater-irrigated field in Tianjin, China. Bull. Environ. Contam. Toxicol. 84 (3), 336–341.
Xia, S., Huang, Y., Tang, J., Wang, L., 2019. Preparation of various thiol-functionalized carbon-based materials for enhanced removal of mercury from aqueous solution. Environ. Sci. Pollut. Control Ser. 26 (9), 8709–8720. https://doi.org/10.1007/s11356-019-04320-0.
Xu, Q., Zhao, L., Wang, Y., Xie, Q., Yin, D., Feng, X., Wang, D., 2018. Bioaccumulation characteristics of mercury in fish in the three gorges reservoir, China. Environ. Pollut. 243, 115–126.
Yan, H., Li, Q., Yuan, Z., Jin, S., Jing, M., 2019. Research progress of mercury bioaccumulation in the aquatic food chain, China: a review. Bull. Environ. Contam. Toxicol. 102 (5), 612–620.

Yang, Y., Liu, J., Liu, F., Wang, Z., Miao, S., 2018. Molecular-level insights into mercury removal mechanism by pyrite. J. Hazard Mater. 344, 104–112. https://doi.org/10.1016/j.jhazmat.2017.10.011, 2018/02/15/.

Yu, R.-Q., Reinfelder, J.R., Hines, M.E., Barkay, T., 2013. Mercury methylation by the methanogen Methanospirillum hungatei. Appl. Environ. Microbiol. 79 (20), 6325–6330.

Yudovich, Y.E., Ketris, M., 2005. Mercury in coal: a review: Part 1. Geochemistry. Int. J. Coal Geol. 62 (3), 107–134.

Zhang, D., Yin, Y., Liu, J., 2017. Removal of Hg2+ and methylmercury in waters by functionalized multi-walled carbon nanotubes: adsorption behavior and the impacts of some environmentally relevant factors. Chem. Speciat. Bioavailab. 29 (1), 161–169. https://doi.org/10.1080/09542299.2017.1378596.

Zhang, T., Kim, B., Levard, C., Reinsch, B.C., Lowry, G.V., Deshusses, M.A., Hsu-Kim, H., 2012. Methylation of mercury by bacteria exposed to dissolved, nanoparticulate, and microparticulate mercuric sulfides. Environ. Sci. Technol. 46 (13), 6950–6958. https://doi.org/10.1021/es203181m.

Zhang, T., Kucharzyk, K.H., Kim, B., Deshusses, M.A., Hsu-Kim, H., 2014. Net methylation of mercury in estuarine sediment microcosms amended with dissolved, nanoparticulate, and microparticulate mercuric sulfides. Environ. Sci. Technol. 48 (16), 9133–9141.

Zhang, W., Chen, Z., Liu, H., Zhang, L., Gao, P., Li, D., 2011. Biosynthesis and structural characteristics of selenium nanoparticles by Pseudomonas alcaliphila. Colloids Surf. B Biointerfaces 88 (1), 196–201. https://doi.org/10.1016/j.colsurfb.2011.06.031.

Zhao, H., Fan, H., Yang, G., Lu, L., Zheng, C., Gao, X., Wu, T., 2018. Integrated dynamic and steady state method and its application on the screening of MoS2 nanosheet-containing adsorbents for Hg0 capture. Energy Fuel. 32 (4), 5338–5344. https://doi.org/10.1021/acs.energyfuels.8b00099.

Zhao, H., Yang, G., Gao, X., Pang, C.H., Kingman, S.W., Wu, T., 2016. Hg0 capture over CoMoS/γ-Al2O3 with MoS2 nanosheets at low temperatures. Environ. Sci. Technol. 50 (2), 1056–1064. https://doi.org/10.1021/acs.est.5b04278.

Zhao, X.C., 2005. Mineral-thermal groundwater in Qicun geothermal field. China Nat 6, 47–48, 01/01.

Zhijia, C., Xiaoshan, Z., Yongguang, Y., Jinsheng, C., Shiwei, W., 2016. Mercury Redox Chemistry in Waters of the Eastern Asian Seas: from Polluted Coast to Clean Open Ocean.

Zhong, H., Li, P., Shi, J., Rinklebe, J., Feng, X., 2019. Recent progress in mercury research by young Chinese scholars. Bull. Environ. Contam. Toxicol. 102 (5), 595–596. https://doi.org/10.1007/s00128-019-02634-w.

Zhou, C., Zhu, H., Wang, Q., Wang, J., Cheng, J., Guo, Y., Zhou, X., Bai, R., 2017. Adsorption of mercury(ii) with an Fe3O4 magnetic polypyrrole–graphene oxide nanocomposite [10.1039/C7RA01147D]. RSC Adv. 7 (30), 18466–18479. https://doi.org/10.1039/C7RA01147D.

Zhou, Y., 2003. Assessment of Mercury Methylation in Aquatic Sediments. University of Cincinnati.

Zhuang, S.T., Yin, Y.N., Wang, J.L., 2018. Simultaneous detection and removal of cobalt ions from aqueous solution by modified chitosan beads. Int. J. Environ. Sci. Technol. 15 (2), 385–394. https://doi.org/10.1007/s13762-017-1388-x.

Žižek, S., Horvat, M., Gibičar, D., Fajon, V., Toman, M.J., 2007. Bioaccumulation of mercury in benthic communities of a river ecosystem affected by mercury mining. Sci. Total Environ. 377 (2–3), 407–415.

Appendix B: Supplementary data

a) Elevated mercury (Hg) in soil and groundwater caused by oil and gas production

Table 2.1S: Physico-chemical parameters of groundwater in the study area (2021, 2022 and 2023)

ID	Latitude (E)	Longitude (N)	pH	Eh (mV)	DO (mg/L)	DO (%)	EC (µS/cm)	TDS (mg/L)	Salinity (PSU)	Temp. (°C)	Alkalinity (mg/L)
1-21	7.102167	4.75059	5	341	5.1	64.2	42	21	0.01	27.2	3.3
1-22	7.102167	4.75059	5	322	4.4	56.6	207	105	0.1	28.9	1.9
1-23	7.102167	4.75059	5.3	ND	6.6	87.6	35	18	0.02	29.4	0
2-21	7.101882	4.750247	5.5	450	4.3	55.4	121	60	0.1	28.4	7
2-22	7.101882	4.750247	5.6	292	4.9	66.4	72	36	0.03	30.9	7.7
2-23	7.101882	4.750247	6.3	ND	7	93.4	67	33	0.03	29.5	14
3-21	7.10135	4.75025	4.7	776	6.3	80.5	55	27	0.01	28.2	0
3-22	7.10135	4.75025	4.6	742	5.3	68.9	46	24	0.02	28.2	1.1
3-23	7.10135	4.75025	5.5	ND	7.3	97.2	27	13	0.01	29.5	0
4-21	7.100967	4.750452	4.7	542	3.3	41.5	37	18	0.01	28	0.3
4-22	7.100967	4.750452	4.7	783	3.3	42	67	34	0.03	28.1	0
4-23	7.100967	4.750452	5.2	ND	5	66.3	26	13	0.01	29.2	0
5-21	7.101127	4.751107	4.5	797	6.6	83.7	37	18	0.01	27.6	0
5-22	7.101127	4.751107	4.7	775	6.9	96	34	17	0.01	32.5	0
5-23	7.101127	4.751107	5.6	ND	6.5	84.3	28	14	0.01	28.2	0
6-22	7.101615	4.74998	4.6	716	4.8	62	41	20	0.02	28	0.8
6-23	7.101615	4.74998	5.6	ND	6.1	81.7	28	14	0.01	29.4	0
7-21	7.097229	4.765065	4.8	734	5.7	78.8	20	10	0.01	32	0
7-22	7.097229	4.765065	4.8	786	6.5	89.9	66	33	0.03	26.6	0.8
7-23	7.097229	4.765065	5.6	ND	7.3	90.6	17	8	0.01	26.4	1.1
8-21	7.10261	4.75113	4.5	450	5.2	67	32	16	0.01	28.5	0
8-22	7.10261	4.75113	4.4	653	5.6	70.7	75	37	0.03	27.7	0.8
8-23	7.10261	4.75113	4.5	ND	6.7	85.8	30	15	0.01	28.1	0
9-22	7.102517	4.7508	4.5	734	3.2	41.4	40	20	0.02	28	0
9-23	7.102517	4.7508	5	ND	6.4	85	21	11	0.01	29.1	0
10-22	7.100998	4.750173	4.8	576	5.6	72.5	39	19	0.02	28.3	1.4
10-23	7.100998	4.750173	6.1	ND	7.2	96	31	15	0.01	29.7	0
11-21	7.100848	4.751698	4.6	801	6.6	84.8	48	24	0.02	28.4	0
11-23	7.100848	4.751698	5.8	ND	7.1	95.6	18	9	0.01	29.7	0
12-22	7.100852	4.75112	4.6	728	5.2	66.6	53	26	0.02	28.3	4.8
12-23	7.100852	4.75112	5	ND	6.5	84.3	32	16	0.01	28.3	0
13-22	7.10209	4.751638	5.6	336	7.4	96.7	79	40	0.04	28.8	4.8
13-23	7.10209	4.751638	5.7	ND	6.4	85.1	50	25	0.02	29.4	4.5
14-22	7.100618	4.750235	5	737	6.2	80.3	45	22	0.02	28.1	1
14-23	7.100618	4.750235	5.6	ND	7.3	92.8	24	12	0.01	27.2	1.4
15-22	7.099858	4.752686	4.6	769	3.1	40.1	59	29	0.03	28.8	0
15-23	7.099858	4.752686	5.2	ND	4.7	63.9	24	12	0.01	30.6	0
16-22	7.1099	4.765987	4.9	561	7.5	95.2	20	10	0.01	27.1	0
16-23	7.1099	4.765987	6.1	ND	1.4	19	64	32	0.03	30.5	22
17-22	7.102928	4.752167	4.8	356	5.7	71.9	40	20	0.01	27.4	0
17-23	7.102948	4.752168	4.8	ND	4.4	57.8	107	54	0.05	28.9	1.7
18-23	7.101615	4.74998	4.5	ND	4.8	93.7	32	16	0.01	28.4	0
19-23	7.100056	4.750556	5.4	ND	7.3	95	16	8	0.01	28.5	0
20-21	7.106843	4.774288	4.5	553	7.6	97	49	25	0.01	27.4	0
21-21	7.1104	4.748702	4.5	645	7	87.1	32	16	0.01	26.9	0
22-21	7.109605	4.750095	4.3	797	4.6	59.2	61	31	0.01	27.9	0
23-21	7.114468	4.767733	6.9	117	2	25.4	388	195	0.2	27.9	12
24-21	7.114897	4.765332	6.4	231	3.3	42.5	100	50	0.01	29	2.5
25-22	7.10029	4.752067	5.4	418	4.5	58.5	52	26	0.02	28.9	3.9
26-22	7.098743	4.750856	4.7	594	6.2	78.6	178	89	0.08	27.6	0.2
27-21	7.107481	4.750064	5	435	5.6	70.7	32	16	0.01	26.9	0
28-23	7.100833	4.751111	4.5	ND	7.2	94.1	18	9	0.01	28.3	0
29-21	7.106223	4.746242	4.7	431	7	86.7	25	13	0.01	26.4	0
30-21	7.106942	4.751678	5.2	297	2.9	35.5	40	20	0.01	25.8	0.5
31-21	7.108108	4.751458	4.8	258	6.1	77.7	39	20	0.01	27.2	0
32-21	7.11643	4.76728	6.3	147	3.3	42.6	281	140	0.1	27.6	4.8
33-21	7.128373	4.772763	6.3	142	3.2	41.9	269	134	0.1	28.9	5.6
34-21	7.105677	4.753635	5.6	316	7.8	95.7	23	12	0.01	25.3	3.4
35-21	7.108347	4.759097	5.3	319	6.4	78.7	29	14	0.01	25.3	4.5
36-22	7.099103	4.749565	4.6	487	7	90.8	133	66	0.06	28.3	0
37-22	7.101355	4.749598	4.5	553	8	101.6	59	30	0.03	27.8	0
38-22	7.108247	4.751522	4.7	395	2.5	32.3	48	24	0.02	27.5	1
39-22	7.105703	4.772383	4.7	487	8.4	106	74	37	0.03	26.9	0.9
40-22	7.099723	4.753902	5	508	7.3	95.6	40	20	0.02	29.3	0.5
40-23	7.099723	4.753902	5.3	ND	6.7	85.2	17	8	0.01	27.5	1.3
41-22	7.099858	4.752686	4.6	ND	3.1	40.1	59	29	0.03	28.8	0

ID	Latitude (E)	Longitude (N)	pH	Eh (mV)	DO (mg/L)	DO (%)	EC (µS/cm)	TDS (mg/L)	Salinity (PSU)	Temp. (°C)	Alkalinity (mg/L)
42-22	7.09597	4.764598	5	769	8.4	106.3	219	110	0.1	27	1.1
43-23	7.100028	4.751111	5.6	ND	7.2	93.7	17	9	0.01	28.5	0
44-22	7.103658	4.750985	4.6	532	7.4	94.2	42	21	0.02	27.4	0.5
45-21	7.098138	4.756732	4.5	564	7.5	94.1	46	23	0.01	27.1	0
46-21	7.10011	4.75034	4.7	555	7.1	90.4	72	36	0.01	27.7	0
47-22	7.106193	4.751553	6.1	238	4.6	58.8	98	49	0.04	28.3	0
48-21	7.112232	4.74903	5.3	436	7.8	98	107	53	0.1	26.6	25
49-21	7.099778	4.767568	4.8	502	7.8	97.6	22	11	0.01	26.4	1
50-21	7.114042	4.751447	4.6	511	7	88.5	51	25	0.01	27.0	1.5
51-21	7.117338	4.756097	5.4	417	7.3	92.8	29	14	0.01	27.2	0
52-21	7.116914	4.754697	4.4	504	6.7	84.2	60	30	0.01	26.7	1.6
53-22	7.115575	4.760697	5	426	6.4	80.6	100	50	0.05	27.2	0
Minimum			4	117	1.4	19	16	8	0.01	25.3	0
Maximum			6.9	801	8.4	106.3	388	195	0.2	32.5	25
Median			4.9	506	6.5	84	41	20	0.01	28.1	0
Mean			5	512	6	76	65	32	0.03	28	2
REF1	7.115556	4.77527	4	516	7.6	103	24	12	0.01	30.9	0.8
REF2	7.114167	4.779167	4.3	497	7.5	100.9	17	9	0.01	30.8	0
REF3	7.082319	4.736111	5.1	448	7.9	100.2	31	15	0.01	27.7	1.2
REF4	7.114722	4.746944	4.6	ND	6.6	83.5	19	9	0.01	27	0

Table 2.2S: Chemical measurements of groundwater in the study area (2021, 2022 and 2023)

ID	Cl (mg/L)	NO_3 (mg/L)	SO_4^{2} (mg/L)	Ca (mg/L)	Na (mg/L)	K (mg/L)	Mg (mg/L)	Si (mg/L)	Sr (mg/L)	Fe (mg/L)	Mn (mg/L)	DOC (mg/L)	BTEX (µg /L)	THg (µg /L)	Hg_{diss} (µg/L)
1-21	11	<0.01	<0.01	0.8	5	0.1	0.1	3	0.003	0.2	0.04	18	ND	2.1	0.1
1-22	3	3	6	1	6	0.4	0.1	1	0.002	0.3	0.1	33	623	0.1	0.03
1-23	5	< 0.01	10	< 0.01	6	0.2	0.1	4	0.001	0.2	0.03	32	357	0.1	< 0.01
2-21	2	1	12	0.2	11	0.1	0.03	3	0.001	< 0.01	0.01	18	ND	3.8	0.1
2-22	3	2	12	1	15	0.4	0.1	1	0.002	0.2	0.03	27	62	0.7	0.1
2-23	5	<0.01	< 0.01	2	14	0.2	0.1	3	0.003	0.2	0.03	ND	ND	0.4	< 0.01
3-21	2	3	< 0.01	0.4	2	0.3	0.2	4	0.004	< 0.01	0.04	23	ND	5.5	4.6
3-22	2	3	4	1	4	1	0.2	1	0.004	0.02	0.1	26	4.4	4	2
3-23	5	2	8	1	4	0.3	0.2	4	0.002	< 0.01	0.04	ND	0.5	6	3.8
4-21	2	2	2	0.3	2	0.3	0.2	4	0.002	< 0.01	0.1	23	ND	3.7	3.2
4-22	3	3	3	1	3	1	0.2	1	0.003	0.01	0.1	24	0.3	2.2	1.7
4-23	4	11	6	0.4	3	0.4	0.2	5	0.002	< 0.01	0.04	ND	ND	2.7	1.1
5-21	2	2	< 0.01	0.3	2	0.3	0.2	4	0.004	< 0.01	0.1	21	ND	4	1.9
5-22	2	3	3	1	2	1	0.3	1	0.01	0.01	0.1	15	1.3	1.2	0.7
5-23	5	2	7	1	2	0.4	0.2	5	0.003	< 0.01	0.1	ND	ND	2.14	1
6-22	2	2	4	1	4	0.2	0.3	2	0.01	0.02	0.1	22	ND	4	0.3
6-23	5	2	9	0.4	4	0.3	0.2	4	0.002	0.02	0.04	3	186	3	1.5
7-21	1	< 0.01	1	< 0.01	1	0.1	0.1	3	0.004	0.02	0.01	26	ND	3.2	0.7
7-22	1	1	1	1	1	0.2	0.1	1	0.004	0.01	0.01	29	0.1	0.6	0.4
7-23	3	3	3	1	1	0.1	0.1	4	0.003	< 0.01	0.01	30	ND	0.4	< 0.01
8-21	1	< 0.01	1	0.3	1	0.1	0.1	3	0.003	< 0.01	0.2	23	ND	1.7	< 0.01
8-22	1	< 0.01	2	1	2	0.4	0.3	1	0.01	0.03	0.5	28	ND	0.4	0.1
8-23	3	< 0.01	6	1	1	0.2	0.2	4	0.003	0.1	0.4	33	2888	0.3	< 0.01
9-22	1	1	1	1	1	1	0.2	1	0.003	0.01	0.2	22	1305	1.5	0.7
9-23	4	1	6	1	1	0.4	0.2	5	0.003	0.01	0.3	4	890	1.2	0.4
10-22	2	3	2	1	3	1	0.2	2	0.003	0.03	0.04	23	0.2	2.7	1.4
10-23	5	3	6	0.4	3	0.4	0.2	5	0.002	0.01	0.03	2	ND	3.3	1.6
11-21	2	2	3	1	2	0.3	0.2	1	0.003	0.01	0.05	14	ND	1.6	1.2
11-23	5	2	7	0.4	2	0.2	0.2	4	0.002	0.02	0.04	ND	0.8	2	0.7
12-22	2	3	3	1	2	0.3	0.2	1	0.003	0.01	0.1	23	0.3	1.7	1.5
12-23	5	2	7	1	2	0.2	0.2	4	0.002	< 0.01	0.04	ND	ND	1.9	1
13-22	4	2	11	1	10	0.3	0.2	1	0.003	1	0.1	22	86	1.7	0.1
13-23	5	1	14	1	10	0.2	0.2	3	0.002	1	0.1	3	70	0.3	0.2
14-22	1	2	2	0.4	3	0.2	0.1	1	0.001	0.01	0.02	30	ND	0.7	0.3
14-23	<0.01	4	5	0.4	3	0.2	0.1	4	0.001	< 0.01	0.01	29	ND	1.1	< 0.01
15-22	2	2	2	0.4	1	1	0.1	1	0.002	< 0.01	0.03	42	ND	0.1	0.1
15-23	4	< 0.01	6	0.3	1	0.4	0.1	5	0.001	< 0.01	0.03	26	ND	0.2	< 0.01
16-22	1	< 0.01	1	2	10	1	0.4	1	0.01	0.01	0.2	47	461	1.4	0.01
16-23	5	< 0.01	6	9	1	1	1	3	0.03	0.3	0.03	35	231	0.3	0.03
17-22	2	< 0.01	< 0.01	1	2	0.1	0.2	3	0.004	1	0.1	33	1439	0.7	0.1
17-23	2	< 0.01	5	1	4	0.4	0.4	1	0.01	4	0.3	25	ND	0.1	0.01
18-23	5	3	7	1	3	0.3	0.2	4	0.004	0.03	0.04	ND	ND	4.3	2.1
19-23	4	2	6	0.4	1	0.3	0.1	5	0.001	< 0.01	0.03	ND	ND	0.8	0.03
20-21	4	7	< 0.01	1	3	0.1	0.2	2	0.01	< 0.01	0.02	21	ND	0.2	< 0.01
21-21	2	1	3	1	1	0.1	0.1	3	0.004	< 0.01	0.1	24	ND	0.3	0.1
22-21	<0.01	2	< 0.01	3	1	0.1	1	3	0.01	< 0.01	0.1	23	ND	0.4	0.3
23-21	5	1	1	40	2	4	1	8	0.6	0.6	0.1	32	ND	0.2	0.02
24-21	2	2	<0.01	8	2	2	4	4	0.1	0.2	0.3	28	ND	0.2	< 0.01
25-22	4	< 0.01	5	0.3	9	0.2	0.02	1	0.001	0.5	0.01	33	ND	0.1	0.01

ID	Cl (mg/L)	NO_3 (mg/L)	SO_4^2 (mg/L)	Ca (mg/L)	Na (mg/L)	K (mg/L)	Mg (mg/L)	Si (mg/L)	Sr (mg/L)	Fe (mg/L)	Mn (mg/L)	DOC (mg/L)	BTEX (µg /L)	THg (µg /L)	Hg_{diss} (µg/L)
26-22	1	1	2	1	2	< 0.01	0.1	2	0.002	0.1	0.1	24	ND	0.2	0.2
27-21	2	4	3	0.4	3	< 0.01	0.2	3	0.003	0.01	0.02	23	ND	0.4	0.01
28-23	4	1	6	1	1	0.2	0.1	4	0.003	0.01	0.03	ND	ND	0.01	< 0.01
29-21	1	1	1	0.2	< 0.01	0.2	0.1	4	0.002	< 0.01	0.03	23	ND	0.01	< 0.01
30-21	2	< 0.01	4	1	4	0.2	0.1	2	0.004	2	0.03	24	ND	0.01	< 0.01
31-21	3	< 0.01	< 0.01	0.2	1	0.1	0.2	4	0.003	1	0.04	27	ND	0.03	< 0.01
32-21	5	1	1	7	2	0.3	0.4	1	0.04	32	0.04	27	ND	0.1	< 0.01
33-21	3	< 0.01	< 0.01	5	2	2	0.3	1	0.01	21	0.1	53	ND	0.1	0.02
34-21	1	1	< 0.01	0.3	1	3	0.1	8	0.01	0.1	0.02	16	ND	0.01	< 0.01
35-21	1	1	1	0.4	1	4	0.2	9	0.01	< 0.01	0.01	26	ND	0.02	0.01
36-22	2	2	2	1	1	0.3	0.2	1	0.002	0.01	0.04	31	ND	0.01	0.01
37-22	2	2	2	0.4	1	0.4	0.2	1	0.003	0.01	0.04	18	ND	<0.01	< 0.01
38-22	4	< 0.01	1	1	2	0.2	0.2	1	0.003	2	0.1	20	ND	0.01	0.03
39-22	1	1	1	1	1	0.2	0.1	1	0.003	< 0.01	0.01	28	ND	0.1	0.01
40-22	1	< 0.01	2	1	1	1	0.1	2	0.004	0.01	0.03	26	ND	<0.01	< 0.01
40-23	2	3	3	1	1	1	0.1	5	0.003	0.001	0.02	29	ND	0.03	< 0.01
41-22	2	2	2	0.4	1	1	0.1	1	0.002	0.004	0.03	42	ND	0.1	0.07
42-22	1	1	1	1	1	1	0.2	2	0.01	0.01	0.02	21	ND	0.03	0.03
43-23	5	3	7	< 0.01	< 0.01	1	0.3	3	0.004	0.02	0.02	ND	ND	0.2	< 0.01
44-22	2	2	1	1	1	1	0.1	1	0.004	0.004	0.03	22	ND	0.03	0.01
45-21	1	< 0.01	< 0.01	0.2	< 0.01	0.4	0.1	4	0.003	< 0.01	0.01	25	ND	0.02	< 0.01
46-21	2	< 0.01	< 0.01	0.2	1	0.4	0.2	5	0.003	< 0.01	0.04	ND	ND	0.02	0.02
47-22	2	< 0.01	6	1	2	0.2	0.2	0.5	0.003	25	0.1	31	ND	< 0.01	0.1
48-21	1	1	1	1	< 0.01	0.1	0.3	3	0.002	0.01	0.02	18	ND	0.01	< 0.01
49-21	1	< 0.01	1	1	< 0.01	0.1	0.1	3	0.004	< 0.01	0.01	21	ND	< 0.01	< 0.01
50-21	1	1	< 0.01	0.1	< 0.01	0.1	0.1	3	0.002	< 0.01	0.02	21	ND	0.03	< 0.01
51-21	2	1	< 0.01	2	1	0.2	0.2	2	0.01	< 0.01	0.02	24	ND	0.01	< 0.01
52-21	3	5	5	1	1	0.03	0.1	2	0.002	< 0.01	0.02	23	ND	0.03	< 0.01
53-22	4	1	2	0.4	3	0.2	0.1	1	0.001	0.2	0.02	17	ND	0.01	0.01
Minimum	<0.01	<0.01	<0.01	<0.01	<0.01	<0.01	0.02	0.5	0.001	<0.01	0.01	2	2888	<0.01	<0.01
Maximum	11	11	14	40	15	4	4	9	1	32	0.5	53	0.1	6	4.6
Median	2	2	3	1	2	0.3	0.2	3	0.003	0.02	0.04	23	78	0.3	0.2
Mean	3	2	4	2	3	1	0.3	3	0.02	2	0.1	23	430	1.2	0.7
REF1	5	3	6	0.3	2	0.1	0.1	3	< 0.01	0.01	0.01	23	<0.01	< 0.01	< 0.01
REF2	5	3	6	1	1	0.1	0.1	2	< 0.01	0.01	0.01	35	<0.01	< 0.01	< 0.01
REF3	2	2	2	1	1	1	0.3	2	0.004	< 0.01	0.03	10	<0.01	< 0.01	< 0.01
REF4	4	< 0.01	6	1	1	0.3	0.1	3	< 0.01	< 0.01	0.01	2	<0.01	< 0.01	< 0.01

Notes: ND = Not Determined, DOC = Dissolved Organic Carbon, REF = Reference sample. Sample names that end with –22 and –23 represent groundwater samples collected in 2022 and 2023, respectively.

Table 2.3S: Hg speciation in groundwater of the study area (2023)

ID	THg (µg /L)	Hg_{diss} (µg/L)	HgIIa+Hg^0	Hg^0	Hg-part	HgIIb	HgIIa
9-23	1.16	0.4	0.29	< 0.01	0.76	0.11	0.29
13-23	0.29	0.01	0	< 0.01	0.28	0.01	< 0.01
4-23	2.5	1.05	1.03	< 0.01	1.45	0.02	1.03
6-23	3.01	1.48	1.39	< 0.01	1.53	0.09	1.39
3-23	6	3.84	3.45	< 0.01	2.16	0.39	3.45
5-23	1.98	0.87	0.77	< 0.01	1.11	0.1	0.77
12-23	1.87	0.41	0.33	< 0.01	1.46	0.08	0.33
29-23	0.01	< 0.01	< 0.01	< 0.01	< 0.01	< 0.01	< 0.01

Table 2.4S: THg and Total Carbon content in sediments of the study area

ID	Depth (cm)	THg (µg/kg)	Total Carbon (mg/kg)	% Carbon	Munsell Notation	Color name	Description sand median
S-1 A	20	71.4	27619	2.8	10YR 5/1	Dark grayish brown	very fine to medium coarse
S-1 B	40	141.7	7418	0.7	10YR 6/1	Grayish brown	very fine to medium coarse
S-1 C	60	85.1	6363	0.6	10YR 6/1	Grayish brown	very fine to very coarse
S-1 D	80	97.6	9773	1	10YR 7/1	Light gray	medium fine to extreme coarse
S-1 E	100	65.1	2646	0.3	10YR 7/2	Light gray	medium fine to extreme coarse
S-2 A	20	34.1	8495	0.9	10YR 6/1	Gray	extreme fine to very coarse
S-2 B	40	46.9	37886	3.8	10YR 6/1	Gray	extreme fine to very coarse
S-2 C	60	53.8	2316	0.2	10YR 7/1	Light gray	medium fine to extreme coarse
S-2 D	80	42.8	3186	0.3	10YR 7/1	Light gray	medium fine to extreme coarse
S-2 E	100	53.2	1313	0.1	10YR 7/1	Light gray	medium fine to extreme coarse

S-3 A	20	337.2	400741	40.1	2.5YR 2/0	Black	extreme fine to very fine
S-3 B	40	400.1	210464	21.5	5YR 5/1	Gray	extreme fine to very fine
S-3 C	60	529	189015	20.3	5YR 6/1	Light olive gray	extreme fine to very fine
S-3 D	80	421.7	165216	16.5	10YR 5/1	Gray	extreme fine to very fine
S-3 E	100	258.1	112532	11.3	10YR 5/1	Gray	extreme fine to medium coarse
S-4 A	20	87.2	19523	2	10YR 6/1	Gray	very fine to medium coarse
S-4 B	40	46.4	4324	0.4	10YR 6/1	Gray	very fine to medium coarse
S-4 C	60	38.3	914	0.1	10YR 7/1	Light gray	very fine to extreme coarse
ID	Depth (cm)	THg (µg/kg)	Total Carbon (mg/kg)	% Carbon	Munsell Notation	Color name	Description sand median
S-4 D	80	69.6	1319	0.1	10YR 7/1	Light gray	medium fine to extreme coarse
S-4 E	100	58.6	928	0.1	10YR 7/1	Light gray	medium fine to extreme coarse
S-5 A	20	199.4	60875	6.1	10YR 5/1	Gray	very fine to medium coarse
S-5 B	40	228.5	54658	5.5	10YR 5/1	Gray	very fine to medium coarse
S-5 C	60	77.4	16801	1.7	10YR 6/1	Gray	very fine to extreme coarse
S-5 D	80	115.4	4070	0.4	10YR 7/1	Light gray	very fine to extreme coarse
S-5 E	100	122.2	1367	0.1	10YR 8/4	very pale brown	very fine to extreme coarse
S-6 A	20	124.6	189888	19	10YR 4/1	Dark gray	very fine to medium coarse
S-6 B	40	99.8	106788	10.8	10YR 5/1	Gray	very fine to medium coarse
S-6 C	60	42.4	31972	3.2	10YR 6/1	Gray	very fine to medium coarse
S-6 D	80	30.5	3587	0.4	10YR 7/1	Light gray	medium fine to extreme coarse
S-6 E	100	28.5	1653	0.2	10YR 7/1	Light gray	medium fine to extreme coarse
S-7 A	20	69.8	7230	0.7	10YR 6/2	Dark gray	very fine to very coarse
S-7 B	40	60.6	16307	1.6	10YR 6/1	Black	very fine to very coarse
S-7 C	60	71.8	5610	0.6	10YR 7/2	Dark gray	very fine to extreme coarse
S-7 D	80	28.2	5139	0.5	10YR 7/2	Dark gray	very fine to extreme coarse
S-7 E	100	30.1	3058	0.3	10YR 7/2	Gray	very fine to extreme coarse
S-8 A	20	30.7	4375	0.4	10YR 7/1	Light gray	very fine to extreme coarse
S-8 B	40	24.9	6006	0.6	10YR 7/3	very pale brown	very fine to extreme coarse
S-8 C	60	24.2	7952	0.8	10YR 7/3	very pale brown	very fine to very coarse
S-8 D	80	19.6	3393	0.3	10YR 7/3	very pale brown	very fine to very coarse
S-8 E	100	10.1	4075	0.4	10YR 7/3	very pale brown	very fine to very coarse
REF A	20	5	778	0.1	10YR 7/1	Light brownish gray	Extremely fine to medium fine sand
REF B	40	2.3	< 0.1	0	10YR 8/2	Gray	medium fine to extreme coarse
REF C	60	2.2	< 0.1	0	10YR 8/2	light gray	very fine to extreme coarse
REF D	80	3.2	< 0.1	0	10YR 8/1	White	very coarse to extreme coarse
REF E	100	1.4	< 0.1	0	10YR 8/1	White	very fine to extreme coarse

Table 2.5S: Batch leaching experiment

ID	THg (µg/kg) before extraction	THg (µg/kg) extracted	% Extracted
S3 B	400	54.4	13.5
S3 C	529	59.5	11.3
S3 D	422	99.3	23.5
S5 B	229	5.6	2.6
S5 A	199	< 0.01	<0.01

Fig. 2.1S Wastewater discharge channel (a) and wastewater reservoir (b) and in the PHRC

Fig. 2.2S Examples of cracks within the concrete WDO in Okochiri.

b) Pipeline-related residential benzene exposure and groundwater natural attenuation capacity in the eastern Niger Delta, Nigeria

Table 3.1: BTEX and DOC measurements of groundwater (2022 and 2023)

Sample Name	Location	DOC (mg/L)	DIC (mg/L)	Benzene (µg/L)	Toluene (µg/L)	Ethylbenzene (µg/L)	Xylenes (µg/L)	Trimethylbenzene (µg/L)	BTEX (µg/L)
1–22	Alode	47	0	460	0.5	0.1	0.4	NA	461
1–23	Alode	35	66	230	0.3	0.1	0.2	< 0.1	231
2–22	Alode	26	55	220	5	65	26	NA	315
2–23	Alode	26	67	190	0.4	3.2	0.4	< 0.1	194
3–22	Alode	34	0	1000	17	2	41	NA	1060
3–23	Alode	32	35	1300	42	6	42	120	1510
4–22	Alode	33	31	1400	80	14	64	NA	1558
4–23	Alode	34	0	1500	130	33	94	150	1907
5–22	Alode	26	0	1100	47	19	49	NA	1215
5–23	Alode	34	8	1300	120	51	94	120	1685
6–22	Alode	22	22	2100	51	120	21	NA	2292
6–23	Alode	35	26	3500	48	150	26	180	3904
7–22	Alode	16	0	46	0.5	24	2	NA	72
7–23	Alode	30	105	1100	4.6	130	9	220	1464
8–22	Alode	24	0	1900	100	10	101	NA	2111
9–23	Alode	26	141	1600	25	5.6	17	69	1717
10–23	Alode	18	21	16	< 0.1	< 0.1	< 0.1	1	17
11–22	Ogale	49	175	910	210	260	283	NA	1573
11–23	Ogale	30	194	1100	64	370	360	140	2034
12–22	Ogale	9	0	1000	4	180	10.4	NA	1194
12–23	Ogale	27	0	880	3	110	6.2	97	1096
13–22	Ogale	14	0	73	1.1	19	3	NA	96
13–23	Ogale	26	0	6.3	0.4	75	1.3	47	130
14–22	Ogale	15	0	54	1	12	2	NA	69
14–23	Ogale	31	0	41	0.3	7.4	1.3	67	117
15–22	Eleme	20	0	480	< 0.1	< 0.1	< 0.1	NA	480
16–22	Ogale	19	145	11	< 0.1	< 0.1	< 0.1	NA	11
17–22	Ogale	27	32	0.1	0.1	11	2	NA	12
18–23	Ogale	30	0	380	1	78	2	20	481
19–23	Ogale	42	160	38	< 0.1	< 0.1	1	4.3	43
20–23	Ogale	22	26	1300	17	140	110	220	1787
21–22	Okochiri	22	0	1300	2	0.2	3	NA	1305
21–23	Okochiri	4	0	850	1.4	1	2.1	36	890
22–22	Okochiri	33	52	620	1	0.2	2	NA	623
22–23	Okochiri	32	0	350	0.4	0.2	1	6	357
23–22	Okochiri	31	82	160	0.3	56	1	NA	217
23–23	Okochiri	29	0	91	1	17	2.2	190	301
24–22	Okochiri	22	34	86	0.1	< 0.1	< 0.1	NA	86
24–23	Okochiri	3	26	66	< 0.1	< 0.1	0.3	3.9	70
25–22	Okochiri	27	58	62	< 0.1	< 0.1	< 0.1	NA	62
25–23	Okochiri	3	0	180	0.1	< 0.1	0.6	5.4	186
26–22	Okochiri	26	69	4.4	< 0.1	< 0.1	< 0.1	NA	4.4
26–23	Okochiri	NA	0	0.5	< 0.1	< 0.1	< 0.1	< 0.1	0.5
27–22	Okochiri	25	66	1400	19	4	16.2	NA	1439
28–23	Okochiri	33	0	2700	20	4	24	140	2888
29–23	Okochiri	NA	137	25	0.1	33	0.3	5.9	64
30–22	Okochiri	24	0	0.3	< 0.1	< 0.1	< 0.1	NA	0.3
31–22	Okochiri	23	320	0.3	< 0.1	< 0.1	< 0.1	NA	0.3
32–22	Okochiri	23	61	0.2	< 0.1	< 0.1	< 0.1	NA	0.2
33–22	Okochiri	29	31	0.1	< 0.1	< 0.1	< 0.1	NA	0.1
34–22	Okochiri	15	0	1.3	< 0.1	< 0.1	< 0.1	NA	1.3
35–22	Okochiri	14	0	0.8	< 0.1	< 0.1	< 0.1	NA	0.8
36–22	Okochiri	26	13	1	< 0.1	< 0.1	< 0.1	NA	0.7
REF1	Alode	23	0	< 0.1	< 0.1	< 0.1	< 0.1	< 0.1	< 0.1
REF2	Alode	35	0	< 0.1	< 0.1	< 0.1	< 0.1	< 0.1	< 0.1
REF3	Ebubu	2	0	NA	NA	NA	NA	NA	NA
REF 4	Okochiri	18	0	< 0.1	< 0.1	< 0.1	< 0.1	NA	< 0.1

NA = Not Analyzed, ND = Not Detected, DOC = Dissolved Organic Carbon, DIC = Dissolved Inorganic Carbon, REF = Reference sampl e. Sample names that end with –22 and –23 represent groundwater samples collected in 2022 and 2023, respectively.

Table 3.2: Physico-chemical parameters of groundwater in the study area (2022 and 2023)

Sample Name	Location	Longitude	Latitude	pH	DO (mg/L)	DO (%)	EC (µS/cm)	TDS (mg/L)	Salinity (PSU)	Temp. (°C)	Alkalinity (mg/L)
1–22	Alode	7.1099	4.765987	4.9	7.5	95	20	10	0.01	27	0
1–23	Alode	7.1099	4.765987	6.1	1.4	19	64	32	0.03	31	22
2–22	Alode	7.122632	4.776868	5.3	3.6	49	63	31	0.03	31	4
2–23	Alode	7.122632	4.776868	5.3	6.8	94	47	24	0.02	31	5
3–22	Alode	7.121092	4.774338	4.8	5.6	74	71	36	0.03	29	0
3–23	Alode	7.121092	4.774338	5.4	5.5	76	35	17	0.02	31	3
4–22	Alode	7.120805	4.774332	5.1	4.9	64	38	19	0.02	28	1
4–23	Alode	7.120805	4.774332	5	6.2	85	30	15	0.01	31	0
5–22	Alode	7.12017	4.772995	4.8	6.2	83	56	28	0.02	30	0
5–23	Alode	7.12017	4.772995	5.2	5.9	81	20	10	0.01	31	1
6–22	Alode	7.118968	4.77318	5.1	3.8	50	36	18	0.02	29	1
6–23	Alode	7.118968	4.77318	5.1	4.6	77	20	10	0.01	31	1
7–22	Alode	7.119302	4.774917	4.8	6.8	60	78	39	0.04	27	0
7–23	Alode	7.119302	4.774917	5	3.7	51	76	38	0.04	31	4
8–22	Alode	7.121002	4.774275	4.7	5.4	67	41	21	0.02	26	0
9–23	Alode	7.124444	4.778056	5.9	3.5	48	106	53	0.05	31	30
10–23	Alode	7.123889	4.776944	5.3	5.4	75	36	18	0.02	31	1
11–22	Ogale	7.129307	4.795973	6.6	2.3	29	364	183	0.17	28	94
11–23	Ogale	7.129307	4.795973	6.5	0.7	9	206	103	0.1	31	100
12–22	Ogale	7.12643	4.788903	5.2	3.6	45	55	27	0.02	28	0
12–23	Ogale	7.12643	4.788903	5.2	4.2	55	32	16	0.01	29	0
13–22	Ogale	7.126427	4.789248	5.2	3.9	74	60	30	0.03	27	0
13–23	Ogale	7.126427	4.789248	5	3.8	51	32	16	0.01	29	0
14–22	Ogale	7.132052	4.791505	5	3.1	38	35	18	0.02	25	0
14–23	Ogale	7.132052	4.791505	4.7	4.4	58	20	10	0.01	29	0
15–22	Eleme	7.120062	4.788458	5.1	4.4	57	228	114	0.11	28	0
16–22	Ogale	7.12799	4.789133	5.7	5.9	75	100	50	0.05	28	24
17–22	Ogale	7.127315	4.786512	5.1	1.5	19	67	33	0.03	26	2
18–23	Ogale	7.126421	4.789252	4.1	3.4	45	41	20	0.02	30	0
19–23	Ogale	7.119444	4.774722	4.7	5.2	67	125	63	0.06	29	3
20–23	Ogale	7.125278	4.790556	5.3	5.5	75	20	10	0.01	31	2
21–22	Okochiri	7.102517	4.7508	4.5	3.2	41	40	20	0.02	28	0
21–23	Okochiri	7.102517	4.7508	5	6.4	85	21	11	0.01	29	0
22–22	Okochiri	7.10224	4.750622	5	4.4	57	207	105	0.1	29	2
22–23	Okochiri	7.10224	4.750622	5.3	6.6	86	35	18	0.02	29	0
23–22	Okochiri	7.106193	4.751553	6.1	4.6	59	98	49	0.04	28	25
23–23	Okochiri	7.106193	4.751553	5.2	5.3	70	27	13	0.01	29	0
24–22	Okochiri	7.10209	4.751638	5.6	7.4	97	79	40	0.04	29	5
24–23	Okochiri	7.10209	4.751638	5.7	6.4	85	50	25	0.02	29	5
25–22	Okochiri	7.101903	4.75027	5.6	4.9	66	72	36	0.03	31	8
25–23	Okochiri	7.101903	4.75027	5.6	6.1	82	28	14	0.01	29	0
26–22	Okochiri	7.101417	4.750313	4.6	5.3	69	46	24	0.02	28	1
26–23	Okochiri	7.101417	4.750313	5.5	7.3	97	27	13	0.01	30	0
27–22	Okochiri	7.102948	4.752168	4.8	4.4	58	107	54	0.05	29	2
28–23	Okochiri	7.102778	4.751111	4.5	5.7	86	30	15	0.01	28	0
29–23	Okochiri	7.105556	4.751389	5.6	6.3	83	64	32	0.03	28	20
30–22	Okochiri	7.10104	4.75044	4.7	3.3	42	67	34	0.03	28	0
31–22	Okochiri	7.100852	4.75112	4.6	5.2	67	53	26	0.02	28	5
32–22	Okochiri	7.100998	4.750173	4.8	5.6	73	39	19	0.02	28	1
33–22	Okochiri	7.097222	4.765118	4.8	6.5	81	66	33	0.03	27	1
34–22	Okochiri	7.10132	4.751203	4.7	6.9	96	34	17	0.01	33	0
35–22	Okochiri	7.100848	4.751698	4.6	6.6	85	48	24	0.02	28	0
36–22	Okochiri	7.099723	4.753902	5	7.3	96	40	20	0.02	29	0.5
REF1	Alode	7.113888	4.77924	4	7.6	103	24	12	0.01	31	0
REF2	Alode	7.115607	4.775545	4.3	7.5	101	17	9	0.01	31	0
REF3	Alode	7.131944	4.747222	4.6	6.6	84	19	9	0.01	27	1.6
REF 4	Okochiri	7.101355	4.749598	4.5	8	102	59	30	0.03	28	0

Table 3.3: Chemical measurements of groundwater in the study area (2022 and 2023)

Sample Name	Cl (mg/L)	NO_2 (mg/L)	NO_3 (mg/L)	SO_4^{2-} (mg/L)	HCO_3 (mg/L)	H_2CO_3 (mg/L)	Ca (mg/L)	Na (mg/L)	K (mg/L)	Mg (mg/L)	Si (mg/L)	Fe (mg/L)	Mn (mg/L)
1–22	1	< 0.01	< 0.01	1	0	0	2	10	1	0.4	1	0.01	0.2
1–23	3	<0.01	<0.01	2	27	39	10	1	1	1	3	0.3	0.03
2–22	7	< 0.01	< 0.01	2	5	50	1	5	1	0.2	1	2	0.01
2–23	12	<0.01	<0.01	6	6	61	1	7	0.2	0.2	3	2.4	0.01
3–22	1	< 0.01	< 0.01	2	0	0	1.4	9	1	0.3	1	0.2	0.03
3–23	2	<0.01	<0.01	4	4	31	1	5	0.4	0.3	4	0.3	0.02
4–22	1	< 0.01	< 0.01	1	2	30	2	1	1	0.3	1	1	0.03
4–23	2	<0.01	<0.01	2	0	0	2	1	0.3	0.3	4	0.4	0.03
5–22	1	< 0.01	< 0.01	2	0	0	1	1	1	0.2	1	0.3	0.03
5–23	1	<0.01	<0.01	1	1	8	1	1	0.4	0.2	4	1	0.02
6–22	1	< 0.01	< 0.01	2	1	21	1	1	1	0.2	1	1	0.03
6–23	2	<0.01	<0.01	1	2	26	1	1	0.3	0.2	4	1	0.04
7–22	6	< 0.01	2	17	0	0	2	5	0.3	0.3	1	6.4	0.05
7–23	10	<0.01	<0.01	17	5	100	1	10	0.1	0.2	2	7	0.02
8–22	1	< 0.01	1	1	0	0	1	1	1	0.4	1	0.2	0.03
9–23	9	<0.01	<0.01	6	37	104	1	3	0.3	0.2	4	3	0.02
10–23	3	<0.01	1	2	2	19	1	3	0.2	0.1	3	0.4	0.01
11–22	6	0.2	2	3	115	60	13	4	1.1	1	0.3	50	0.1
11–23	10	<0.01	<0.01	7	122	72	12	4	7	1	1	46	0.1
12–22	5	< 0.01	< 0.01	2	0	0	0.3	3	0.3	0.1	1	4	0.02
12–23	6	<0.01	<0.01	1	0	0	0.2	3	0.1	0.1	3	4	0.02
13–22	3	< 0.01	< 0.01	1	0	0	1	2	1	0.1	1	2	0.02
13–23	6	<0.01	<0.01	2	0	0	0.1	5	0.1	0.02	3	1	0.01
14–22	3	< 0.01	2	2	0	0	0.4	1	0.3	0.1	1	1	0.1
14–23	3	<0.01	<0.01	2	0	0	0.3	1.4	0.1	0.1	3	1	0.04
15–22	18	1	39	23	0	0	13	14	12	4	1	0.01	0.01
16–22	8	0.2	12	2	29	119	2	11	1	1	1	0.04	0.2
17–22	6	< 0.01	<0.01	2.4	2	30	0.4	5	0.2	0.04	1	2	0.01
18–23	8	<0.01	<0.01	2	0	0	0.4	5	0.1	0.2	4	1	0.04
19–23	10	<0.01	29	14	4	156	7	9	7	1.9	3	0.01	0.02
20–23	3	<0.01	<0.01	2	3	23	0.3	3	0.1	0.03	3.4	0.4	0.01
21–22	1	< 0.01	1	1	0	0	1	1	1	0.2	1.4	0.01	0.2
21–23	2	<0.01	0.2	1	0	0	1	1	0.4	0.2	5	0.01	0.01
22–22	3	< 0.01	3	6	2	50	1	7	0.4	0.1	1	0.3	0.1
22–23	3	<0.01	<0.01	6	0	0	1	6	0.2	0.1	4	0.2	0.01
23–22	2	< 0.01	<0.01	6	31	52	1	2	0.2	0.2	1	25	0.1
23–23	4	<0.01	<0.01	2	0	0	0.2	2	0.1	0.04	3	2	0.01
24–22	4	< 0.01	2	11	6	28	1	10	0.3	0.2	1	1	0.1
24–23	3	0.1	<0.01	11	5	20	1	10	0.2	0.2	3	1	0.01
25–22	3	< 0.01	2	12	9	48	1	15	0.3	0.1	1	0.2	0.03
25–23	2	<0.01	0.4	5	0	0	1	4	0.3	0.2	4	0.02	0.01
26–22	3	< 0.01	3	4	1	67	1	4	1	0.2	1.4	0.02	0.1
26–23	3	<0.01	1	5	0	0	1	4	0.3	0.2	4.4	0.01	0.01
27–22	2	< 0.01	<0.01	5	2	64	1	4	0.4	0.4	1.4	4	0.3
28–23	2	<0.01	<0.01	1	0	0	1	1.4	0.2	0.2	4	0.1	0.4
29–23	3	<0.01	0.1	12	25	112	1	3	0.1	0.2	1	14	0.1
30–22	3	< 0.01	3	3	0	0	1	3	1	0.2	1.4	0.01	0.1
31–22	3	< 0.01	3	3	6	314	1	2	0.3	0.2	1	0.01	0.1
32–22	2.4	< 0.01	4	3	2	59	1	3	1	0.2	2	0.03	0.04
33–22	2	< 0.01	1	1.4	1	30	1	1	0.2	0.1	1	0.01	0.01
34–22	3	< 0.01	3	3	0	0	1	2	1	0.3	1	0.01	0.1
35–22	2	< 0.01	2	3	0	0	1	2	0.3	0.2	1	0.01	0.1
36–22	2	< 0.01	<0.01	2	1	13	1	1	1	0.1	2	0.01	0.03
REF1	2	< 0.01	1	1	0	0	0.3	2	0.1	0.1	3	0.01	0.01
REF2	3	< 0.01	<0.01	1	0	0	1	1	0.1	0.1	2	0.01	0.01
REF3	2	< 0.01	<0.01	1	0	0	1	1	0.3	0.1	3	<0.01	0.01
REF 4	2	< 0.01	2	2	0	0	1	1	0.4	0.2	1	0.01	0.04

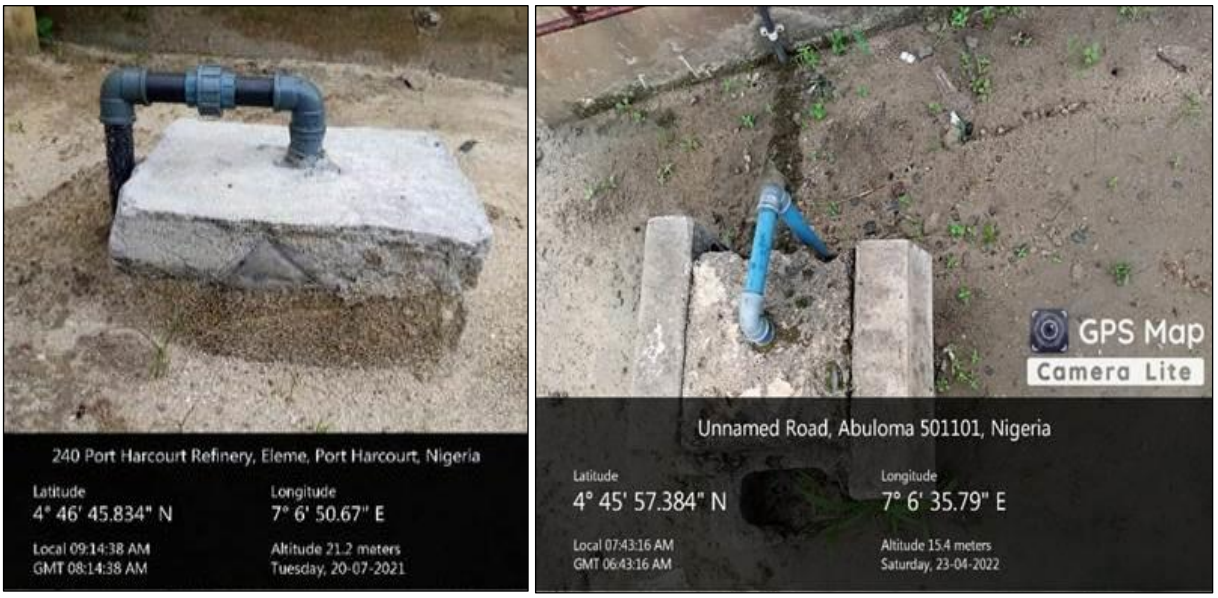

Fig. 3.1S Well heads sealed with concrete slabs to prevent surface contamination from run-offs and theft of the installed submersible pump.

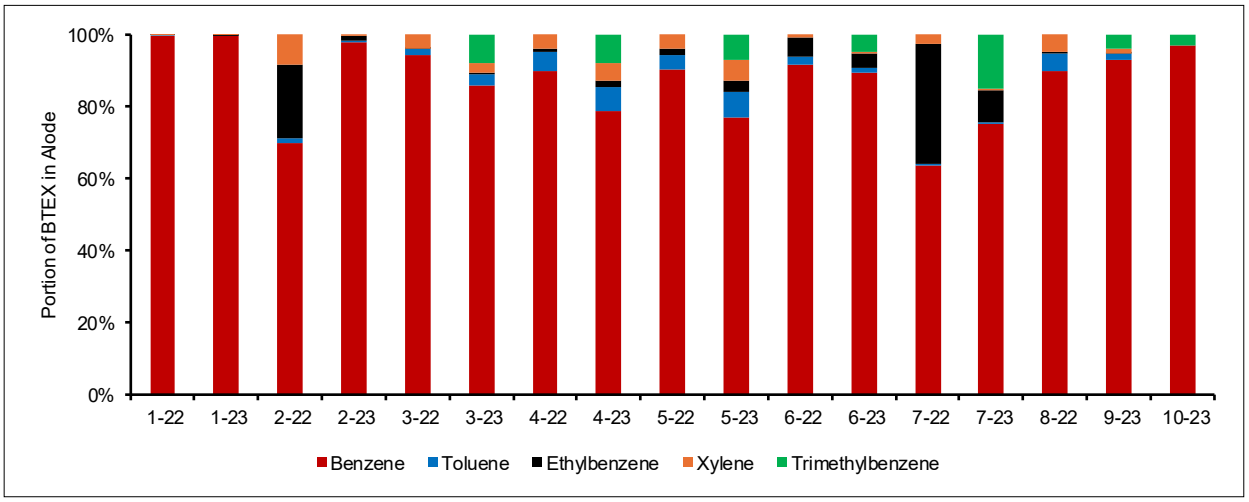

Fig. 3.2S Comparison between concentrations of benzene, toluene, ethylbenzene, xylenes and trimethylbenzene in the shallow aquifers of Alode.

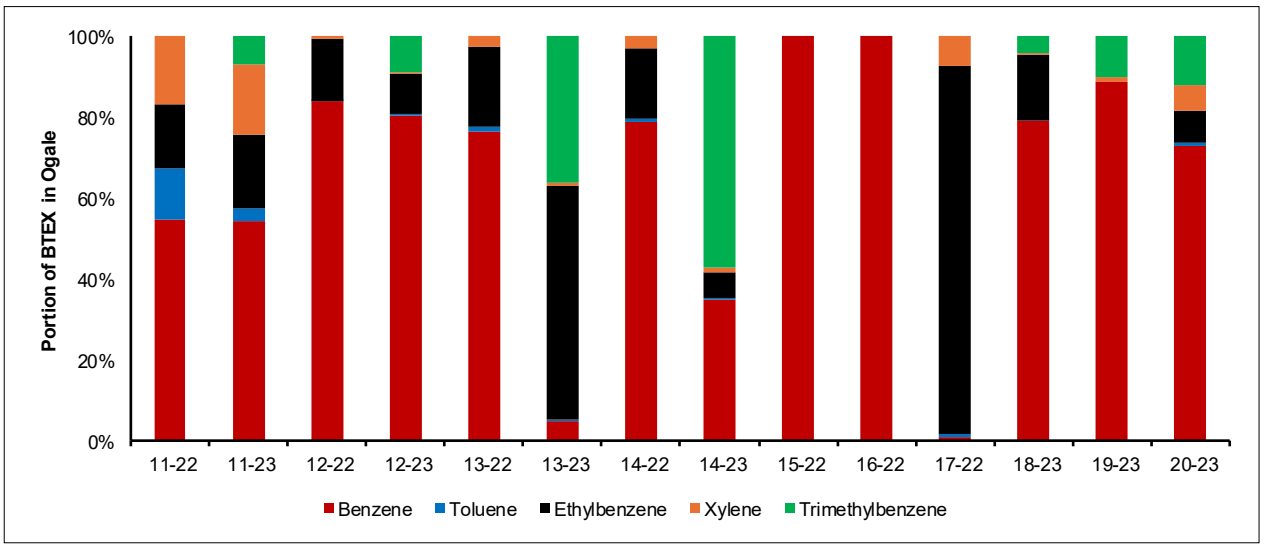

Fig. 3.3S Comparison between concentrations of benzene, toluene, ethylbenzene, xylenes and trimethylbenzene in the shallow aquifers of Ogale.

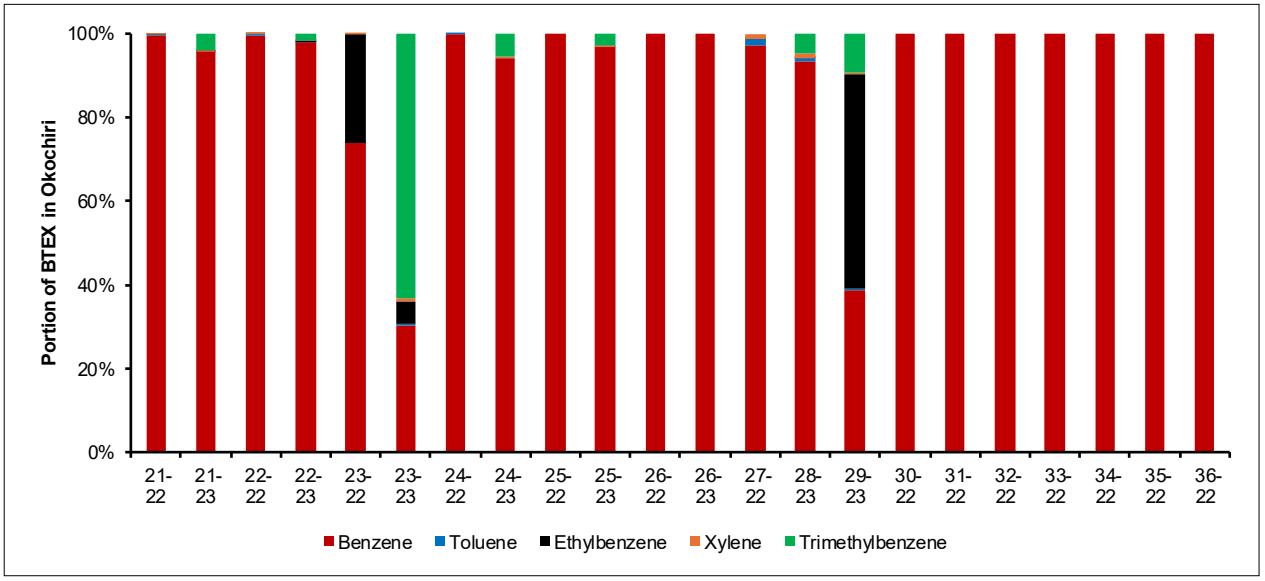

Fig. 3.4S Comparison between concentrations of benzene, toluene, ethylbenzene, xylenes and trimethylbenzene in the shallow aquifers of the eastern Niger Delta

Fig. 3.5S Reddish-brown precipitate on domestic water containers in Ogale.

c) Source, transport and fate of nitrate in shallow groundwater in the eastern Niger Delta

Table 4.1S: Physico-chemical parameters of groundwater in the study area (2022 and 2023)

ID	Site	Longitude	Latitude	pH	Eh (mV)	DO (mg/L)	DO (%)	EC (µS/cm)	TDS (mg/L)	Salinity (PSU)	Temp. (°C)	Alkalinity (mg/L)
1–22	Alesa	7.112087	4.796872	5.8	451	3.3	43	512	256	0.2	27.2	3
1–23	Alesa	7.112087	4.796872	5.8	ND	2.8	37	395	198	0.1	30.5	31
2–22	Alesa	7.120062	4.788458	5.1	596	4.4	57	228	114	0.1	28.3	0
2–23	Alesa	7.120062	4.788458	4.7	ND	3	39	187	93	0.1	29.3	1
3–22	Alesa	7.120909	4.795887	4.5	538	5.8	77	302	151	0.1	29.1	3
3–23	Alesa	7.120909	4.795887	4.6	ND	4.9	64	215	108	0.1	29.3	0
4–22	Alesa	7.104822	4.794335	6.3	414	6.6	83	185	91	0.1	26.5	4
4–23	Alesa	7.104822	4.794335	4.7	ND	4.8	64	77	38	0.1	30.1	0
5–22	Alesa	7.106808	4.799022	4.4	488	7.6	97	327	163	0.2	27.5	0
5–23	Alesa	7.106808	4.799022	4.5	ND	5.8	77	245	122	0.2	30.5	0
6–22	Alesa	7.111695	4.78944	4.5	490	6.7	86	321	160	0.2	28.1	0
6–23	Alesa	7.111695	4.78944	4.4	ND	5.8	76	192	96	0.1	30.4	0
7–22	Alesa	7.109185	4.800108	4.2	579	4.5	57	400	200	0.2	27.6	0
7–23	Alesa	7.109185	4.800108	4.2	ND	4.8	63	322	161	0.2	28.8	0
8–22	Alesa	7.118945	4.78445	4.9	501	6.2	78	165	82	0.1	26.6	1
8–23	Alesa	7.118945	4.78445	4.7	ND	5.2	67	125	63	0.1	29.4	3
9–22	Alesa	7.120667	4.787682	6.1	405	7.3	93	298	147	0.1	28.3	14
9–23	Alesa	7.120667	4.787682	5.1	ND	5.5	73	244	122	0.1	29.9	14
10–22	Alesa	7.122352	4.78513	4.5	554	7.8	100	90	45	0.04	27.7	0
10–23	Alesa	7.122352	4.78513	3.5	ND	6.3	85	82	41	0.04	31.1	0
Minimum				3.5	405	2.8	37	77	38	0.04	26.5	0
Maximum				6.3	596	7.8	100	512	256	0.2	31.1	31
Median				4.7	496	5.7	75	236	118	0.1	29	0
Average				4.8	502	5.5	71	246	123	0.1	28.8	3.7
11–22	Ogale	7.128107	4.788077	5.4	348	2	26	67	33	0.03	27.8	15
12–22	Ogale	7.129307	4.795973	6.6	113	2.3	29	364	183	0.2	28.1	94
13–22	Ogale	7.128767	4.78765	6	307	3	39	162	81	0.1	27.7	17
13–23	Ogale	7.128767	4.78765	6.1	ND	0.7	9	206	103	0.1	30.7	100
14–22	Ogale	7.128502	4.787285	5.9	331	3.9	50	520	260	0.3	27.5	45
15–22	Ogale	7.120435	4.787102	5.6	348	5.6	71	126	62	0.1	27.1	2.5
15–23	Ogale	7.120435	4.787102	5.5	ND	3.8	48	374	187	0.2	29.2	35
16–22	Ogale	7.127315	4.786512	5.1	391	1.53	19	67	33	0.03	26.5	2
16–23	Ogale	7.127315	4.786512	5.6	ND	5.1	69	31	16	0.01	30.1	2
17–22	Ogale	7.126735	4.787023	6.1	368	6.8	87	852	427	0.4	27.6	0
17–23	Ogale	7.126735	4.787023	4.4	ND	4.7	60	17	8	0.1	28.8	1
18–22	Ogale	7.12799	4.789133	5.7	431	5.9	75	100	50	0.1	27.3	24
19–22	Ogale	7.132052	4.791505	5	428	3.1	38	35	18	0.02	25.1	0
19–23	Ogale	7.132052	4.791505	4.1	ND	3.4	45	41	20	0.02	30	0
20–22	Ogale	7.126753	4.781363	4	584	5.7	73	371	185	0.2	28.6	0
20–23	Ogale	7.126753	4.781363	4.7	ND	4.4	58	20	10	0.01	29.2	0
21–22	Ogale	7.133773	4.778295	5.1	529	8.2	103	91	46	0.04	27.7	0
21–23	Ogale	7.133773	4.778295	3.9	ND	5.5	73	230	115	0.1	29.5	0
22–22	Ogale	7.12643	4.788903	5.2	313	3.6	45	55	27	0.02	27.6	0
23–22	Ogale	7.126427	4.789248	5.2	401	3.9	74	60	30	0.03	26.7	0
23–23	Ogale	7.126427	4.789248	5.2	ND	4.2	55	32	16	0.01	29.2	0
24–22	Ogale	7.133198	4.775068	4.6	509	7.2	93	105	53	0.1	28.7	0
24–23	Ogale	7.133198	4.775068	5	ND	3.8	51	32	16	0.01	29	0
25–22	Ogale	7.12786	4.778627	4.4	591	8.1	106	118	59	0.1	28.9	0
25–23	Ogale	7.12786	4.778627	4	ND	7.3	91	87	44	0.04	27.1	0
26–22	Ogale	7.126795	4.783217	4	575	8.4	107	294	147	0.1	27.7	0
26–23	Ogale	7.126795	4.783217	4	ND	7.4	93	78	39	0.04	27.9	0
27–22	Ogale	4.787298	7.128548	5.7	371	3	36	327	163	0.2	27.5	17
27–23	Ogale	4.787298	7.128548	4.1	ND	6	80	172	86	0.1	30.1	0
Minimum				3.9	113	0.7	9	17	8	0.01	25.1	0
Maximum				6.6	591	8.4	107	852	427	0.4	30.7	100
Median				5.1	391	4.4	60	100	50	0.1	27.9	0
Average				5	408	4.7	62	174	87	0.1	28	12
28–22	Ebubu	7.155532	4.75196	5.1	487	8.6	109	21	10	0.01	27.9	2
29–22	Ebubu	7.156438	4.758375	4.4	538	3.4	43	341	171	0.2	27.8	0
30–22	Ebubu	7.150593	4.781777	4.6	573	7.9	103	81	41	0.04	28.5	0
31–22	Ebubu	7.159867	4.783162	4.9	505	8.9	115	38	18	0.02	27.9	0
31–23	Ebubu	7.159867	4.783162	3.5	ND	7.5	97	51	25	0.02	29.5	0
32–22	Ebubu	7.157197	4.77655	4.5	520	7.2	94	154	76	0.1	28.8	0
33–22	Ebubu	7.151137	4.77939	4.8	516	8.3	105	73	36	0.03	27.5	0
33–23	Ebubu	7.151137	4.77939	4.6	ND	7	92	119	60	0.1	28.9	0
34–22	Ebubu	7.150657	4.776055	5.4	480	6.4	84	447	225	0.2	29.1	4
34–23	Ebubu	7.150657	4.776055	5.2	ND	7.5	97	376	188	0.2	29.5	3

ID	Site	Longitude	Latitude	pH	Eh (mV)	DO (mg/L)	DO (%)	EC (µS/cm)	TDS (mg/L)	Salinity (PSU)	Temp. (°C)	Alkalinity (mg/L)
35–22	Ebubu	7.146193	4.77285	5.9	424	6.1	78	93	46	0.04	28.5	8
35–23	Ebubu	7.146193	4.77285	5.2	ND	5.5	72	376	188	0.2	28.3	3
36–22	Ebubu	7.153428	4.771623	5.3	462	8.3	106	72	35	0.03	27.7	1
36–23	Ebubu	7.153428	4.771623	3.6	ND	7.1	94	59	29	0.03	29.2	0
37–22	Ebubu	7.147802	4.766063	5	506	8.6	112	41	20	0.02	29	0
38–22	Ebubu	7.138585	4.783827	4.4	641	6.9	87	84	42	0.04	27.2	0
38–23	Ebubu	7.138585	4.783827	4.1	ND	4.1	53	86	43	0.04	28.8	0
39–22	Ebubu	7.150598	4.781781	4.9	506	7.9	103	81	41	0.04	27.9	0
39–23	Ebubu	7.150598	4.781781	4.1	ND	6.4	83	72	31	0.02	29	0
Minimum				3.5	424	3.4	43	21	10	0.01	27.2	0
Maximum				5.9	641	8.9	115	447	225	0.2	29.5	8
Median				4.8	506	7.2	94	81	41	0.04	28.5	0
Average				4.7	513	7	91	140	70	0.07	28.5	1.1
40–22	Alode	7.1099	4.765987	4.9	561	7.5	95	20	10	0.01	27.1	0
40–23	Alode	7.1099	4.765987	6.1	ND	1.4	19	64	32	0.03	30.5	22
41–22	Alode	7.115575	4.760697	5	426	6.4	81	100	50	0.1	27.2	1
42–22	Alode	7.122632	4.776868	5.3	118	3.6	49	63	31	0.03	30.6	4
42–23	Alode	7.122632	4.776868	5.3	ND	6.8	94	47	24	0.02	31	5
43–22	Alode	7.123132	4.776448	6.3	214	2	26	351	175	0.2	28	62
44–22	Alode	7.12319	4.778118	4.9	669	5.1	67	87	44	0.04	28.9	6
44–23	Alode	7.12319	4.778118	5	ND	7.9	100	53	27	0.03	29.1	1
45–22	Alode	7.121092	4.774338	4.8	374	5.6	74	71	36	0.03	28.6	0
45–23	Alode	7.121092	4.774338	5.4	ND	5.5	76	35	17	0.02	30.7	3
46–22	Alode	7.120805	4.774332	5.1	418	4.9	64	38	19	0.02	28.4	1
46–23	Alode	7.120805	4.774332	5	ND	6.2	85	30	15	0.01	30.5	0
47–22	Alode	7.12017	4.772995	4.8	435	6.2	83	56	28	0.02	29.9	0
47–23	Alode	7.12017	4.772995	5.2	ND	5.9	81	20	10	0.01	30.9	1
48–22	Alode	7.118968	4.77318	5.1	293	3.8	50	36	18	0.02	29	1
48–23	Alode	7.118968	4.77318	5.1	ND	5.6	77	20	10	0.01	30.8	1
49–22	Alode	7.118422	4.774342	4.8	473	5.2	74	59	30	0.03	33.5	0
49–23	Alode	7.118422	4.774342	3.5	ND	6	79	151	75	0.1	29.7	0
50–22	Alode	7.128068	4.774547	4.5	576	8.9	115	175	88	0.1	28.5	0
51–22	Alode	7.119213	4.774785	5.2	479	7.9	103	37	18	0.02	28.5	1
52–22	Alode	7.119302	4.774917	4.8	453	4.8	60	78	39	0.04	26.9	0
52–23	Alode	7.119302	4.774917	5	ND	3.7	51	76	38	0.04	30.5	2
53–22	Alode	7.121002	4.774275	4.7	489	5.4	67	41	21	0.02	26.5	0
54–22	Alode	7.121198	4.771883	5.6	474	8.5	107	23	12	0.01	26.9	2
55–22	Alode	7.121875	4.773352	4.9	754	7.5	99	43	21	0.02	28.9	0
56–22	Alode	7.123095	4.775877	5.1	536	8	105	22	11	0.01	28.6	0
57–22	Alode	7.120873	4.7731	5.1	454	7.6	94	199	100	0.1	26.6	0
58–22	Alode	7.121163	4.77653	5.1	438	3.9	47	127	63	0.1	25.4	0
59–22	Alode	7.11643	4.76728	6.3	147	3.3	43	281	140	0.1	27.6	5
60–22	Alode	7.114468	4.767733	6.9	117	2	25	388	195	0.2	27.9	12
61–22	Alode	7.114897	4.765332	6.4	231	3.3	43	100	50	0	29	3
62–22	Alode	7.128373	4.772763	6.3	140	3.2	42	269	134	0.1	28.9	6
63–23	Alode	7.124539	4.77805	5.9	ND	3.5	48	106	53	0.1	30.9	30
64–23	Alode	7.123953	4.776968	5.6	ND	5.9	81	31	15	0.01	30.9	6
65–23	Alode	7.120892	4.773005	5.3	ND	5.4	75	36	18	0.02	31	1
Minimum				3.5	117	1.4	19	20	10	0	25.4	0
Maximum				6.9	754	8.9	115	388	195	0.2	33.5	62
Median				5.1	438	5.5	75	59	30	0.03	28.9	1
Average				5	403	5	71	95	48	0.04	29	5
66–22	Okochiri	7.10224	4.750622	5	322	4.4	57	207	105	0.1	28.9	2
67–22	Okochiri	7.101903	4.75027	5.6	292	4.9	66	72	36	0.03	30.9	8
67–23	Okochiri	7.101903	4.75027	6.3	ND	7	93	67	33	0.03	29.5	14
68–22	Okochiri	7.101417	4.750313	4.6	742	5.3	69	46	24	0.02	28.2	1
68–23	Okochiri	7.101417	4.750313	5.5	ND	7.3	97	27	13	0.01	29.5	0
69–22	Okochiri	7.10104	4.75044	4.7	783	3.3	42	67	34	0.03	28.1	0
69–23	Okochiri	7.10104	4.75044	5.2	ND	5	66	26	13	0.01	29.2	0
70–22	Okochiri	7.10209	4.751638	5.6	336	7.4	97	79	40	0.04	28.8	5
70–23	Okochiri	7.10209	4.751638	5.7	ND	6.4	85	50	25	0.02	29.4	5
71–22	Okochiri	7.100852	4.75112	4.6	728	5.2	67	53	26	0.02	28.3	5
71–23	Okochiri	7.100852	4.75112	5	ND	6.5	84	32	16	0.01	28.3	0
72–22	Okochiri	7.100598	4.75093	4.7	513	7.5	96	32	16	0.01	28.1	1
73–22	Okochiri	7.100998	4.750173	4.8	576	5.6	73	39	19	0.02	28.3	1
73–23	Okochiri	7.100998	4.750173	6.1	ND	7.2	96	31	15	0.01	29.7	0
74–22	Okochiri	7.101615	4.74998	4.6	716	4.8	61	41	20	0.02	28	1
74–23	Okochiri	7.101615	4.74998	5.6	ND	6.1	82	28	14	0.01	29.4	0
75–22	Okochiri	7.102665	4.751113	4.4	653	5.6	71	75	37	0.03	27.7	1
75–23	Okochiri	7.102665	4.751113	4.5	ND	6.7	86	30	15	0.01	28.1	0
76–22	Okochiri	7.102948	4.752168	4.8	273	4.4	58	107	54	0.1	28.9	2
77–22	Okochiri	7.108247	4.751522	4.7	395	2.5	32	48	24	0.02	27.5	1
78–22	Okochiri	7.102517	4.7508	4.5	734	3.2	41	40	20	0.02	28	0

ID	Site	Longitude	Latitude	pH	Eh (mV)	DO (mg/L)	DO (%)	EC (µS/cm)	TDS (mg/L)	Salinity (PSU)	Temp. (°C)	Alkalinity (mg/L)
78–23	Okochiri	7.102517	4.7508	5	ND	6.4	85	21	11	0.01	29.1	0
79–22	Okochiri	7.10132	4.751203	4.7	775	6.9	96	34	17	0.01	32.5	0
79–23	Okochiri	7.10132	4.751203	5.6	ND	6.5	84	28	14	0.01	28.2	0
80–22	Okochiri	7.100848	4.751698	4.6	801	6.6	85	48	24	0.02	28.4	0
81–22	Okochiri	7.100475	4.751938	4.7	613	6.6	85	23	12	0.01	27.7	0
82–22	Okochiri	7.10029	4.752067	5.4	418	4.5	59	52	26	0.02	28.9	4
82–23	Okochiri	7.10029	4.752067	5.8	ND	7.1	96	18	9	0.01	29.7	0
83–22	Okochiri	7.100463	4.751511	4.7	542	7.7	99	121	60	0.1	28.2	0.3
84–22	Okochiri	7.100348	4.751697	4.7	507	6.2	81	68	33	0.03	29	0
85–22	Okochiri	7.099723	4.753902	5	508	7.3	95	40	20	0.02	29.3	1
85–23	Okochiri	7.099723	4.753902	5.3	ND	6.7	85	17	8	0.01	27.5	1
86–22	Okochiri	7.113888	4.77924	4.6	497	8.2	102	35	17	0.01	26.1	1
87–22	Okochiri	7.115607	4.775545	4.7	516	8.3	102	29	14	0.01	26.1	0
88–22	Okochiri	7.097222	4.765118	4.8	786	6.5	81	66	33	0.03	26.6	1
88–23	Okochiri	7.097222	4.765118	5.6	ND	7.3	91	17	8	0.01	26.4	1
89–22	Okochiri	7.106193	4.751553	6.1	238	4.6	59	98	49	0.04	28.3	25
89–23	Okochiri	7.106193	4.751553	5.1	ND	6	78	35	18	0.02	27.9	5
90–22	Okochiri	7.098743	4.750856	4.7	594	6.2	79	178	89	0.1	27.6	0.2
91–22	Okochiri	7.105703	4.772383	4.7	487	8.4	106	74	37	0.03	26.9	1
92–22	Okochiri	7.09597	4.764598	5	478	8.4	106	219	110	0.1	27	1
93–22	Okochiri	7.099103	4.749565	4.6	487	7	91	133	66	0.1	28.3	0
94–22	Okochiri	7.099858	4.752686	4.6	769	3.1	40	59	29	0.03	28.8	0
94–23	Okochiri	7.099858	4.752686	5.2	ND	4.7	64	24	12	0.01	30.6	0
95–22	Okochiri	7.101355	4.749598	4.5	553	8	102	59	30	0.03	27.8	0
96–22	Okochiri	7.103658	4.750985	4.6	535	7.4	94	42	21	0.02	27.4	0
97–22	Okochiri	7.115943	4.753642	4.7	516	8	105	136	68	0.1	29.1	0
98–22	Okochiri	7.103875	4.771045	4.8	458	8.3	105	55	28	0.02	27.2	0
99–22	Okochiri	7.09639	4.767717	4.9	457	8.1	106	132	66	0.1	28.6	0
100–22	Okochiri	7.11692	4.754807	4.8	477	7	87	56	28	0.02	26.1	0
101–22	Okochiri	7.11262	4.75071	5.3	583	6.9	87	52	26	0.02	26.8	0
102–22	Okochiri	7.115581	4.742069	4.8	493	7.3	93	27	13	0.01	27.3	0
103–22	Okochiri	7.116902	4.749518	5.1	491	8.3	108	83	41	0.04	28.7	1
104–22	Okochiri	7.11887	4.751762	5.4	457	8.3	108	42	21	0.02	28.8	0
105–22	Okochiri	7.116783	4.747585	5.5	451	7.9	99	26	13	0.01	26.6	0.3
106–22	Okochiri	7.109768	4.749522	4.8	781	5.7	74	52	26	0.02	28.6	0
107–22	Okochiri	7.109265	4.746812	4.8	539	7.9	100	24	12	0.01	27.4	0
108–22	Okochiri	7.100618	4.750235	5	737	6.2	80	45	22	0.02	28.1	1
108–23	Okochiri	7.100618	4.750235	5.6	ND	7.3	93	24	12	0.01	27.2	1
109–23	Okochiri	7.100833	4.751111	4.5	ND	7.2	94	18	9	0.01	28.3	0
110–23	Okochiri	7.100833	4.750556	4.5	ND	4.8	62	32	16	0.01	28.4	0
111–23	Okochiri	7.100028	4.751111	5.6	ND	7.2	94	17	9	0.01	28.5	0
112–23	Okochiri	7.100028	4.750557	5.4	ND	7.3	95	16	8	0.01	28.5	0
113–23	Okochiri	7.099083	4.750546	5.6	ND	6.3	83	64	32	0.03	28.3	14
114–23	Okochiri	7.105556	4.751389	5.2	ND	5.3	70	27	13	0.01	29	0
115–23	Okochiri	7.097785	4.657397	4.7	ND	4.4	58	20	10	0.01	29	0
Minimum				4.4	238	2.5	32	16	8	0.01	26.1	0
Maximum				6.2	801	8.4	108	219	110	0.1	32.5	25
Median				4.8	516	6.7	85	42	21	0.02	28.3	0
Average				5	549	6.4	83	56	28	0.03	28	1.6
All data												
Minimum				3.5	113	0.7	9	16	8	0.01	25.1	0
Maximum				6.9	801	8.9	115	852	427	0.4	33.5	100
Median				5	489	6.2	81	67	33	0.03	28.5	0
Average				5	485	5.9	76	120	60	0.1	28.5	5
REF1	Alode	7.11569	4.775232	4	491	7.6	103	24	12	0.01	30.9	0
REF2	Alode	7.114142	4.779242	4.3	516	7.5	101	17	9	0.01	30.8	0
REF3	Okochiri	7.114741	4.747028	4.6	451	6.6	84	19	9	0.01	27	2
REF4	Okrika	7.079138	4.738417	5.1	450	7.9	100	31	15	0.01	27.7	1
REF5	Ogale	7.14101	4.774265	5	641	8.2	107	69	32	0.03	28.4	0

Table 4.2S: Chemical measurements and hydrochemical ratios of groundwater in the study area (2022 and 2023)

ID	Site	NO_3 (mg/L)	NO_2 (mg/L)	Cl (mg/L)	SO_4^2 (mg/L)	Ca (mg/L)	Na (mg/L)	K (mg/L)	Mg (mg/L)	Si (mg/L)	Sr (mg/L)	Fe (mg/L)	Mn (mg/L)	DOC (mg/L)	NO_3^- /Cl^-
1–22	Alesa	142	0.3	49	< 0.01	27	32	19	5	2	0.1	<0.01	0.1	21	2.9
1–23	Alesa	106	<0.01	41	21	27	33	18	5	2	0.1	<0.01	0.1	31	2.6
2–22	Alesa	39	1	17	23	13	14	12	4	1	0.01	<0.01	<0.02	20	2.3
2–23	Alesa	34	1	17	23	12	15	10	3	3	0.01	<0.01	<0.02	36	2
3–22	Alesa	83	<0.01	30	4	10	25	4	2	1	0.03	<0.01	0.1	31	2.8
3–23	Alesa	83	<0.01	27	4	8	23	2	2	3	0.03	<0.01	0.1	27	3.1
4–22	Alesa	19	<0.01	10	2	12	10	1	3	1	0.02	<0.01	0.04	33	1.9
4–23	Alesa	17	<0.01	9	1	3	9	1	1	3	0.01	<0.01	0.02	37	1.9
5–22	Alesa	90	<0.01	27	5	12	27	7	3	1	0.04	<0.01	0.1	17	3.3
5–23	Alesa	73	<0.01	24	5	10	22	6	2	2	0.04	<0.01	0.1	38	3
6–22	Alesa	58	<0.01	18	14	11	15	11	3	1	0.02	<0.01	0.02	41	3.2
6–23	Alesa	53	<0.01	18	13	10	16	9	2	3	0.02	<0.01	0.02	37	2.9
7–22	Alesa	99	<0.01	40	21	18	29	14	4	1	0.1	0.04	0.2	32	2.5
7–23	Alesa	97	<0.01	38	18	16	29	12	3	3	0.1	<0.01	0.2	37	2.6
8–22	Alesa	33	<0.01	10	14	7	10	8	2	1	0.01	<0.01	0.03	26	3.3
8–23	Alesa	32	<0.01	11	14	7	9	7	2	3	0.01	<0.01	0.02	42	2.9
9–22	Alesa	68	<0.01	24	13	51	18	14	8	2	0.1	<0.01	0.3	24	2.8
9–23	Alesa	66	<0.01	24	12	16	20	12	4	2	0.03	<0.01	0.1	35	2.8
10–22	Alesa	18	<0.01	5	2	1	7	1	0.3	1	0.01	<0.01	0.1	15	3.6
10–23	Alesa	22	<0.01	6	1	2	7	1	0.3	3	0.01	<0.01	0.1	32	3.7
Minimum		17	<0.01	5	1	1	7	1	0.3	1	0.01	<0.01	<0.02	15	1.9
Maximum		142	1	49	23	51	33	19	8	3	0.1	0.04	0.3	42	3.7
Median		62	1	21	13	12	17	9	3	2	0.03	0.04	0.1	32	2.9
Average		62	0.8	22	11	14	19	9	3	2	0.04	0.04	0.1	31	2.8
11–22	Ogale	<0.01	<0.01	11	3	0.3	11	0.3	0.1	1	0.001	2	<0.02	16	<0.01
12–22	Ogale	2	0.2	5	3	13	4	1	1	0.3	0.01	50	0.1	49	0.4
13–22	Ogale	3	<0.01	7	31	15	8	7	3	0.4	0.04	0.03	0.1	24	0.4
13–23	Ogale	<0.01	<0.01	10	7	12	4	7	1	1	0.01	46	0.1	30	<0.01
14–22	Ogale	93	0.2	57	17	14	50	19	3	0.4	0.04	0.02	0.4	32	1.6
15–22	Ogale	12	<0.01	4	4	0.4	3	1	0.1	1	0.002	3	0.02	28	3
15–23	Ogale	64	<0.01	49	18	10	39	18	2	1	0.03	0.03	0.2	27	1.3
16–22	Ogale	<0.01	<0.01	6	2	0.4	5	0.2	<0.01	1	0.001	2	<0.02	27	<0.01
16–23	Ogale	<0.01	<0.01	5	3	0.2	4	0.3	0.1	4	<0.001	2	0.02	32	<0.01
17–22	Ogale	211	<0.01	66	80	42	56	59	14	1	0.1	<0.02	0.2	47	3.2
17–23	Ogale	<0.01	<0.01	2	3	1	1	1	0.2	6	<0.001	0.02	0.02	5	<0.01
18–22	Ogale	12	0.2	8	2	2	11	1	1	1	0.02	0.04	0.2	19	1.5
19–22	Ogale	2	<0.01	3	2	0.4	1	0.3	0.1	1	0.003	1	0.1	15	0.7
19–23	Ogale	<0.01	<0.01	8	2	0.4	5	0.1	0.2	4	<0.001	1	0.04	30	<0.01
20–22	Ogale	124	<0.01	30	2	13	30	5	3	1	0.05	0.03	1	17	4.1
20–23	Ogale	<0.01	<0.01	3	2	0.3	1.4	0.1	0.1	3	<0.001	1	0.04	31	<0.01
21–22	Ogale	20	<0.01	5	2	3	6	2	1	1	0.01	<0.01	0.1	17	4
21–23	Ogale	81	<0.01	21	1	7	19	4	2	3	0.03	<0.01	1	36	3.9
22–22	Ogale	<0.01	<0.01	5	2	0.3	3	0.3	0.1	1	0.001	4	0.02	9	<0.01
23–22	Ogale	<0.01	<0.01	3	1	1	2	1	0.1	1	0.001	2	0.02	14	<0.01
23–23	Ogale	<0.01	<0.01	6	1	0.2	3	0.1	0.1	3	<0.001	4	0.02	27	<0.01
24–22	Ogale	29	<0.01	6	2	0.4	1	0.2	0.1	1	0.001	0.1	0.02	16	4.8
24–23	Ogale	<0.01	<0.01	6	2	0.2	5	0.1	<0.01	3	<0.001	1	<0.02	26	<0.001
25–22	Ogale	29	<0.01	7	2	3	10	0.4	1	1	0.02	<0.01	0.1	14	4.1
25–23	Ogale	28	<0.01	7	1	2	11	0.4	0.4	3	0.01	<0.01	0.1	36	4
26–22	Ogale	88	<0.01	24	2	7	25	1	3	2	0.1	0.02	1	11	3.7
26–23	Ogale	22	<0.01	6	<0.01	2	9	0.2	0.3	3	0.01	0.02	0.1	35	3.7
27–22	Ogale	51	0.2	36	21	6	29	10	2	1	<0.001	0.02	0.1	25	1.4
27–23	Ogale	62	<0.01	19	1	5	17	2	2	3	0.03	<0.01	1	35	3.3
Minimum		<0.01	<0.01	2	<0.01	0.2	1	0.1	<0.01	0.3	<0.001	<0.01	<0.02	5	<0.001
Maximum		211	0.2	66	80	42	56	59	14	6	0.1	50	1	49	4.8
Median		29	0.2	7	2	2	6	1	1	1	0.01	1	0.1	27	3.3
Average		57	0.2	16	10	7	14	7	2	2	0.03	7	0.3	25	2.7
28–22	Ebubu	2	<0.01	1	2	1	1	0.2	0.1	1	0.004	<0.01	<0.02	25	1.4
29–22	Ebubu	<0.01	<0.01	1	8	15	26	7	3	1	0.1	0.4	0.4	32	<0.01
30–22	Ebubu	13	<0.01	3	2	3	5	<0.01	1	2	0.01	0.05	0.2	26	3.9
31–22	Ebubu	2	<0.01	1	2	0.3	1	0.2	0.1	1	0.001	<0.01	<0.02	35	1.4
31–23	Ebubu	15	<0.01	4	<0.01	1	6	0.2	0.3	3	0.01	<0.01	0.1	31	3.8
32–22	Ebubu	51	<0.01	12	1	12	12	2	3	2	0.03	0.2	2	31	4.3
33–22	Ebubu	8	<0.01	3	2	1	3.4	0.3	0.1	1	0.003	0.02	0.02	34	2.7
33–23	Ebubu	44	<0.01	9	1	3	11	2	1	3	0.01	0.03	1	32	4.9
34–22	Ebubu	120	0.2	40	2	31	27	16	8	1	0.1	0.05	0.1	34	3
34–23	Ebubu	10	1	6	6	1	5	0.1	0.2	3	<0.001	<0.02	0.02	27	1.7
35–22	Ebubu	15	0.2	4	4	8	5	0.3	2	1	0.02	0.1	0.1	19	3.8
35–23	Ebubu	148	<0.01	42	26	29	27	14	7	3	0.1	0.02	0.1	33	3.5
36–22	Ebubu	11	<0.01	4	6	4	3	3	1	1	0.004	0.02	0.02	25	2.8
36–23	Ebubu	3	<0.01	4	1	1	5	0.1	0.2	3	<0.001	<0.01	0.02	27	0.8

ID	Site	NO_3 (mg/L)	NO_2 (mg/L)	Cl (mg/L)	SO_4^{2} (mg/L)	Ca (mg/L)	Na (mg/L)	K (mg/L)	Mg (mg/L)	Si (mg/L)	Sr (mg/L)	Fe (mg/L)	Mn (mg/L)	DOC (mg/L)	NO_3^- /Cl$^-$
37–22	Ebubu	2	<0.01	1	2	1	1	0.2	0.1	1	0.002	<0.01	<0.02	35	1.4
38–22	Ebubu	19	< 0.01	7	2	1	8	0.4	1	1	0.01	<0.01	0.2	47	2.6
38–23	Ebubu	25	<0.01	8	1	1	11	0.3	1	3	0.01	<0.01	0.2	39	3.1
39–22	Ebubu	11	<0.01	3	2	3	5	0.3	1	1	0.01	0.02	0.1	32	3.2
39–23	Ebubu	28	<0.01	8	3	1	11	0.3	1	3	0.01	<0.01	0.2	39	3.3
Minimum		<0.01	<0.01	1	<0.01	0.3	1	<0.01	0.1	1	<0.001	<0.01	<0.02	19	<0.01
Maximum		148	1	42	26	31	27	16	8	3	0.1	0.4	2	47	4.9
Median		14	0.2	4	2	1	5	0.3	1	1	0.01	0.04	0.1	32	3
Average		34	0.5	10	5	7	10	3	2	2	0.03	0.1	0.4	32	2.9
40–22	Alode	<0.01	<0.01	1	1	2	10	1	0.4	1	0.01	<0.01	0.2	47	<0.01
40–23	Alode	<0.01	<0.01	3	1	10	1	1	1	3	0.03	0.3	0.03	35	<0.01
41–22	Alode	0.824	<0.01	4	2	0.4	4	0.2	0.1	1	0.001	0.2	0.02	17	0.2
42–22	Alode	<0.01	<0.01	7	2	1	5	1	0.2	1	0.002	2	<0.02	26	<0.01
42–23	Alode	<0.01	<0.01	10	2	1	7	0.2	0.2	3	<0.001	2.4	<0.02	26	<0.01
43–22	Alode	2	<0.01	10	33	27	6	0.4	4	1	0.1	19	0.3	26	0.2
44–22	Alode	13	<0.01	9	2	3	9	0.4	0.4	1	0.01	0.02	0.02	17	1.4
44–23	Alode	1	0.2	9	4	2	9	0.3	0.3	3	0.01	<0.02	<0.02	28	0.1
45–22	Alode	<0.01	<0.01	1	2	2	1	1	0.3	1	0.01	0.2	0.03	34	<0.01
45–23	Alode	<0.01	<0.01	2	4	1.3	5	0.4	0.3	4	<0.001	0.3	0.02	32	<0.01
46–22	Alode	<0.01	<0.01	1	1	2	1	1	0.3	1	0.01	1	0.03	33	<0.01
46–23	Alode	<0.01	<0.01	2	1	2	1	0.3	0.3	4	0.01	0.4	0.03	34	<0.01
47–22	Alode	<0.01	<0.01	1	2	1	1	1	0.2	1	0.004	0.3	0.03	26	<0.01
47–23	Alode	<0.01	<0.01	1	1	1	1	0.4	0.2	4	<0.001	1	0.02	34	<0.01
48–22	Alode	<0.01	<0.01	1	2	1	1	1	0.2	1	0.004	1	0.03	22	<0.01
48–23	Alode	<0.01	<0.01	2	1	1	1	0.3	0.2	4	<0.001	1	0.04	35	<0.01
49–22	Alode	<0.01	<0.01	1	2	1	1	1	0.3	1	0.004	0.1	0.03	33	<0.01
49–23	Alode	55	<0.01	12	2	3	16	2	1	3	0.02	0.03	1	42	4.6
50–22	Alode	50	<0.01	11	2	3	15	2	1	1	0.02	0.1	0.3	10	4.5
51–22	Alode	4	<0.01	2	2	1	2	1	0.1	2	0.003	0.1	0.03	25	2
52–22	Alode	2	<0.01	6	17	2	5	0.3	0.3	1	0.01	6	0.1	16	0.3
52–23	Alode	<0.01	<0.01	9	17	1	10	0.1	0.2	2	<0.001	7	0.02	30	<0.01
53–22	Alode	1	<0.01	1	1	2	1	1	0.4	1	0.01	0.2	0.03	24	1
54–22	Alode	2	<0.01	2	2	2	1	0.4	0.1	1	0.002	<0.01	<0.02	20	1
55–22	Alode	7	<0.01	3	2	1	4	1	0.2	1	0.004	<0.01	0.02	29	2.3
56–22	Alode	2	<0.01	2	1	1	1	0.3	0.1	1	0.002	0.1	0.02	16	0.7
57–22	Alode	2	<0.01	2	2	1	1	0.4	0.1	1	0.001	1	<0.02	16	1
58–22	Alode	1	<0.01	6	9	2	6	1	0.3	1	0.01	3	0.03	23	0.2
59–22	Alode	2	<0.01	5	2	7	2	0.3	0.4	1	<0.001	32	<0.02	27	0.3
60–22	Alode	1	2	5	1	40	2	4	1	8	1	1	0.1	32	0.2
61–22	Alode	2	<0.01	2.4	<0.01	8	2	2	4	4	0.1	0.2	0.3	28	0.8
62–22	Alode	<0.01	<0.01	3	<0.01	5	2	2	0.3	2	<0.001	21	0.1	54	<0.01
63–23	Alode	<0.01	<0.01	9	6	1	3	0.3	0.2	4	<0.001	3	0.02	26	<0.01
64–23	Alode	<0.01	<0.01	3	2	3	6	0.1	1	1	<0.001	21	0.1	29	<0.01
65–23	Alode	2	<0.01	3	3	1	3	0.2	0.1	3	<0.001	0.4	0.01	18	0.7
Minimum		<0.01	<0.01	1	<0.01	0.4	1	0.1	0.1	1	<0.001	<0.01	<0.02	10	<0.01
Maximum		55	2	12	33	40	16	4	4	8	1	32	1	54	4.6
Median		2	1	3	2	2	2	0.4	0.3	1	0.01	1	0.03	27	0.8
Average		10	1	4.4	5	5	4.4	11	1	2	0.1	5	0.1	28	1.3
66–22	Okochiri	3	<0.01	3	6	1	7	0.4	0.1	1	0.002	0.3	0.1	33	1
67–22	Okochiri	2	<0.01	3	12	1	15	0.4	0.1	1	0.002	0.2	0.03	27	0.7
67–23	Okochiri	<0.01	<0.01	3	12	2	14	0.2	0.1	3	<0.001	0.2	0.03	ND	<0.01
68–22	Okochiri	3	<0.01	3	4	2	4	1	0.2	2	0.004	0.02	0.1	26	1
68–23	Okochiri	1	<0.01	3	5	2	4	0.3	0.2	5	<0.001	<0.01	0.04	ND	0.3
69–22	Okochiri	3	<0.01	3	3	2	3	1	0.2	2	0.003	<0.01	0.1	24	1
69–23	Okochiri	2	<0.01	3	2	0.4	3	0.4	0.2	5	<0.001	<0.01	0.04	ND	0.7
70–22	Okochiri	2	<0.01	4	11	1	10	0.3	0.2	1	0.003	1	0.1	22	0.5
70–23	Okochiri	<0.01	0.2	3	11	1	10	0.2	0.2	3	<0.001	1	0.1	3	<0.01
71–22	Okochiri	3	<0.01	3	3	1	2	0.3	0.2	1	0.003	<0.01	0.1	23	1
71–23	Okochiri	2	<0.01	3	3	1	2	0.2	0.2	4	<0.001	<0.01	0.04	ND	0.7
72–22	Okochiri	2	<0.01	2	2	1	1	0.4	0.2	2	0.002	0.02	0.04	29	1
73–22	Okochiri	4	<0.01	2	2	1	3	1	0.2	2	0.003	0.03	0.04	23	2
73–23	Okochiri	3	<0.01	3	2	1	3	0.4	0.2	5	< 0.001	<0.02	0.03	2	1
74–22	Okochiri	2	<0.01	2	4	2	4	0.2	0.3	3	0.01	0.02	0.1	22	1
74–23	Okochiri	<0.01	<0.01	2	5	1	4	0.3	0.2	4	<0.001	0.02	0.04	3	<0.01
75–22	Okochiri	<0.01	<0.01	1.4	2	1	2	0.4	0.3	1	0.01	0.03	1	28	<0.01
75–23	Okochiri	<0.01	<0.01	2	1	1	1.4	0.2	0.2	4	<0.001	0.1	0.4	33	<0.01
76–22	Okochiri	<0.01	<0.01	2	5	1	4	0.4	0.4	2	0.01	4	0.3	25	<0.01
77–22	Okochiri	<0.01	<0.01	4	1	1	2	0.2	0.2	1	0.003	2	0.1	20	<0.01
78–22	Okochiri	1	<0.01	1	1	1	1	1	0.2	2	0.003	<0.01	0.2	22	1
78–23	Okochiri	0	<0.01	2	1	1	1	0.4	0.2	5	<0.001	<0.01	0.3	4	<0.01
79–22	Okochiri	3	<0.01	2	3	1	2	1	0.3	2	0.01	<0.01	0.1	15	1.5
79–23	Okochiri	2	<0.01	3	2	1	2	0.4	0.2	5	<0.001	<0.01	0.1	ND	0.7
80–22	Okochiri	2	<0.01	2	3	1	2	0.3	0.2	1	0.003	<0.01	0.1	14	1.2

ID	Site	NO_3 (mg/L)	NO_2 (mg/L)	Cl (mg/L)	SO_4^{2} (mg/L)	Ca (mg/L)	Na (mg/L)	K (mg/L)	Mg (mg/L)	Si (mg/L)	Sr (mg/L)	Fe (mg/L)	Mn (mg/L)	DOC (mg/L)	NO_3^- /Cl$^-$
81–22	Okochiri	2	<0.01	2	1	1	1	0.4	0.2	1	0.002	<0.01	0.04	30	1
82–22	Okochiri	<0.01	<0.01	4	5	0.3	9.4	0.2	<0.01	1	<0.001	1	0.01	33	<0.01
82–23	Okochiri	1	<0.01	2	2	0.4	2	0.2	0.2	4	<0.001	0.02	0.04	ND	0.5
83–22	Okochiri	2	<0.01	2	2	1	1	0.2	0.2	1	0.002	0.02	0.04	17	1
84–22	Okochiri	3	<0.01	2	2	1	1	0.4	0.3	2	0.004	0.02	0.1	34	1.5
85–22	Okochiri	<0.01	<0.01	2	2	1	1	1	0.1	2	0.004	<0.01	0.03	26	<0.01
85–23	Okochiri	<0.01	<0.01	2	1	1	1	1	0.1	5	<0.001	<0.01	0.02	29	<0.01
86–22	Okochiri	1	<0.01	1	1	1	1	0.2	0.1	1	0.002	<0.01	0.02	26	1.4
87–22	Okochiri	3	<0.01	2	2	0.4	2	0.2	0.1	1	0.002	0.02	0.02	29	1.5
88–22	Okochiri	1	<0.01	2	1	1	1	0.2	0.1	1	0.004	<0.01	<0.02	29	0.5
88–23	Okochiri	<0.01	<0.01	2	3	1	1	0.1	0.1	4	<0.001	<0.01	<0.02	30	<0.01
89–22	Okochiri	<0.01	<0.01	2	6	1	2	0.2	0.2	1	0.003	25	0.1	31	<0.01
89–23	Okochiri	<0.01	<0.01	3	7	1	2	0.1	0.1	1	<0.001	6	0.1	26	<0.01
90–22	Okochiri	1.4	<0.01	2	2	1	2	<0.01	0.1	2	0.002	0.1	0.1	24	0.7
91–22	Okochiri	1	<0.01	1	1	1	1	0.2	0.1	1	0.003	<0.01	<0.02	28	1
92–22	Okochiri	1	<0.01	1	1	1	1	1	0.2	7	0.01	<0.01	0.02	21	1
93–22	Okochiri	2	<0.01	2	2	1	1	0.3	0.2	2	0.002	<0.01	0.04	31	1
94–22	Okochiri	2	<0.01	2	2	0.4	1	1	0.1	2	0.002	<0.01	0.03	42	1
94–23	Okochiri	<0.01	<0.01	2	1	0.3	1	0.4	0.1	5	<0.001	<0.01	0.03	26	<0.01
95–22	Okochiri	2	<0.01	2	2	1	1	0.4	0.2	1	0.003	<0.01	0.04	18	1
96–22	Okochiri	2	<0.01	2	1	1	1	1	0.1	1	0.004	<0.01	0.03	22	1
97–22	Okochiri	2	<0.01	1.4	2	0.4	1	0.4	0.2	1	0.001	<0.01	0.04	25	1.4
98–22	Okochiri	2	<0.01	2	1	1	1	0.3	0.1	1	0.003	<0.01	<0.02	18	1
99–22	Okochiri	2	<0.01	1	2	1	1	0.3	0.1	1	0.004	<0.01	0.02	14	2
100–22	Okochiri	10	<0.01	2	4	4	2	0.4	0.3	1	0.01	0.04	0.04	43	5
101–22	Okochiri	2	<0.01	2	3	1	1	0.3	0.2	1	0.003	<0.01	0.1	29	1
102–22	Okochiri	1	<0.01	2	2	1	1	0.4	0.2	1	0.001	0.02	0.02	32	0.5
103–22	Okochiri	2	<0.01	2	2	2	1	0.2	0.4	1	0.01	<0.02	<0.02	30	1
104–22	Okochiri	2	<0.01	2	2	1	1	0.2	0.1	1	0.003	0.02	<0.02	37	1
105–22	Okochiri	<0.01	<0.01	2	2	1	1	0.4	0.2	1	0.002	<0.01	0.02	23	<0.01
106–22	Okochiri	2	<0.01	2	6	2	1	0.4	0.3	1	0.01	<0.01	0.1	29	1
107–22	Okochiri	2	<0.01	1	2	1	1	0.2	0.1	1	0.002	<0.01	0.02	34	2
108–22	Okochiri	2	<0.01	1	2	0.4	3	0.2	0.1	1	0.001	<0.01	0.02	30	2
108–23	Okochiri	<0.01	<0.01	2	1	0.4	4	0.2	0.1	5	0.001	<0.01	<0.02	29	<0.01
109–23	Okochiri	1	<0.01	2	1	1	1	0.2	0.1	4	<0.001	<0.01	0.03	ND	0.5
110–23	Okochiri	2	<0.01	3	3	1	3	0.3	0.2	5	<0.001	0.03	0.04	ND	0.7
111–23	Okochiri	3	<0.01	5	7	1	2	0.2	0.1	4	<0.001	<0.01	0.02	ND	0.6
112–23	Okochiri	1	<0.01	2	2	0.4	1.4	0.3	0.1	5	<0.001	<0.01	0.03	ND	0.5
113–23	Okochiri	1	<0.01	3	12	1	3	0.1	0.2	1	<0.001	14	0.1	ND	0.3
114–23	Okochiri	<0.01	<0.01	4	2	0.2	2	0.1	< 0.01	3	<0.001	2	0.01	29	<0.01
115–23	Okochiri	<0.01	<0.01	5	6	0.3	1.4	0.1	0.1	3	<0.001	1	0.04	31	<0.01
Minimum	<0.01	<0.01	1	1	0.2	1	<0.01	<0.01	1	<0.001	<0.01	<0.02	2	<0.01	<0.01
Maximum	10	0.2	5	12	4	15	1	0.4	7	0.01	25	1	43	5	5
Median	2	<0.01	2	2	1	2	0.3	0.2	2	0.003	0.1	0.04	26	1	1
Average	2	<0.01	2	3	1	3	0.4	0.2	2	0.004	3	0.1	25	1	1
Minimum	<0.01	<0.01	1	<0.01	0.2	1	0.1	<0.01	0.3	<0.001	<0.01	<0.02	2	<0.01	<0.01
All data															
Maximum	211	2	66	80	51	56	59	14	8	1	50	2	54	5	5
Median	3	0.2	3	2	1	3	0.4	0.2	1	0.01	0.2	0.04	28	1.4	1.4
Average	25	1	8	6	5	8	3	1	2	0.03	4	0.2	27	2	2
REF1	Alode	3	<0.01	5	6	0.3	2	0.1	0.1	3	<0.001	<0.01	<0.01	23	0.6
REF2	Alode	3	<0.01	5	6	1	1	0.1	0.1	2	<0.001	<0.01	<0.01	35	0.6
REF3	Okochiri	<0.01	<0.01	4	6	1	1	0.3	0.1	3	<0.001	<0.01	<0.01	2	<0.01
REF4	Okrika	2	<0.01	2	2	1	1	0.6	0.3	2	0.004	<0.01	0.03	10	1
REF5	Ogale	1	<0.01	2	2	1	0.4	0.3	0.1	1	0.001	<0.01	0.02	22	0.7

Notes: ND = Not Determined, DOC = Dissolved Organic Carbon, REF = Reference sample. Sample names that end with –22 and –23 represent groundwater samples collected in 2022 and 2023, respectively.

Table 4.3S: Chemical measurements of sewage in the study area

Sample Name	NO_3 (mg/L)	NO_2 (mg/L)	Cl (mg/L)	F (mg/L)	PO_4^3 (mg/L)	SO_4^2 (mg/L)	Ca (mg/L)	Na (mg/L)	K (mg/L)	Mg (mg/L)	Si (mg/L)	Sr (mg/L)	Fe (mg/L)	Mn (mg/L)
EF1	127	<0.01	45	0.3	<0.01	21	30	36	19	5	2	0.1	0.4	0.1
EF2	131	0.4	99	<0.01	10	8	39	5	1	2	5	0.3	1	0.2
EF3	<0.01	<0.01	248	<0.01	54	2	37	363	74	13	31	0.2	7	0.3
EF4	103	<0.01	43	<0.01	<0.01	20	60	65	50	12	6	0.3	3	1
EF5	145	<0.01	123	0.1	2	10	65	83	40	7	8	0.4	1	1
EF6	1	<0.01	68	0.1	<0.01	6	39	28	16	1	5	0.3	0.3	0.2
EF7	31	<0.01	26	<0.01	2	9	22	23	10	2	3	0.1	0.1	0.2
EF8	42	<0.01	31	0.1	2	6	34	30	13	3	5	0.2	0.3	0.2
Minimum	<0.01	<0.01	26	<0.01	<0.01	2	22	5	1	1	2	0.1	0.1	0.1
Maximum	145	0.4	248	0.3	54	21	65	363	74	13	31	0.4	7	1
Median	103	<0.01	57	0.1	2.3	8.5	38	33	17.5	4	5	0.3	0.7	0.2
Average	83	<0.01	85	0.2	14	10	41	79	28	6	8	0.2	2	0.4
REF1	<0.01	<0.01	6	0.1	<0.01	1	18	12	5	1	3	0.1	0.1	0.0
REF2	1	<0.01	12	<0.01	<0.01	4	65	37	44	8	8	0.3	8	1

Fig. 4.1. (A), (B), (C), (D), and (E) municipal sewage in the Alesa, (F), (G), and (H) municipal sewage in the Ogale, and (I) municipal sewage in the Ebubu drainage systems. The arrow shows the flow direction.

Fig. 4.2. (A), and (B) solid waste dumpsite in the Alode, (C) solid waste dumpsite in the Ogale, and (D) solid waste dumpsite in the Alesa.

Fig. 4.3. Municipal drainage systems in Okochiri. Municipal sewage was not observed in the community's drainages. The arrow shows the flow direction.

Fig. 4.4. The overhead storage tank for drinking water in the (A) Alode, (B), (E), and (F) Okochiri, (C), (D), and (G) Ogale.